Trinity College Dublin
Coláiste na Tríonóide, Baile Átha Cliath
The University of Dublin

The Production and Characterisation of Itraconazole Multicomponent Systems

A dissertation submitted for the degree of

Doctor of Philosophy

at the School of Pharmacy & Pharmaceutical Sciences,

Trinity College Dublin,

the University of Dublin, Ireland

by Agnieszka Kozyra

Under the supervision of Dr Lidia Tajber

March 2019

Declaration

I declare that this thesis has not been submitted as an exercise for a degree at this or any other university. A small proportion of the work described in this thesis was carried out by others, and this is duly acknowledged in the text wherever relevant. I declare that all other work is entirely my own.

I agree to deposit this thesis in the University's open access institutional repository or allow the Library to do so on my behalf, subject to Irish Copyright Legislation and Trinity College Library conditions of use and acknowledgement.

_____

Agnieszka Kozyra

Table of Contents

Summary ..... **i**

Acknowledgements ..... **iii**

Publications and Presentations ..... **iv**

List of Abbreviations and Symbol ..... **v**

Chapter 1: General Introduction **1**

1.1 The Oral Route of Administration 2

1.1.1 The Biopharmaceutics Classification System (BCS) 2

1.1.2 Solubility, Dissolution and Dissolution Rate 3

1.1.3 Strategies to Improve Solubility and Dissolution Rate of Drugs 5

1.2 Pharmaceutical Solids 5

1.2.1 Crystalline Solids 6

1.2.2 Amorphous Solids 8

1.2.3 Liquid Crystalline 11

1.3 Classification of Solid Dispersions 12

1.3.1 Eutectic Mixtures 13

1.3.2 Solid Solutions 14

1.3.3 Glass Solutions 15

1.3.4 Glass Suspensions 17

1.4 Miscibility 17

1.4.1 Glass Transition Temperature (T_g) 18

1.4.2 Hansen Solubility Parameters 19

1.4.3 The Flory-Huggins Theory 19

1.5 Itraconazole 20

1.6 Project Aims 22

Chapter 2: Comparative Study of Different Methods for the Prediction of Drug/Polymer Solubility **23**

2.1 Introduction 24
2.2 Materials and Methods 27
2.2.1 Materials 27
2.2.2 Melting Point Depression Method 27
2.2.2.1 Preparation of physical mixtures 27
2.2.2.2 Content Uniformity Determination 27
2.2.2.3 Thermal Analysis 28
2.2.2.4 Powder X-ray Diffraction (PXRD) 29
2.2.3 Crystallization Method 29
2.2.3.1 Sample Preparation 29
2.2.3.2 Solubility Determination 29
2.2.3.3 Solid State Characterisation 30
2.2.4 Dissolution Endpoint Method 30
2.2.4.1 Sample Preparation 30
2.2.4.2 Thermal Analysis 31
2.2.4.3 Solid State Characterisation 31
2.2.5 True Density Measurements 31
2.3 Results and Discussion 32
2.3.1 Prediction of Drug/Polymer Solubility from DSC Data 32
2.3.2 Melting Point Depression Method 32
2.3.3 Comparison of the Different Methods 36
2.4 Conclusions 39
Chapter 3: Phase Diagrams of Polymer-Dispersed Liquid Crystal Systems of Itraconazole-Component Immiscibility Induced by Molecular Anisotropy 40
3.1 Introduction 41
3.2 Materials and Methods 44
3.2.1 Materials 44
3.2.2 Methods 44

3.2.2.1 Preparation of physical mixtures 44
3.2.2.2 Content Uniformity Determination 45
3.2.2.3 Thermal Analysis 45
3.2.2.3.1 Melting point depression measurements 45
3.2.2.3.2 Liquid Crystalline (LC) Phase Transition Measurements 45
3.2.2.3.3 Determination of Glass Transition Temperatures (T_gs) 45
3.2.2.3.4 Thermogravimetric Analysis (TGA) 45
3.2.2.4 Powder X-ray Diffraction (PXRD) 46
3.2.2.5 Polarised Light Microscopy and Hot Stage (PLM-HS) 46
3.2.2.6 True Density Measurements 46
3.2.2.7 Solid-State Fourier Transform Infrared Spectroscopy (FT-IR) 46
3.2.2.8 Mathematical Modelling and Statistical Analysis 47
3.3 Results and Discussion 48
3.3.1 Liquid Crystalline Properties of Itraconazole 48
3.3.2 Thermomicroscopic Studies of ITZ/Polymer Systems 54
3.3.3 DSC Analysis of Liquid Crystalline Transitions for ITZ/polymer Systems 56
3.3.4 Phase Diagrams of ITZ/Polymer Systems 60
3.3.4.2 Solid-Isotropic (Liquid) Line 64
3.3.4.3 Liquid Crystalline Phase Separation 66
3.3.4.4 Glass Transition Temperatures 67
3.4 Conclusions 68
Chapter 4: Phase Diagrams and Thermodynamic Properties of Binary Systems of Itraconazole and Succinic Acid 69
4.1 Introduction 70
4.2 Materials and Methods 73
4.2.1 Materials 73
4.2.2 Methods 73
4.2.2.1 Preparation of Physical Mixtures 73

4.2.2.2 Fast - Evaporation Crystallisation 73
4.2.2.3 Slow - Evaporation Crystallisation 74
4.2.2.4 Differential Scanning Calorimetry (DSC) 74
4.2.2.5 Powder X-ray Diffraction (PXRD) 75
4.2.2.6 Polarised Light Microscopy and Hot Stage (PLM-HS) 75
4.2.2.7 Solid-State Fourier Transform Infrared Spectroscopy (FT-IR) 75
4.3 Results and Discussion 76
4.3.1 Determination of ITZ and SUC Thermodynamic Phase Diagram 76
4.3.2 Crystallisation of pure binary ITZ/SUC phases 82
4.3.2.1 Slow-Evaporation Crystallisation 82
4.3.2.2 Fast - Evaporation Crystallisation 84
4.3.3 Physicochemical properties of ITZ-SUC and eutectic form E_1 87
4.3.4 Second heating 91
4.4 Conclusions 97
Chapter 5: Solid State Characterisation and Solubility Behaviour of Itraconazole–Succinic Acid and Itraconazole–Succinic Acid-Polymer Systems 98
5.1 Introduction 99
5.2 Materials and Methods 101
5.2.1 Materials 101
5.2.1.1 Preparation of Media for Solubility Studies 101
5.2.2 Synthesis of Itraconazole and Succinic Acid Cocrystal (ITZ-SUC) 101
5.2.3 Preparation of Milled Samples 102
5.2.4 Differential Scanning Calorimetry (DSC) 102
5.2.5 Powder X-ray Diffraction (PXRD) 102
5.2.6 Solid-State Fourier Transform Infrared Spectroscopy (FT-IR) 102
5.2.7 Dynamic Solubility Study 102
5.2.8 High-Performance Liquid Chromatography (HPLC) 103
5.2.9 Dynamic Vapour Sorption (DVS) 103

5.2.10 Computer Modelling 104

5.4 Results and Discussion 105

5.4.1 Thermal Behaviour of Milled ITZ 105

5.4.2 Comparison of Physicochemical Properties of Milled ITZ-SUC and Milled Physical Mixture of ITZ and SUC in a 2:1 Molar Ratio 109

5.4.3 Preparation of Solid Dispersions (SDs) of ITZ and SUC 115

5.4.4 Preparation of Solid Dispersions of ITZ and SUC with Eudragit L100-55 119

5.4.5 Dynamic Solubility Studies 122

5.5 Conclusions 129

Chapter 6: General Discussion and Conclusions 131

6.1 General Discussion and Conclusions 132

6.2 Main Findings 135

6.3 Future Directions 136

References 138

Summary

This thesis focuses on the poorly soluble triazole antifungal agent, itraconazole (ITZ). This compound was reported to form hydrochloride salts and cocrystals with a wide range of aliphatic dicarboxylic acids, which have shown some potential to enhance the solubility of ITZ. In addition, ITZ has the unusual ability to form liquid crystalline (LC) phases. Liquid crystalline materials have been utilised for decades in a wide range of non-pharmaceutical applications, however their applications have not been extensively recognised in the field of pharmaceutical materials.

The primary aim of this work was to produce and characterise a number of multicomponent systems containing ITZ and investigate their solubility behaviour. For this reason, it was necessary to examine the LC properties of ITZ and, for the first time, to generate full thermodynamic phase diagrams for ITZ/polymer systems considering isotropic and anisotropic (LC) phases that this drug can form. In addition, the two-component phase diagrams were constructed for the ITZ and succinic acid (SUC) system to investigate the possible solid-state (eutectic and cocrystal) phases for the binary mixtures of ITZ and SUC. Several binary (composed of ITZ and SUC) and ternary (composed of ITZ, SUC and methacrylic acid-ethyl acrylate copolymer (EUD)) systems were produced by ball milling to investigate if the addition of SUC and EUD to ITZ formulation could create a favourable pH-microenvironment and thus enhance the solubility of ITZ.

Studies of LC properties of ITZ suggested that supercooled ITZ forms a vitrified smectic (vSm) phase with a glass transition temperature (T_g) of 59.3°C, as evident from X-ray diffraction and thermomicroscopic (PLM) experiments. Two endothermic LC events with the onset temperature values for the smectic to the nematic transition of 73.2 ± 0.4 °C and nematic to isotropic transformation at 90.4±0.35 °C and enthalpies of transition of 416 ± 34 J/mol and 842 ± 10 J/mol, respectively, were recorded. For the binary supercooled mixtures, PLM and differential scanning calorimetry (DSC) showed that both, smectic and nematic phases were detected for the supercooled ITZ/hypromellose acetate succinate (HAS) and ITZ/EUD mixtures, while geometric restrictions inhibited the smectic formation in the ITZ/polyacrylic acid (CAR) systems. The Flory-Huggins lattice theory coupled with the Maier-Saupe-McMillan approach was successfully utilised to create phase diagrams for all ITZ/polymer mixtures. It was concluded that the presence of LC phase of ITZ in the ITZ/polymer system might lead to immiscibility of components in such systems.

The thermodynamic phase diagram of the binary mixtures of ITZ and SUC was determined experimentally, using DSC, and theoretically, using the Schroeder-van Laar and Prigogine-Defay equations. The constructed diagram was characteristic for a congruently melting system with the ability of cocrystal formation. It signified the cocrystal formation with a stoichiometry of 2:1 ITZ and SUC (ITZ-SUC). Three eutectic phases were also identified: metastable (m-E) at 132.8 ± 0.22 °C, a stable eutectic phase composed of ITZ-SUC and SUC (E_1) at 147.9 ± 0.08 °C, and a stable eutectic phase made by ITZ-SUC and ITZ (E_2) at 157.1 ± 0.28 °C. The composition of E_1 was determined from the Tamman plot as *x* (ITZ) = 0.31 and x (SUC) = 0.69. The composition of the E_2 phase was found to be very close to the ITZ-SUC composition and was *x* (ITZ) = 0.67 and x (SUC) = 0.33. The E_1 was successfully produced by a fast-evaporation crystallisation method, and its identity was confirmed by DSC and powder X-ray diffraction (PXRD) analyses.

Dynamic solubility studies of a number of binary and ternary ITZ milled (amorphous or semi-amorphous) systems were conducted in the simulated gastric fluid (SGF) and in the fasted state simulated intestinal fluid (FaSSIF) at 37 °C and ITZ concentrations were determined using High-Performance Liquid Chromatography (HPLC). It was found that ITZ-SUC was able to extend, up to 30 minutes, supersaturation levels that were ~7.7-fold and ~330-fold higher than ITZ thermodynamic solubility, in SGF and FaSSIF, respectively. Solid dispersions with higher SUC and EUD content significantly enhanced the solubility of ITZ in FaSSIF. Incorporation of 20% or 40% of EUD into a system composed of ITZ and SUC in a 1:2 molar ratio resulted in supersaturation levels that were ~400 and ~2,500-fold higher than that of crystalline ITZ, respectively.

Acknowledgements

Firstly, I would like to express my sincere gratitude to my supervisor, Dr Lidia Tajber, for all her support and guidance during my PhD studies and for giving me the opportunity to be a part of her research group.

I also wish to thank the past and current members of my lab, as well as the other researchers in the Panoz Institute, for all their help and friendship over the years. In particular Hanah, Kate, Svenja, David, Kieran, Alan, Ricardo, Jeremiah, Emer, Zelalem and Mah. Also, a massive thank you to Peter for his time, help and invaluable advice. I am also thankful to the technical staff in the School of Pharmacy, Trevor, Brian and Ray, for their time and assistance. And a very special thank you to Rhona and Irene for all their support.

This research project would not have been possible without the funding provided by Science Foundation Ireland, under the Synthesis and Solid State Pharmaceutical Centre (SSPC) for which I am very thankful.

And finally, I would like to thank my family for their constant moral support and encouragement. In particular my mum Boguslawa, who spent so much time away from home to help look after my daughter. A special thank you to my partner David for all his motivation and understanding, and without whose support I would not have completed this PhD. Thank you to my beautiful daughter Emilia. You being you fills me with so much love and the resolve to keep going, even when I feel that I can't.

Publications and Presentations

Publications Associated with the Thesis:

- M. M. Knopp, L. Tajber, Y. Tian, N. E. Olesen, D. S. Jones, A. Kozyra, K. Löbmann, K. Paluch, C. M. Brennan, R. Holm, A. M. Healy, G. P. Andrews, and T. Rades, "Comparative study of different methods for the prediction of drug-polymer solubility," *Mol. Pharm.*, 2015, 12, 3408–3419

- A. Kozyra, N. A. Mugheirbi, K. J. Paluch, G. Garbacz, and L. Tajber, "Phase Diagrams of Polymer-Dispersed Liquid Crystal Systems of Itraconazole/Component Immiscibility Induced by Molecular Anisotropy," *Mol. Pharm*., 2018, 15, 5192–5206

- A. Kozyra, K. Paluch, L. Tajber "Phase diagrams and thermodynamic properties of binary systems made of itraconazole and succinic acid," In preparation.

- A. Kozyra, K. Paluch, L. Tajber "Characterisation and solubility behaviour of itraconazole solid dispersion systems," In preparation.

Other Publications:

- K. Wlodarski, W. Sawicki, A. Kozyra, and L. Tajber, "Physical stability of solid dispersions with respect to thermodynamic solubility of tadalafil in PVP-VA," *Eur. J. Pharm. Biopharm.*, 2015, 96, 237–246.

Poster Presentations:

- A. Kozyra, L. Tajber "Characterisation of itraconazole polymer mixtures" 38th All Ireland Schools of Pharmacy Conference, RCSI, Dublin, Ireland. 2016, Mar 21-22.
- A. Kozyra, L. Tajber "Studies of Phase Transitions in Itraconazole and Itraconazole/polymer mixtures" SFI 2 year review of SSPC, University of Limerick, Ireland. 2015, Dec 10.
- A. Kozyra, K. Paluch, L. Tajber "Application of theoretical and practical approaches in the prediction of itraconazole-polymer miscibility for the design of solid dispersions" AAPS Annual Meeting and Exposition, Orlando, FL, USA, 2015, Oct 25-29; M1225
- A. Kozyra, D. Colgan, K. Paluch, L. Tajber "Ionic liquids of lidocaine with dicarboxylic acids" 9th PBP World Meeting, Lisbon, Portugal, 2014, Mar 31-Apr 3

List of Abbreviations and Symbol

2θ	2 theta (diffraction angle)
ΔH_m	heat of fusion
^exo	exothermic direction
Ø	volume fraction
χ	interaction parameter
API	active pharmaceutical ingredient
BCS	biopharmaceutics classification system
CAP	chloramphenicol
CAR	polyacrylic acid (Carbopol 981)
CCDC	Cambridge Crystallographic Data Centre
CCX	celecoxib
C_{max}	maximum concentration
CSD	Cambridge Structural Database
d	true density
dm/dt	change in mass per unit time
DSC	differential scanning calorimetry
DVS	dynamic vapor sorption
E_1	eutectic phase formed between ITZ-SUC and SUC
E_2	eutectic phase formed between ITZ-SUC and ITZ
EUD	Methacrylic acid - ethyl acrylate copolymer (Eudragit L100-55)
FaSSIF	fasted state simulated intestinal fluid
FDP	felodipine
F-H	Florry-Huggins
FT-IR	Fourier transform infrared spectroscopy

GIT	gastrointestinal tract
G-T	Gordon-Taylor
HAS	hypromellose acetate succinate (HPMCAS-MG)
HPLC	high-performance liquid chromatography
IMC	Indomethacin
ITZ	itraconazole
LC	liquid crystal
m-E	metastable eutectic phase
M_w	molecular weight
n	number of moles
PCM	paracetamol
pKa	negative base-10 logarithm of the acid dissociation constant
PLM	polarised light microscopy
PLM-HS	polarised light microscopy and hot stage
PXRD	powder X-ray diffraction
r	correlation coefficient
R	gas constant
rpm	revolutions per minute
RT	room temperature
SGF	simulated gastric fluid
SIF	simulated intestinal fluid
SD	solid dispersion
T_m	melting temperature
T_g	glass transition temperature
TGA	thermogravimetric analysis

Chapter 1: General Introduction

1.1 The Oral Route of Administration

The oral route of administration is the most preferred method for delivery of drug products, as it offers good patient compliance due to its acceptability, convenience and ease of use Examples of oral medication include tablets and capsules. Also, the overall production cost of oral formulations is less as oral formulations do not require sterile manufacturing environment. However, the oral route may not be suitable for all drugs. The fundamental parameters for effective delivery of oral formulations are aqueous solubility, dissolution rate and ability of drug molecule to permeate the gastrointestinal tract (GIT) membrane.[1]

Over the last decade, the drug discovery process has changed dramatically. The development of technologies such as combinatorial chemistry and High Throughput Screening (HTS) have proven highly successful in the discovery of new compounds with outstanding *in vitro* potency. However, they ignore issues of drug absorption and metabolism. Poor aqueous solubility is now recognised as a major issue during drug development process, as this characteristic is directly related to reduced bioavailability of oral formulations.[2][3]

1.1.1 The Biopharmaceutics Classification System (BCS)

The Biopharmaceutics Classification System (BCS) was first proposed by Amidon et al. in 1995.[4] This classification system is based on aqueous solubility and gastrointestinal permeability of drugs. Amidon recognised that major parameters controlling the rate and extent of drug absorption are the drug dissolution and gastrointestinal permeability. Therefore, the active pharmaceutical ingredients (APIs) are categorised as having either rapid or slow in vitro dissolution[5] and then classified based on their aqueous solubility and permeability into four groups as shown in Figure 1.1-1. Molecules with high solubility and high permeability belong to Class I BCS; drugs with low solubility and high permeability to Class II; high soluble and low permeable drugs to Class III and Class IV of molecules is characterised by low solubility and low permeability.[4]

A drug product is considered to have high solubility when the highest dose strength is soluble in 250 ml or less of aqueous media over the pH range of 1 - 6.8 at 37 ± 1 °C. The estimated volume of 250 ml is based on a typical bioavailability study protocols. These protocols prescribe administration of a drug to fasting human volunteers with an 8 fluid ounce (250 ml) glass of water. A highly permeable drug has an extent of absorption that is greater than 85% of the administered dose. Regarding dissolution, a drug is considered rapidly dissolving if more than 85% of the dose dissolves within 30 minutes, using United States Pharmacopeia (USP) Apparatus

1 or 2 in a volume of 500 mL or less (or 900 mL when appropriately justified) in the dissolution medias such as: (1) 0.1 N HCl or Simulated Gastric Fluid USP without enzymes; (2) a pH 4.5 buffer; and (3) a pH 6.8 buffer or Simulated Intestinal Fluid USP without enzymes.[6]

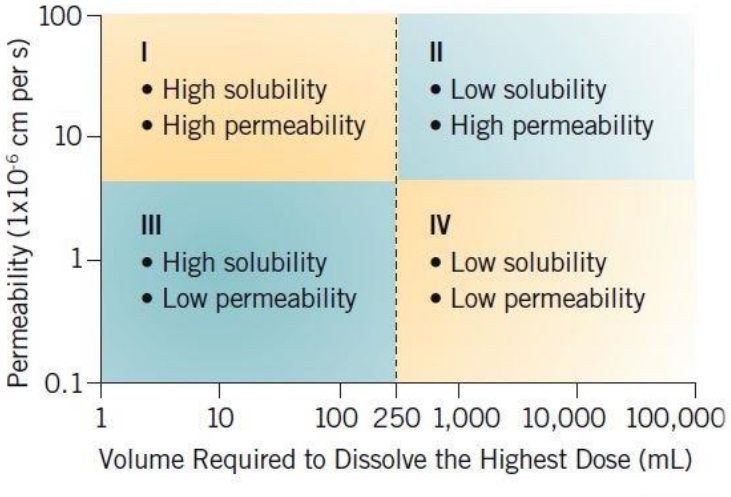

Figure 1.1-1 The Biopharmaceutics Classification System. Reproduced from[7]

1.1.2 Solubility, Dissolution and Dissolution Rate

Solubility and dissolution are related to each other. However, there is a difference between them.

Solubility is the maximum amount of a solute that the pure solvent can hold in solution, under certain conditions, such as temperature and pH. Solubility is a thermodynamically driven process. It is possible to exceed the saturation level of a solute in the solution and create a supersaturation.[8] It can be done by manipulation of certain conditions such as temperature, pH, volume, or formulation. The supersaturation can improve intestinal absorption of drugs by generation and prolonging supersaturation state. This process has been described by Guzmán et al. [9] as a “spring” and “parachute”, as shown in Figure 1.1-2.The supersaturated solutions are considered thermodynamically unstable, they can be generated starting from a higher energy form of the API (as compared to its crystalline form), that is the ‘‘spring’’. This could be achieved by formulation, including use of amorphous materials, crystalline salt forms, higher energy polymorphic forms or the delivery of drugs in solution, for example co-solvent systems, and lipid-based formulations.[9] Once supersaturation has been generated, the excess of the solute (drug molecules) will precipitate out of solution reaching the equilibrium solubility.[10] Therefore, to benefit from the supersaturated state, pharmaceutical excipients that interfere

with nucleation and/or crystal growth, may be required to extend the duration of supersaturation state, that is the ‘‘parachutes’’.[9]

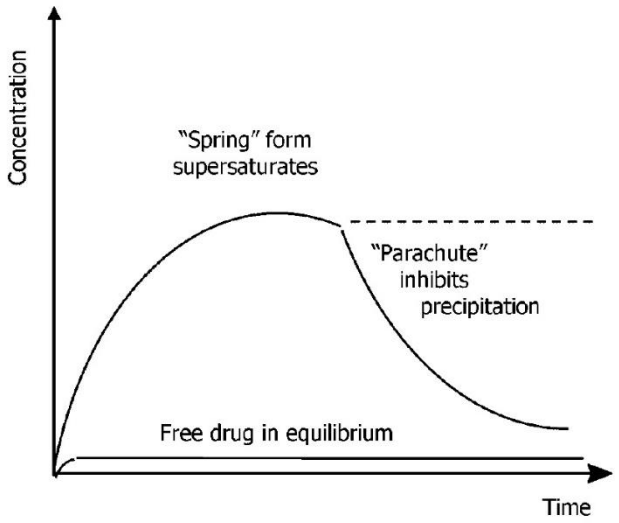

Figure 1.1-2 Schematic drug concentration versus time profiles illustrating the “spring” and “parachute” approach to promote and maintain supersaturation of drug in solution. Reproduced from[9]

Dissolution is the process during which a solute is disaggregating and dispersing in a solvent to form a solution. It is a kinetic process expressed by dissolution rate.[8][10] Dissolution rate represents the speed of solution formation. It tells us how long it takes to reach a certain API concentration. It is possible for a drug to have a poor solubility but fast dissolution rate. It is also possible that some very soluble drugs will take an inordinate amount of time to reach the desired concentration.[8]

The original dissolution model was developed in 1897 by Noyes and Whitney[11]. Their work was later modified by Nernst and Brunner.[12], [13] The modified Noyes–Whitney equation (Equation 1.1-1), shown below, describes how different factors can influence a dissolution rate of a compound.[14]

$$DR = \frac{A\ x\ D}{h}\left(C_s - \frac{X_d}{V}\right) \qquad \text{(Equation 1.1-1)}$$

Where DR is the dissolution rate, A is the surface area of the drug available for dissolution, D is the diffusion coefficient of the drug, h is the thickness of the boundary layer adjacent to the dissolving drug surface, Cs is the saturation solubility of the drug, X_d is the amount of dissolved drug and V is the volume of dissolution media.

If the solvent volume is very large, or the solute (drug) is removed from the solvent faster than it dissolves, then the amount of dissolved drug is approximately zero. Therefore, the second part of the Noyes-Whitney equation simplifies to Cs. Under these circumstances the dissolution is said to occur under "sink" conditions. This can occur *in vivo* when a drug is absorbed into the body faster than it dissolves.[15]The parameters D and h, in Equation 1.1-1, are difficult to improve. These parameters are directly related to the molecule properties and conditions of the human gastrointestinal tract (GIT). The diffusion coefficient is affected by the viscosity of the dissolution medium, solution temperature and size of the diffusing drug molecules.[8] As the temperature *in vivo* is constant, the viscosity of the gastrointestinal fluids could be influenced by food or fluid intake.[14] The thickness of the diffusion layer (h), through which the drug particles pass, on their way to the bulk solution can be decreased *in vitro*, simply by stirring in a beaker, however not possible to achieve *in vivo*.[8] In contrast, both surface area and solubility can be manipulated by formulation.[14]

1.1.3 Strategies to Improve Solubility and Dissolution Rate of Drugs

Several techniques can be adapted to enhance solubility or dissolution rate of hydrophobic drugs. These techniques include particle size reduction (micronisation and nanoparticles), amorphisation, solid dispersions, crystal modification (metastable polymorphs, cocrystals, and salts), use of cyclodextrins, co-solvents, surfactants, and pH modification. Techniques such as amorphisation, solid dispersions, crystal modification are discussed in Sections 1.2 and 1.3.

Particle size reduction of an API increases the surface area available for interaction with solvent. Micronisation and nanosizing techniques have been demonstrated to result in significant improvement of dissolution rate[16], and several pharmaceutical nanocrystal products entered a marked in the recent years.[17] However, not all drugs may have physicochemical properties suitable for effective particle size reduction and can be susceptible to polymorphic transition during manufacture or storage. Also, nanoparticles are highly cohesive, and stabilising agents must be added to prevent aggregation.[16], [18]

1.2 Pharmaceutical Solids

Solid drugs can exist in different solid state forms, including crystalline, liquid crystalline or amorphous form (Figure 1.2-1). Crystalline solids are characterised by the presence of three-dimensional long-range order. In contrast, amorphous solids lack long-range order but can have short-range order.[19] Liquid crystalline solids are referred to as "mesophases" with the intermediate molecular order.[20] Such differences in the molecular arrangement are expressed

by unique physiochemical properties of each form. Consequently, each form can profoundly influence solubility, bioavailability, stability, manufacturability and other performance characteristics of the formulated API.[21]

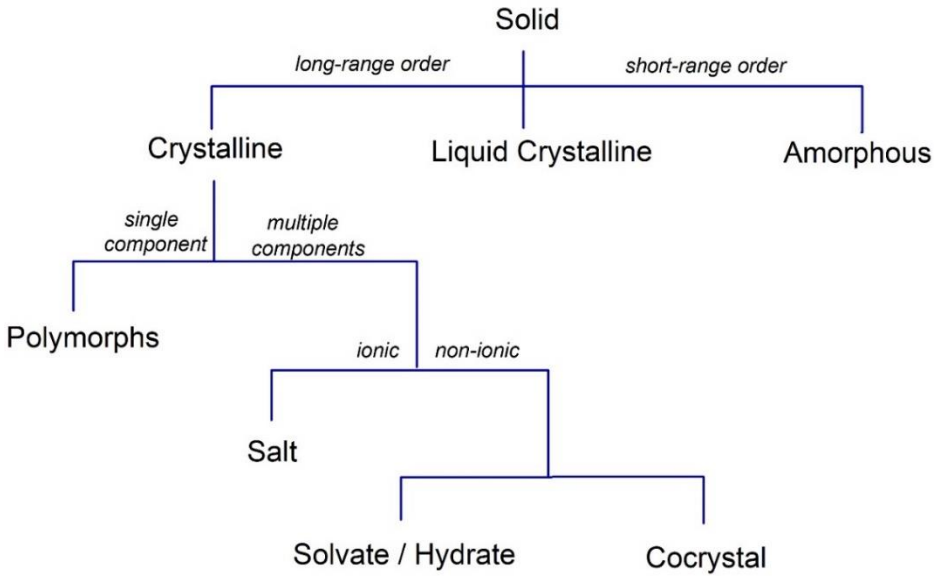

Figure 1.2-1 Classification of pharmaceutical solids.

1.2.1 Crystalline Solids

When a crystalline API has a poor physicochemical property, such as solubility, dissolution rate, stability, or hygroscopicity, drug developers often look for alternative solid forms. These include salts, polymorphs, hydrates/solvates, and cocrystals, as illustrated in Figure 1.2-2. [22]

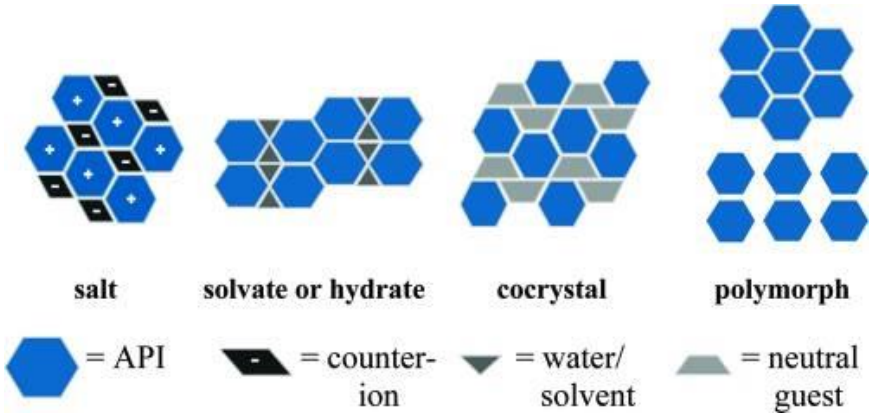

Figure 1.2-2 Common solid-state strategies to alter the chemical and physical solid-state properties of APIs. Reproduced from[22]

Majority of marketed drugs are present in crystalline forms, which often can transform into different polymorphic forms. Polymorphism is the ability of a solid crystalline material to exist in two or more crystalline phases that have different arrangements of molecules in the crystal lattice.[23] Therefore they have different physical and chemical properties. Developing a polymorphic form may seem like a promising route to enhance solubility and bioavailability of drugs. However, metastable polymorphs only show a slight solubility improvement and stability is a major concern. Metastable polymorphs tend to convert to thermodynamically stable form impacting shelf-life and drug performance[24], which was the reason to withdraw the drug ritonavir from the market until a new formulation was developed.[25]

Hydrates and solvates, also known as pseudo-polymorphic forms, are crystalline solids that contain water or solvents molecules within the crystal lattice.[23] Though some of the existing APIs can be developed as hydrates or solvates, they are not often regarded as preferred solids. Poor thermal stability and potential toxicity concerns eliminate most of these formulations from human therapeutics.[24], [26], [27] Pudipeddi and Serajuddin[28] have studied the solubility ratios of anhydrate/hydrate pairs compiled from literature. The results of their study indicated that for pharmaceutical compounds, anhydrous forms are usually two times more soluble than hydrates. However, a significantly higher solubility ratio was observed for some compounds, for example, succinyl sulfathiazole (13 fold) and niclosamide (23 fold).[28]

A pharmaceutical salt is formed when a basic or acidic drug molecule reacts with acidic/basic salt former (counter-ion), as shown in Figure 1.2-2. Currently, salt formation is the most common approach used to modify physical properties of APIs. It is estimated that over 50% of the marketed drugs are formulated as salts.[29]–[31] However, a major setback with the salt formation is that the approach is limited to the APIs, which have a suitable (basic or acidic) ionisable site for proton transfer. The success of forming a stable salt form is believed, to depend mainly on the pKa values of the components. A difference in the pKa values by ≥3 units is expected to favour salt formation.[32], [33] For example, potassium salts of ampicillin showed higher dissolution rates compared with the free ampicillin trihydrate.[29] Celecoxib salts (e.g., sodium and sodium propylene glycol salts) resulted in increased bioavailability when compared to the pure API.[9] The oxalate and acesulfame salts of salinazid shown superior solubility improvement of 33 and 18 times, respectively, compared to pure drug.[34]

Over the past two decades, cocrystals gained much attention as a promising alternative to modify physicochemical properties of drugs and consequently improve their solubility. Cocrystal can be defined as a crystalline complex of two or more different components in a stoichiometric

ratio, which are solids at ambient conditions. These components are held together in the same crystal lattice by non-covalent bonds such as hydrogen bonds.[35]–[38] A pharmaceutical cocrystal is composed of an API and an appropriate coformer, that should be non-toxic and approved for human consumption.[39] For example pharmaceutical excipients and compounds approved by FDA may have the status "generally recognised as safe" (GRAS) and thus deemed as appropriate for internal administration.[35], [36] Cocrystal design is based on the Desiraju's "supramolecular synthon" approach[40] and Etter's hydrogen-bonding "rules".[41] The term "synthons" was first introduced by Corey as "structural units within molecules which can be formed and/or assembled by known or conceivable synthetic operations".[40] Desiraju further utilised this concept to introduce "supramolecular synthons", defined as "structural units within supermolecules which can be formed and/or assembled by known or conceivable intermolecular interactions".[40] Supramolecular synthons are further classified into two classes. One class that involves the same functional groups is called supramolecular homosynthon. The other class involves different but complementary functional groups and is defined as supramolecular heterosynthon.[42] It is suggested that analysis of crystal structures deposited in the Cambridge Structural Database (CSD) should be the first step in cocrystal design experiment.[35] Once the prospective coformers are selected, various approaches to cocrystal synthesis are possible. The most common techniques include solution crystallisation, mechanical grinding and melt crystallisation.[36] Acetaminophen/theophylline is an example of pharmaceutical cocrystal, which showed increased bioavailability and efficacy than separate administration of these two drugs.[43] The meloxicam-aspirin cocrystal decreased the time needed to reach the human therapeutic concentration compared with the drug on its own.[44] Remenar et al.[45] reported improved solubility of itraconazole by formulating it into cocrystals with succinic acid, L-malic acid, and L-tartaric acid.

1.2.2 Amorphous Solids

Amorphous solids lack long-range order, however, at the molecular level, they may possess some short-range order.[19][46] The highly disordered molecular arrangement of amorphous materials also results in a greater specific volume and higher free energy, enthalpy and entropy than the corresponding crystalline state.[19][47] These properties may lead to enhanced dissolution and bioavailability of amorphous APIs. However, this can also create a risk of spontaneous conversion of amorphous materials back to the crystalline state during processing or storage.[46] To delay the crystallisation process of amorphous drugs, and to further enhance their solubility, various amorphous formulations containing one or more stabilisers have been developed. These formulations, known as glass solutions are briefly discussed in Section 1.3.

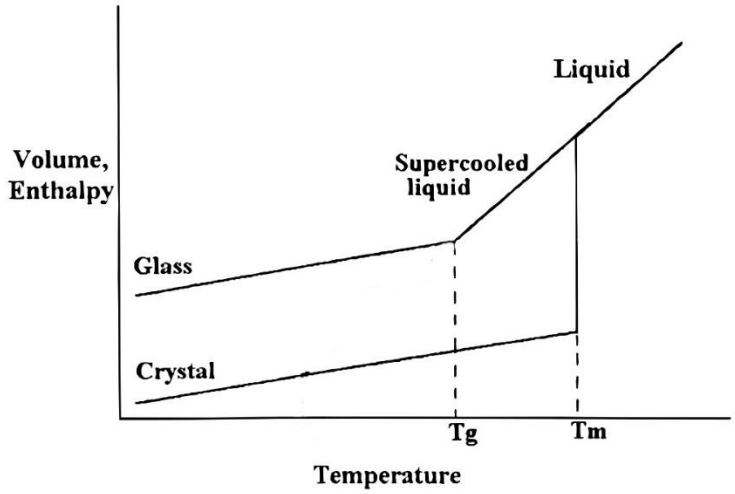

Figure 1.2-3 Thermodynamic relationship of crystalline and amorphous (glassy) state as a function of temperature. Where T_g represents the glass transition temperature and Tm represents the melting temperature. Reproduced from[46]

Figure 1.2-3 shows a schematic plot of enthalpy or volume versus temperature for crystalline and amorphous (glassy) system.[46] One can see that when a crystalline drug is heated up, the increase in enthalpy or volume is small with respect to temperature. When the temperature reaches the melting point (Tm), there is a discontinuity in both the enthalpy and volume, representing the first order phase transition of solid to liquid. When a liquid is cooled, it usually crystallises below the Tm. However, when the molten drug is cooled rapidly, the liquid state may persist leading to the formation of a supercooled liquid. Further, on cooling, a change in slope is seen at the experimentally observed temperature, known as the glass transition temperature (T_g). Below T_g, the molecular mobility of material is reduced, and the material is "kinetically frozen" in a thermodynamically unstable glassy state.[46] Therefore, amorphous materials are more likely to crystallise at temperatures above their T_g, as the increased molecular mobility facilitates nucleation and crystallisation. Although, some materials may possess sufficient molecular mobility to support crystallisation below the T_g.[48] The molecular mobility, at a temperature of 50K or more, below the T_g is considered negligible.[49][50] Therefore, an amorphous material stored at a temperature of T_g-50 °C, should remain stable for years at a time, without crystallisation.[46]

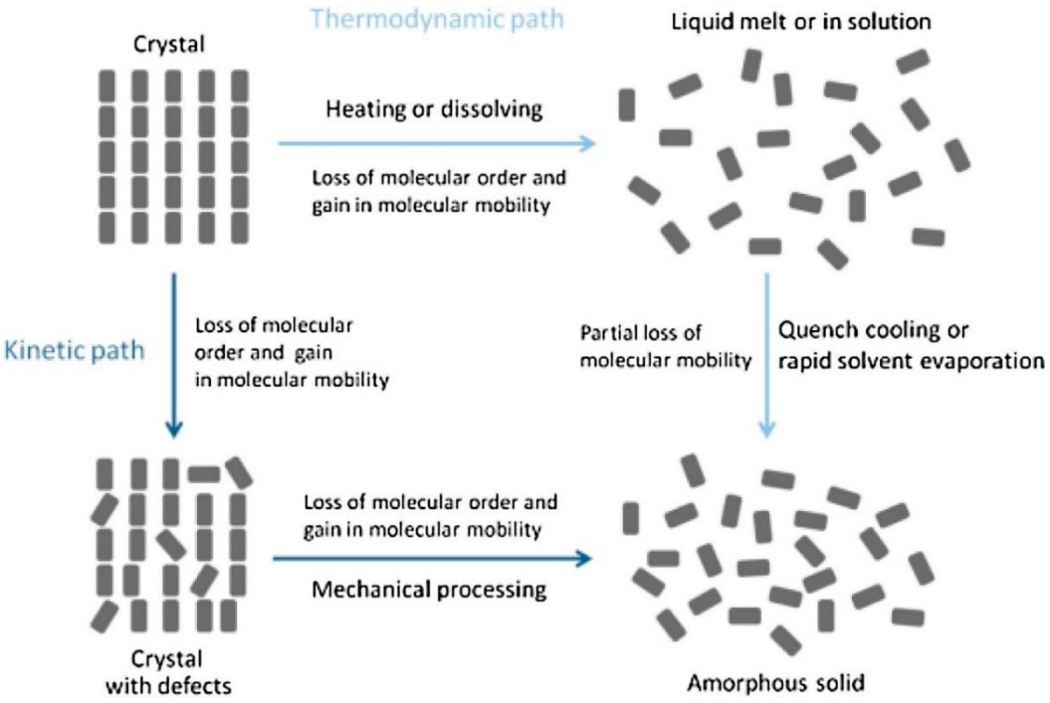

Figure 1.2-4 Amorphisation of crystalline material through thermodynamic and kinetic pathways. Reproduced from[51]

The most common techniques of preparation of amorphous solids follow the thermodynamic pathway or the kinetic pathway, as illustrated in Figure 1.2-4. On the thermodynamic pathway, the crystalline material is converted into a thermodynamically stable, non-crystalline, disordered form (melt or solution). Quench cooling, or rapid solvent evaporation is then introduced to "trap" the material in amorphous form. When following the kinetic pathway, the thermodynamically stable crystalline state is converted to an amorphous form by mechanical activation such as milling. During milling, an amount of crystal defect increases until the amorphous form is obtained.[51]

Amorphous materials prepared via thermodynamic or kinetic pathways may exhibit different properties. Salvonien et al.[52] reported that the cryo-milled simvastatin showed decreased physical stability in relation to amorphous simvastatin prepared by melt quenching. Karmwar et al.[53] found that the cryo-milled amorphous form of indomethacin was physically less stable than amorphous forms prepared by melt-quench and spray drying methods. Blaabjerg et al.[51] investigated the preparation method, the thermodynamic path versus kinetic path, on stability of amorphous itraconazole and celecoxib. They reported that both drugs when amorphised using melt quench method were more stable than the ball milled samples. It was also mentioned that stability of amorphous samples was dependant on the degree of disorder and the

preparation technique. Most likely, the amorphous materials prepared by ball milling may still contain a large number of nuclei. These nuclei will subsequently act as seeds and induce crystallisation. In contrast, the melt-quenched samples may have a very low number of nuclei, which consequently gives them better stability.[51] Furthermore, amorphous materials prepared by different techniques will have different molecular arrangements, which can be detected using terahertz spectroscopy or solid state NMR methods.[54], [55]

1.2.3 Liquid Crystalline

Liquid crystals (LCs) can be defined as a state of matter in which the degree of molecular order is between that of a crystalline solid and an isotropic material. [56] Therefore LCs, or mesophases, are also referred to as the fourth state of matter, as they possess mechanical, optical and structural properties between that of a three dimensionally ordered solid crystal and a completely disordered liquid or amorphous solid. [57], [58] LC materials can be divided into two broad categories: thermotropic LCs and lyotropic LCs. Thermotropic mesophases are formed by heating a crystalline solid or by heating or cooling a mesogen.[58] When a mesophase appears on both heating and cooling it is termed enantiotropic. The mesophase that appears only on cooling of a material below its melting point or heating a solid is termed monotropic. On the other hand, lyotropic LCs are formed by dissolving an amphiphilic mesogen in a suitable solvent.[59], [60]

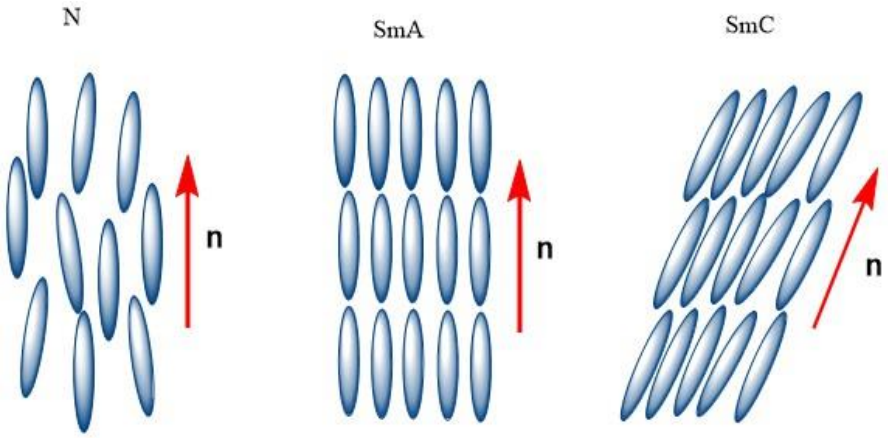

Figure 1.2-5 Orientation of rodlike molecules in the nematic phase (N), the smectic A phase (SmA) and in the smectic C phase (SmC), where n is the director.

Based on the orientation of LC molecules one can distinguish different phases. Possibly the most studied ones are nematic (N), smectic A (SmA) and smectic C (SmC) mesophases (Figure 1.2-5).

The nematic phase (N) is the least ordered phase. For rod-like molecules, the long molecular axes of individual molecules are preferably oriented in one direction and defined as the director *n* (Figure 1.2-5). In the SmA phases, the molecules are parallel to one another. They are arrayed in layers, with the long axes of the molecules perpendicular to the layer plane. In the smectic C (SmC) molecular arrangement is also layered. However, the long axes are tilted to the layers planes.[61], [62]

A mini-review of pharmaceutical LC mesophases was published by Stevenson et al.[20] Authors reviewed a number of low and large molecular weight APIs including fenoprofen, itraconazole, nafcillin, methotrexate, cromolyn, folic acid, tobramycin, leuprolide, cyclosporine and calcitonin. All of the above pharmaceutical compounds showed the ability to form LC mesophases. It was highlighted that pharmaceutical research should be expanded above the crystalline or amorphous states and investigate the existence of the LC state. Although the LC phases had been characterised for some drugs, still much exploration is needed. Formulations that include LC phases may be a promising route to improve the stability of a formulation, as well as to enhance solubility and bioavailability of APIs.

1.3 Classification of Solid Dispersions

The term “solid dispersions” (SD) was introduced by Chiou and Riegelmann in relation to “the dispersion of one or more active ingredients in an inert carrier or matrix at solid state prepared by the melting (fusion), solvent, or melting-solvent method”.[63] Based on the possible physical state, SD were classified into six groups: simple eutectic mixtures, solid solutions, glass solutions and glass suspensions, amorphous precipitations in a crystalline carrier, compound or complex formation and combinations of the previous five types.[63] Table 1.3-1 shows classification of SD according to their number of solid-state phases and the physical state of these phases.[64]

Table 1.3-1 Classification of solid dispersions. Letters C and A, in the column Physical state of phase(s), represent crystalline and amorphous phase, respectively. Reproduced from [64].

Solid dispersion	Number of phases	Physical state of phase(s)
Eutectic mixture	2	C/C
Solid solution	1	C
Glass solution	1	A
Glass suspension	2	A/A or A/C

1.3.1 Eutectic Mixtures

A simple eutectic mixture is made up of two components that are miscible in the liquid state, however immiscible in the solid state. When the mixture of components A and B at eutectic composition E is cooled down, both components crystallise out simultaneously. For any other compositions, one of the components will separate out before the other.[65] Thermodynamically, the eutectic system is regarded as a fully blended physical mixture of its two crystalline components.[63] A thermodynamic diagram of a simple eutectic system is shown in Figure 1.3-1. The solubility enhancement shown by eutectic mixtures may be related to very fine crystalline form, to each components A and B crystallise out. A reduction of particle size of a drug increases a surface area and consequently may increase the dissolution rate and bioavailability of poorly soluble drugs. Solubility improvement in the case of a eutectic mixture may also be related to solubilisation of the drug by the carrier, improved wettability because of the presence of the carrier, and hindrance of agglomeration and aggregation of the drug particles.[63] For example a 1:1 eutectic mixture formed between two anti-tubercular drugs pyrazinamide and isoniazid, showed significantly improved dissolution rate compare to pure pyrazinamide.[66] Dissolution rate improvement was also reported for fenofibrate-PEG [67] and for fenofibrate-acetylsalicylic acid [68] eutectic systems.

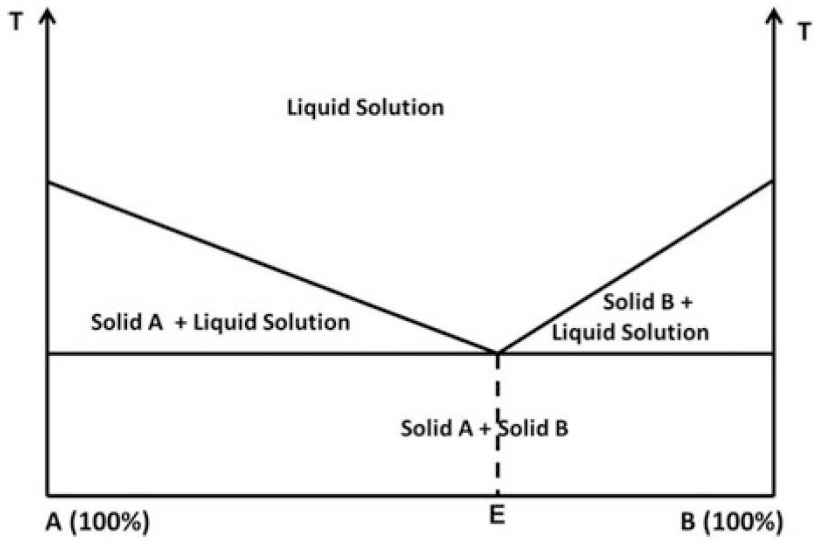

Figure 1.3-1 Phase diagram of a simple eutectic system. Reproduced from[69].

1.3.2 Solid Solutions

Solid solutions are comparable to liquid solutions as they are composed of a solid solute dissolved in a solid solvent. They are also called a mixed crystal, because the two components crystallise together to form a homogeneous one-phase system.[63]

Solid solutions can be classified according to two methods. Based on the solubility of the solute in the crystal lattice, one can recognise continuous and discontinuous solid solutions. In relation to the distribution of the solute molecules, there are substitutional and interstitial solid solutions.[69]

In a continuous solid solutions system, the components are miscible in all proportions. Theoretically, this can occur when the strength of the bonds between the two components (A-B) is stronger than the bond between molecules of each of the individual components (A-A or B-B). However, this type of solid solution has not been reported in the pharmaceutical field.[65]

In contrast, in the discontinuous solid solutions, the solubility of one of the components in the other component is limited. Figure 1.3-2 shows a typical phase diagram of a discontinuous solid solution. The solid solution regions are shown as α and β, where each component is capable of completely dissolving the other component. The solubilisation capability of the components is temperature dependent. As the temperature is lowered, the solid solution regions become narrower.[63], [65], [69]

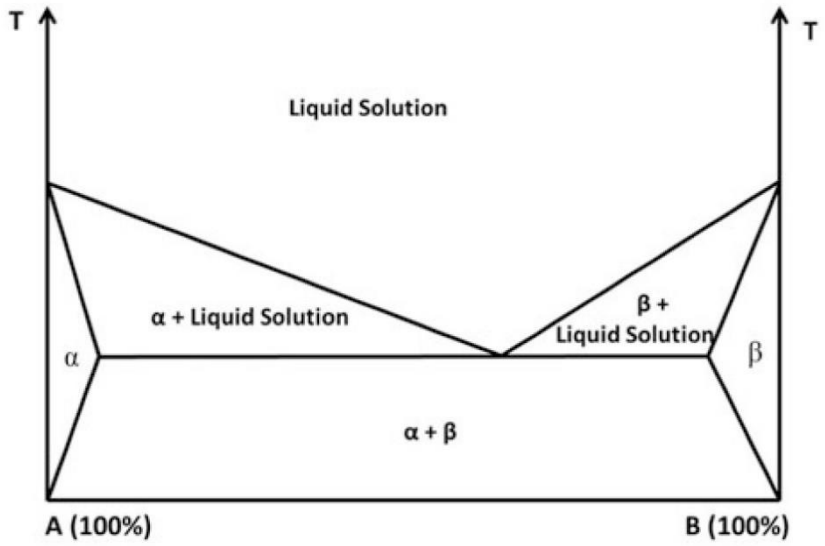

Figure 1.3-2 Phase diagram of a discontinuous solid solution. Reproduced from[69].

Substitutional and interstitial crystalline solid solutions are shown in Figure 1.3-3. In the case of a substitutional solid solution, a solute molecule can be substituted by a solvent molecule in the crystal lattice, as illustrated in Figure 1.3-3 a. However, this is only possible when the size of the solute and solvent molecules are very similar and differs by less than 15% from each other.[63][65] When the solute molecules are much smaller than the solvent molecules, they may be able to occupy the interstitial spaces in the crystalline lattice, as shown in Figure 1.3-3 b. This interstitial crystalline solid solutions can be formed only if case when the diameter of the solute molecules does not exceed 0.59 times the diameter of the solvent. [63][65]

Goldberg et al. reported formation of solid solutions for acetaminophen−urea[70], griseofulvin−succinic acid[71], and chloramphenicol−urea systems[72]. They reported, that these systems showed higher dissolution rate than the pure drugs. Mishra et al.[73] observed that omeprazole crystallises as a tautomeric solid solution. They reported that tautomeric composition affects hardness of the crystals. which may be relevant in manufacturing processes.

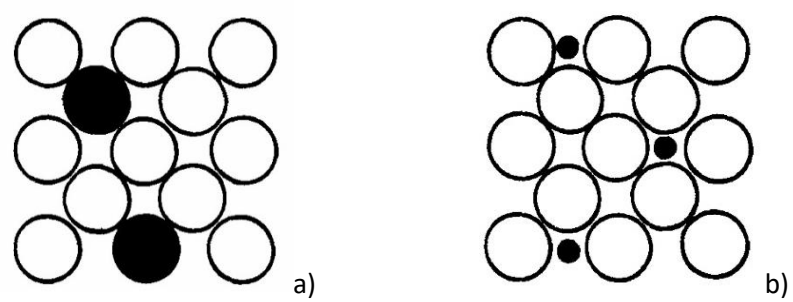

Figure 1.3-3 Substitutional crystalline solid solution (a) and interstitial crystalline solid solution (b). Reproduced from[63].

1.3.3 Glass Solutions

A glass solution is a homogeneous, miscible mixture of two or more compounds that forms a single amorphous phase. Often, it is referred to as an amorphous solid dispersion (ASD). [69][64] The glass solutions can be further divided based on the excipients that stabilise the amorphous drug, as shown in Figure 1.3-4. Based on this classification, there are two groups, polymer-based glass solutions, also referred to as polymeric amorphous solid dispersion and non-polymeric excipients glass solutions. The second group, non-polymeric excipients, can be subdivided into mesoporous silica-based glass solutions and co-amorphous formulations, containing only low molecular weight components.[64]

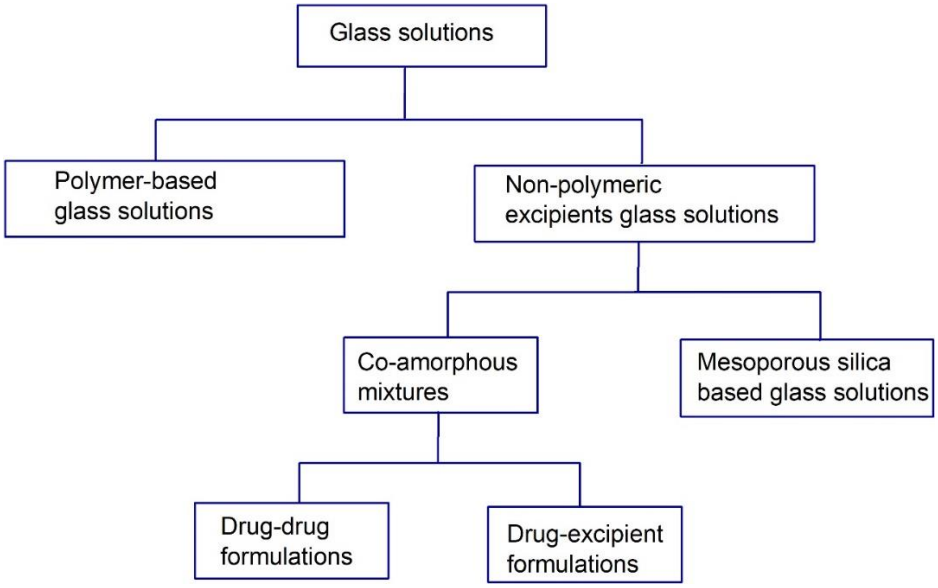

Figure 1.3-4 Classification of glass solutions based on the choice of the stabilising excipient.

Polymer-based glass solutions are perhaps the most investigated group of amorphous formulations. The stabilisation of amorphous API, in the presence of a polymer, can be achieved via different mechanisms. Polymers can stabilise amorphous drug by antiplasticization, which is defined as a reduction of plasticity and hardening of a material, leading to an increase in T_g of the compound and therefore an increase in the free energy required for crystallisation.[74] Intermolecular interactions between the drug and functional groups of the polymer such as hydrogen bonding, also have been found to play an important role in the stabilisation mechanism. These week intermolecular interactions reduce the molecular mobility of a drug in the polymer matrix and increase the energy required for crystallisation. [74][75][76][77] Examples of commercially available polymeric glass solution include: Sporanox® (itraconazole/HPMC and PEG)[78], Cesamet® (nabilone/PVP)[79], and Prograf® (tacrolimus/HPMC)[80]

In mesoporous silica-based glass solutions, amorphous drugs are stabilised via molecular interactions between the API and the functional groups of the silica matrix.[64] [81] Due to the porous nature of silica (pore size of 2 – 50 nm), drug particles can also be confined and stabilised within the pores and crystallisation may be physically inhibited by the pore diameter of the silica matrix.[64], [81], [82]

The co-amorphous mixtures have been intensively investigated in the past few years as an alternative to polymeric ASD. The co-amorphous formulation is composed of two or more low molecular weight compounds that form a homogeneous amorphous single-phase system.[64]

The term “co-amorphous” was coined by Chieng et al. to differentiate glass solutions containing two small molecules from a polymer or mesoporous silica-based glass solutions.[83] Due to poor miscibility of the drug in a polymer carrier, a polymeric ASD usually requires a high concentration of a polymer to stabilise amorphous API. Therefore, depending on a drug dose, the final volume of a formulation may be too high to be used conveniently in a solid dosage form.[84] In contrast, the co-amorphous formulation approach can drastically reduce the amount of stabilising excipient (if used), this is achieved due to the low molecular weight of the co-amorphous co-former. [64] Two types of co-amorphous systems have been proposed so far. These include drug-drug, and drug–excipient combinations.[64][85] In the first type, two pharmacologically active drugs are amorphised together. They therapeutic use is combined, and they can stabilise each other in the amorphous form. Co-amorphous mixture of Indomethacin and naproxen showed increased dissolution rate of both drugs[86], and a long-lasting supersaturation was reported for both atorvastatin and glibenclamide.[87] In the second type of co-amorphous formulation, low molecular weight excipients such as amino acids can be used as co-former.[88], [89]

1.3.4 Glass Suspensions

Due to limited miscibility of an amorphous API in the amorphous carrier, phase separation can occur. In case when the drug forms a separate amorphous phase, the glass converts to a glass suspension. Because the separated drug phase is still in the present in the amorphous form, glass suspensions may show an increased dissolution rate compared to the crystalline form.[69] This type of solid dispersion is usually found when the drug load is high. For example, for PVP–diazepam system two T_g's were observed for drug loads above 35%w/w indicating phase separation and the presence of amorphous diazepam clusters, partially dispersed in the carrier at a molecular level.[90] However, the risk of crystallisation of the amorphous drug is also high due to a decrease in T_g. The T_g of the drug or drug-rich phase is usually lower than the T_g of the polymer or polymer-rich phase.[69] For example, it has been found that fenofibrate (T_g = -19.6 °C) incorporated in inulin, PVP or hydroxypropyl-b-cyclodextrin (HPbCD) at a drug load of 48% w/w was partially crystalline and partially amorphous.[91]

1.4 Miscibility

The term miscibility refers to the formation of a single phase amorphous system through liquid-liquid mixing where one liquid is an amorphous polymer, and the other liquid is an amorphous drug.[92] It can be assumed that when the two components (drug and polymer) are mixed homogeneously at the molecular level, they can form uniform composition. more resistant to

drug crystallisation than the amorphous drug alone.[93] Therefore, drug/polymer miscibility is important in the development of glass solutions that maintain stability over prolonged shelf-life. Different methods, such as solubility parameter approach, Flory-Huggins theory, melting point depression, glass transition temperature and molecular modelling can be used as pre-formulation tools trying to predict drug and polymer miscibility.[74]

1.4.1 Glass Transition Temperature (T_g)

Glass transition temperature (T_g) can be used as an indicator of the physical stability of formulated glass solution. If the two components (drug and polymer) are fully miscible, a single T_g should be obtained. In contrast, if the compounds are not homogeneously mixed, phase separation may occur, and such system may display more than one T_g.[94] Polymers used to form glass solution usually have much higher T_g than that of the amorphous drug. Thus, for a miscible system, a single T_g should be obtained, in between the T_g of the pure drug and the polymer.[95] Accordingly, the miscibility of the system may be estimated by comparing the experimentally obtained T_g to a theoretical value.[96] To predict T_g of a mixture the Gordon-Taylor equation (Equation 1.4-1) is often used. This equation assumes additivity of free volumes of the individual components characteristic of ideal mixing. [97]

$$T_g = \frac{w_1 T_{g1} + k w_2 T_{g2}}{w_1 + k w_2} \qquad \text{(Equation 1.4-1)}$$

where T_g is the glass transition temperature, *w* is the weight fraction of the component, and *k* is a constant that can be calculated using true density (*d*) of the amorphous components as follows:

$$k = \frac{d_1 T_{g1}}{d_2 T_{g2}} \qquad \text{(Equation 1.4-2)}$$

If the experimentally determined T_g of a glass solution is very similar to that calculated by the Gordon-Taylor equation, it suggests that components mix ideally in the liquid and are fully miscible at the molecular level. In other words, it means that there are no specific interactions between the components. However, if the theoretical T_g values deviate from the experimental T_g, it may indicate that the components are not completely miscible. The positive deviation from the theoretical T_g value suggests that the interactions between unlike molecules (drug-polymer) are greater either in number or strength than the interactions between the individual components. In contrast, if the specific interactions, such as hydrogen bonding, between the two components is weaker than between the individual molecules, the observed T_g will be lower than predicted.[98]

1.4.2 Hansen Solubility Parameters

The miscibility and compatibility of the components of solid solution may also be estimated using Hansen solubility parameter approach. It was developed by Charles M. Hansen in 1967 [99] as an extension of the Hildebrand parameter, to estimate the miscibility of polar and hydrogen bonding systems. Hansen solubility parameters (Equation 1.4-3), divide the total solubility parameter (δ_t) into individual parts arising from different types of interactions present in a molecule, such as dispersive forces (δ_d), dipole-dipole interactions between polar groups (δ_p) and hydrogen bonding (δ_h).[100]

$$\delta_t = \sqrt{{\delta_d}^2 + {\delta_p}^2 + {\delta_h}^2} \qquad \text{(Equation 1.4-3)}$$

If the two components have similar Hansen solubility parameters (differing by < 7 $MPa^{1/2}$), they are expected to have a high affinity for each other and to form uniform, miscible system. However, if there is a difference of more than 10 $MPa^{1/2}$ between solubility parameters of the two compounds, they are likely to be immiscible.[101]Hansen's solubility parameters can be predicted using group contribution methods[102][103] or experimental technique, such as inverse gas chromatography (IGC). [103]

1.4.3 The Flory-Huggins Theory

The Flory-Huggins (F-H) lattice theory was initially developed for polymer-solvent binary systems and is an extension of the concept of regular solutions on polymer solutions.[104] Over the last decade, this theory has been applied to predict compatibility and miscibility of API/polymer systems.[105]–[111] The F-H theory is a mathematical approach based on the Gibbs free energy of mixing ΔG_m, which is related to enthalpic ΔH_m and entropic ΔS_m components through the relationship shown in Equation 1.4-5, where T is the temperature.

$$\Delta G_m = \Delta H_m - T\Delta S_m \qquad \text{(Equation 1.4-4)}$$

For the two components to be miscible at a given temperature, the total Gibbs free energy of mixing should be less than zero. As mixing always increases the disorder of the system, ΔS_m is a positive quantity, and this is particularly evident for low molecular weight materials, where the large entropic change that occurs on mixing provides the driving force to miscibility. For such systems, ΔG_m becomes more negative with increasing temperature, and this favours miscibility.[112]

According to the F-H theory, the entropy of mixing long-chain molecules, ΔS_m, can be calculated with the assumption that a polymer chain in the lattice can be divided into a number of segments.

Each segment is equal in size to a solvent molecule and each occupying single lattice sites.[113] Another important assumption is that no volume change takes place during mixing, while for real polymer blends and solutions, very small, but measurable volume changes on mixing are present.[113]

The following formula (Equation 1.4-5) defines the change in the free energy of mixing (ΔG_m):

$$\Delta G_m/RT = n_{drug} ln\phi_{drug} + n_{poly} ln\phi_{poly} + n_{drug}\phi_{poly}\chi \quad \text{(Equation 1.4-5)}$$

where R is the gas constant, n and ϕ are the number of moles and volume fractions of drug and polymer respectively, and χ is the Flory–Huggins interaction parameter between drug and polymer. The first two terms on the right-hand side in the Equation 1.4-5 represent combinatorial entropy contributions, and the last term describes the enthalpic contribution. Systems with polymers having a large molecular weight have a limited number of possible configurations within the lattice. Therefore, the entropy of mixing is very small, although always positive. Consequently, the miscibility or immiscibility of such systems depends mainly on the value of the enthalpic part of the Equation 1.4-5, which can be either positive (opposing mixing) or negative (promoting mixing), depending on the sign of the interaction parameter χ.[113] At its simplest, χ characterises the difference of interaction energies in the mixture. Therefore, two situations are possible. One, if there is a net attraction between molecules (i.e. they like each other more than themselves), $\chi < 0$ and a single-phase mixture should be favourable for all compositions. In the other scenario, there is a net repulsion between molecules (i.e. they like themselves more than each other), $\chi > 0$, and the phase separation is most likely to occur in this case. To summarise, a necessary condition of miscibility is that ΔG_m is negative; therefore the χ has to be negative or slightly positive. [113]

1.5 Itraconazole

Itraconazole (ITZ) is an API from a group of triazole antifungal drugs used against various fungal species including Cryptococcus, Candida, Aspergillus, Blastomyces and Histoplasma capsulatum var. capsulatum.[114] ITZ is classified as a BCS II compound with extremely low aqueous solubility and poor dissolution rate. Its aqueous solubility is approximately 1 ng/ml at neutral pH and around 4 µg/ml at pH 1. [114], [115] ITZ has a melting point of approximately 170 °C and a reported glass transition temperature of 59 °C.[116] The chemical structure of ITZ is shown in Figure 1.5-1.

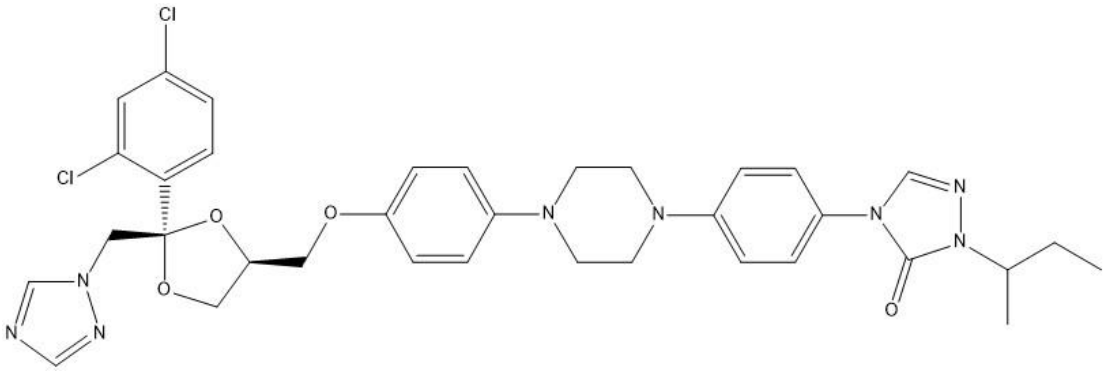

Figure 1.5-1 Chemical structure of Itraconazole (ITZ).

Two formulations of ITZ are commercially available under the trade name Sporanox® as capsules (FDA approved in 1992) and Sporanox® oral solution (FDA approved in 1997). Due to the low ITZ solubility, hydroxypropyl-β-cyclodextrin is used as a solubilising agent in the liquid formulations,[114] while a polymeric solid dispersion approach is employed in the formulation of the oral solid.[117]

The absorption of ITZ is facilitated by an acidic environment. It has been shown that administration of capsules in the fasted state or with neutralising agents such as antacids negatively affected the bioavailability of ITZ, while administration together with acidic beverages such as Coca-Cola has resulted in improved blood levels of ITZ. [118] The absorption of ITZ oral solution was reported to be better when taken without food.[119] Furthermore it was reported that under optimal conditions, the bioavailability of ITZ oral solution is approximately 60% higher than that of the capsules.[120] However, it should be noted that absorption mechanism and behaviour of ITZ formulations in the gastrointestinal tract (GIT) has not been fully elucidated.[121]

Due to the very unfavourable biopharmaceutical properties of ITZ, many studies in relation to manufacturing its polymeric SDs have been published. Sarode et al. prepared X-ray diffraction amorphous SDs of ITZ with hydrophilic polymers, including Eudragit EPO, Eudragit L-100-55, Eudragit L 100, HPMCAS-LF, HPMCAS-MF, Pharmacoat 603, and Kollidon VA-64.[122] The supersaturation levels of ITZ in non-sink conditions of simulated intestinal fluid (SIF) achieved with HPMCAS-LF, HPMCAS-MF, and Eudragit L 100-55 were respectively 22, 19, and 7- times higher than the equilibrium solubility of ITZ in SIF.[122] Enteric polymers, including cellulose acetate phthalate (CAP) and polyvinyl acetate phthalate (PVAP) were selected by DiNunzio et al.[123] to produce amorphous SDs by ultra-rapid freezing. ITZ-CAP formulations demonstrated a significant improvement in the supersaturation level of ITZ in neutral media. This was due to

the stabilising effect of the polymer and a 2-fold improvement in ITZ bioavailability in comparison to the currently marketed product (Sporanox®) was demonstrated.[123] Ternary amorphous SDs of ITZ in Eudragit L 100-55 containing either 20% or 40% Carbopol® 974P produced by hot melt extrusion were investigated by Miller et al.[124] The addition of 20% Carbopol® 974P very markedly extended the in vitro release of ITZ at 1 and 2 h after the acid-to-neutral pH change, respectively.[124]

Studies of cocrystal formation of ITZ with aliphatic dicarboxylic acids are described in Chapter 4.

Liquid crystalline properties of ITZ are addressed in Chapter 3.

1.6 Project Aims

The solubility of a drug is one of its most important physicochemical properties as it is directly related to bioavailability of drugs and thus effectiveness of drug product formulations.[2] The determination of drug solubility and, if necessary, ways of enhancing it, are important steps during any pharmaceutical development process.[2] Itraconazole (ITZ) was chosen as a model drug with very low solubility, and with a limited number of marketed, also generic, formulations.

The main aim of this work was to improve solubility of ITZ, concentrating on the solid state manipulation of the drug.

Therefore, the specific objectives of this thesis were to:

1. Compare different thermal analysis methods, based on the Flory-Huggins (F-H) theory, currently applied in research to search for a compatible drug-polymer combination (Chapter 2).
2. Investigate liquid crystalline (LC) properties of ITZ and construct full thermodynamic phase diagram based on F-H theory and the Maier-Saupe-McMillan theory, to include LC nature of ITZ (Chapter 3).
3. Study the mechanism of ITZ and succinic acid (SUC) cocrystal (ITZ-SUC) formation by constructing thermodynamic phase diagram (Chapter 4).
4. Determine if addition of an organic acid (SUC) and/or polymer (EUD) can create favourable microenvironmental pH to increase solubility of ITZ (Chapter 5).

Chapter 2: Comparative Study of Different Methods for the Prediction of Drug/Polymer Solubility

2.1 Introduction

The use of amorphous solid dispersions (ASDs) to enhance solubility and dissolution rates of poorly water soluble drugs has gained much interest in the pharmaceutical industry over the past decade.[74], [125], [126] However, a major drawback of this approach is the poor physical stability of such disordered systems. The high energy, entropy and free energy of amorphous drugs often result in fast crystallisation and leads to loss of solubility and dissolution rate advantages. [127], [128] [93] As mentioned in Chapter 1, in order to produce a physically stable formulation, the drug and the polymer need to be mixed homogeneously at the molecular level.[93] It means that the drug/polymer system will form a single phase amorphous system through liquid-liquid mixing where one liquid is an amorphous polymer, and the other liquid is an amorphous drug.[92] The drug concentration in the mixture with the polymer should be below its supersaturation in order to form a thermodynamically stable, homogenous solution, and to prevent crystallisation.[129] Therefore determination of the solubility and miscibility of the drug within the polymer matrix is required to generate stable amorphous formulations.

The first protocols which were developed to predict drug/polymer miscibility were based on the melting point depression of a drug in the presence of a polymer.[92], [130], [131] As mentioned in Chapter 1, if a drug and a polymer are miscible, the addition of an amorphous polymer to the crystalline drug may reduce the chemical potential of the crystalline material, consequently leading to melting point depression. According to the Flory-Huggins (F-H) theory, discussed in Chapter 1, it is possible to relate the extent of the melting point depression to the solubility of the crystalline drug in the polymer. This concept was exploited by Marsac et al.[92] to calculate the Flory-Huggins interaction parameters for nifedipine/PVP K12 and felodipine/PVP K12 systems. The authors prepared physical mixtures of known concentrations of drug and polymer by geometric mixing and analysed them by differential scanning calorimetry (DSC). The onset of melting of the bulk melting endotherm was taken, and it was reported that the melting point decreased linearly with increasing concentration of polymer in the physical mixture.[132] Zhao et al. [109] published a study on the prediction of the thermal phase diagram of indomethacin and PVP-VA amorphous solid dispersions by the Flory–Huggins theory. Zhao et al. [109] also suggested that the onset of the melting peak represents the sample property better by eliminating the impact of sample preparation. The authors reported that they had used a sufficiently slow heating rate to facilitate the complete mixing.[109] However, in another protocol published by Marsac et al.[93] it was recommended to use offset (endpoint) values when studying the melting point depression, as they represent the melting point of the final composition, assuming that complete mixing has occurred.[93] Tao et al.[133] developed this

protocol further and introduced a cryo-milling step to mix the components before DSC analysis. This cryo-milling step was added to improve the uniformity and facilitate the determination of dissolution endpoints.[133] Sun et al.[128] developed even further the previously reported method by introducing an annealing step. In their method, drug/polymer mixtures were cryo-milled to prepare uniform samples of small particle sizes to help attain solubility equilibrium. Samples were annealed at a various temperature to achieve phase equilibrium and then analysed by DSC at a heating rate of 10°C/min to check for the presence of undissolved crystals. The endpoint of the dissolution endotherm was considered the equilibrium solubility temperature of the given composition.[128] The endpoint values are currently the most commonly used in the literature to determine the drug and polymer miscibility.[93], [105], [107], [128], [133]–[135]

Tao et al.[133] reported that measuring the solubility of a crystalline drug in a polymer may be difficult due to the high viscosity of polymers. It was reported that DSC measurements were carried out with reasonable confidence down to 20% w/w D-mannitol in PVP, and the dissolution endpoint did not depend on the heating rate. However, at lower D-mannitol concentrations, the solution was too viscous for the dissolution endpoint to be determined with confidence. For such mixtures, dissolution eventually becomes too slow, and such a system cannot achieve solubility equilibrium even at the slowest heating rate achieved practically.[133] Ultimately, this may result in a higher dissolution endpoint and possibly lead to an underestimation of the drug/polymer solubility.[128] Therefore, Mahieu et al.[136] proposed a new protocol to determine the solubility of drugs in polymers. This method takes advantage of the fact that crystallisation (demixing) is generally faster than dissolution. In this method, a supersaturated glass solution is annealed above its crystallisation temperature until the equilibrium solubility is reached. The equilibrium solubility concentration is then derived directly from the Gordon−Taylor plot.[136]–[138]

Although the different approaches reported in the literature to determine the solubility of drugs in the polymers vary in detail, they can be divided into three general thermal analysis methods: the crystallisation method, the dissolution endpoint method, and the melting point depression method.[139] Despite the high interest in the determination of solubility of drugs in polymers, no comparative study across methods has been reported in the literature. Therefore, the aim of this study was to compare the three aforementioned thermal analysis methods for the prediction of drug/polymer solubility using binary systems consisting of five model drugs (celecoxib, chloramphenicol, paracetamol, indomethacin, and felodipine) and polyvinylpyrrolidone/vinyl acetate copolymers (PVP/VA) of different vinylpyrrolidone/vinyl

acetate weight ratios (30/70, 50/50, 60/40, 70/30 and 100/0).[139] The drug molecules were chosen based on their physiochemical properties, which were typical of low molecular weight compounds and reported as thermally stable and readily amorphising with glass transition temperatures around 20-60 °C. This work was done collaboratively between Trinity College Dublin (using the melting point depression method), Queen's University Belfast (using the dissolution endpoint method) and University of Copenhagen (using the crystallisation method). The focus in this Chapter is on the results attained from the melting point depression approach and comparisons to the results obtained from the other tests.

2.2 Materials and Methods

2.2.1 Materials

Paracetamol (PCM, M_w = 151.17 g/mol) and chloramphenicol (CAP, M_w = 323.13 g/mol) were purchased from Sigma-Aldrich Co. (St. Louis, MO, USA). Celecoxib (CCX, M_w = 381.37 g/mol) was purchased from AK Scientific, Inc. (Union City, CA, USA). Indomethacin (IMC, M_w = 357.79 g/mol) was purchased from Hawkins Pharmaceutical Group (Minneapolis, MN, USA). Felodipine (FDP, M_w = 384.26 g/ mol) was purchased from Combi-Blocks, Inc. (San Diego, CA, USA). Plasone K-17 (PVP K17, M_w = 10000 g/mol), PVP-VA copolymer E-335 (PVP- VA 335, M_w = 28000 g/mol), PVP-VA copolymer E-535 (PVP-VA 535, M_w = 36700 g/mol), and PVP-VA copolymer E-635 (PVP-VA 635, M_w = 38200 g/mol) were kindly supplied by Ashland Chemical Co. (Columbus, OH, USA). Since the PVP-VA copolymers were sourced as solutions, they were converted to the solid forms by spray drying. The supplied liquids were diluted with ethanol to form 5% (w/w) solutions and processed, using the Mini Spray Dryer B-290 from Büchi (Flawil, Switzerland) in the open pressure mode with air as drying gas, applying the following conditions: inlet temperature 140 °C, aspirator rate 100%, and pump speed 30%. These parameters resulted in an outlet temperature of around 80 °C.[139]

2.2.2 Melting Point Depression Method

2.2.2.1 Preparation of physical mixtures

All physical mixtures (in w/w ratios) of drug and polymer were prepared by ball milling at 400 rpm for 10 min with a planetary ball mill PM 100 (Retsch, Germany) at room temperature. A total amount of 500 mg was loaded to the stainless-steel milling container with a volume of 25 mL, and two stainless steel balls (15 mm in diameter) were used. Care was taken to ensure that no polymorphic transition occurred and crystalline API was still present at the end of milling (confirmed by XRPD).[135] Collected samples were stored in a desiccator over silica gel at 5 °C until use.

2.2.2.2 Content Uniformity Determination

The content uniformity test was carried out on the 9:1 API/polymer w/w physical mixtures after ball milling and this analysis was performed five times for each system. A UV spectrophotometric method was used on a double beam UV-visible spectrophotometer (model 1700Pharma, Shimadzu, Japan) with two matched quartz cells with a 1 cm light path. Ethanol was used as a solvent for all analyses. The absorbance of each solution against ethanol was recorded. Lambda

max values were as follows: 243 nm, 318 nm, 255 nm, 278 nm, and 238 nm for PCM, IMC, CCX, CAP and FDP, respectively. Six point calibration curves were obtained for each API/polymer system with a correlation coefficient (R^2) of at least 0.998. The individual results were found to be not more than ±1.2% from the desired 90% API content, and the average results were not more than ±0.6% from the 90% API content.

2.2.2.3 Thermal Analysis

Melting Point Depression Measurements

The melting events of the physical mixtures prepared as described in Section 2.2.2.1 were measured using a PerkinElmer Diamond DSC unit (Waltham, MA, USA) with HyperDSC. The unit was refrigerated using a ULSP B.V. 130 cooling system (Ede, Netherlands) and operated under a nitrogen flow of 40 ml/min. The gas flow was controlled using a PerkinElmer Thermal Analysis Gas Station (TAGS). The instrument was calibrated for melting temperature onset and enthalpy with indium. Before the measurement, the samples loaded in the DSC standard aluminium pans (5-8 mg) were first annealed in an oven (Memmert, Germany) at a temperature 10 °C above the glass transition temperature (T_g) of the polymer for 2 h. The annealing time was chosen to be 2 h based on a comparison of the heat of fusion values obtained for the non-annealed and annealed for 2, 4, and 6 h 9:1 API/polymer w/w physical mixtures. The heat fusion of samples annealed for 2, 4, and 6 h did not differ; therefore, it was assumed that the annealing time of 2 h would be sufficient. Samples were then cooled down to room temperature, and the final sample weight was calculated.

The DSC programme used to determine the melting point depression due to the presence of the polymer was as follows: samples were first heated from 25 to 120 °C at a heating rate of 10 °C/min and then a heating rate of 1 °C/min was applied to obtain the melting temperature value as close to the equilibrium as possible. All curves were evaluated and the values of melting onsets, melting endsets (offsets), and heat of fusions was calculated. All analyses were performed in duplicate for each sample.

Determination of Glass Transition Temperatures (T_gs)

T_gs of API/polymer mixtures were determined using the Perkin Elmer Diamond DSC setup as described above. Samples (physical mixtures prepared as described in Section 2.2.2.1) weighing between 5-8 mg were preheated in the DSC pans from 100 to 170 °C at a 10 °C/min heating rate, cooled to 30-40 °C below the expected T_g at a programmed cooling rate of 300 °C/min (flash cooling) and then a step scan (modulated temperature) method was applied to determine the

T_g. For the step scan, the samples were heated to 30-40 °C above the expected T_g at 5 °C/min in 2 °C steps. A 1 min isothermal step was applied between each of the dynamic steps. All analyses were performed in duplicate for each sample.

2.2.2.4 Powder X-ray Diffraction (PXRD)

Powder X-ray diffraction measurements at room temperature (RT-PXRD) were performed on samples placed on a low background silicon sample holder using a Rigaku Miniflex II desktop X-ray diffractometer (Rigaku, Japan) with a Haskris cooling unit (Grove Village, IL, USA). RT-PXRD patterns were recorded from 5 to 40 on the 2θ scale at a step of 0.05 /s. The X-ray tube was operated under a voltage of 30 kV and current of 15 mA.

2.2.3 Crystallization Method

The crystallisation method was applied by a research team from the University of Copenhagen.[139]

2.2.3.1 Sample Preparation

Supersaturated amorphous solid dispersions were prepared by a film casting method. The drug and polymer (80:20 or 85:15 w/w, 500 mg) were dissolved in 5 mL of acetone: ethanol (80:20 v/v) and cast onto a Teflon coated 76 × 26 mm Menzel glass. The solvent was evaporated on a Jenway 1100 hot plate from Bibby Scientific Ltd. (Staffordshire, U.K.) using a plate temperature of 150 °C. The dried samples were scraped of the Teflon coated glass plate and gently ground using a mortar and pestle. Thermal Analysis. The cast film powders and pure compounds were analysed using a Q2000 DSC from TA Instruments Inc. (New Castle, DE, USA). Sample powders (2− 3 mg) were scanned under 50 ml/min pure nitrogen gas purge using Tzero aluminium hermetic pans with a perforated lid. The temperature and enthalpy of the DSC instrument were calibrated using indium. The melting temperature (T_m, onset), melting enthalpy (ΔH_m), glass transition temperature (T_g, inflection), and heat capacity change (Δ_{Cp}) were determined using the Universal Analysis 2000 (version 4.5A) software.[139]

2.2.3.2 Solubility Determination

The supersaturated amorphous solid dispersions were loaded into the DSC and annealed at different temperatures below the T_m of the particular drug under investigation for 3 h to crystallise the excess drug in the mixture and to reach equilibrium solubility. After annealing, the sample was cooled to −10 °C and ramped at a rate of 5 °C/min to determine the T_g of the

annealed material. The concentration of drug remaining in the polymer matrix was then derived directly from the T_g of the annealed material. In order to determine the composition dependence of the T_g, physical mixtures of drug/polymer of known composition were prepared using a mortar and pestle. The samples were then heated above the T_m of the pure drug, quench cooled to −10 °C in situ in the DSC and ramped at a rate of 5 °C/min to determine the T_g. For a detailed description of the method, please refer to Mahieu et al.[136]

2.2.3.3 Solid State Characterisation

X-ray powder diffraction (XRPD) analysis was performed using an X'Pert PRO MRD diffractometer from PANalytical (Almelo, The Netherlands) equipped with a TCU 100 temperature control unit and an X'Celerator detector using nickel-filtered Cu Kα radiation (λ = 1.5406 Å) at 45 kV and 40 mA. Approximately 1 mg of sample powder was placed on zero background Si plates and measured over the angular range 3−40° 2θ at a scan rate of 1.20° 2θ/min. The diffractograms were analysed using the X'Pert Data Viewer (version 1.2) software.[139]

2.2.4 Dissolution Endpoint Method

The dissolution endpoint method was employed by a research team from Queen's University Belfast.[139]

2.2.4.1 Sample Preparation

Drug and polymer mixtures with different compositions were first mixed using a mortar and pestle followed by mixing in an MM200 ball mill mixer from Retsch GmbH (Haan, Germany). The individual materials were kept in a drying chamber for at least 24 h at 50 °C before sample preparation. In a typical milling procedure, pure drug or drug/polymer powder samples of 500 mg were loaded in 25 mL stainless steel milling containers with two stainless steel balls (15 mm in diameter) and milled at 20 Hz. A predefined milling time of 2 min was chosen, which was subsequently followed by a 2 min cooling time. The number of milling−cooling cycles to be used for each drug/polymer combination was determined by measuring the melting end point of the mixture, where no further decrease in the melting end point was observed with an increased number of milling−cooling cycles. Longer milling time enhanced the dissolution rate of the crystalline drug into the polymer but decreased the sensitivity of the DSC measurement due to increased amorphous content (observed by XRPD). Thus, fewer milling−cooling cycles were used for mixtures containing lower drug loadings.[139]

2.2.4.2 Thermal Analysis

Samples were analyzed using the power compensation DSC8000 from PerkinElmer (Waltham, MA, USA). Nitrogen was used as the purge gas for low-speed scanning. Approximately 8−10 mg of freshly ball-milled sample was packed into an aluminium pan with a perforated lid. Melting point end point determination was conducted at a heating rate of 1 °C/min from 20 to 200 °C. The end point of the melting endotherm (Tend) was calculated from the intercept point of the endothermic trace and the post-melting baseline.[139]

2.2.4.3 Solid State Characterisation

The solid-state properties of the ball-milled samples were determined using a MiniFlex II X-ray powder diffractometer from Rigaku Corp. (Tokyo, Japan). Radiation was generated from a copper source operating at a voltage of 30 kV and a current of 15 mA. The test samples were packed into a glass sample holder and scanned from 0 to 40° 2θ, using a step width of 0.01° 2θ and a scan rate of 1° 2θ/min; continuous mode was used. There were certain levels of increased amorphous halo background in the XRPD pattern of ball-milled samples in comparison to crystalline drug and amorphous polymer physical mixtures, but the polymorphic form of all crystalline drugs was determined to be the same as that of the starting drug materials.[139]

2.2.5 True Density Measurements

The amorphous densities of the materials were determined using an AccuPyc 1330 helium pycnometer from Micromeritics Instruments Corp. (Norcross, GA, USA). Before the measurements, approximately 1 g of the samples were melt quenched to remove any sorbed moisture and to obtain the amorphous form. The samples were weighed before analysis and purged with 19.5 psig dry helium. The reported results are averages of 10 consecutive measurements. The true density measurements were carried out by a research team from the University of Copenhagen.[139]

2.3 Results and Discussion

2.3.1 Prediction of Drug/Polymer Solubility from DSC Data

The experimental solubility of the drug in the polymer was determined using the analytical protocols described in Section 2.2. The data sets for the three methods were fitted with the F-H model to predict the solubility at ambient temperature by extrapolation[92], [108] using the following equation (Equation 2.3-1):

$$\frac{\Delta H_m}{R}\left(\frac{1}{T}-\frac{1}{T_m}\right)=\left[ln\phi+\left(1-\frac{1}{m}\right)(1-\phi)+\chi(1-\phi)^2\right] \quad \text{(Equation 2.3-1)}$$

where ΔH_m and T_m are the enthalpy of fusion and melting temperature for the pure drug respectively, R is the gas constant, ϕ is the volume fraction of drug, m is the volume ratio of the polymer to drug volume and χ is the F-H interaction parameter. T is the annealing temperature, the onset temperature of melting or dissolution endpoint temperature depending on the method in question.

The parameter m, the volume ratio of the polymer to drug volume, was calculated as per Equation 2.3-2, where M_w is the molecular weight and d is the true density:

$$m=\frac{M_{w\,(poly)}}{d_{poly}}\Big/\frac{M_{w\,(drug)}}{d_{drug}} \quad \text{(Equation 2.3-2)}$$

The parameter ϕ is the volume fraction of drug and was be calculated from Equation 2.3-3, where d_{drug} and d_{poly} are the densities of drug and polymer respectively, and X_{drug} is the mass fraction of drug:

$$\emptyset=\frac{\frac{X_{drug}}{d_{drug}}}{\frac{X_{drug}}{d_{drug}}+\frac{1-X_{drug}}{d_{poly}}} \quad \text{(Equation 2.3-3)}$$

2.3.2 Melting Point Depression Method

The phase diagrams for each drug/polymer system shown in Figure 2.3-1 were constructed using the onset of melting and the physicochemical characteristics of the components are presented in Table 2.3-1. The solid-liquid line was constructed based on the melting point depression phenomenon, originally applied in polymer science to predict miscibility between two polymers. [140] Later, this method was further developed and applied to study miscibility of API/polymer systems.[108], [132] The melting point of a pure drug is directly related to the chemical potential

energy. For a pure crystalline drug, the melting point is defined as the point at which the chemical potential of the crystalline drug equals the chemical potential of the molten drug.[132], [141] If the drug is miscible with a polymer, then negative energy results from mixing, and the chemical potential of the drug in the mixture must be lower than that of the pure drug. This will result in a decrease in the melting point of the crystalline dug. In other words, this is the melting point depression.[132], [141] In contrast, if the drug and polymer are immiscible, no melting point depression is expected as the chemical potential of the melted drug remains unchanged. The heating rate of 1 °C/min was applied to provide sufficient time to achieve the melting temperature values as close to the solubility equilibrium as possible (Section 2.2.2.3). As previously mentioned, both the heating rate and the annealing time have an impact on the melting point measurements.[108], [128] The values of F-H interaction parameter χ shown in Table 2.3-2 were calculated for each drug/polymer system using Equation 2.3-1.

Table 2.3-1 Physical properties of components, where ΔHm is the heat of fusion and T_m is the melting point measurement of crystalline API, T_g, d and M_w are glass transition temperatures, true density and molecular weight of pure components, respectively.

	M_w[a] (g/mol)	T_m (K)	ΔH_m ($J \cdot g^{-1}$)	T_g (K)	d (g/cm^3)
PCM	151.17	441.9 ± 0.1	166.5 ± 0.9	294.5 ± 0.2	1.22 ± 0.01
CAP	323.13	422.1 ± 0.1	107.7 ± 0.5	299.8 ± 0.2	1.47 ± 0.00
CCX	381.37	434.2 ± 0.1	86.1 ± 0.5	328.5 ± 0.1	1.35 ± 0.01
IMC	357.79	433.0 ± 0.0	99.2 ± 0.0	316.4 ± 0.2	1.31 ± 0.01
FDP	384.26	415.3 ± 0.1	76.0 ± 1.1	315.6 ± 0.0	1.29 ± 0.00
PVP-VA 335	28,000	––	––	337.8 ± 0.3	1.18 ± 0.00
PVP-VA 535	36,700	––	––	356.7 ± 0.1	1.19 ± 0.01
PVP-VA 635	38,200	––	––	372.5 ± 0.1	1.18 ± 0.01
PVP-VA 735	56,700	––	––	387.5 ± 0.1	1.18 ± 0.01
PVP K17	10,000	––	––	379.4 ± 0.3	1.20 ± 0.00

[a]Average M_w according to the supplier.

The experimental and theoretical values of T_g for each API/polymer systems are shown in Figure 2.3-1. The theoretical T_g values were calculated using the Gordon–Taylor equation (Chapter 1, Equation 1.4-1). As shown in Figure 2.3-1, the experimental T_g values for PMC/PVP-VA 335, CAP/PVP-VA 535 and FDP/PVP K17 systems generally correlate well with those predicted by the Gordon-Taylor equation. Positive and negative deviations from the theoretical T_g values were observed for CCX/PVP-VA 635 and IMC/PVP-VA 735 systems, respectively. The Gordon and Taylor equation is based on the assumption of ideal mixing of the components (volume additivity, and a linear change in volume with temperature), therefore deviations from the ideal behaviour are the result of entropy effects beyond combinatorial mixing such as strong intermolecular interactions.[142] The intermolecular interactions (e.g. hydrogen bonds) may be seen as positive deviations from the theoretically predicted T_g values, suggesting good miscibility between the components.[142][98] In contrast, the negative deviations indicate that interactions between the individual molecules may be stronger than interactions between the between the two components.[98][143] As single T_g values were measured for all drug/polymer systems, this indicated that the mixtures were miscible across the entire composition range.

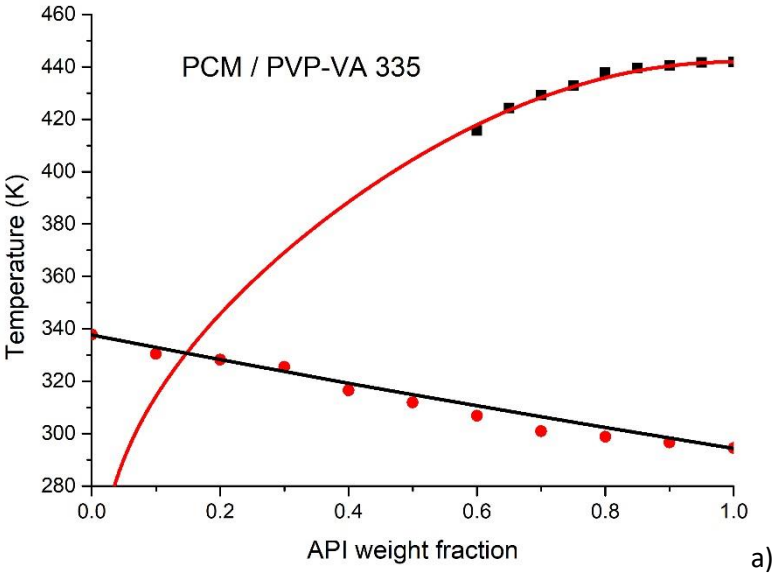

a)

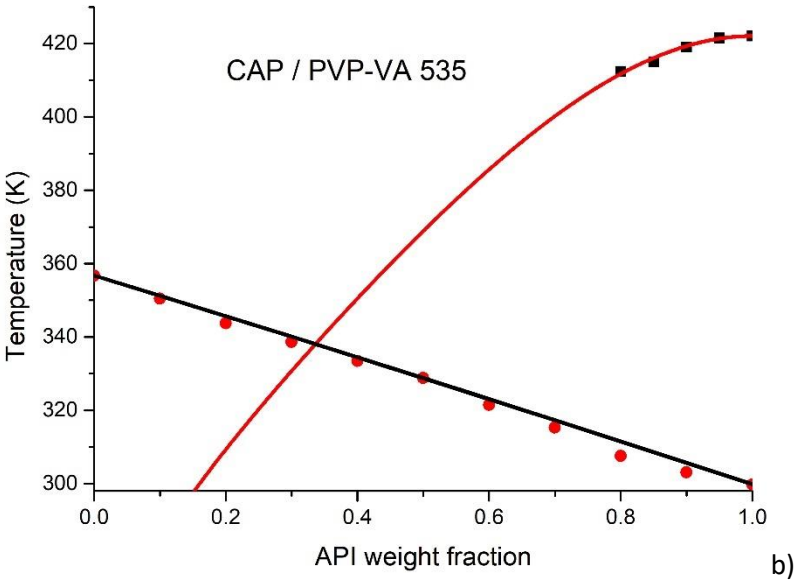
CAP / PVP-VA 535
Temperature (K)
API weight fraction
420
400
380
360
340
320
300
0.0
0.2
0.4
0.6
0.8
1.0

b)

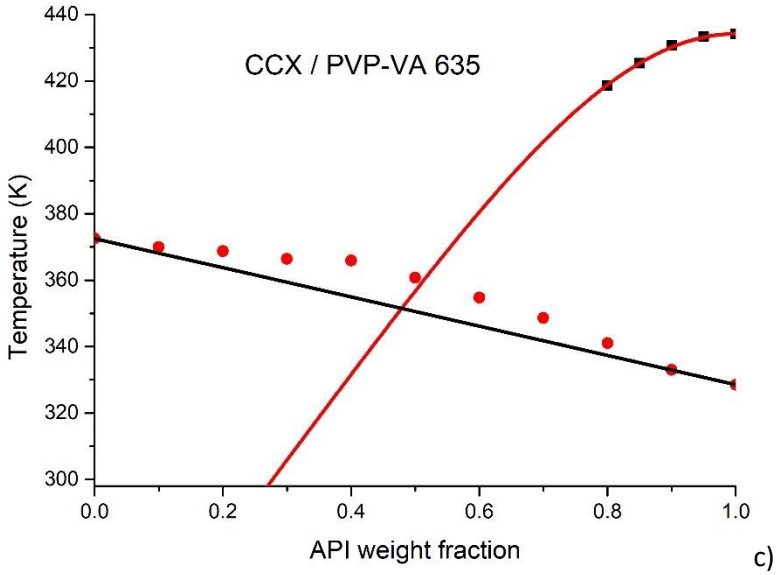
CCX / PVP-VA 635
Temperature (K)
API weight fraction
440
420
400
380
360
340
320
300
0.0
0.2
0.4
0.6
0.8
1.0

c)

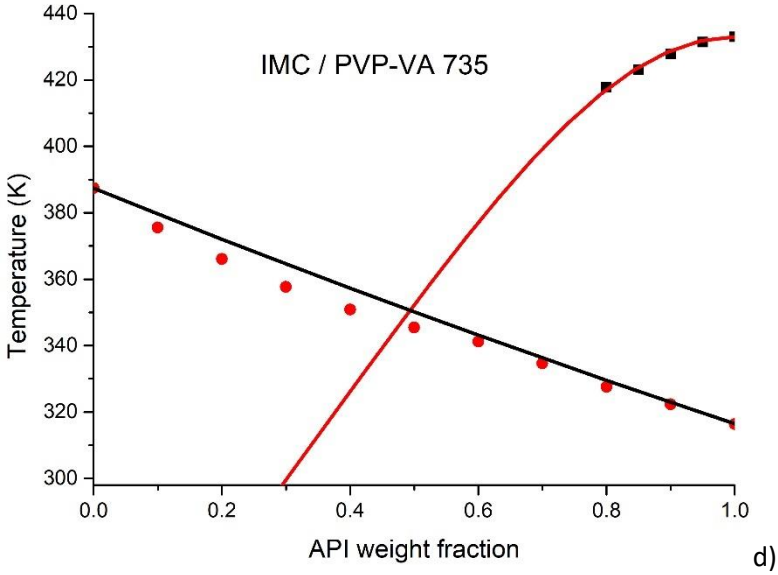
IMC / PVP-VA 735
Temperature (K)
API weight fraction
440
420
400
380
360
340
320
300
0.0
0.2
0.4
0.6
0.8
1.0

d)

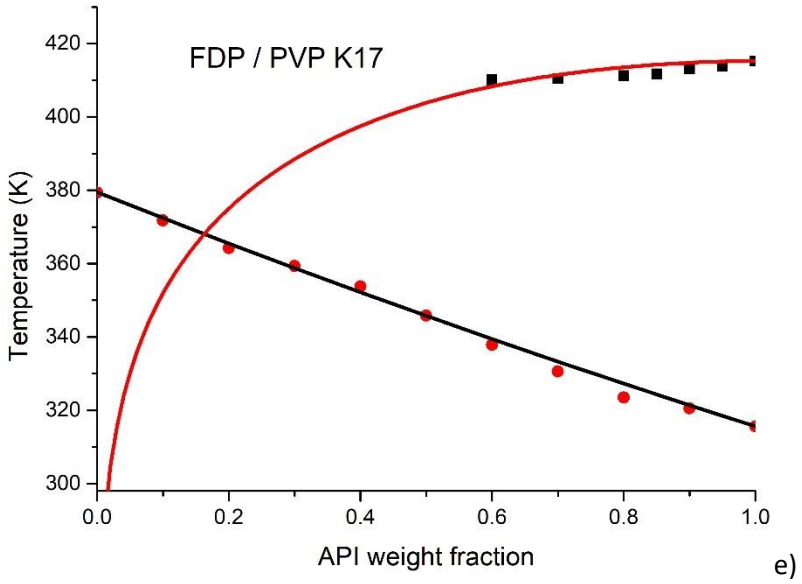

Figure 2.3-1 Phase diagrams for the drug/polymer systems: a) PCM/PVP-VA 335; b) CAP/PVP-VA 535; c) CCX/PVP-VA 635; d) IMC/PVP-VA 735; e) FDP/PVP K17. The black squares (■) represent the experimental onset of melting values. Red lines represent solid-liquid lines generated by fitting experimental points (black squares) to the F-H theory. The red circles (●) represent the experimental T_g values, and the black lines are the theoretical Gordon-Taylor relationships.

2.3.3 Comparison of the Different Methods

The predicted solubility at 25 °C, based on the Flory-Huggins theory, and χ values of the five drug/polymer systems using the three different methods are given in Table 2.3-2. Graphical illustration of predicted solubility at 25 °C for the analysed systems is shown in Figure 2.3-2.

From Table 2.3-2 and Figure 2.3-2 it is evident that the predicted solubility results at 25 °C, obtained from melting point depression methods and crystallisation method correlate closely. However, those produced by dissolution end point deviate significantly. Both, melting point depression methods and crystallisation method rank the predicted solubility in the same order, IMC/PVP-VA 735 > CCX/PVP-VA 635 > CAP/PVP-VA 535 > FDP/PVP K17 > PCM/PVP-VA 335, except for the FDP/PVP K17 system.

The solubility predictions based on the melting point depression method were consistently higher than the predictions based on the crystallisation method. Furthermore, the predictions based on the crystallisation method (except FDP/PVP K17) were higher than the predictions based on the dissolution end point method. It was concluded, that the difference between the solubility predictions based on crystallisation method and dissolution end point method, may be related to the mechanism of two methods. [139] The crystallisation method approaches

equilibrium solubility from the supersaturated state. Therefore, the equilibrium thermodynamics is driven by crystallisation kinetics. In contrast, the dissolution end point method approaches equilibrium solubility from an undersaturated state. In this case, the equilibrium thermodynamics is driven by dissolution kinetics. Trying to understand the discrepancy between the two methods, Knopp et al.[139] related to the fact that when the drug concentration approaches equilibrium solubility, the crystallisation and dissolution kinetics slow down. Therefore, it may be possible that the crystallisation kinetics slow down to the extent that it is not detectable in the DSC. Thus, such a system can falsely be considered in equilibrium, and this might suggest that the crystallisation method might be overestimating the solubility. In contrast, the dissolution endpoint method depends on dissolution kinetics. As the dissolution kinetics are expected to be slower than crystallisation kinetics, this may result in underestimating the solubility. This hypothesis was not verified in this study; however, it could explain the differences between the solubility results obtained from the two methods. Furthermore, the solubility results provided by melting point depression method were for some samples almost equal to that of the crystallisation method, suggesting that the melting point depression method may overestimate solubility.[139]

Table 2.3-2 Combined results for the three different methods presenting the values of the interaction parameter χ and API weight fraction solubility at 25 °C. Adapted from [139]

	PCM/PVP-VA 335	**CAP/PVP-VA 535**	**CCX/PVP-VA 635**	**IMC/PVP-VA 735**	**FDP/PVP K17**
Values predicted from the melting point depression method					
Interaction parameter χ	-1.3 ± 0.8	-3.9 ± 1.8	-5.7 ± 1.1	-8.8 ± 3.7	-1.5 ± 3.0
Solubility at 25 °C (w/w)	0.05	0.15	0.25	0.35	0.06
Values predicted from the crystallisation method					
Interaction parameter χ	-1.2 ± 0.3	-4.1 ± 1.0	-5.2 ± 0.9	-6.3 ± 1.6	-2.2 ± 0.6
Solubility at 25 °C (w/w)	0.03	0.14	0.17	0.19	0.07
Values predicted from the dissolution endpoint method					
Interaction parameter χ	-0.6 ± 0.9	-1.9 ± 0.8	-2.9 ± 1.6	-2.9 ± 0.9	-1.4 ± 0.6
Solubility at 25 °C (w/w)	0.02	0.05	0.06	0.06	0.08

[a] According to supplier information

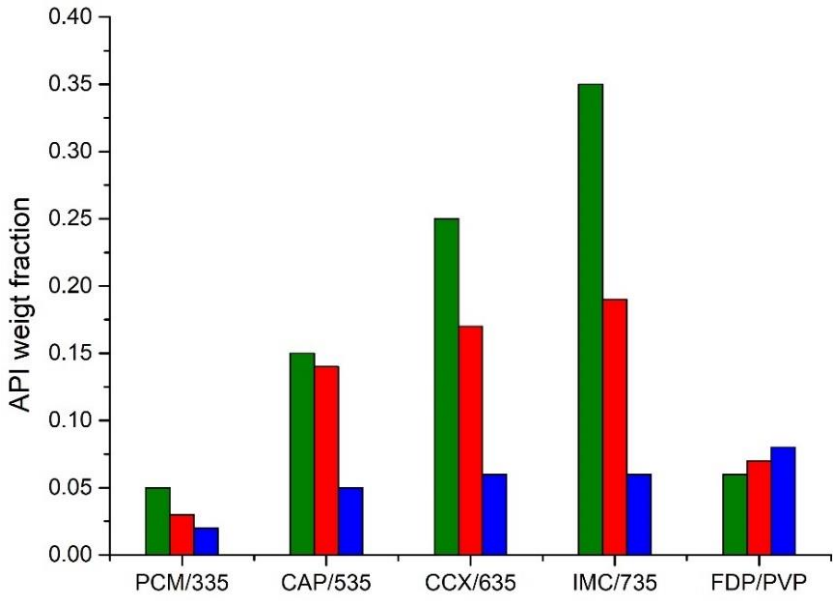

Figure 2.3-2 Graphical illustration of predicted solubility at 25 °C of the five drug/polymer systems from the three methods presented in Table 2.3-2. The green bars represent the melting point depression method, the red bars represent the crystallisation method, and the blue bars represent the dissolution end point method. Adapted from [139]

The advantages and disadvantages of the three methods are summarised in Table 2.3-3. As previously mentioned, all three thermal analysis methods provided reproducible data and fitted with the Flory−Huggins model thermal relatively well. Therefore, in choosing an optimal method for the prediction of drug/polymer solubility, the thermal properties of both the drug and polymer should also be considered. The crystallisation method should be used if the T_g of the polymer is higher than the Tm of the drug or if the difference between the Tm of the drug and T_g of the polymer is less than 20 °C. As in such case, the mixing of the components might be slower than the timescale of the DSC measurement. However, if the difference between T_g of the polymer and the T_g of the drug is less than 20 °C, the experimental composition dependence of the T_g might not be sufficient to obtain the equilibrium solubility concentration with satisfactory precision after annealing. In this case, melting point depression or dissolution end point methods are recommended for prediction of drug/polymer solubility. If none of the above restrictions applies, all three methods can be used to predict the drug/polymer solubility.[139]

Table 2.3-3 Advantages and disadvantages of three different methods, where T_g is the glass transition temperature and T_m is the melting temperature, respectively. Adapted from [139]

	Advantages	**Disadvantages**
Melting point depression method	• Applicable for most polymers with $T_g < 120$ °C [a] • Relatively fast	• Heating rate dependent • May overestimate solubility • Requires 100% crystallinity • Not applicable if the drug is thermally decomposed at T_m
Crystallization method	• Heating rate independent • Applicable for most polymers with $T_g > 90$ °C [a]	• Time-consuming • May overestimate solubility
Dissolution endpoint method	• Applicable for most polymers with $T_g < 120$ °C [a] • Relatively fast	• Heating rate and milling conditions dependent • May underestimate solubility • Not applicable if the drug is thermally decomposed at T_m

[a] Estimation based on a general assumption of the T_m (>140 °C) and T_g (<70 °C) of low molecular weight drugs.[144]

2.4 Conclusions

The drug/polymer solubility for a range of systems at 25 °C was predicted using the Flory-Huggins theory. The solubility predictions from melting point depression and crystallisation methods gave similar results that were consistently higher than the predictions made from the dissolution endpoint method. The negative F-H interaction parameter (χ) values, supported by a presence of a single T_g, indicated miscibility of all five drug/polymer systems in the whole composition range. The data generated from all the three methods was with satisfactory reproducibility and fitted relatively well with the Flory−Huggins model. Therefore, this comparative study may be used as general guidance for the selection of the most suitable thermal analysis method for the screening of drug/polymer solubility.

Chapter 3: Phase Diagrams of Polymer-Dispersed Liquid Crystal Systems of Itraconazole-Component Immiscibility Induced by Molecular Anisotropy

3.1 Introduction

Poor solubility and dissolution of many active pharmaceutical ingredients (APIs) has become an industry-wide concern. Approximately 40% of marked drugs are classified as class II drugs with high permeability and low solubility, according to the Biopharmaceutics Classification System (BCS).[145] Conversion of crystalline APIs into dis(ordered), amorphous or liquid crystal (LC) forms is a route, which promises to greatly improve the solubility and consequently the oral bioavailability of these BCS class II drugs, as the solubility of disordered (translationally and/or orientationally) forms is likely to be several times higher than their crystalline counterparts.[146], [147]

As previously discussed in Chapter 1, disordered APIs have higher energy, entropy and free energy than the corresponding crystalline state. [127] This may lead to their enhanced solubility and bioavailability. However, it also creates the possibility of chemical degradation or spontaneous crystallisation upon storing or processing conditions. [21]LC phases are expected to be more chemically and physically stable than fully disordered, amorphous materials of the same composition.[148] Also, due to the higher Gibbs free energy in comparison to crystalline materials, the (apparent) solubility of mesophases is higher, as shown for fenofibrate calcium.[149] Physical stability of disordered materials can be imparted by mixing them with polymers to form solid dispersions (SDs).[150] This approach is well known for fully disordered API molecules and if the drug and polymer are miscible and the drug loading is below the solubility equilibrium, the drug is molecularly dispersed in the polymer matrix and should form a thermodynamically stable, homogeneous solution without supersaturation and a risk of crystallisation.[132], [135], [139] LC phases are also able to form LC/polymer blends, in literature often referred to as polymer dispersed liquid crystals (PDLCs), and a wide range of non-pharmaceutical applications of PDLCs, such as electrooptical displays, shutters and membranes, have been investigated.[151] These materials, however, typically consist of LC droplets dispersed in a polymer matrix, thus are phase separated systems. As from the point of view of pharmaceutical applications homogenous dispersions are preferred, the phase behaviour of mesophases in binary mixtures is of utmost importance as it directly impacts the physical stability and performance of SDs. Thermodynamic phase diagrams have been recognised as a very beneficial tool in determining stability of binary polymer/API SDs, with the Flory-Huggins approach allowing miscibility/immiscibility of components to be determined.[92], [135], [139]

As previously discussed in Chapter 1, Itraconazole (ITZ) is poorly soluble, making it a class II BCS drug. [123] In addition to solubility issues, ITZ has the unusual ability to form a number of LC

phases.[116], [152], [153] It forms two thermotropic LC phases, nematic and smectic A,[154], [155] however a nematic, process-induced phase was also characterised for nanosized and spray dried ITZ as well as a 1:1 water:ITZ complex forming a smectic phase was recently isolated.[156]

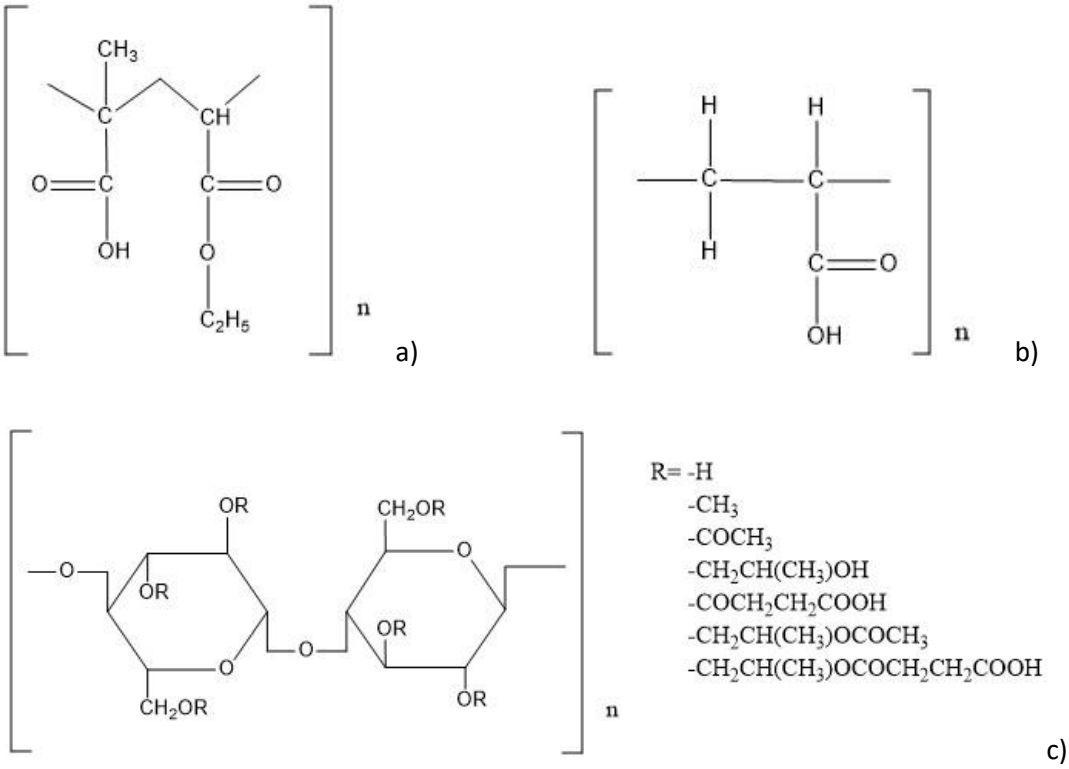

Figure 3.1-1 Chemical structures of monomers: a) Eudragit L100-55 (EUD), b) Carbopol 981 (CAR), and c) hypromellose acetate succinate (HPMCAS, HAS).

Numerous studies have been carried out into the miscibility of ITZ with other commonly used polymers, and many solid dispersions (SDs) have been manufactured. This was described in Chapter 1. These SDs were identified as amorphous. However interestingly, Six et al.[152] and Janssens et al.[153], [157] observed a phase separation of ITZ from Kollicoat IR® and Eudragit E100-based SDs. This phase separation was dependent on the API concentration and the drug phase identified as a "chiral nematic mesophase", but not as an amorphous solid. Phase separation of ITZ in its hydroxypropyl methylcellulose (HPMC) amorphous SD was recently observed by Purohit and Taylor using nanoscale infrared spectroscopy and nanothermal analysis, however the state of matter of ITZ in the separated phase was not identified.[158]

Considering the scarcity of data in relation to ITZ LC behaviour in polymeric SDs, the main aim of this study was to consolidate information of ITZ LC, investigate the phase behaviour of ITZ

when in binary mixtures with polymers and construct, for the first time, full phase diagrams for a pharmaceutical drug showing a liquid crystalline behaviour when mixed with polymers. The Flory-Huggins theory for isotropic systems was coupled with the Maier-Saupe-McMillan for anisotropic mixing to support the construction of phase diagrams. Based on the previous reports, the following polymers presenting the benefits when incorporated in ITZ SDs and resulting in an improvement of the drug biopharmaceutical properties: Eudragit L100-55[122] (EUD), HPMCAS-MG[122] (HAS) and Carbopol[124] were selected.

3.2 Materials and Methods

3.2.1 Materials

Itraconazole (ITZ) was donated by Welding GmbH (Hamburg, Germany). Methacrylic acid - ethyl acrylate copolymer (Eudragit L100-55, EUD) was kindly donated by Evonik Industries AG (Germany), polyacrylic acid (Carbopol 981, CAR) was purchased from BF Goodrich (USA), while hypromellose acetate succinate (Shin-Etsu AQOAT) grade MG (HPMCAS-MG, HAS) was donated by Shin-Etsu Chemical Co. Ltd. (Japan). Table 3.2-1 presents the physicochemical characteristics of the components used. HAS starting material was a coarse powder and it was comminuted at 400 rpm for 30 minutes with a planetary ball mill PM 100 (Retsch, Germany) at room temperature prior to mixing with ITZ. Ethanol (98%, analytical grade) used for content uniformity experiments was purchased from Cooley distillery.

Table 3.2-1 Physicochemical properties of ITZ, EUD, HAS and CAR. M_w - molecular weight, T_m onset – onset temperature of melting, Tm endset – endset temperature of melting, ΔH - heat of fusion, T_g – glass transition temperature and d - true density, N/A – not applicable.

Component	M_w (g/mol)	T_m onset (°C)	T_m endset (°C)	ΔH (J/g) and (J/mol)	T_g (°C)	d (g/cm^3)
ITZ	705.6	166.1 ± 0.2	168.05 ± 0.35	81.54 ± 0.35 (57534 ± 247)	59.35 ± 0.35	1.4 ± 0.0
EUD	320,000	N/A	N/A	N/A	114.4 ± 0.25	1.3 ± 0.0
HAS	18,000	N/A	N/A	N/A	117.3 ± 0.2	1.3 ± 0.0
CAR	1,250,000	N/A	N/A	N/A	129.4 ± 0.3	1.5 ± 0.0

3.2.2 Methods

3.2.2.1 Preparation of physical mixtures

All physical mixtures (in w/w ratios) of ITZ (crystalline, as supplied) and each of the polymers investigated (EUD, HAS or CAR) were prepared as described in Chapter 2.

3.2.2.2 Content Uniformity Determination

The content uniformity test was performed as described in Chapter 2. Absorbance of each solution against ethanol was recorded at 262 nm. Six point calibration curves were obtained for each of the ITZ/polymer systems with a correlation coefficient (R^2) of at least 0.998. The single results were found to be deviating by no more than ±1.5% from the desired 90% ITZ content and the average results were deviating by no more than ±1.1% from the 90% ITZ content.

3.2.2.3 Thermal Analysis

3.2.2.3.1 Melting point depression measurements

The melting events of crystalline ITZ in the physical mixtures prepared as described in Section 3.2.2.1 were performed as described in Chapter 2.

3.2.2.3.2 Liquid Crystalline (LC) Phase Transition Measurements

LC phase transition events of ITZ and ITZ/polymer mixtures were determined using the Perkin Elmer Diamond DSC as described in Chapter 2. Analysis were performed on samples (physical mixtures prepared as described in Section 3.2.2.1) weighing between 3-5 mg. All samples were first heated from 25 to 180 °C, cooled to 25 °C and then re-heated to 180 °C. A heating/cooling rate of 10 °C/min was used in all steps. All analyses were performed in duplicate for each sample.

3.2.2.3.3 Determination of Glass Transition Temperatures (T_gs)

T_gs of ITZ/polymer mixtures were determined as described in Chapter 2.

3.2.2.3.4 Thermogravimetric Analysis (TGA)

TGA of the polymers used for this study was performed using a Mettler TG 50 module linked to a Mettler MT5 balance (Mettler Toledo, Switzerland). Sample weights between 9-11 mg were used and placed into open aluminium pans. Measurements were performed from 25 to 200 °C at a 10 °C/min heating rate. Analysis was carried out in the furnace under nitrogen purge and monitored by Mettler Toledo STARe software (version 6.10). TGA analysis of polymers used in this study was carried out to ensure that the melting point measurements would not be affected by polymer decomposition. It was confirmed that all polymers and ITZ were stable within the desired temperature range of 25 to 180 °C.

3.2.2.4 Powder X-ray Diffraction (PXRD)

Powder X-ray diffraction measurements at room temperature (RT-PXRD) were performed as described in Chapter 2. Samples for RT-PXRD analysis first were melted in the oven at 180 °C on glass supports and cooled down to room temperature prior to the analysis.

Temperature controlled PXRD (VT-PXRD) was performed on an X'Pert-PRO (PANalytical, Netherlands) X-ray diffractometer equipped with an Anton Paar TTK-450 sample stage (Anton Paar, Austria). VT-PXRD patterns were collected from 5 to 40 2θ at a continuous scanning rate of 0.12 2θ/second. The X-ray tube was operated under a voltage of 40 kV and current of 40 mA.

3.2.2.5 Polarised Light Microscopy and Hot Stage (PLM-HS)

PLM-HS experiments were performed using an Olympus BX53 polarising optical microscope equipped with a U-POT cross polarizer, a Linkam hot stage and a Q IMAGING Fast 1394 camera (Olympus, Japan) at x500 magnification. The hot stage ramp, for thermomicroscopic investigations, was performed from 25 to 180 °C using a heating rate of 10 °C/min. Samples for PLM-HS experiments were prepared by melting on a microscope glass slide at 170 and 180 °C in the oven (Memmert, Germany). When the powdered mixture was fully melted, a glass coverslip was placed on top, and the sample was allowed to cool at room temperature.

3.2.2.6 True Density Measurements

True density was measured by an AccuPyc 1330 Pycnometer Micromeritics™, using helium (99.995% purity) to determine the volume of the sample. A 1 cm^3 aluminium sample cup was used for all samples. The instrument was calibrated immediately before the analysis. All analyses were performed in duplicate for each sample.

3.2.2.7 Solid-State Fourier Transform Infrared Spectroscopy (FT-IR)

Samples for FT-IR analysis were mixed with potassium bromide (KBr) at a ratio of 1:100 w/w using an agate mortar and pestle. Disks were produced using a 13 mm KBr die set (Perkin Elmer, England) by direct compression of approximately 10 bar for 1 min. Spectra were recorded on the Spectrum 100 FT-IR Spectrometer (PerkinElmer, England) under Spectrum software version 6.1.0. A spectral range of 650–4,000 cm^{-1}, resolution 2 cm^{-1}, and accumulation of 10 scans were used.

3.2.2.8 Mathematical Modelling and Statistical Analysis

Modelling of phase diagrams and statistical analysis was performed by Dr Lidia Tajber using Origin 2018 software. Non-linear least squares curve fits to experimentally determined data were obtained by applying the Levenberg-Marquardt iteration algorithm until the Chi-square tolerance value of 1×10^{-9} was reached and the fit converged. No weighting for parameters was applied.

3.3 Results and Discussion

3.3.1 Liquid Crystalline Properties of Itraconazole

The ability of itraconazole (ITZ) to form liquid crystal phases was previously reported by Six and co-workers.[116] The authors stated that on reheating, the melted drug showed a glass transition temperature (T_g) at 59 °C and two endothermic reversible transitions at 74 and 90 °C. The peak at 90 °C was interpreted as the transition of the isotropic liquid into a chiral nematic mesophase, while the transition occurring at a lower temperature (at 74 °C) was assigned as being most likely due to rotational restriction of the molecules.[116] Further research on the molecular dynamics of ITZ by dielectric spectroscopy was later conducted by Tarnacka et al.[154] and Mapesa et al.[155] concluding that these endothermic transitions are in fact related to the formation of a nematic phase (LC_{N-I}), seen as an endothermal transition at 90 °C, and a smectic A phase (LC_{Sm-N}), represented as an endothermal transition at 74 °C, phase.

With the previously published literature in mind, in this work, a range of characterisation techniques were applied to characterise ITZ further. ITZ was subjected to a thermal analysis cycle consisting of a first heating to 170 °C (as the melting point of ITZ is 166 °C)[116], flash cooling to 25 °C and then re-heating at 10 °C/min. At higher temperatures crystallisation and melting processes were seen. A small endotherm at around 160 °C, preceding the main melting peak, was observed (Figure 3.3-1a). Recently, polymorphism of ITZ was described by Zhang et al.[159], however no sign of a polymorphic transition was observed for this sample under polarising light microscopy (Figure 3.3-1a) and by PXRD (data not shown). Thus it is likely that the origin of this low magnitude endotherm is the presence of small crystallising particles of ITZ with the melting point following a Gibbs-Thomson relationship, similarly as described previously for fenofibrate.[160]. The positions of the LC thermal transitions (Figure 3.3-1a) were in agreement with the data reported by Six et al.[116] Nevertheless, this group observed that the glassy ITZ prepared by cooling from its melt did not crystallise on heating and that crystallisation was mechanically induced by scratching.[116]

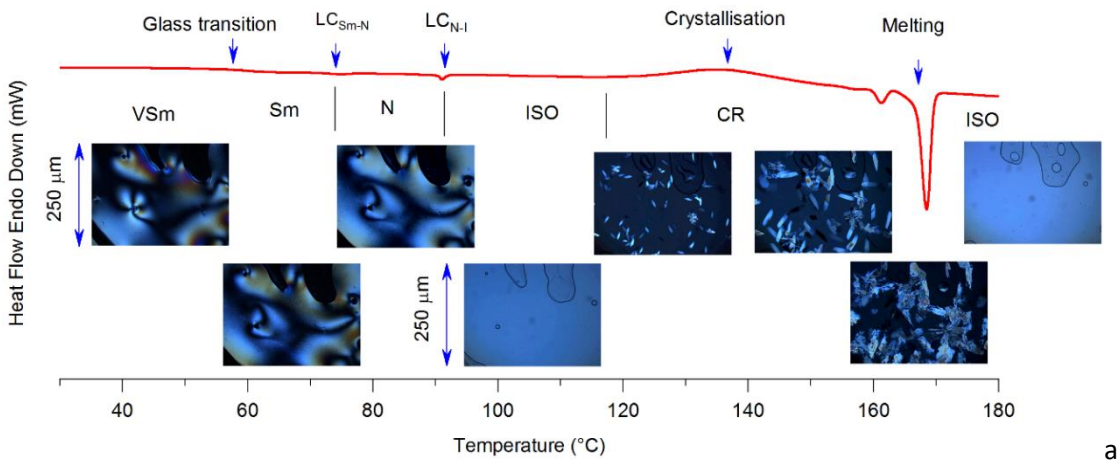

a)

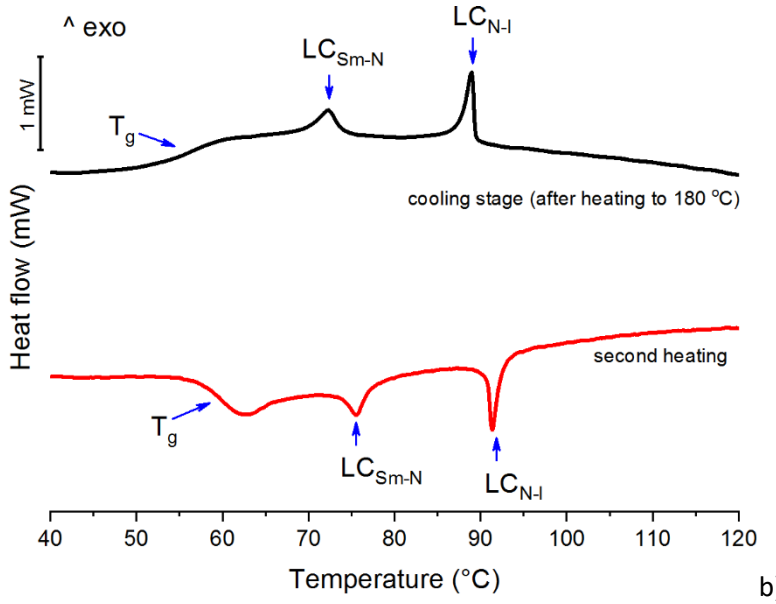

b)

Figure 3.3-1 a) DSC and thermomicroscopical analysis of second heating of ITZ, previously heated to 170 °C and cooled to 25 °C. The images present morphology of ITZ phases identified: VSm – vitrified smectic, Sm – smectic, N - nematic phase, ISO – isotropic phase, CR-crystallisation. b) DSC thermograms of ITZ on cooling after heating to 180 °C (black solid line) and reheating the sample from its vitrified phase.

Thus, in another experiment the end temperature of the first heating stage was increased to 180 °C, followed by cooling to 25 °C (slow cooling at 10 °C/min) and reheating at the same. As shown in Figure 3.3-1b, the DSC trace on reheating (second heating) showed a T_g at 59.3 ± 0.25 °C, followed by two endothermic LC transitions with the onset temperature values for the LC events of 73.2 ± 0.4 °C (LC_{Sm-N}) and 90.4 ± 0.35 °C (LC_{N-I}) with the enthalpies of transition of 416 ± 34 J/mol and 842 ± 10 J/mol, respectively. Thus, these values are typical of nematic and smectic

transitions as tabulated by Sackmann.[161] No cold crystallisation on reheating was observed and the position and the heat of transition of the LC events was unaffected by the thermal treatment applied. It was also determined that a decrease in the heating rate from 300 °C/min to 10 °C/min during the cooling step had no effect on the position and magnitude of the LC peaks. A consecutive heating/cooling treatment showed the reversibility of the LC transitions (Figure 3.3-1b), thus the enantiotropic nature of both LC transitions. The most likely explanation for crystallisation of ITZ on the DSC run when the sample was first heated to 170 °C might be in the thermal lag of the sample (the melting point is only 166 °C) that resulted in some crystalline material still being present in the melted sample when the cooling stage began. Therefore, to avoid sample crystallisation, heating to 180 °C in the first stage was applied to all further investigations.

Polarised light microscopy (PLM) is probably the most widely used technique to identify different LC phases as they appear to have distinct textures.[62] Based on the orientation of LC molecules one can distinguish between different phases. A sample of nematic or smectic C LC viewed by PLM often appears as a colourful Schlieren texture. Between crossed polarisers, Schlieren textures show an irregular network of dark brushes, which correspond to the extinction position of the nematic LC.[62] A smectic A phase viewed by PLM appears as a focal-conic fan texture. It develops directly from a nematic phase or isotropic liquid (ISO) as batonnets grow, merge and eventually generate this characteristic texture.[62] The ITZ sample prepared by first heating the crystalline material to 180 °C and then cooling down to room temperature was clearly birefringent at 25 °C under PLM, showing a mixture of focal-conic fan and Schlieren textures along with spontaneously formed homeotropic fields (dark areas) (Figure 3.3-2a). Therefore, this material cannot be classified as an amorphous or a completely disordered phase. Several samples of vitrified ITZ were prepared proving reproducibility of the technique developed (Figure 3.3-2a). For most of the samples colourful focal-conic fan textures as well as four-brush Schlieren textures were seen (Figure 3.3-2a) suggesting a material with a smectic (A or C) arrangement.

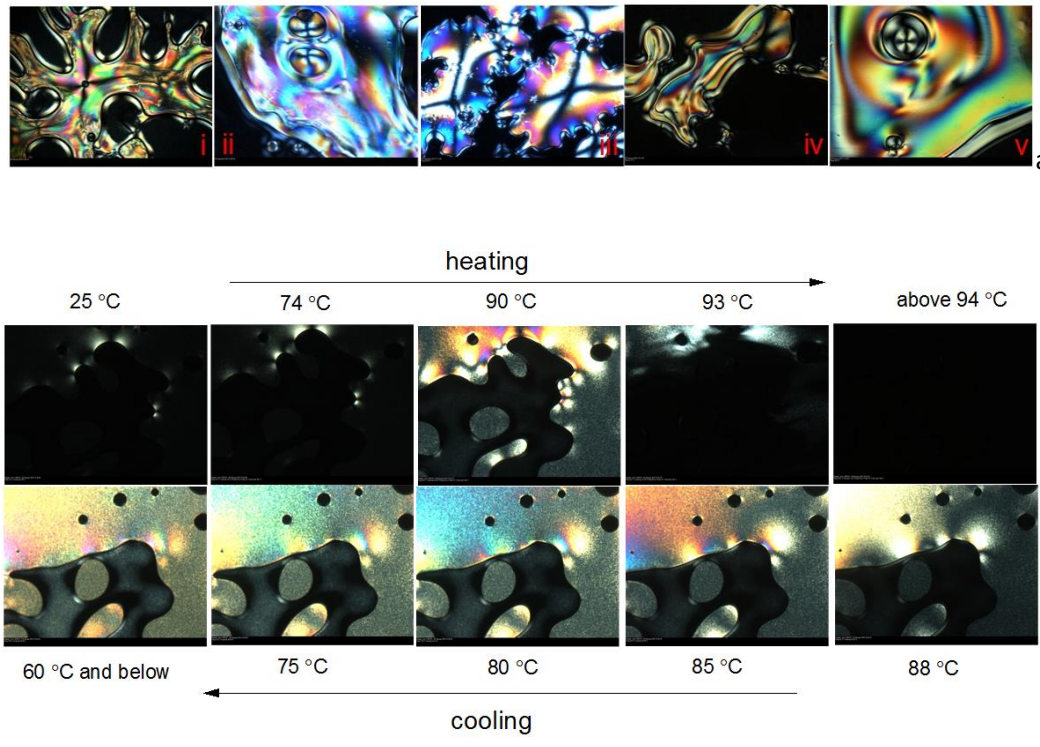

Figure 3.3-2 Textures of unaligned LC phases on untreated glass observed between crossed polarizers. a) ITZ at 25 °C. The sample was first heated to 180 °C and melt cooled down to 25 °C. b) PLM-HS analysis of ITZ.

Morphology of vitrified ITZ sample subjected to a heating/cooling cycle of 25-100 °C at a rate of 10 °C/min is shown in the Figure 3.3-2b. On heating, a change that was noticeable at about 74 °C. This corresponds to the first LC transition recorded in the DSC thermogram (Figure 3.3-1) at the same temperature. A growing increase in light intensity was visible up to 90 °C, where it reached its maximum intensity. This relates to another LC transition at 90 °C consistent with the DSC data. Above 90 °C, a gradual decrease in light intensity was noticed, reaching its minimum value at 93 °C. During the cooling stage, the first change was observed at about 88 °C. A growing increase in light intensity was visible cooling down to 60 °C, where it reached its maximum (Figure 3.3-2b).

RT-PXRD analysis performed on ITZ which was heated to 180 °C and then cooled down to room temperature showed two sharp peaks at 2θ=2.97° (d-spacing 29.67 Å) and 5.96° (d-spacing 14.92 Å). There was also a major diffuse maximum at 2θ=19° (Figure 3.3-3a). The peaks at around 3 and 19° 2θ corresponded well to the position of predicted maxima, normally located at $Q = 2\pi/l_o$ and $Q=2\pi/w_o$, where Q is the scattering wavevector and l_o and w, are the length and

width of the molecule, respectively.[58] Molecular dimensions of ITZ were calculated from the crystal structure, CSD code: TEHZIP using Mercury 3.7 and the length and width of ITZ measured as 28.05 Å and 5.42 Å, respectively. For a smectic phase the position and intensity of the diffraction peaks, typically sharp due the high degree of periodicity over large distances, are related to the long range organisation of the phase and in the ITZ sample shown as the peak at app. 6° 2θ.[58] Thus the phase, resulting from heating ITZ past its melting point and cooled down to room temperature has a smectic arrangement, as suggested by PLM.

VT-PXRD was used to further investigate the LC phase transitions of ITZ (Figure 3.3-3b). The crystalline sample of ITZ was melted on the XRD sample holder at 180 °C. It was then cooled down to 25 °C followed by reheating to 100 °C at a heating rate of 10 °C/min. VT-PXRD spectra collected during cooling stage, showed a peak at 2θ=5.88° (d-spacing 15.01 Å) beginning to appear at 60 °C. The sharpness of this peak was visible during further cooling down to 25 °C (Figure 3.3-3b). This clearly indicates the long range organisation of the LC phase and strongly suggests the smectic phase formation. Similarly, on reheating the same peak was evident, but this time reduction of peak intensity was noticed (Figure 3.3-3c).

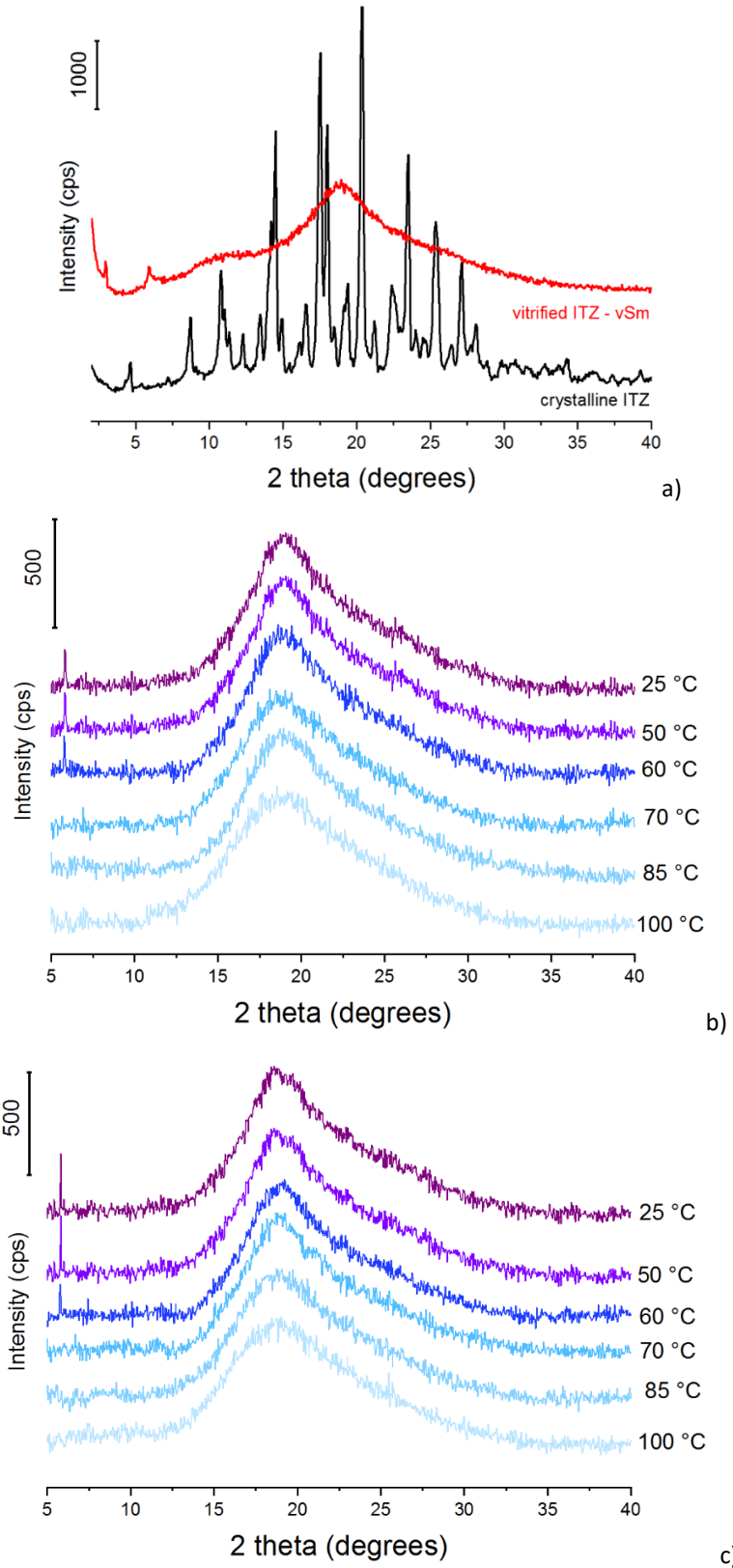

Figure 3.3-3 a) RT-PXRD of crystalline and vitrified ITZ. b) VT-PXRD of ITZ on cooling. The sample was first heated to 180 °C. c) VT-PXRD of ITZ on second heating. The sample was first heated to 180 °C and cooled to 25 °C.

PLM-HS and PXRD studies clearly indicate that ITZ forms an ordered, anisotropic structure at 25 °C on cooling from melt and that the molecular organisation of this phase is of a smectic and not a fully disordered, amorphous phase, as sometimes misinterpreted and referred to in many pharmaceutical publications.[159], [162]–[164] DSC, however, displays a T_g transition on cooling at 56 °C and therefore, consistent with the accepted nomenclature[165], this phase should be referred to as a vitrified smectic phase. It should be highlighted that the phenomenon of a glass transition is not exclusive to amorphous materials. It has been long recognised that many other substances, even with a partly crystalline structure and with a long-range structural order (e.g. plastic crystals, liquid crystals, spin glasses etc.) may exhibit this transition.[166], [167] Another interesting observation that can be made in relation to the T_g of ITZ (56 °C, 329 K) is that it can be considered as relatively high in comparison to its melting point (T_m) of 166 °C (439 K) with the T_g/T_m ratio of 0.75. This value falls within the range of 0.6-0.8 as reported by Kerc and Srcic[168], however it needs to be acknowledged that T_g values of nematic or smectic glasses (vitrified phases) are generally higher than those of fully disordered materials.[169]

3.3.2 Thermomicroscopic Studies of ITZ/Polymer Systems

Having observed the formation of a vitrified, glassy phase of ITZ on quench cooling, a frequent method used to obtain amorphous pharmaceuticals, an important question arises: Is this phase observed when in a mixture with polymers? The production of polymeric solid dispersion of ITZ, as a means of improving apparent solubility and dissolution rates thus enhancing bioavailability of the drug is well known and numerous accounts in this area have been published.[122]–[124] However, when screening the published information, it becomes evident that only one research group has reported that a liquid crystal phase of ITZ may be present in such solid dispersions.[152], [153], [157] A phase separation induced by anisotropy of a liquid crystal phase can be detrimental to the performance and long term stability of ITZ formulations, as discussed further.

A screening approach was adopted first, whereby 8:2 w/w ITZ/polymer mixtures were first prepared as described in Section 3.2.2.5 and then subjected to a heating/cooling treatment. Birefringence of the samples was clearly observed at 25 °C for the vitrified samples (Figure 3.3-4), regardless of the polymer (EUD, HAS or CAR) used.

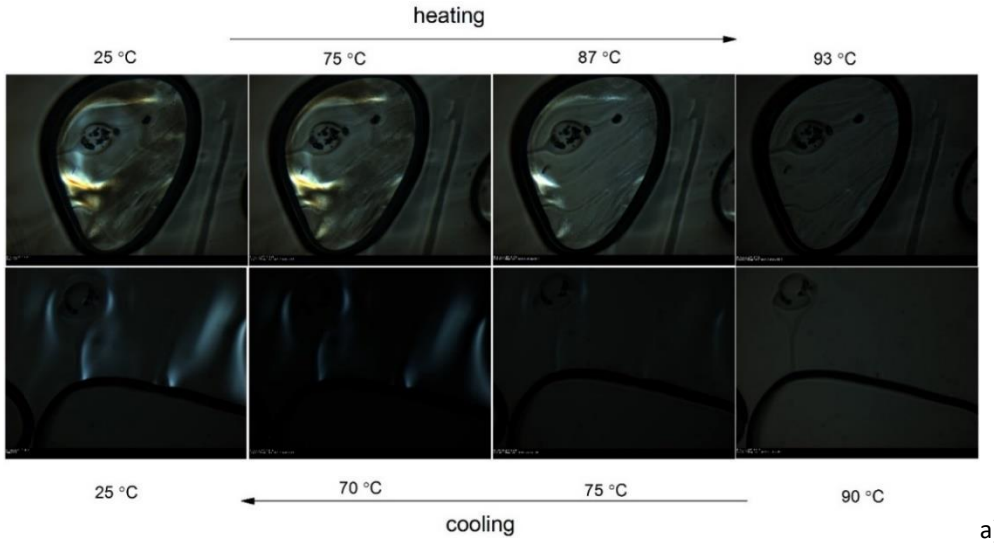

a)

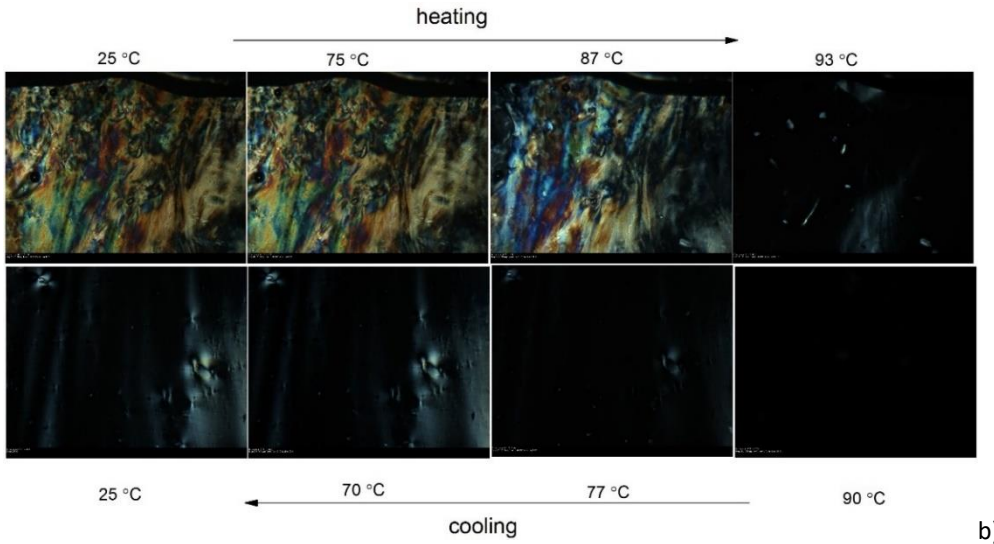

b)

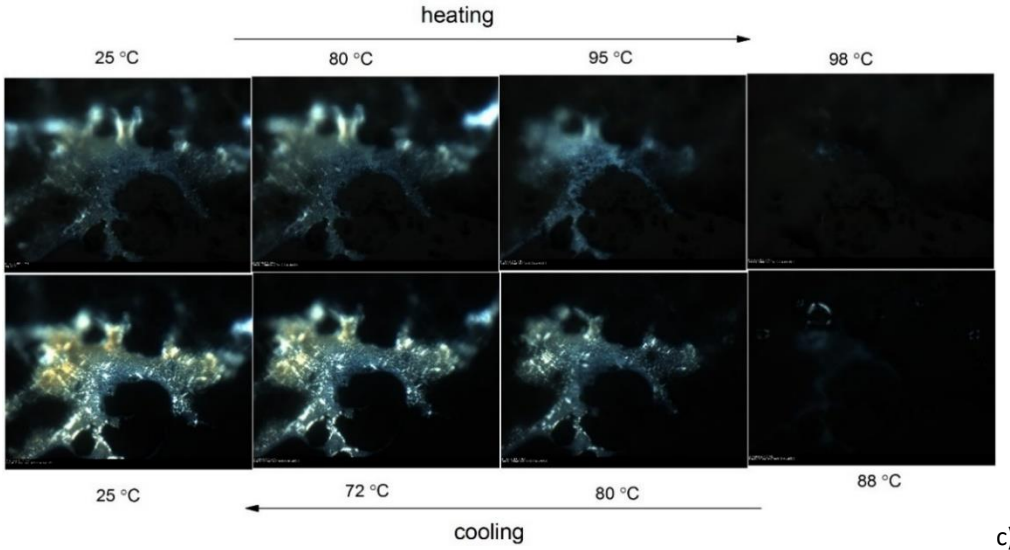

c)

Figure 3.3-4 PLM-HS analysis of: a) 8:2 ITZ/EUD w/w, b) 8:2 ITZ/HAS w/w and c) 8:2 ITZ/CAR w/w. A heating/cooling cycle at a rate of 10 °C/min was used for all samples.

During the heating stage, the LC_{Sm-N} transition, expected at about 74-75 °C, was not perceptible in any of the analysed ITZ/polymer systems as no visible change was recorded regarding birefringence of these samples (Figure 3.3-4). In relation to the LC_{N-I} transition, expected to be seen at around 90 °C, a clear change in the appearance of the ITZ/EUD and ITZ/HAS samples was recorded at 93 °C, while for the ITZ/CAR combination at 98 °C. Above 100 °C all samples remained isotropic and no birefringent regions were visible.

During the cooling stage, the birefringent regions started to emerge only at 75 °C for ITZ/EUD and at 77 °C for ITZ/HAS samples (Figure 3.3-4ab). No signs of the LC_{N-I} transition were apparent. The ITZ/CAR system showed a different behaviour as morphology of this sample changed at 88 °C with birefringent droplets forming at this temperature (Figure 3.3-4c). At 80 °C these droplets were fully formed and no further change in their birefringence upon cooling to 25 °C was seen (Figure 3.3-6). Inspecting closely the microscopic images it became obvious that the shape and position of the droplets remained almost the same during the heating/cooling cycle. Therefore, this system appears to be more viscous (also consistent with the high molecular weight of this polymer as presented in Table 3.2-1) in comparison to the ITZ/EUD or ITZ/HAS samples. The results also suggest that the ITZ/CAR system is more likely to form only one LC phase, most likely a nematic, rather than the more organised, smectic phase as the ITZ molecules may have restricted movement due to the high viscosity of CAR.

3.3.3 DSC Analysis of Liquid Crystalline Transitions for ITZ/polymer Systems

DSC analysis of ITZ/EUD and ITZ/HAS systems revealed the presence of both, LC_{Sm-N} and LC_{N-I}, transitions for ITZ contents of at least 80% of drug. A decrease in the onset temperature values for the LC events was noticed in comparison to the values for pure ITZ (Figure 3.3-5a and b).

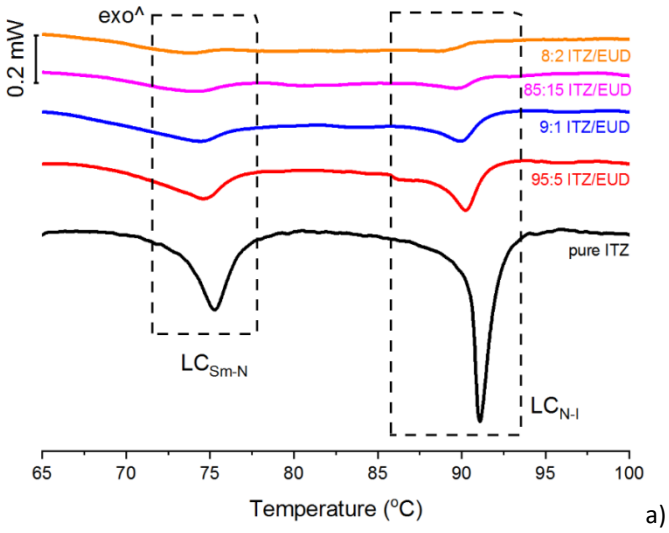

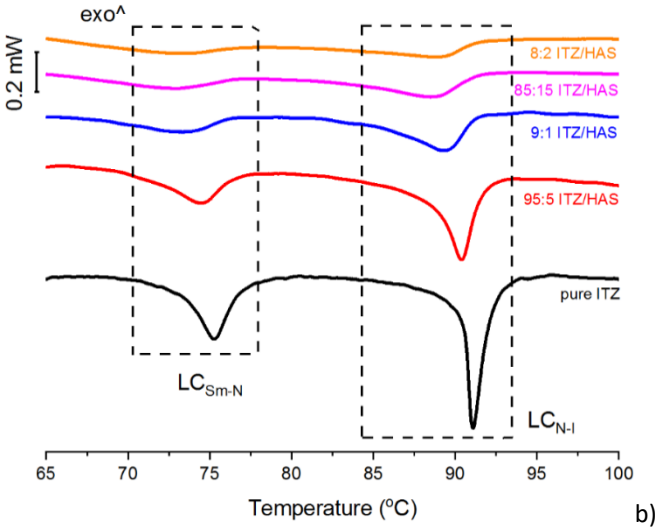

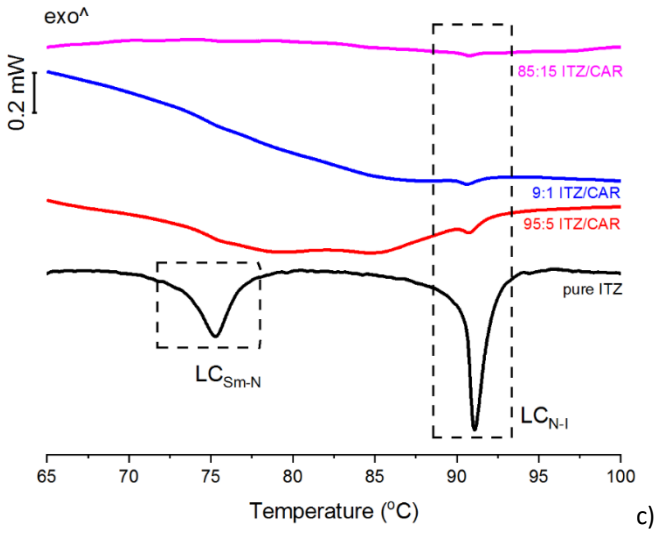

Figure 3.3-5 DSC thermograms of ITZ/polymer systems presenting the liquid crystalline transitions in ITZ. a) ITZ/EUD, b) ITZ/HAS and c) ITZ/CAR. The ITZ/polymer ratios are weight ratios; the temperature range for the LC transitions are marked by broken lines.

The largest decrease in the onset temperature for the LC transitions, in comparison to pure ITZ, was observed for the 8:2 ITZ/HAS w/w sample, with 66.65 ± 0.1 and 82.1 ± 0.5 °C recoded for LC_{Sm-N} and LC_{N-I}, respectively. For the EUD/ITZ combination the decrease in the onset temperature values was moderate, with the LC_{Sm-N} transition beginning at 70.0 ± 0.1 °C and the LC_{N-I} transformation starting at 87.6 ± 0.2 °C. This compares with 73.2 ± 0.4 °C and 90.4 ± 0.35 °C recoded for pure ITZ. Thus, EUD and HAS are able to depress the onset temperature of LC transitions and work on the principles of miscible impurities. Interpreting these results in relation to ITZ miscibility, HAS is more likely to be miscible with ITZ than EUD. For the ITZ/CAR system only the LC_{N-I} transition was recorded by DSC and no significant difference was observed in relation to the onset temperature of this transition (Figure 3.3-5c).

Dispersions of ITZ/Eudragit E100 containing more than 13% of ITZ and produced by extrusion were identified by Six et al. as mixtures of molecular dispersions of the drug and polymer as well as liquid crystalline ITZ.[152] In fact, while the authors report the presence of only a "chiral nematic" phase, both LC transitions were clearly visible on the DSC thermogram shown in the report. Janssens and co-workers seen signs of a "glassy chiral nematic mesophase" of ITZ appearing at a drug load of 30% w/w for spray dried samples and at 22.5% w/w for the film casted systems. For the spray dried system only one LC endotherm was present, of the LC_{N-I} transformation, interpreted that ITZ was made to a disordered mesophase resulting from the interference of the polymer and the process.[153] Two LC transitions in samples composed of ITZ and Kollicoat IR® (a polyvinyl alcohol–polyethylene glycol copolymer) and processed by hot stage extrusion were recorded for the drug concentration 40% or higher.[157] Regarding the behaviour of ITZ/CAR systems exhibiting only one LC transition, this could be caused by the strong polymer-polymer interactions[170]. However, no evidence of intermolecular interactions was found in the present work using FT-IR (data not shown). It may also be the result of geometric inhibitions restricting the formation of a smectic phase, which is more ordered than a nematic phase and requires more space for the molecules to assembly.[171]

As evident from the DSC studies and data presented above, at least a part of ITZ was present in the drug/polymer mix as a liquid crystal. As numerous studies show, typically part of the liquid crystal remain separated (as evident from Figure 3.3-5) and some of the LC phase dissolves in the polymer matrix to form a molecular dispersion.[151], [172] The fraction of ITZ remaining in the LC phase can be quantified taking into consideration the enthalpy of a LC transition (Equation 3.3-1):

$$P(x) = \frac{\Delta H_{LC}(x)}{\Delta H_{LC}(LC)} \qquad \text{(Equation 3.3-1)}$$

where x is the weight ratio of ITZ, P(x) is the ratio of the mass of phase-separated LC to the total mass of the blend and $\Delta H_{LC}(x)$ and $\Delta H_{LC}(LC)$ are the enthalpies for the LC transitions (LC_{Sm-N} and LC_{N-I}) for the blend and pure LC, respectively.[151] Relationships between P(x) and x for the various ITZ/polymer blends considering both LC transitions, LC_{Sm-N} and LC_{N-I}, separately are presented in Figure 3.3-6.

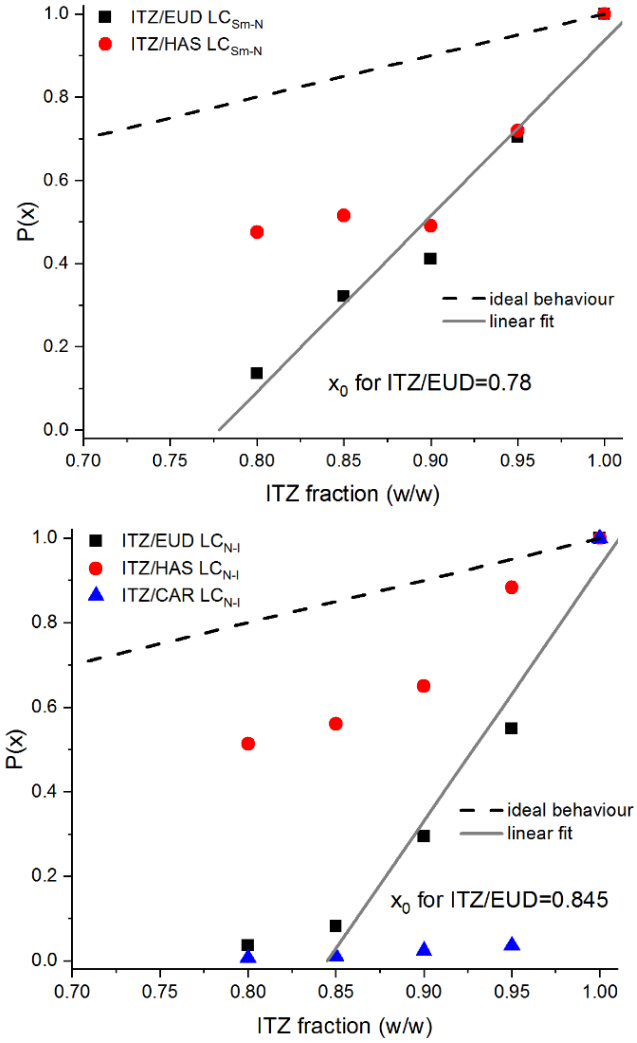

Figure 3.3-6 The mass ratio of phase separated ITZ as a liquid crystalline phase (P(x)) versus the total weight fraction of ITZ in the polymer blend. The dashed black line indicates the ideal P(x) versus ITZ weight fraction relationship if there was no solubility of ITZ in the polymer. The solid grey lines represent linear fits to ITZ/EUD data, while x_0 is ITZ weight fraction when P(x)=0, i.e. the drug concentration fully soluble in the polymer. Please note that the experimental data point for LC_{N-I} at x=0.8 was omitted in the linear fit for ITZ/EUD.

Some researchers found that the P(x) versus x relationship can be linear[151], [172], however this applies here to the ITZ/EUD system only with the drug solubility limits in the polymer determined to be close for LC_{Sm-N} and LC_{N-I}, at 0.78 and 0.845 ITZ weight fraction, respectively. Therefore, considering just the linear fits to the experimental points, the EUD content in those blends must be at least around 20% w/w to form a homogenous, non-separated blend. For the HAS systems, the LC phases of the drug were well persistent at concentrations much lower than 80% w/w ITZ and a non-linear relationship of P(x) versus x was observed. However, both LC_{Sm-N} and LC_{N-I} were seen to behave in a similar, non-linear manner. For the CAR/ITZ systems, a very abrupt decrease in the LC ITZ fraction was noted, as at 95% w/w ITZ only 3.6% of ITZ was separated from the blend. At 85% w/w ITZ the content of separated drug was only 1%.

3.3.4 Phase Diagrams of ITZ/Polymer Systems

The phase behaviour of a low molecular weight drug substance and a polymer binary mixture in the isotropic state can be described by the Flory-Huggins (F-H) lattice theory. As mentioned in Chapter 1 this theory has been applied to describe and predict compatibility/miscibility of a number of API/polymer systems.[105]–[109], [135] However, the F-H theory alone cannot be used to describe the phase behaviour of a binary composition made of a liquid crystalline compound with a polymer due to the inherent anisotropy of LC phases. Thus an extended approach to the F-H theory needs to be employed with the total Gibbs free energy of such a system (f) represented as the combination of two constituents, the free energy ($f^{(i)}$) of mixing of isotropic liquids, as described by the F-H lattice theory, and the free energy ($f^{(a)}$) due to anisotropic ordering of molecules.[172]–[175]

The F-H free energy ($f^{(i)}$) of mixing of isotropic liquids can be described by Equation 3.3-2[134], [173]:

$$\frac{\Delta f^{(i)}}{RT} = \phi ln\phi + \frac{1-\phi}{m}\ln(1-\phi) + \chi\phi(1-\phi) \qquad \text{(Equation 3.3-2)}$$

where R is the gas constant, φ is the volume fraction of the API (ITZ), m - the volume ratio of the polymer to drug volume and χ is the F-H interaction parameter. As described in Chapter 1, a necessary condition of miscibility is that the free energy of mixing is negative, therefore χ has to be negative or slightly positive.[113]

The free energy ($f^{(a)}$) due to anisotropic ordering of molecules for the nematic and/or smectic arrangement is described by the Maier-Saupe-McMillan (M-S-M) theory[172], [176]:

$$\frac{\Delta f^{(a)}}{RT} = \phi\left[\frac{1}{2}\,\upsilon(S^2 + \xi\sigma^2)\phi - lnZ\right]$$ (Equation 3.3-3)

where ν is the temperature-dependent (ν=4.54T_{I_N}/T, where T_{I_N} is the isotroptic-nematic transition temperature) parameter describing interactions between the molecules in the nematic phase and S is the nematic order parameter, where S=0.5(3<$\cos^2\theta$>-1) with θ being the angle between a reference axis and the director of the liquid crystalline molecule, ξ is a smectic interaction parameter, σ is a smectic order parameter and Z is the partition function in the smectic order. The parameters V, S, θ, ξ, and Z were determined by fitting the equation to expected points by using the Levenberg-Marquardt iteration algorithm.

In relation to fitting the ITZ solid-liquid (isotropic) transition in the polymer systems, the parameter χ was calculated using the melting point depression method based on the F-H theory[92], [108] using the following Equation 2.3-1 (Chapter2).

The phase diagrams presented in Figure 3.3-7 were constructed using the values presented in Table 3.3-1 and the data points were obtained in the following manner. Firstly, the solid-isotropic (liquid) line was constructed using the heating rate of 1 °C/min to provide sufficient time to achieve the melting temperature values as close to the solubility equilibrium as possible (Section 3.2.2.3.1). It was previously documented that both the heating rate and the annealing time have an impact on the melting point measurements.[108], [128] Secondly, the T_g values were determined by heating ITZ/polymer physical mixtures past the melting point of ITZ and flash cooled to prevent, as far as possible, ITZ ordering upon cooling. A modulated DSC programme was then used to determine the experimental Tg midpoints (Section 3.2.2.3.3). Thirdly and finally, LC transitions were measured on samples melted past the melting point of ITZ, cooled to 25 °C at a rate of 10 °C/min and re-heated at 10 °C/min, thus applying a “standard” thermal treatment (Section 3.2.2.3.2).

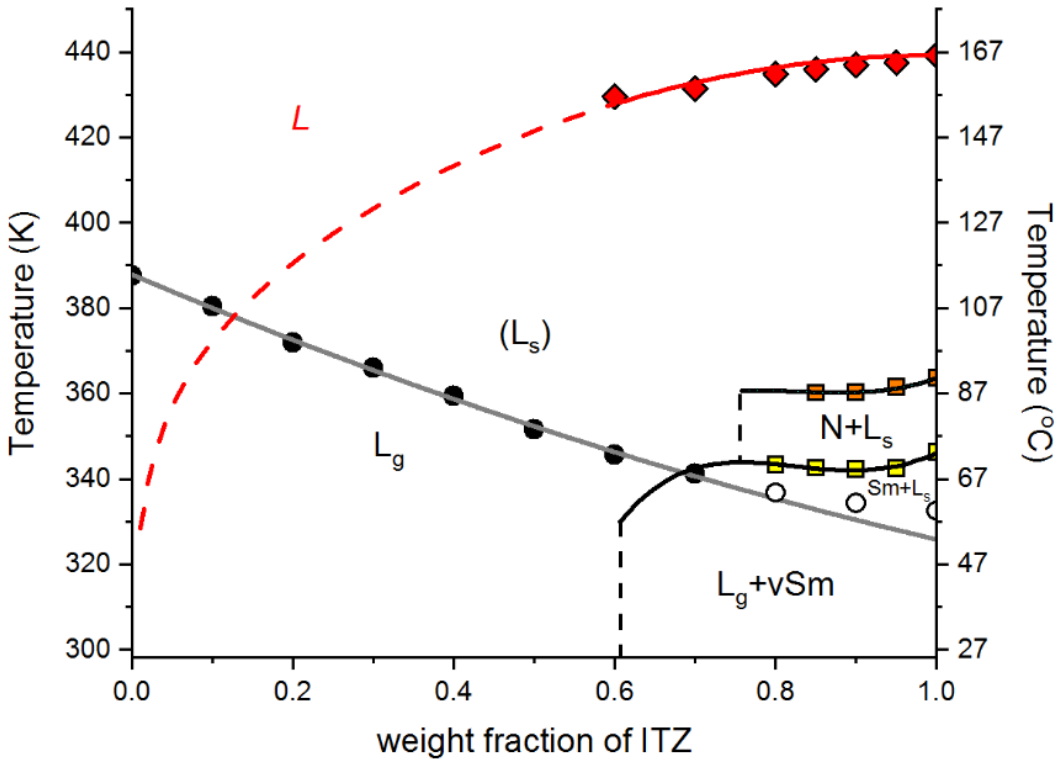
Temperature (K)
Temperature (°C)
weight fraction of ITZ
L
(L_s)
L_g
N+L_s
Sm+L_s
L_g+vSm
440
420
400
380
360
340
320
300
167
147
127
107
87
67
47
27
0.0
0.2
0.4
0.6
0.8
1.0

a)

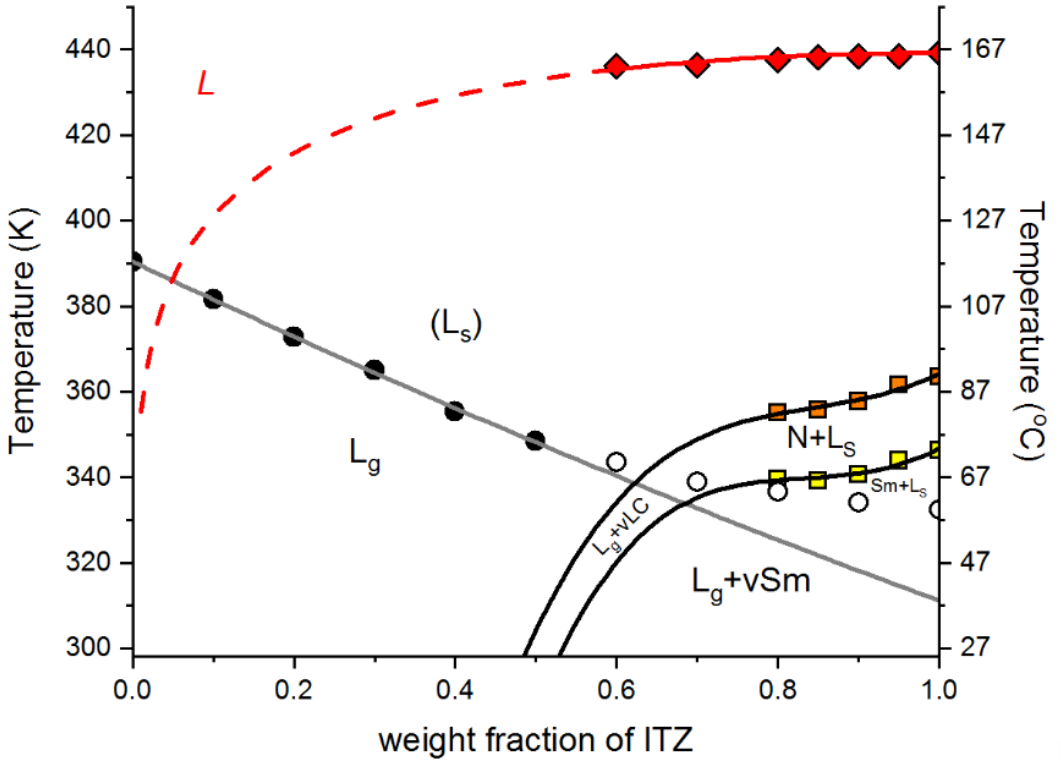
Temperature (K)
Temperature (°C)
weight fraction of ITZ
L
(L_s)
L_g
N+L_S
Sm+L_s
L_g+vLC
L_g+vSm
440
420
400
380
360
340
320
300
167
147
127
107
87
67
47
27
0.0
0.2
0.4
0.6
0.8
1.0

b)

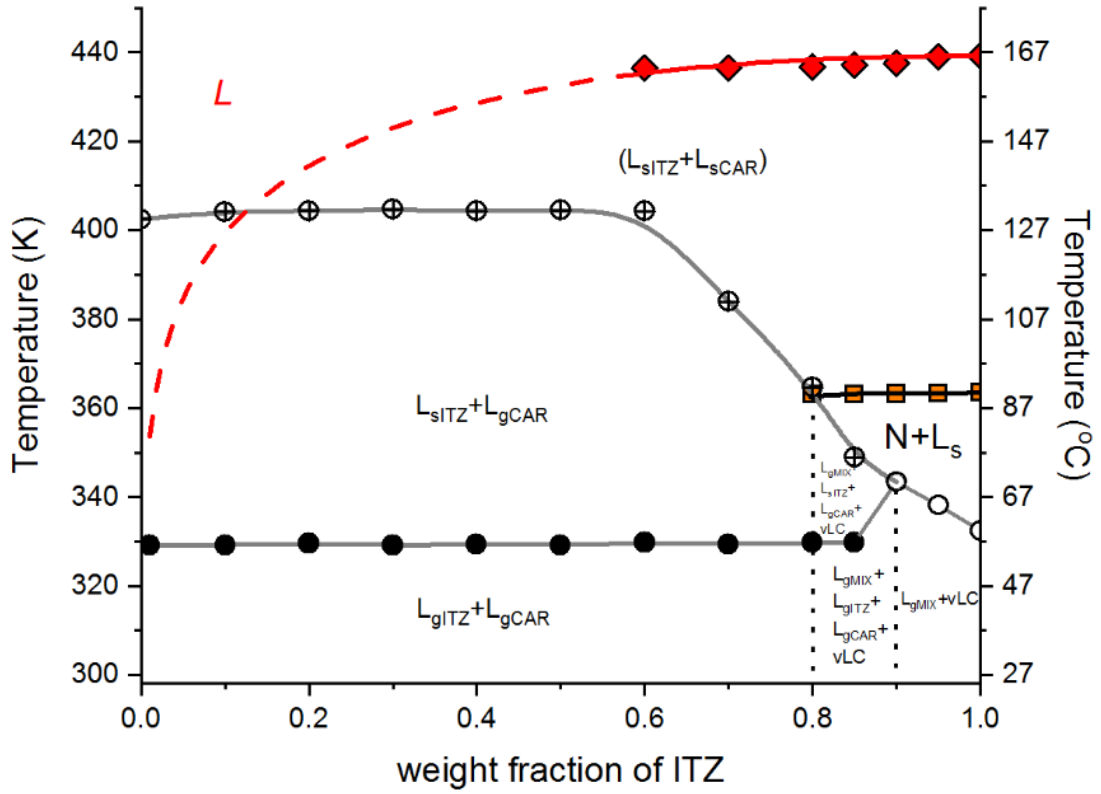

c)

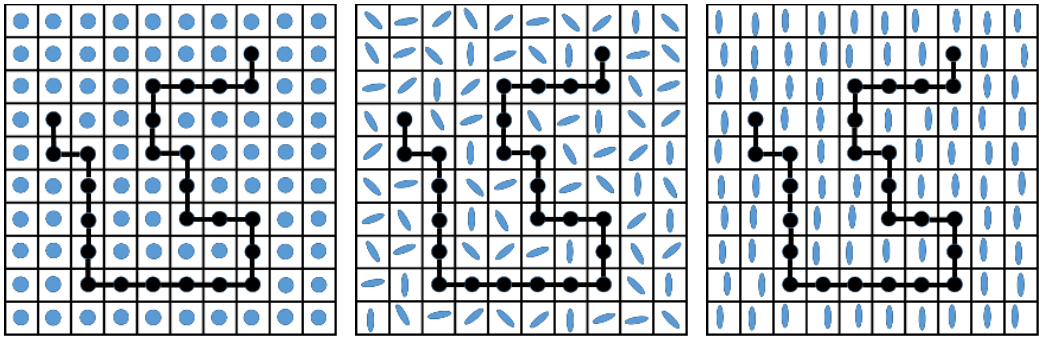

d)

Figure 3.3-7 Phase diagrams for the ITZ/polymer systems: a) ITZ/EUD, b) ITZ/HAS and c) ITZ/CAR. Symbols used: L – liquid, L_g – glass phase (below Tg), L_S – supercooled phase (above T_g), N – nematic, Sm – smectic , vSm – vitrified smectic, vLC – vitrified liquid crystal phase (uncertain identification), ITZ – Iitraconazole, CAR – carbopol and MIX – binary ITZ and CAR mixture. Grey lines through the T_g points (circles) are for visual guide only. Red lines are solid-isotropic (liquid) lines generated by fitting experimental points (diamonds) to the F-H theory, black lines are fitted LC lines (smectic–nematic and nematic-isotropic) to the experimental data (squares) using the F-H and M-S-M theories, while the broken lines indicate prediction beyond the experimental range. d) Schematic representation of polymeric ITZ dispersions with ITZ in an isotropic (left), anisotropic nematic considering an orientation order parameter (middle) and anisotropic smectic considering a one-dimensional translational order parameter (right) arrangements.

3.3.4.2 Solid-Isotropic (Liquid) Line

The solid-liquid lines presented in Figure 3.3-7 are constructed based on the onset temperature of the ITZ melting peak, however there are differing opinions as to whether the onset[92], [177] or endset (offset)[107], [108], [135] temperature of the melting endotherm of the drug better describes the miscibility of the API in the polymer. Thus, in order to compare and provide full information on ITZ miscibility in polymers in this study, both, the onset and endset temperature values for the drug were evaluated. The solid-liquid lines in Figure 3.3-7 represent the best case scenario of two component miscibility, determined on the ability of the melting point of crystalline ITZ to be depressed by the polymer presence.

Reliable DSC results forming the solid-liquid line were obtained only for the systems containing up to 40% w/w polymer. When comparing the data for the onset temperature of the melting event, there was an evident depression of the melting point in comparison with pure ITZ. The onset temperature of melting of pure crystalline ITZ, 166.1 ± 0.2 °C, decreased with an increase in the polymer content as shown in Figure 3.3-7. For instance, at 60% w/w ITZ content, the largest reduction in the onset temperature was observed for the EUD sample, by approximately 3 degrees (163.1 ± 0.2 °C). Smaller decreases, to 163.85 ± 0.2 and 163.3 ± 0.3 °C were recorded for the HAS and CAR samples, respectively. Therefore, considering the melting point depression results, EUD is more likely to be miscible with ITZ than HAS or CAR. No significant difference was observed in relation to the endset values of melting points. The variation in the endset of melting for all systems and at all compositions analysed was not more than ± 0.46 °C from the temperature determined for pure, crystalline ITZ. Table 3.3-1 summarises the values of the interaction parameter (χ) calculated based on Equation 2.3-1 (Chapter2).

Table 3.3-1 Values of the F-H interaction parameter χ for the various ITZ/polymer systems estimated using the H-F theory (solid-isotropic (liquid) lines) and a combination of F-H and M-S-M theories (LC lines).

System	Based on crystalline ITZ (solid-isotropic (liquid) line)		Based on LC ITZ (smectic-nematic line)	Based on LC ITZ – (nematic-isotropic line)
	Onset points	Endset points		
ITZ / EUD	-1.65 ± 0.28	0.71 ± 0.05	0.715 ± 0.02	0.70 ± 0.01
ITZ / HAS	-0.03 ± 0.12	0.65 ± 0.04	0.72 ± 0.04	0.69 ± 0.065
ITZ / CAR	-0.27 ± 0.26	0.67 ± 0.02	N/A	0.59 ± 0.01

As explained in Chapter 1, the sign of χ indicates whether the components in the binary system are miscible or not. For a system with χ<0 a single phase mixture should be favourable for all compositions (miscible system), while for χ>0, the phase separation is most likely to occur (immiscible system). From the endset points of the melting results, only positive values of χ were calculated. This suggests that ITZ and each of the polymers analysed should not be miscible. When the onset temperature values of the melting events were used, the values of χ were generally negative, however considering the standard deviation values (Table 3.3-1) some of them were only marginally negative, meaning that the components might not be fully miscible with the potential of forming not completely molecularly dispersed systems. The most negative value of χ was calculated for the ITZ/EUD system (Table 3.3-1).

The temperature and/or compositional dependence of the interaction parameter χ was also investigated, as if such dependence can be determined, it would allow extrapolation of the solid-liquid line beyond the experimental points, thus be able to predict stability of a miscible blend and determine spinodal and binodal regions of the phase diagram.[107], [134] A number of mathematical models were employed, described in details elsewhere[113], [178], [179], using the following equations:

$$\chi(T) = A + \frac{B}{T} \qquad \text{(Equation 3.3-4)}$$

where A and B are constants related to entropic and enthalpy contributions, respectively.[113]

$$\chi(\phi, T) = \left(A + \frac{B}{T}\right) \cdot (c_1 + c_2 \cdot \phi + c_3 \cdot \phi^2) \qquad \text{(Equation 3.3-5)}$$

where c_1, c_2 and c_3 are adjustable constants allowing to model the compositional dependence of χ.[113], [178]

$$\chi(\phi) = c_1 + c_2 \cdot \phi \qquad \text{(Equation 3.3-6)}$$

where c_1 and c_2 have the same meaning as the parameters used in Equation 3.3-5.

In contrast to other researchers, no “transformation to linearity” [105]–[107], [134] was employed and the whole dataset was fitted with Equations 3.3-4, 3.3-5, and 3.3-6 using the least-square fitting procedure, following the recommendation of Knopp and co-workers[180], who stated that: “From a statistical perspective, the potential of DSC measurements to make miscibility predictions should be examined by deriving an objective function, which results in the unbiased, minimum variance properties of the least-square estimator.” Table 3.3-3 presents the fitting parameters for the ITZ/EUD system as an example. Both datasets, determined from the

onset and endset temperature values of the melting point were used. However, similar to the finding of Knopp et al.[180], the large standard deviations obtained for many of the adjustable parameters prevent an unambiguous description of the solid-liquid line beyond the points measured experimentally and thus a part of the boundary between a fully isotropic and solid ITZ in Figure 3.3-7 in the range of ITZ concentrations 0-60% w/w is marked with a broken line marking uncertainty of the predictions. However, Table 3.3-3 infers that the interaction parameter χ might be dependent on the concentration of ITZ in the blends.

Table 3.3-3 Fitting parameters with standard deviation values as well as relative standard deviation values in parentheses. If the relative standard deviation was larger than 100%, it is expressed as >100%

Equation	Onset temperature values of ITZ melting event (RSD)	Endset temperature values of ITZ melting event (RSD)
Equation 3.3-4	A = -174 ± 38 (22%) B = 74172 ± 16263 (22%)	A = 685 ± 164 (>100%) B = -301846 ± 72488 (>100%)
Equation 3.3-5	A = -50 ± 28246 (>100%) B = 23172 ± $1.3 \cdot 10^7$ (>100%) c_1 = -3.7 ± 2091 (>100%) c_2 = 12.5 ± 7046 (>100%) c_3 = -11.6 ± 6492 (>100%)	A = 129 ± 547128 (>100%) B = -56955 ± $2.41 \cdot 10^8$ (>100%) c_1 = 4.72 ± 32056 (>100%) c_2 = 2.17 ± 15668 (>100%) c_3 = -2.19 ± 3605 (>100%)
Equation 3.3-6	c_1 = 4.50 ± 1.23 (27%) c_2 = -9.63 ± 1.92 (20%)	c_1 = 1.47 ± 0.42 (29%) c_2 = -1.20 ± 0.66 (55%)

3.3.4.3 Liquid Crystalline Phase Separation

The phase diagrams for ITZ/polymers inclusive of LC phases are presented in Figure 3.3-7. Only onset temperature values were taken into considerations. The experimental enthalpy of the LC_{Sm-N} and LC_{N-I} transitions was taken to determine the boundary of the LC phase persistence shown by the broken lines parallel to the y-axis (Figure 3.3-7).

For the ITZ/EUD combination, the smectic phase was determined to be present in the system for ITZ concentration above 60% w/w, while the nematic phase was persistent for ITZ contents above 85% w/w. The interaction parameter χ for the smectic-nematic and nematic-isotropic lines was determined to be 0.715 ± 0.02 and 0.70 ± 0.01, respectively, (Table 3.3-1) suggesting immiscibility of the LC phases with the polymer. These values are close to that calculated for the solid-isotropic line, based on the endset points, which is 0.71 ± 0.05 (Table 3.3-1). In contrast, the LC phases for the ITZ/HAS mixtures were still present at around 50% w/w ITZ, however χ

indicated, again, immiscibility of the API in a liquid crystalline state and the polymer (Table 3.3-1). The ITZ/CAR system only showed one LC phase, nematic, disappearing at ITZ concentrations below 80% w/w. The ITZ nematic phase was immiscible with CAR judging by the interaction parameter of 0.59 ± 0.01 (Table 3.3-1).

The phase diagrams suggest that, depending on the polymer, the LC phase might be present even at a relatively large content of polymer in the binary combination, even up to 50% w/w. The interaction parameters calculated for the smectic-nematic and nematic-isotropic lines were in line with those determined for the solid-isotropic lines based on the endset transition values, implying immiscibility of liquid crystalline ITZ and the polymer studied. Thus, it can be concluded, that in an ITZ/polymer mix, if ITZ is present in a liquid crystalline phase, immiscibility as a result of molecule anisotropy is expected.

3.3.4.4 Glass Transition Temperatures

If some of the liquid crystal dissolves in the polymer matrix, then it will affect the T_g of the polymer.[151] T_g values were measured for the ITZ/polymer blends and presented, excluding the fractions of separated LC ITZ (Figure 3.3-7). For miscible blends, the presence of a single T_g generally indicates that there is a single amorphous phase present. In contrast, the presence of more than one T_g would suggest that more than one amorphous phase is present in the system. However, it needs to be kept in mind that blends showing only one T_g might be an indicator of miscibility achieved kinetically, due to intimate molecular mixing occurring in some of the processes.[181]

Single T_g values were measured for ITZ/EUD and ITZ/HAS at all compositions. For the ITZ/CAR dispersions, single T_g values were recorded at 90% and 95% of ITZ, however between 70% ITZ and 85% ITZ, two T_g values were shown on DSC thermograms. One of these T_g events appeared at a temperature of approximately 57 °C and most likely it corresponds to T_g of ITZ, while the temperature of the other T_g was seen to increase until it reached approximately 131 °C. The presence of two T_g events for ITZ/CAR systems imply a phase separation that is dependent on the API content. At and below 60% of ITZ, two T_g events were noticed, one that was of ITZ and the other of CAR. It was however clear from the phase diagrams (Figure 3.3-7) that no single T_g events should have been detected as at higher ITZ content the samples were phase separated due to the ITZ LC phase content.

Extrapolating only the T_g values for ITZ concentrations where no presence of LC phases was determined to 100% API content, the ITZ T_g values were found to be 46 and 33 °C, for ITZ/EUD

and ITZ/HAS system, respectively. These values show some disparity but are lower than that determined experimentally for the vitrified smectic phase of the drug and perhaps closer to the T_g of “amorphous” ITZ.

3.4 Conclusions

This work, for the first time, presents full phase diagrams for itraconazole/polymer systems showing a great abundance of phases, isotropic and anisotropic, that this drug substance, often used as a model drug substance to study amorphous polymeric solid dispersions, can form. With the phase identification sometimes misinterpreted, as evident from the published literature, this work aimed to systemise the information on disordered itraconazole and show that binary mixtures of this substance with polymers not always are able to form fully disordered systems, however, depending on the itraconazole and polymer ratio, anisotropic, liquid crystalline and phase separated mixtures form. The formation of such liquid crystalline blends is especially evident at high itraconazole to polymer content. The construction of thermodynamic phase diagrams, taking into consideration the presence of smectic and nematic phases, can be considered as a very beneficial guide to predict the correct identity of the phases, of a key relevance to stability and formulation works.

Chapter 4: Phase Diagrams and Thermodynamic Properties of Binary Systems of Itraconazole and Succinic Acid

4.1 Introduction

The aqueous solubility of an API is a significant parameter that controls the rate and extent of drug absorption, thus its bioavailability.[4] Currently, various techniques, as previously described in Chapter 1, have been developed to improve the solubility and dissolution rates of APIs, including physical or chemical modifications of a drug. These techniques involve particle size reduction, amorphisation of drugs, making of solid dispersions (SDs), creation of eutectic mixtures, modification of the crystal habit, cocrystallisation, salt formation, derivatisation and using surfactants.

In 2003, a study was undertaken by Remenar et al. to screen for salts and cocrystals of ITZ using high-throughput crystallisation.[45] There were no salts or cocrystals of ITZ found with monoprotic carboxylic acids, such as acetic and benzoic acid however, new cocrystals of ITZ with fumaric acid, succinic acid, L-malic acid and (L-, D- and LD-) tartaric acid were reported. Interestingly, maleic acid was the only 1,4-dicarboxylic acid tested that did not produce cocrystals with ITZ. Additionally, cocrystallisation of ITZ with malonic, glutaric, and adipic acid was not successful, and it was suggested by the authors that crystallisation of ITZ with 1,4-dicarboxylic acids may be controlled by geometric fit rather than acid-base chemistry. The crystal structure of ITZ cocrystal with succinic acid (SUC) was successfully solved.[45] In the structure of the cocrystal, two antiparallel ITZ molecules form a pocket, which is filled with a succinic acid molecule forming a hydrogen-bonded trimer (Figure 4.1-1). Thus, the stoichiometry of this cocrystal is 2:1 mole/mole in respect to ITZ and SUC.

Dissolution studies on ITZ cocrystals were conducted in 0.1M HCl solution at 25 °C with all successfully produced cocrystals achieving 4 to 20-fold higher concentrations than crystalline ITZ.[45] The solubility of the ITZ and SUC cocrystal (ITZ-SUC) was ~4-fold higher compared to that of ITZ. It was also reported that the ITZ-SUC formed hexagonally-shaped crystalline plates, facilitating easiness to filter and dry to a free-flowing powder.[45]

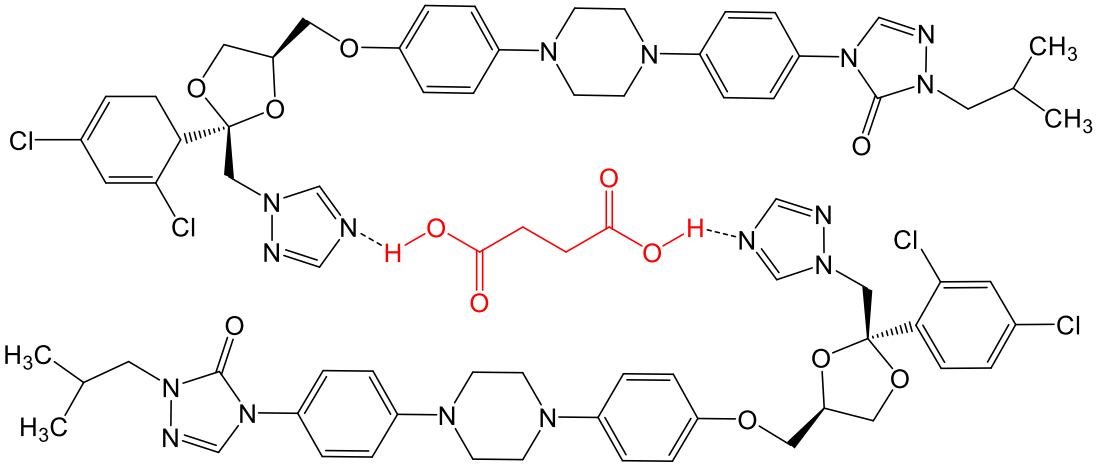

Figure 4.1-1. Chemical structure of ITZ-SUC.

Subsequent to the studies of Remenar et al.[45], Shevchenko and co-workers [182] investigated the potential of the ITZ cocrystal formation with C2-C10 aliphatic dicarboxylic acids. They used solvent-drop grinding and slow evaporation techniques to screen for new products. The authors reported that they were able to successfully synthesise cocrystals of ITZ with dicarboxylic acids containing 2 to 7 carbon molecules. Anhydrous cocrystals of ITZ with malonic, succinic, glutaric and pimelic acids, a cocrystal hydrate with adipic acid, and cocrystal solvates with acetone and tetrahydrofuran for oxalic acid were isolated and characterised. The C8-C10 aliphatic dicarboxylic acids did not produce cocrystals with ITZ and the authors suggested that C7 is the maximum carbon number of the aliphatic dicarboxylic acids chain to produce ITZ cocrystals successfully.[182]

Another study published by Shevchenko et al.[183] reported a synthesis of a new cocrystal of ITZ with malonic acid and two new hydrochloride salts (dihydrochloride and trihydrochloride) of ITZ. The intrinsic dissolution rate (IDR), thermodynamic stability, and hygroscopicity study were performed for the obtained new products and compared to those of the ITZ-SUC. The IDR study was carried out at pH=1.2 at 37 °C. The highest IDR was recorded for both hydrochloric salts of ITZ. The dissolution rate of ITZ-SUC and ITZ-MAL cocrystals were about 11 and 5-fold higher, respectively, than the dissolution rate of the crystalline ITZ. However, the results of this study indicated that the hydrochloric salts of ITZ indeed showed higher intrinsic dissolution rates but were less stable. Both cocrystals, ITZ-SUC and ITZ-MAL, were found to be promising materials for pharmaceutical applications due to their good physical stability in solution and high dissolution rates.

The production of ITZ-SUC using liquid antisolvent and gas antisolvent (GAS) cocrystallisation methods was studied by Courtney and Gupta.[184] These researchers reported the formation

of the ITZ-SUC, however the final product was not pure and contained free ITZ and SUC. The cocrystal samples produced by the both techniques showed broad endothermic events between 145 °C and 165 °C. The authors assumed that these endothermic events were related to melting of the eutectic formed between the residues of uncocrystallised, free pure components followed by melting of the ITZ-SUC. The published differential scanning calorimetry (DSC) thermogram of a 1:1 w/w (equivalent to 1:6 mole/mole) physical mixture of ITZ and SUC [184] showed another endothermic event between 130 °C and 140 °C, which, however, was not discussed by the authors.

Considering the favourable properties of ITZ-SUC and lack of information about the fundamentals of its formation and physicochemical stability, the main aim of this study was to determine these characteristics by constructing a two-component thermodynamic phase diagram to elucidate the possible solid-state (eutectic and cocrystal) phases for the binary mixtures of ITZ and SUC. Thermal analysis, X-ray diffraction and infrared spectroscopy were utilised to understand the interactions between the pure components and to determine the optimum composition of ITZ and SUC for the formation of the various phases. Another aim of this work was to optimise the crystallisation method of ITZ-SUC using acetone as a “green alternative” to the solvents employed to date.

4.2 Materials and Methods

4.2.1 Materials

Itraconazole (ITZ) was donated by Welding GmbH (Hamburg, Germany). Succinic acid (SUC) ACS reagent grade, potassium bromide (KBr) IR grade, and acetone HPLC grade were purchased from Sigma-Aldrich Ireland Limited.

4.2.2 Methods

4.2.2.1 Preparation of Physical Mixtures

Physical mixtures of ITZ and SUC were prepared in mole:mole ratios as 20:1, 12:1, 10:1,8:1, 6:1, 5:1, 4:1, 3:1, 2:1, 3:2, 1:1, 2:3, 1:2, 1:3, 1:4, 1:5, 1:6, 1:8, 1:10, 1:12, and 1:20. All physical mixtures of the ITZ and SUC were prepared by weighing the exact quantities of ITZ and SUC powders to obtain a total weight of 200 mg of each physical mixture. The analytical balance Mettler Toledo MT5 (Schwerzenbach, Switzerland) was used to accurately weight the ITZ and SUC, then the weighted powders were gently mixed using an agate mortar and pestle. Prepared samples were stored in a desiccator over silica gel at 5 ˚C until use.

4.2.2.2 Fast - Evaporation Crystallisation

Fast-evaporation crystallisation experiments were carried out using a Rotavapor R-210 (Buchi, Switzerland) equipped with a vacuum controller V-850 (Buchi, Switzerland), a vaccum pump V-700 (Buchi, Switzerland) and a water bath B-491 (Buchi, Switzerland) using conditions stated below.

Preparation of ITZ-SUC

The ITZ-SUC was synthesised from an acetone solution. A quantity of 1 mmol of SUC (118 mg) was dissolved in a 500 ml round bottom containing 250 ml of HPLC grade acetone at room temperature. Afterwards, 2 mmol of ITZ (1411 mg) was added to the SUC solution and dissolved over a water bath at 50 °C. Once a clear solution was obtained, the solvent was removed, under a vacuum of 350 mbar at 50 °C until approximately 10 ml of acetone was left in the flask. The precipitated crystals were filtered using a paper filter and dried in air at room temperature for approximately 24 hours. The sample was then stored in a desiccator over silica gel at 5 ˚C until use.

Preparation of the eutectic (E_1) composition

A quantity of 20 mmol of SUC (2362 mg) was dissolved in a 500 ml round bottom flask containing 250 ml of HPLC grade acetone at room temperature. Afterwards, 1 mmol of ITZ (705 mg) was added to the SUC solution and dissolved over a water bath at 50 °C. The solvent was removed, under a vacuum of 350 mbar at 50 °C, until approximately 50 ml of acetone was left in the flask. Then the flask was closed with a glass stopper and left to stand at room temperature for 24 hours. The produced crystals were filtered using a paper filter and dried in air at room temperature for approximately 24 hours. The collected crystals were stored in a desiccator over silica gel at 5˚C until use.

Preparation of the eutectic (E_1) composition by fast evaporation to dryness

To prepare the E_1 phase, an amount of 0.45 mmol of SUC (52.6 mg) was dissolved in a 100 ml round bottom flask containing 50 ml of HPLC grade acetone at room temperature. Afterwards, 0.2 mmol of ITZ (141.1 mg) was added to the SUC solution and dissolved over a water bath at 50 °C. The solvent was removed to dryness, under a vacuum of 350 mbar at 50 °C. The collected crystals were stored in a desiccator over silica gel at 5˚C until use.

4.2.2.3 Slow - Evaporation Crystallisation

The slow-evaporation crystallisation experiments were performed using HPLC grade acetone as a solvent. A quantity of 0.2 mmol of ITZ (141 mg) and an appropriate amount of SUC was used to obtain 2:1, 1:1 and 2:1 molar mixtures of ITZ and SUC. The mixtures were dissolved in 25 ml of acetone over a water bath at 50 °C with continuous stirring. Afterwards, each solution was filtered using a 0.45 µm PTFE membrane filters (VWR, USA) to 50 ml glass vials and covered with a perforated parafilm to allow for slow solvent evaporation at room temperature. Once the formation of crystals was observed, the excess of solvent was removed, and crystals were dried in air at room temperature for approximately 24 hours. The collected crystals were stored in a desiccator over silica gel at 5˚C until use.

4.2.2.4 Differential Scanning Calorimetry (DSC)

DSC was performed using a PerkinElmer Diamond DSC as described in Chapter 2.

All samples for DSC experiments were initially heated to 200 °C at a heating rate of 10°C/min (first heating). They were cooled down to 25 °C at a heating rate of 300 °C/min and reheated again to 200°C (second heating) at a heating rate of 10°C/min. For the phase diagram construction, temperatures of the invariant points were determined as onset temperature of

the transition, while the temperature of the liquidus effects (LIQ) was recorded as midpoint temperature of the transition. All experiments were performed in duplicate.

4.2.2.5 Powder X-ray Diffraction (PXRD)

PXRD was performed as described in Chapter 2.

The melted physical mixtures of ITZ and SUC with mole/mole ratios of 2:1, 1:1 and 1:2 that were prepared for PXRD analysis as follows: about 100 mg of physical mixtures, prepared as described in Section 4.2.2.1, was placed on a microscope glass slide and melted at 200 °C in an oven type UL 40 (Memmert, Germany). When the powdered mixtures were fully melted, the samples were allowed to cool down at room temperature and were first visualised using the polarising optical microscope as described in Section 4.2.2.4, then gently removed from the microscope glass slides and analysed by PXRD.

4.2.2.6 Polarised Light Microscopy and Hot Stage (PLM-HS)

PLM-HS experiments were performed using equipment described in Chapter 3.

The hot stage ramp, for thermomicroscopic investigations, was performed from 25 to 200 °C using a heating/cooling rate of 10 °C/min. Samples for PLM-HS experiments were placed on a microscope glass slide and covered with a glass coverslip.

4.2.2.7 Solid-State Fourier Transform Infrared Spectroscopy (FT-IR)

FT-IR analysis were performed as described in Chapter 3.

4.3 Results and Discussion

4.3.1 Determination of ITZ and SUC Thermodynamic Phase Diagram

A simple eutectic mixture made up of two components that are miscible in the liquid state, however immiscible in the solid state was described in Chapter 1. Such a system does not interact to form a new compound (cocrystal) as shown in the thermodynamic diagram presented in Figure 1.3-1 (Chapter 1). However, a case when a two compounds A and B can react to form a third compound (cocrystal) C is also possible. If the cocrystal C is stable in the liquid state and does not decompose upon melting (congruent melting), the phase diagram will look like shown in Figure 4.3-1.[185]

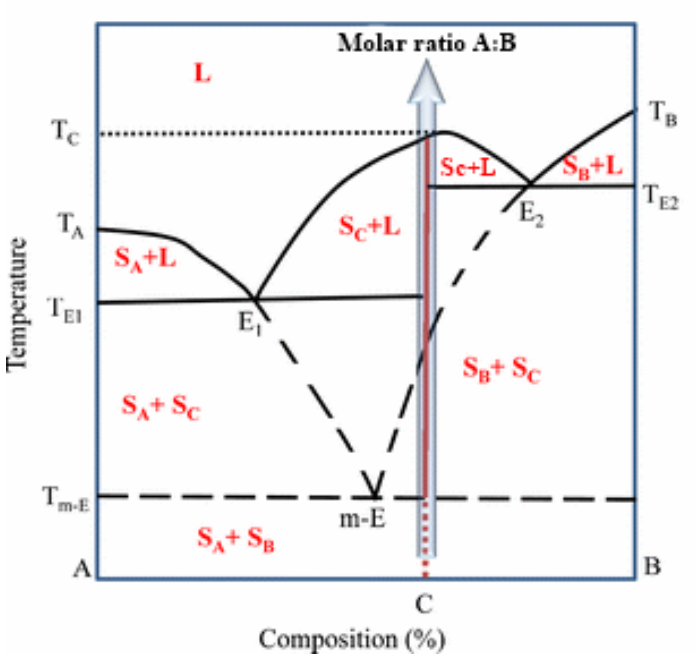

Figure 4.3-1 Binary phase diagrams of congruently melting system, capable of cocrystal formation. Where L - liquid; S_A - solid of component A; S_B - solid of component B; S_C – solid of cocrystal; E -eutectic point; m-E is metastable eutectic point; Tm-E is metastable eutectic temperature; T_E - eutectic temperature; T_A - melting temperature of component A; T_B - melting temperature of component B; T_C-melting temperature of cocrystal. Reproduced from [185]

The phase diagram in Figure 4.3-1 has two eutectic points. It resembles two simple phase diagrams like Figure 1.3-1 (Chapter1) placed side by side. Therefore, the eutectic phase E_1 is composed of compound A and cocrystal, while E_2 is composed of cocrystal and compound B. As shown in Figure 4.3-1 when a physical mixture of a molar ratio A:B is heated, it melts at the metastable eutectic temperature (Tm-E), forming a cocrystal which then melts at the melting

point (Tc).[185] In general, when the DSC is used, the molecular compound formation is indicated by the consecutive appearance of endothermic and exothermic peaks.[186] In the congruent melting system, the DSC curve should show an endothermic peak corresponding to melting of the m-E followed by an exothermic peak associated with the cocrystal formation. Another endothermic peak related to cocrystal melting should also be observed. [185], [187]

The thermal behaviour of physical mixtures of ITZ and SUC, prepared as per Section 4.2.2.1, and of the pure components of ITZ and SUC was investigated by DSC (Figure 4.3-2) in order to construct the thermodynamic phase diagram of ITZ and SUC shown in Figure 4.3-3. The phase diagram was constructed by plotting the melting temperatures obtained from DSC analysis from the first heating, versus ITZ molar composition (Figure 4.3-3). The theoretical liquidus curves (the dashed black lines) were calculated using the Schroeder-van Laar equation (Equation 4-1)[188] and Prigogine-Defay equation (Equation 4-2)[189]:

$$\frac{1}{T_x} = \frac{1}{T_m} - \frac{R}{\Delta H_m} \ln x \qquad \text{(Equation 4-1)}$$

$$\frac{1}{T_x} = \frac{1}{T_{ITZ-SUC}} - \frac{R}{\Delta H_{ITZ-SUC}} \{\ln[x_{ITZ}^2\ (1 - x_{ITZ})] - \ln[(2/3)^2\ (1/3)]\} \qquad \text{(Equation 4-2)}$$

where x is the molar ratio of one of the pure components, x_{ITZ} is the molar ratio of ITZ; T_x is the liquidus temperature of the corresponding mixture, ΔH_m and T_m are the heat of fusion and the melting points of either of the pure compounds, respectively. The $T_{ITZ\text{-}SUC}$ and $\Delta H_{ITZ\text{-}SUC}$ are experimental results of melting temperature and the heat of fusion of ITZ-SUC produced by fast-evaporation crystallisation method (Section 4.2.2.2). The experimental melting and eutectic point values (T_m) and enthalpies of fusion (ΔH_m) of the pure components, ITZ-SUC and eutectic composition E_1 (as discussed later) are presented in Table 4.3-1

Table 4.3-1 Thermal data for ITZ, SUC, ITZ-SUC and eutectic composition E_1, where T_m and ΔH_m are the melting temperature and the heat of fusion, respectively.

	T_m (°C)	T_m (K)	ΔH_m (J·g^{-1})
ITZ	167.5 ± 0.09	440.6 ± 0.09	83.86 ± 1.82
SUC	187.8 ± 0.15	461.0 ± 0.15	293.74 ± 7.64
ITZ-SUC	160.6 ± 0.07	433.7 ± 0.07	86.37 ± 3.73
E_1	150.5 ± 0.18	423.7 ± 0.18	88.09 ± 0.05

For the pure ITZ and SUC starting materials, only one melting peak on the DSC curve was observed for each compound, at 167.5 ± 0.09 and 187.8 ± 0.15 °C, respectively (Figure 4.3-2 and Table 4.3-1).

For the physical mixtures of ITZ and SUC, depending on composition, several peaks were detected, representing different points on the constructed phase diagram (Figure 4.3-3). For samples with the composition ranging 0.05 < *x* (ITZ) < 0.33, three endothermic peaks were recorded. The first peak at a constant temperature of about 133 °C is related to a metastable eutectic phase (m-E). The second peak, also at a constant temperature of about 148 °C was interpreted as of eutectic phase E_1. This eutectic phase is formed not between ITZ and SUC, but the ITZ-SUC and SUC, as concluded from Figure 4.3-3. The third peak corresponds to the liquidus effect (LIQ) of SUC, and its position was in a good agreement with the theoretical liquidus curve on the phase diagram, as determined by Equation 4-1 (Figure 4.3-3). It was possible to evaluate the LIQ effect for the SUC component for ITZ composition only up to *x*(ITZ)=0.14 and only these points are included in the phase diagram shown in Figure 4.3-3.

The composition of *x*(ITZ)=0.4 also showed three endothermic peaks corresponding to m-E, E_1, and LIQ and an exothermic peak. A small increase in melting temperature of m-E, from 132.7 to 134.1 °C of was noticed. The composition of *x*(ITZ)=0.5 appeared to be an intermediate composition between the eutectic phase E_1 and another phase, referred to as E_2 (Figure 4.3-2). The E_2 was ascribed to a eutectic phased and composed of ITZ-SUC and ITZ. For samples with compositions ranging 0.60 < *x* (ITZ) < 0.95, the E_2 peak position was recorded at a constant temperature at about 157.1 °C. Samples with compositions ranging 0.88 < *x* (ITZ) < 0.95, the E_2 peak position was recorded at a constant temperature at about 157.1 °C. The m-E peak followed by the exothermic peak were visible for compositions ranging 0.05 < *x* (ITZ) < 0.86.

To summarise, the constructed diagram based on DSC studies of ITZ and SUC physical mixtures suggests the formation of ITZ-SUC with a stoichiometry of 2:1 and melting at 157.6 °C. The phase diagram shows that three eutectic phases can be identified. A metastable eutectic phase (m-E, T_m= 132.8 ± 0.22 °C), a stable eutectic phase composed of ITZ-SUC and SUC (E_1, T_m= 147.9 ± 0.08 °C) and another stable eutectic phase made by ITZ-SUC and ITZ (E_2, T_m= 157.1 ± 0.28 °C).

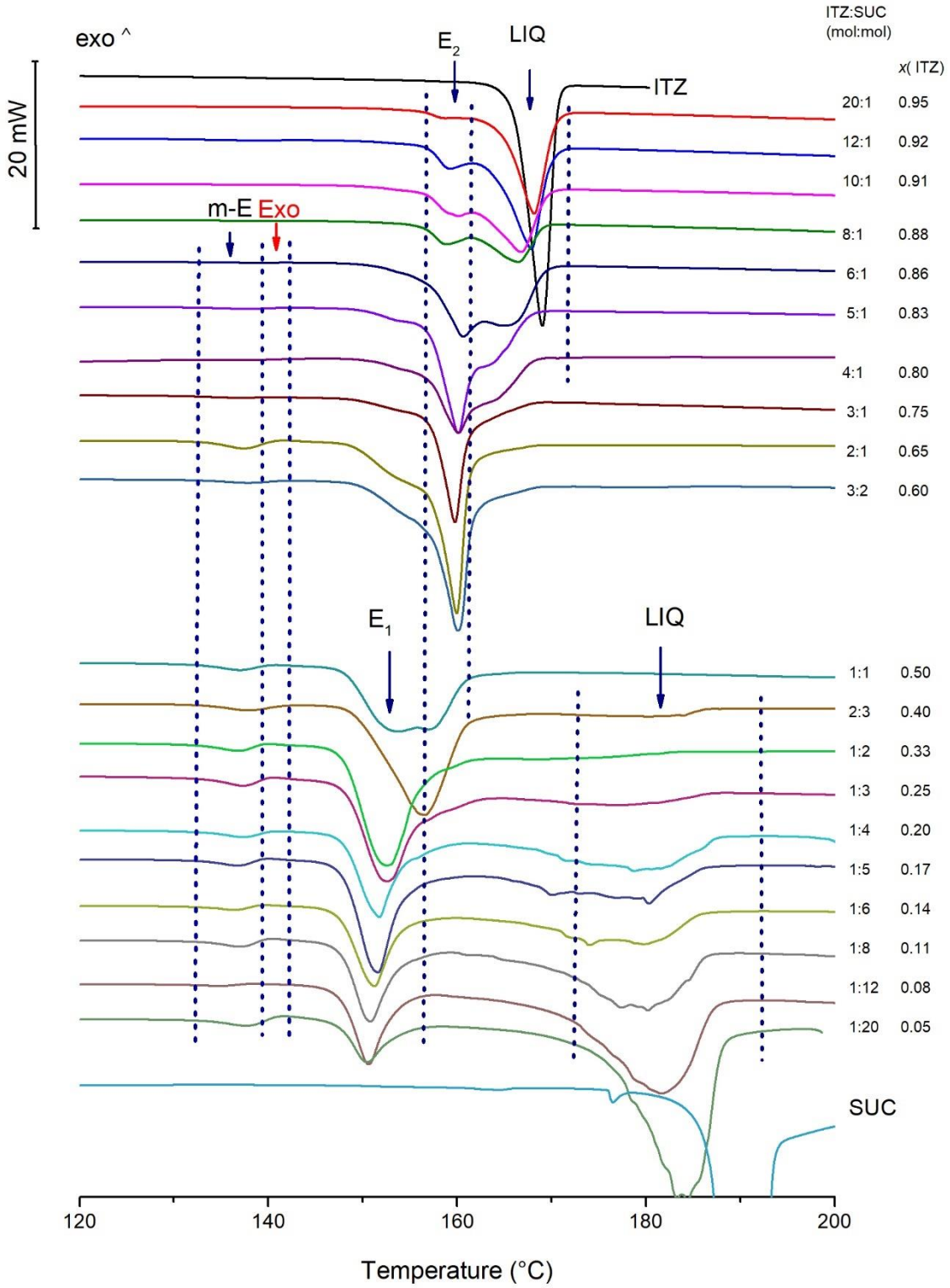

Figure 4.3-2. DSC thermograms of pure ITZ, SUC and physical mixtures of ITZ and SUC. The ITZ content in each physical mixture is given beside corresponding DSC curve and is shown as the molar ratio of ITZ to SUC and as total ITZ molar content in the mixture: x(ITZ). The dashed, solid vertical lines are drawn to guide the eye.

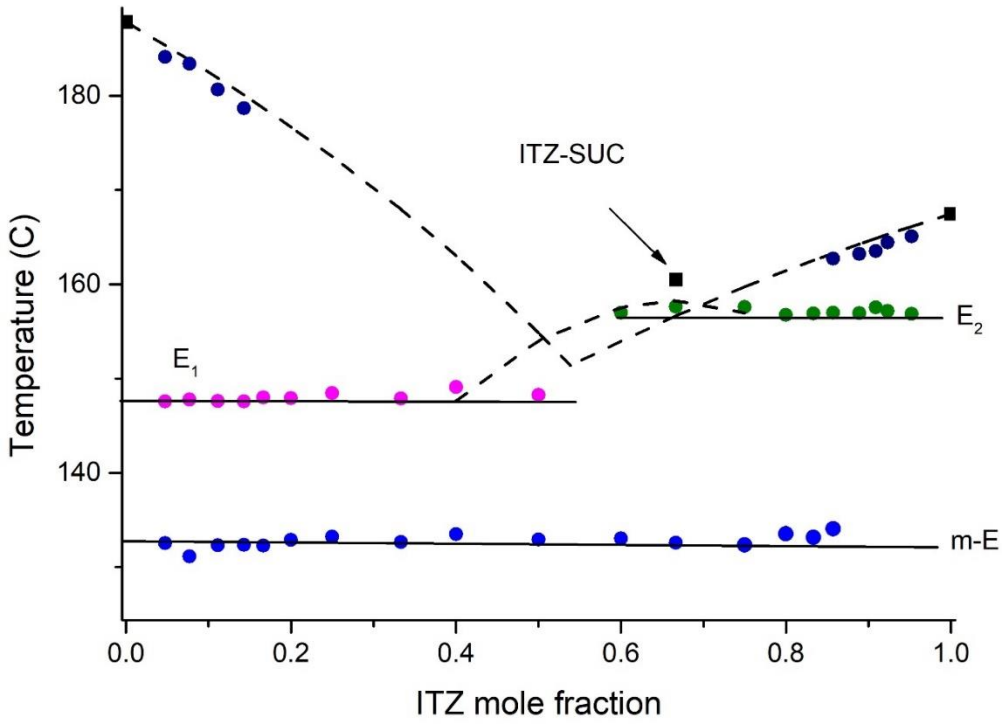

Figure 4.3-3. The binary phase diagram of ITZ and SUC. The dashed black lines represent the theoretical liquidus curves. The experimentally determined points for the liquidus curves are shown as dark blue dots (●). The experimentally determined points for eutectic lines are shown as pink dots (●), green dots (●), and light blue dots (●) for E_1, E_2, and m-E respectively. The black squares (■) are the experimental onset results of the pure compound melting endotherm. The black solid horizontal lines are drawn to guide the eye.

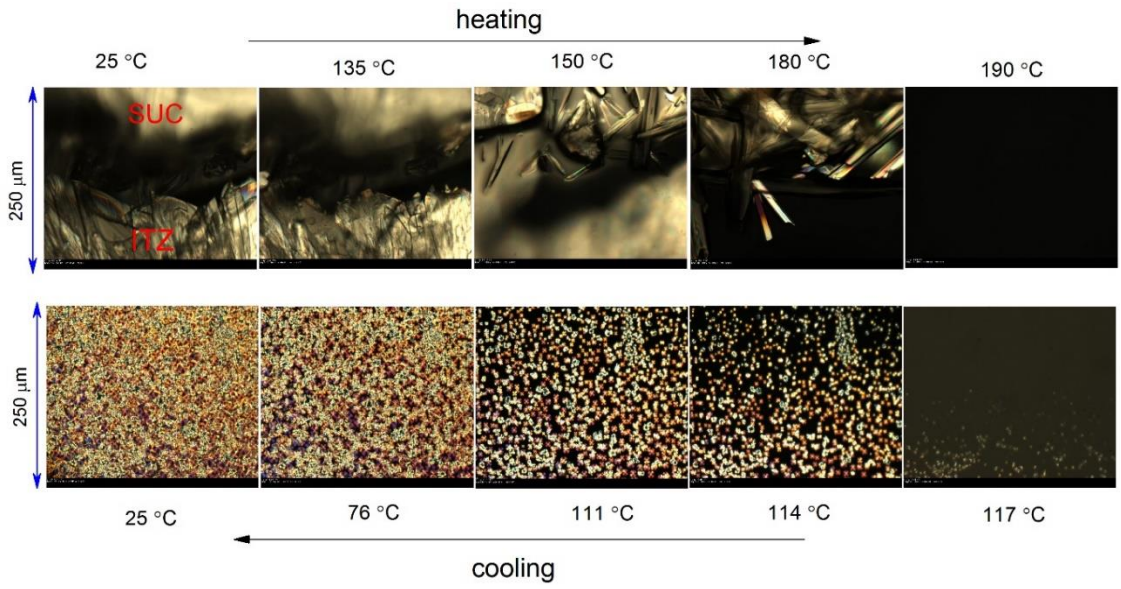

Figure 4.3-4 PLM-HS analysis of ITZ and SUC crystals placed beside each other, during a heating/cooling cycle, at a heating rate of 10 °C/min.

Figure 4.3-4 shows the behaviour of ITZ and SUC crystals, placed side by side on a microscope slide, during a heating/cooling cycle at a rate of 10 °C/min. On heating, the first noticeable change on the ITZ side was observed at about 135 °C, corresponding to the m-E transition recorded by DSC (Figure 4.3-2). Further changes were visible during the heating cycle up to 190 °C. These conversions corresponded to transitions recorded by DSC for physical mixtures of ITZ and SUC. Above 190 °C, the analysed sample was fully melted. During the cooling stage, the first change was observed at about 117 °C when first crystals, in apparent spherulitic forms appeared. These spherulites continued to grow as the sample continued to be cooled and entirely covered the observed part of the microscope slide (Figure 4.3-4). When the cooling cycle to 25 °C was completed, different parts of the sample were investigated (Figure 4.3-5). Even though it was not possible to identify the observed phases, this experiment showed that the formation of new phase(s) upon heating a physical mixture of ITZ and SUC is apparent. Figure 4.3-5a show the SUC-rich side of the slide moving to Figure 4.3-5f showing the ITZ-rich part. The differences between the crystalline structures, seen on the images in Figure 4.3-5a, and Figure 4.3-5b, are noticeable. Images in Figure 4.3-5c, and Figure 4.3-5d, most likely, represent the mixing zone between ITZ and SUC. The crystals visible in this zone can be described as spherulites. The images in Figure 4.3-5e, and Figure 4.3-5f are on the ITZ-rich side.

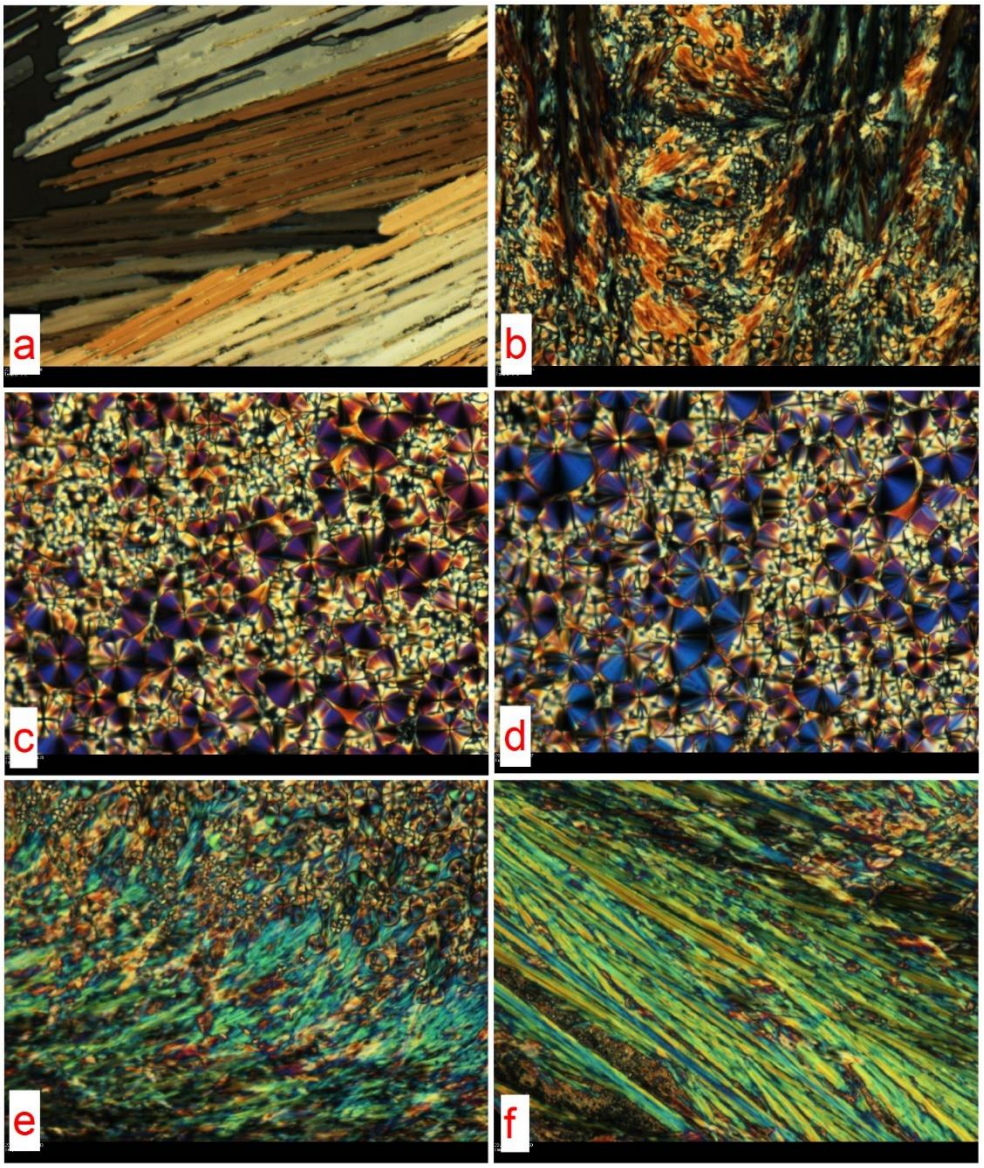

Figure 4.3-5 Microscopic images at RT, after PLM-HS analysis on ITZ and SUC crystals, were completed. Different parts of the microscope slide are shown in the ascending order a-b-c-d-e-f, where a, corresponds to SUC side, f, represents ITZ side, c and d, are assigned to middle section.

4.3.2 Crystallisation of pure binary ITZ/SUC phases

4.3.2.1 Slow-Evaporation Crystallisation

Following construction of the full ITZ/SUC binary phase diagram and identifying a number of phases, crystallisation experiments from a solvent system were conducted. Pharmaceutical cocrystals are mainly produced by solvent based crystallisation such as slurry, evaporation, antisolvent addition, and solvent based techniques including grinding and melt extrusion. Grinding and slow evaporation from solutions of cocrystal components with stoichiometric compositions are generally the most used methods to produce cocrystals.[190]–[192]. A slow

evaporation method was utilised by Shevchenko et al. [182] when investigating the ITZ potential for cocrystal formation with aliphatic dicarboxylic acids. The authors reported using a mixture of tetrahydrofuran (THF) with chloroform with a solution of ITZ in chloroform and a solution of SUC in THF prepared separately due to solubility differences between ITZ and dicarboxylic acids in organic solvents. ITZ is highly soluble in chloroform (363 mg/ml), while dicarboxylic acids have high solubility in THF (>100 mg/ml). Solutions of ITZ and SUC were mixed in 20 mL glass bottles to obtain 1:1 and 2:1 molar mixtures of ITZ and SUC, respectively. Nonappa et al.[193] also synthesised ITZ-SUC by slow evaporation using a mixture of three solvents, consisting of 1,2-dichloroethane, ethyl acetate and 1,4-dioxane (10/2/1 v/v/v). A mixture of ITZ and SUC in a 2:1 mole:mole ratio was dissolved in 15 ml of the solvents mixture, resulting in ITZ concentration of 13.3 mg/ml. Both published methods were reported to be successful in the cocrystal synthesis. However, the solvents used during the above processes are considered undesirable, and belong to the hazardous materials group, according to the pharmacopoeia classification and Pfizer Medicinal Chemistry Solvent Selection Guide[194], [195]. Therefore, in the current method of ITZ-SUC cocrystallisation, acetone was chosen as a “green alternative”.

Figure 4.3-6 presents the DSC thermograms and PXRD traces of the crystalline materials yielded by slow crystallisation experiments. The DSC and PXRD results indicate that these attempts were unsuccessful in the synthesis of pure ITZ-SUC, and a mixture of ITZ, ITZ-SUC and eutectic (E_1) was produced. These results could be explained by the difference in solubility of ITZ and SUC in acetone (ITZ is very soluble in acetone and solubility of SUC is reported to be 27 mg/ml[196]) leading to the crystallisation of a mixture of the ITZ-SUC and ITZ.[197], [198]

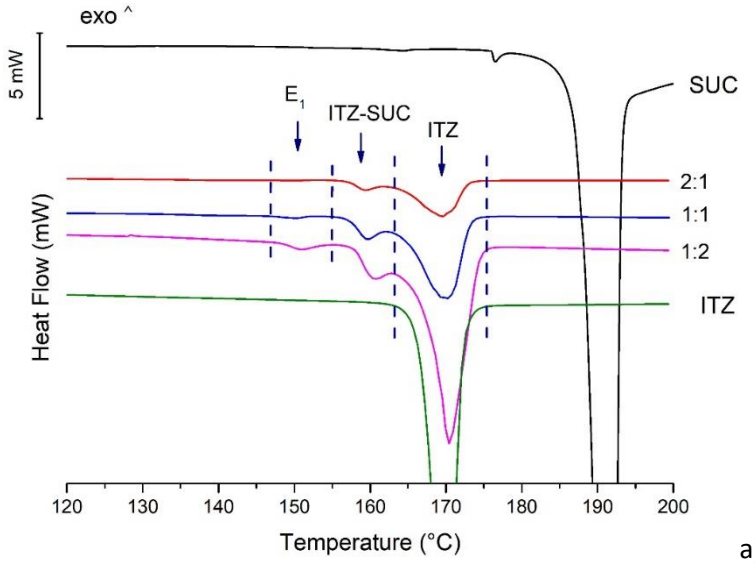

a)

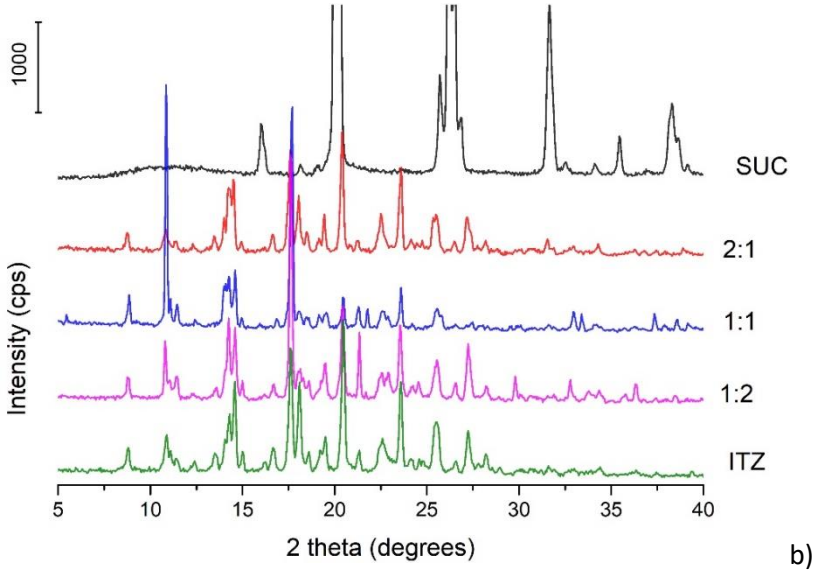

Figure 4.3-6 a) DSC thermograms and b) PXRD results of ITZ, SUC and crystalline material obtained from slow evaporation experiments (section 4.2.2.3), where 2:1, 1:1 and 1:2 is the molar composition of ITZ and SUC.

4.3.2.2 Fast - Evaporation Crystallisation

Considering the limited success of the slow evaporation method, fast solvent evaporation, described in Section 4.2.2.2, was then used in efforts to optimise the production of ITZ-SUC from acetone. At first, the experiments included ITZ to SUC molar ratios of 3:1, 2:1, 1:1, and 1:2. It was discovered that the ITZ to SUC molar ratio concentration played a significant role during crystallisation process. Figure 4.3-7 shows the DSC thermograms and PXRD traces of samples obtained from the fast solvent evaporation method using different molar ratios of ITZ and SUC. The PXRD spectra did not show any differences between samples, identifying only ITZ-SUC phase. However, as it can be seen on the DSC thermograms, that the pure ITZ-SUC was only synthesised when an ITZ to SUC molar ratio of 3:1 or 2:1 was used. The 1:1 combination resulted in an impure ITZ-SUC as evidenced by the presence of the eutectic form (E_1). Samples of ITZ to SUC mixed in the 1 to 2 mole ratios also produced an impure ITZ-SUC. However, the peak area corresponding to the eutectic form (E_1) increased when compared to the sample obtained from the 1:1 molar concentration crystallisation experiment. The DSC thermogram of samples from this experiment are shown in Figure 4.3-7a. It has been reported that crystallisation of a molecular complex can be directed by decreasing solubility of this complex. To generate the supersaturation required for cocrystal formation the components of the cocrystal should be added to solutions in excess of the stoichiometric composition.[199]

The above statement may also apply to the synthesis of the pure E_1 form. The molar ratios of ITZ to SUC of 1:10 and 1:20 were investigated. As described in Section 4.2.2.2, acetone was removed from the crystallisation mixture, however not to dryness. The amount of acetone left in the flask after evaporation was further modified. The crystalline materials were then collected and analysed by DSC and PXRD. The pure E_1 form was produced when the ITZ to SUC molar ratio of 1:20 was used with approximately 50 ml of acetone left in the flask after evaporation.

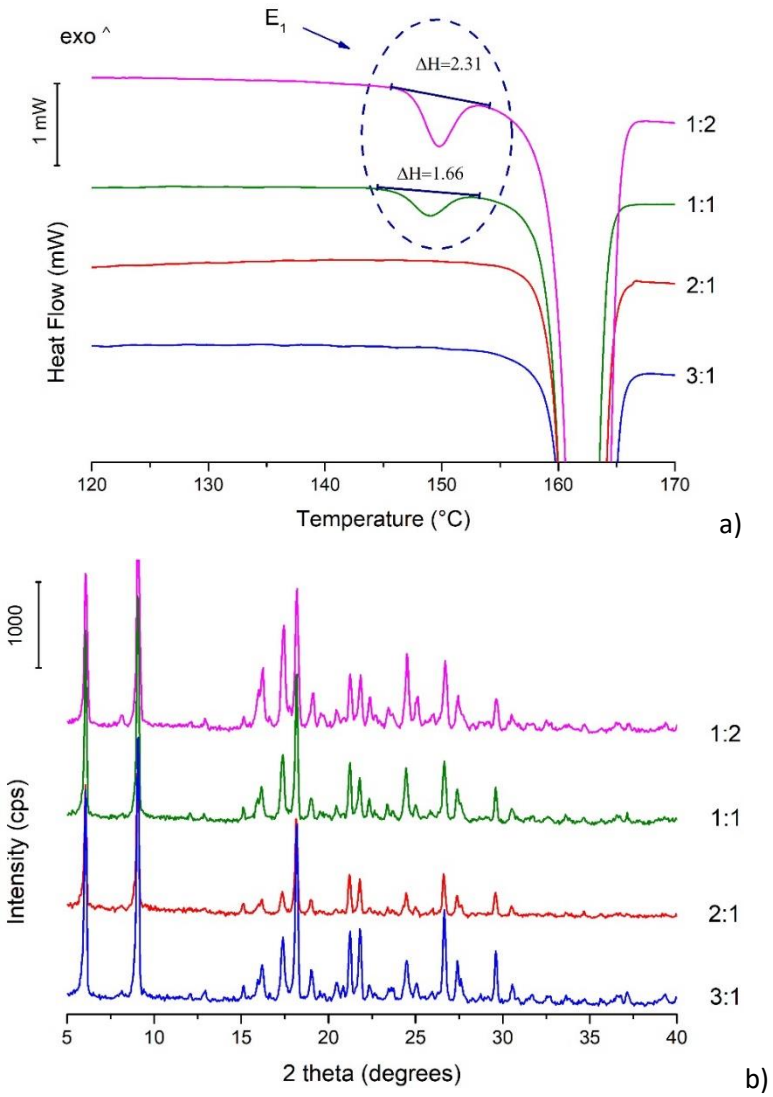

Figure 4.3-7 DSC thermograms (a) and PXRD spectra (b) obtained from fast solvent evaporation method (Section 4.2.2.2), where 2:1, 1:1 and 1:2 is the molar composition of ITZ and SUC.

Sample A shown in Figure 4.3-8 corresponds to the molar ratio of ITZ to SUC of 1:20 (mol/mol) when about 20 ml of acetone was left in the flask after evaporation. The first peak at 150 °C corresponds to the E_1 and the second peak is related to the excess of SUC in the sample (Figure

4.3-8a). The sample A was then washed with water which resulted in “washing out” SUC from the eutectic form and producing an almost pure ITZ-SUC. The characteristic, sharp peaks at 2Θ=19.97° and 2Θ=26.22° corresponding to SUC, are not present after the second wash (Figure 4.3-8b). The intensity of the peak at 2Θ=31.59°, corresponding to SUC, was significantly reduced after the first wash. The liquid phase from the water wash was collected and evaporated to dryness at RT. The obtained residue was then identified by DSC and PXRD as SUC (data not shown).

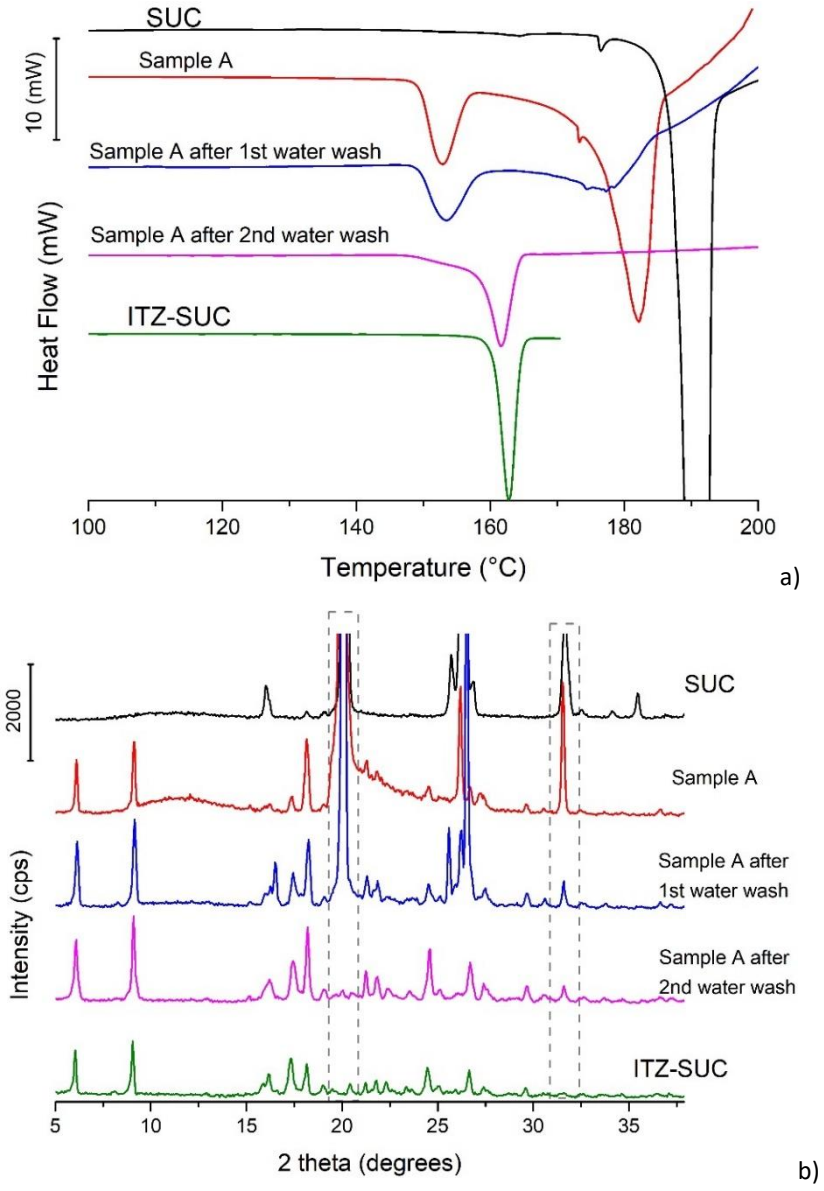

Figure 4.3-8 a) DSC thermograms and b) PXRD results of Sample A from crystallisation experiment described in Section 4.2.2.2. The dashed grey boxes show the position of the two characteristic SUC peaks at 19.97°, 26.22°, and 31.59° 2Θ.

4.3.3 Physicochemical properties of ITZ-SUC and eutectic form E_1

The XRPD pattern of the pure ITZ-SUC produced by the method described in Section 4.2.2.2 matches well the trace calculated based on the single crystal data (CSD Mercury, REWTUK) shown in Figure 4.3-9. The melting point of ITZ-SUC was recorded at 160.5 ± 07 ºC (Figure 4.3-10a).

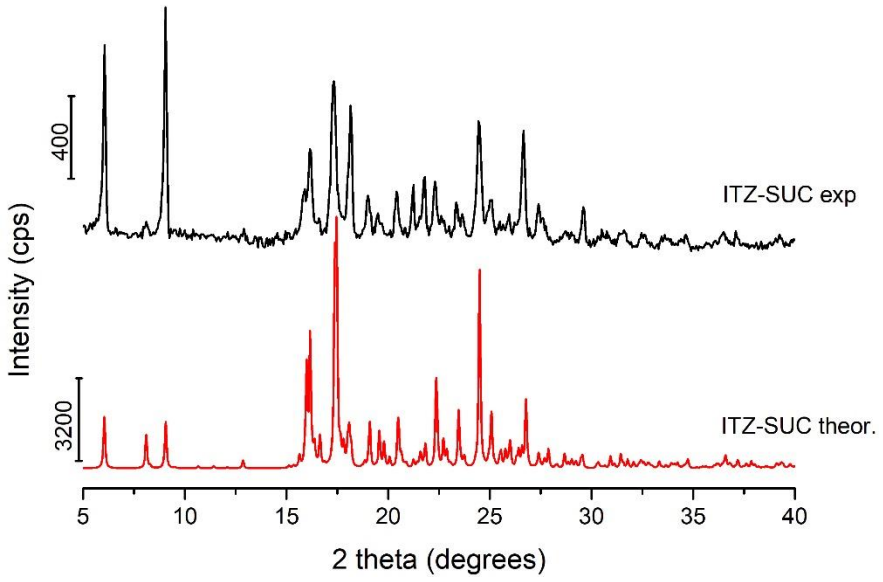

Figure 4.3-9 The XRPD pattern of TZ-SUC produced by this fast evaporation method and corresponding theoretically calculated PXRD pattern.

The E_1 was produced by fast crystallisation method as described in Section 4.2.2.2 and Section 4.3.2.2. The melting temperature was recorded at 150.5 ± 16 ºC (Figure 4.3-10a). The PXRD spectra of E_1 is shown in Figure 4.3-10b. Presence of characteristic peaks corresponding to SUC and peaks corresponding to ITZ-SUC suggests formation of E_1, composed of ITZ-SUC and SUC, the β form of the acid. Peaks corresponding to SUC were recorded at 19.97°, 26.22°, and 31.59° 2Θ and peaks corresponding to ITZ-SUC at 6.10°, 9.05°, and 18.21° 2Θ. The microscopic images if ITZ-SUC and E_1 are shown in Figure 4.3-11. The crystalline sample of E_1 shows similar hexagonal crystal shape as seen for ITZ-SUC crystals.

The fast crystallisation method described in Section 4.2.2.2 and Section 4.3.2.2. was successful in preparation of E_1 phase. However, one may argue about reproducibility of this method. Therefore, a fast evaporation to dryness, described in Section 4.2.2.2, was also applied to produce E_1 form. The exact concentration of both pure components (ITZ and SUC) that was used in the experiment was predicted from the Tamman plot (Section 4.3.4). In this method ITZ and

SUC were dissolved in acetone and then the solution was evaporated to dryness. The collected powered material was confirmed as E_1 by DSC and PXRD. One melting peak was recorded at 148.2 °C (data not shown). The PXRD spectra showed characteristic peaks corresponding to SUC at 19.97°, 26.22°, and 31.59° 2Θ and peaks corresponding to ITZ-SUC at 6.10°, 9.05°, and 18.21° 2Θ (data not shown).

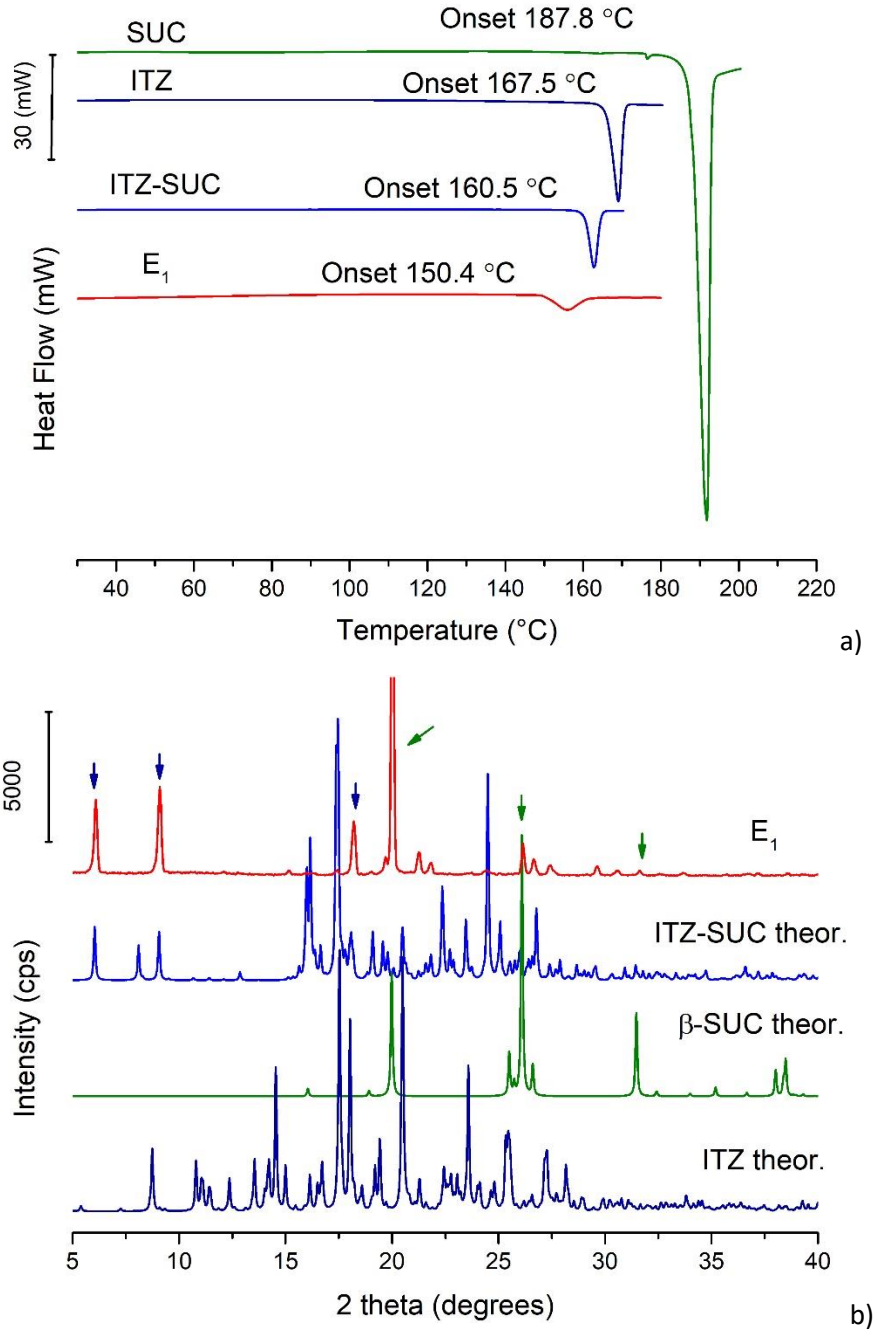

Figure 4.3-10 DSC thermograms (a) and PXRD results (b) of pure ITZ, SUC, ITZ-SUC and E_1. The navy and green arrows show the position of peaks corresponding to ITZ-SUC and β-SUC, respectively.

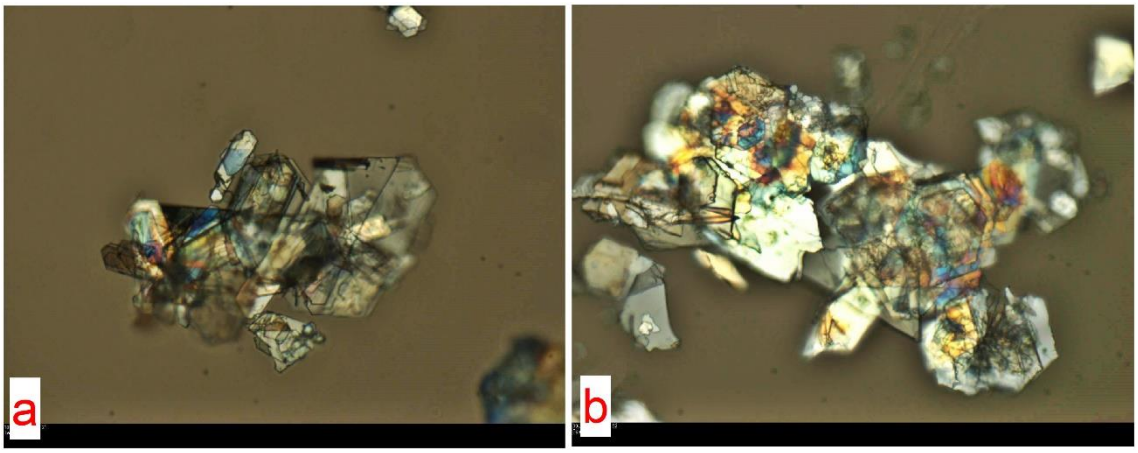

Figure 4.3-11 Microscopic images at RT, of ITZ-SUC (a) and E_1 (b) crystals.

The FT-IR spectrum of pure ITZ shows characteristic peaks at 3069, 2967, 2878 and 2824 cm^{-1} assigned to –CH stretching. A sharp peak occurring at 1700 cm^{-1} is due to a C=O stretching vibration. Peaks at 1614 and 1451 cm^{-1} correspond to C-N and C=N stretches, respectively. The peaks observed at 1554, 1511 and 825 cm^{-1} may be of aromatic C=C bending. The peak at 1381 cm^{-1} can be attributed to the C-H bending of the methyl group. Peaks observed at 1229 and 1041 cm^{-1} could be the result of C-O stretching. The FT-IR spectrum of SUC shows peaks at 2632, and 2538 cm^{-1} assigned to the OH stretching band. The C=O stretching appears at 1731 $cm^{-1,}$ and is shown as a doublet due to neighbouring chain vibrations. The C-O stretching and OH bending vibrations are coupled and appear at 1420 and 1310 cm^{-1}. Two peaks at 1201 and 1177 cm^{-1} are assigned to CH_2 wagging and CH_2 twisting vibrations, respectively. The OH out-of-plane bending vibration correspond to peak at 910 $cm^{-1.}$ The peak at 893 cm^{-1} is assigned to the antisymmetric C-C stretching vibration, and the peak at 803 cm^{-1} is related to the CH2 rocking vibrations. The peaks at 637 and 544 cm^{-1} correspond to O-C=O deformation vibration and C=O out-of-plane bending, respectively.[200]

ITZ-SUC is made by two antiparallel ITZ molecules which form a pocket filled by SUC molecule. The SUC is connected to the 1,2,4,-triazole group of ITZ by hydrogen bond. [45], [182], [193] Generally, when hydrogen bond is formed with either the carbonyl oxygen (HO-C=**O**), or the hydroxyl hydrogen (**H**O-C=O), the C=O stretching frequency is downshifted.[201] The peak corresponding to C=O group in the FT-IR spectra of SUC at 1731 cm^{-1} was shifted to 1711 cm^{-1} in the ITZ- SUC spectrum suggesting the H –bond formation between ITZ and SUC (Figure 4.3-12). There were no differences observed between spectra of E_1 and ITZ-SUC spectra (Figure 4.3-13).

However, this is not surprising as E_1 is composed of ITZ-SUC and SUC and most likely the concentration of pure SUC in E_1 phase is below the detection limit.

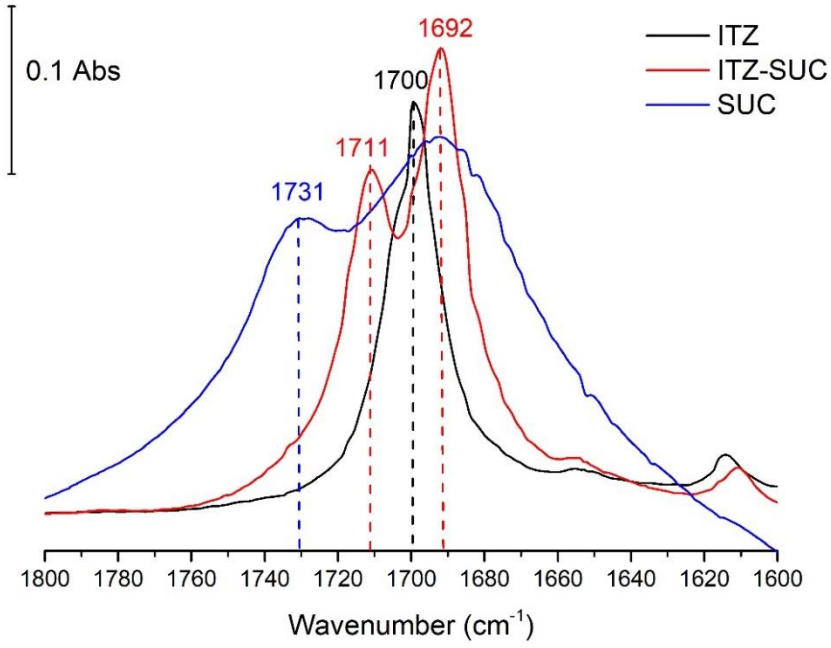

Figure 4.3-12 The carbonyl region of FT-IR spectrum of pure ITZ, SUC, and ITZ-SUC.

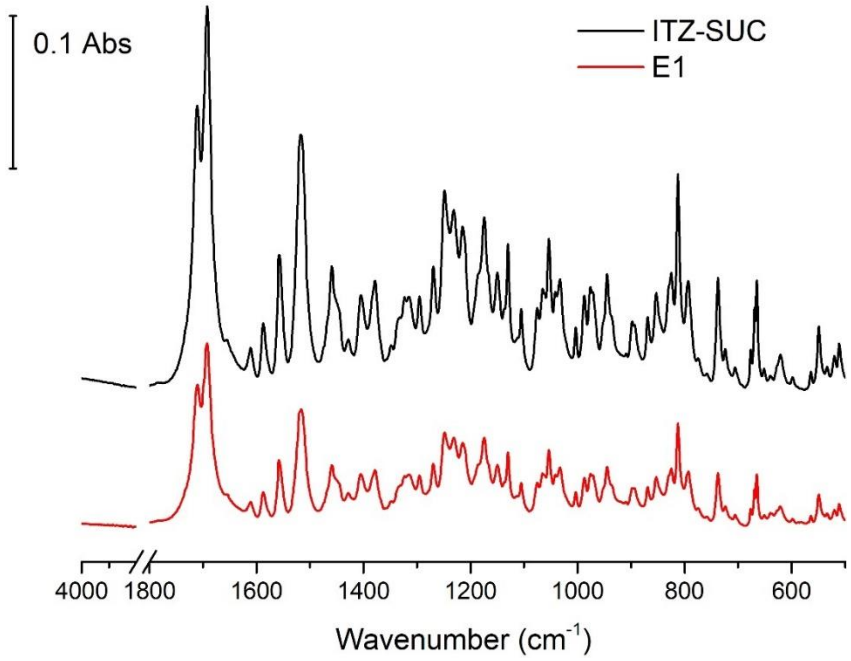

Figure 4.3-13 FT-IR fingerprint regions of ITZ-SUC and E_1.

4.3.4 Second heating

The thermal behaviour of ITZ, SUC, and physical mixtures of ITZ and SUC during second heating, after very rapid cooling of the melts, is shown in Figure 4.3-14. This thermal treatment was chosen to determine if the samples are able to supercool and possibly form disordered phases. The thermodynamic phase diagram of ITZ and SUC based on the results from second heating was constructed by plotting the melting temperatures obtained from DSC analysis, versus ITZ-SUC molar composition (Figure 4.3-15). The theoretical liquidus curves (the dashed black lines) were calculated using the Schroeder-van Laar equation (Equation 4-1)[188] and Prigogine-Defay equation (Equation 4-2).[189]

The sample of pure ITZ showed a T_g at 59 °C, followed by two endothermic LC transitions peaking at 75 °C (LC_{N-I}), and 91 °C (LC_{Sm-N}) (Chapter 3). The melting peak of SUC was observed at 188.3 °C. For the physical mixtures of ITZ and SUC, depending on the composition, several endothermic and exothermic peaks were detected.

For samples of the composition range $0.92 < x$ (ITZ) < 0.95, one small endothermic event, corresponding to the LC_{Sm-N} transition was observed at around 94 °C. The LC_{N-I} transition however was not detected.

The samples of the composition range $0.80 < x$ (ITZ) < 0.91 had two endothermic peaks. The first peak was at about 92 °C and therefore it was assigned to the LC_{Sm-N} transition. The second peak at 151 °C is related to eutectic phase E_2, formed between ITZ and ITZ-SUC.

For samples of the composition range $0.60 < x$ (ITZ) < 0.75, one exothermic and one endothermic event were recorded. The crystallisation peak was observed at 107.7 °C, 103.3 °C, and 100.8 °C for x (ITZ) of 0.75, 0.65, and 0.60, respectively. The endothermic peak was shown at 153.2 °C, 155.0 °C, and 154.2 °C for x (ITZ) of 0.75, 0.65, and 0.60, respectively, and characteristic of the E_2 phase.

The composition of x (ITZ) = 0.50 can be taken as an intermediate composition as both eutectic phases, E_2 and E_1, were detected by DSC. The endothermic peak at 142.8 °C corresponded to the eutectic E_1 phase formed between SUC and ITZ-SUC. The endothermic peak recorded at 150.4 °C was assigned to the eutectic E_2 phase. For this composition two exothermic peaks were recorded, at 38.5 °C and 93.7 °C (Figure 4.3-14).

The samples of the composition of x (ITZ) = 0.40, and x (ITZ) = 0.33 showed two exothermic peaks and one endothermic peak. The first exothermic peak was recorded at 35.6 °C and 38.2 °C for samples of x (ITZ) = 0.4, and x (ITZ) = 0.33, respectively. The second exothermic event peaked at

88.0 °C and 85.6 °C for samples of composition *x* (ITZ) = 0.40 and *x* (ITZ) = 0.33, respectively. The endothermic peak corresponding to eutectic E_1, was recorded at 143.6 °C for both of the compositions, *x* (ITZ) = 0.40 and 0.33. Two peaks were recorded for the sample containing *x* (ITZ) = 0.25, an exothermic peak at 90.4 °C and an endothermic peak at 143.0 °C.

For the samples of the composition range 0.11 < *x* (ITZ) < 0.20, one exothermic and two endothermic events were recorded. The crystallisation peak was detected at about 89 °C. The first endothermic peak, related to the formation of the E_1 phase, was recorded at a constant temperature at about 140.8 °C. The second endothermic peak, with a characteristic tail shape, corresponds to LIQ effect (Figure 4.3-14). The samples of the composition of *x* (ITZ) = 0.08 and *x* (ITZ) = 0.05 had two endothermic peaks. The first peak corresponds to the E_1 phase was recorded at 134.5 °C for (ITZ) = 0.08 and at 130.0°C for (ITZ) = 0.05. The second endothermic peak is related to the LIQ effect.

To summarise, the $LC_{Sm\text{-}N}$ transition was observed for the composition of 0.8 < *x* (ITZ) < 1. The E_1 phase was recorded for samples of the composition of 0.05 < *x* (ITZ) < 0.50. As shown in the diagram in Figure 4.3-15, the temperature corresponding to the E_1 phase decreased from about 143 °C to 130 °C, indicating a non-eutectic behaviour. The E_2 phase was recorded for samples of the composition of 0.50 < *x* (ITZ) < 0.91 and shows the formation of ITZ-SUC with a stoichiometry of 2:1 that melts at 155.0 °C. The exothermic event at about 38 °C was detected only for the samples of *x* (ITZ) = 0.50, 0.40, and 0.33.

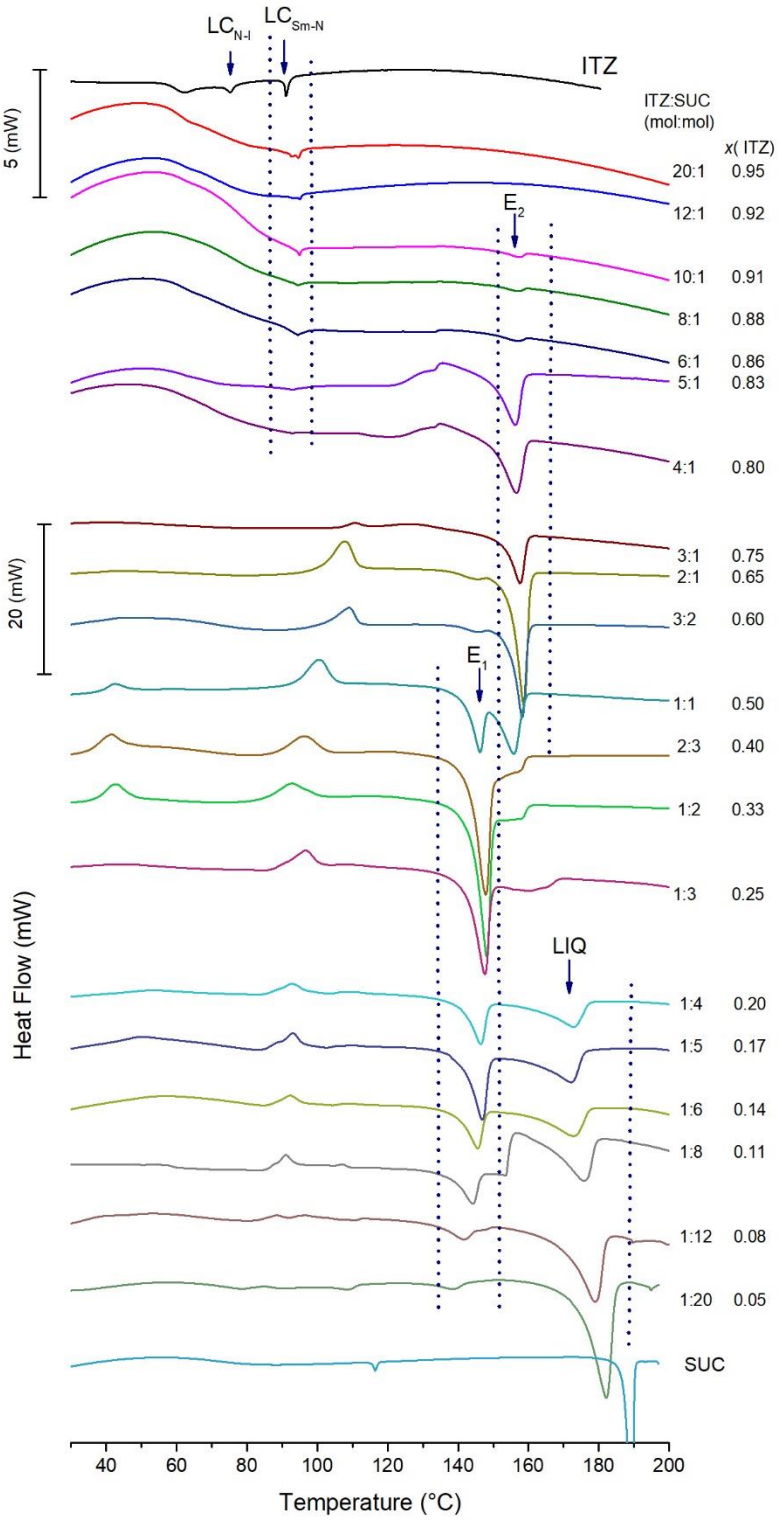

Figure 4.3-14 DSC thermograms during second heating of pure ITZ, SUC and physical mixtures of ITZ and SUC. The ITZ content in each physical mixture is given beside corresponding DSC curve and is shown as the molar ratio of ITZ to SUC (mol/mol) and as total ITZ molar content in the mixture: *x*(ITZ). The dashed, solid vertical lines are drawn to guide the eye.

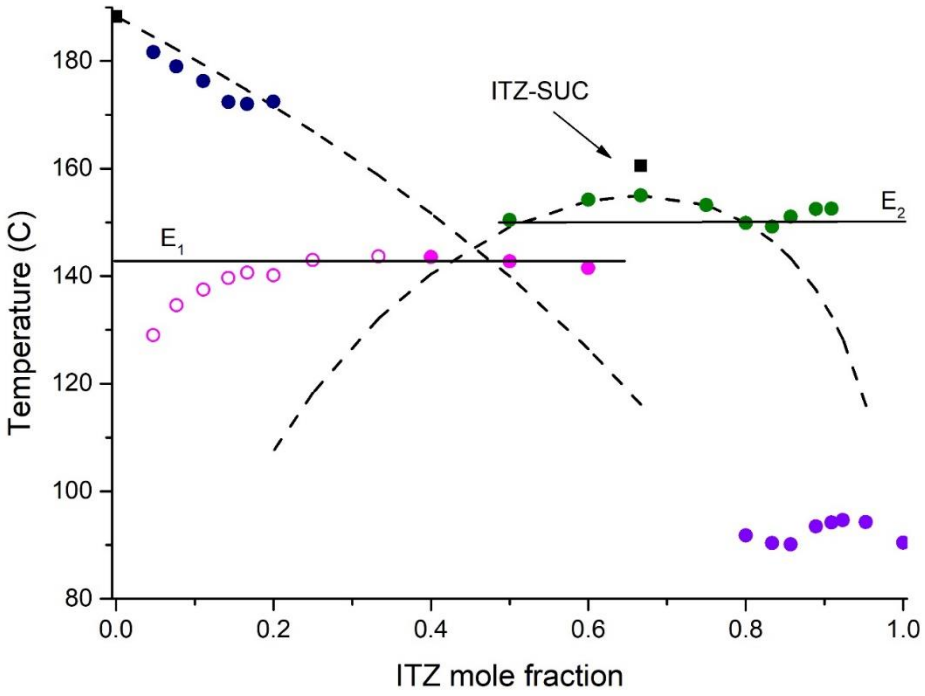

Figure 4.3-15 The binary phase diagram of ITZ and SUC (for second heating results). The dashed black lines represent the theoretical liquidus curves. The experimentally determined points for the liquidus curves are shown as dark blue dots (●). The experimentally determined points for eutectic lines are shown as pink dots (●), and green dots (●) for E_1 and E_2 respectively. The pink circles (○) correspond to compositions, for which the polymorphic transition of β-SUC into α-SUC was observed. The violet dots (●) represent the experimentally obtained points of LC_{Sm-N} transition. The black squares (■) are the experimental onset results of the pure compound melting endotherm. The black solid horizontal lines are drawn to guide the eye.

The molar composition of the E_1 phase obtained from the Tamman plot is shown in Figure 4.3-16. The constructed Tamman diagram was based on the DSC results from the second heating and was obtained by plotting the melting enthalpy of the eutectic phases versus ITZ molar composition. The composition of E_1 was found at the apex of the triangle and was determined to be *x* (ITZ) = 0.31 and x (SUC) = 0.69. The composition of the E_2 phase was found to be very close to ITZ-SUC composition and was *x* (ITZ) = 0.67 and x (SUC) = 0.33. Interestingly, the experimental enthalpies related to LC_{Sm-N} transition plotted against ITZ composition also formed a triangle with the apex at x (ITZ) = 0.87.

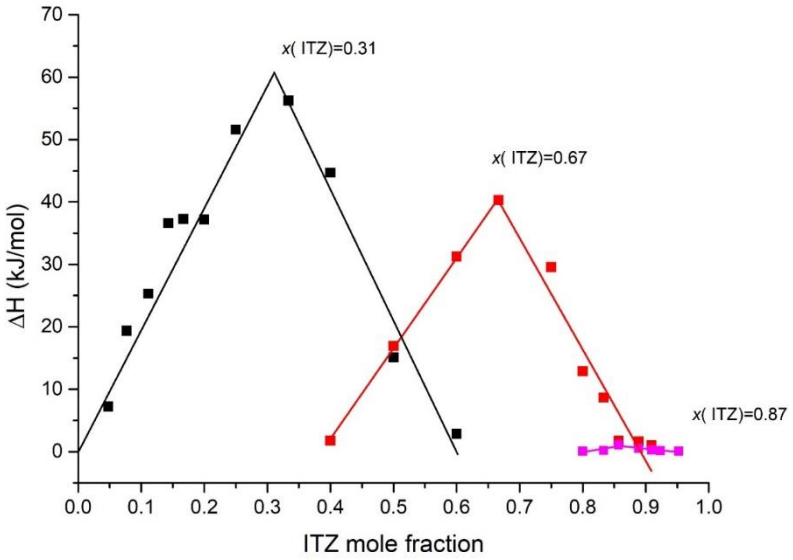

Figure 4.3-16 Tamman plot for ITZ and SUC system. The black squares (■) are the experimental melting enthalpies of E_1. The red squares (■) are the experimental melting enthalpies of E_2, and the pink squares (■) are the experimental enthalpies related to $LC_{Sm\text{-}N}$ transition.

The phase diagram constructed from the first and second heating steps suggested a new phase formation between ITZ and SUC with a stoichiometry of 2:1, a cocrystal, with melting at 157.6 °C. However, the melting temperature of this cocrystal was found to be very close to the melting temperature of eutectic E_2 phase of about 157.1 °C. To investigate it further the physical mixtures of ITZ and SUC at molar ratios of 2:1, 1:1, and 1:2 were analysed by PXRD and PLM-HS. Samples for PXRD analysis were prepared as per Section 4.2.2.5 and the results are shown in Figure 4.3-17.

SUC is known to crystallise in two polymorphic forms, α and β. The β polymorph is stable and commercially available, and it was the polymorphic form used to prepare the physical mixtures analysed in this work. The form α is reported to be metastable at room temperature and stable only above 137 °C.[202]–[206] The two polymorphic forms can be easily distinguished by their PXRD pattern and the powder diffraction patterns of α and β polymorphic forms of SUC, calculated based on the single crystal data (CSD Mercury, SUCACB07 and SUCACB06), are shown in Figure 4.3-17. The physical mixtures of ITZ and SUC in molar ratios of 2:1, 1:1, and 1:2, first melted and cooled down as described in Section 4.2.2.5, showed two characteristic peaks of ITZ-SUC at 6.08° and 9.04° 2θ. The peak corresponding to the β-SUC polymorph was found at 20.01° 2θ for the three compositions. However, the characteristic peaks corresponding to the α-SUC polymorph at 22.02°, 26.20°, 27.11 and 32.21° 2θ were clearly visible in the PXRD spectra of the 1:2 melted physical mixture of ITZ and SUC. This indicates a polymorphic transition of β-SUC to

α-SUC in this mixture upon rapid heat treatment. Thus, the peak of the E_1 phase shifting to the lower temperatures is most likely due to the presence of α- SUC. The E_1 phase is formed between β-SUC and ITZ-SUC and partial replacement of β-SUC by α- SUC may lead to the formation of a different solid state phase.

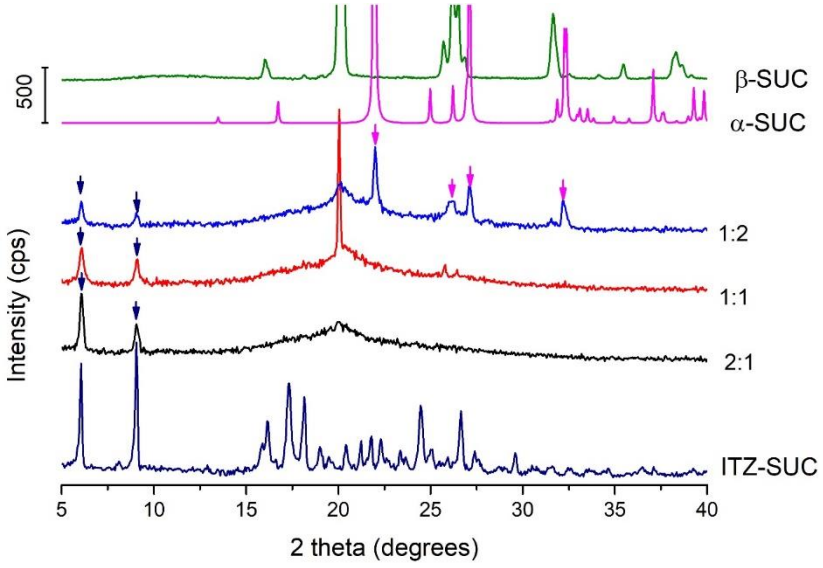

Figure 4.3-17 The XRPD pattern of physical mixtures of ITZ and SUC with 2:1, 1:1 and 1:2 molar ratio of ITZ and SUC, which were melted and cooled to room temperature, and theoretically calculated PXRD patterns of α and β polymorphic forms of SUC. The navy and pink arrows are showing the position of peaks corresponding to ITZ-SUC and α-SUC, respectively.

The microscopic images of physical mixtures, melted and cooled down to room temperature, of ITZ and SUC in molar ratio 2:1, 1:1, and 1:2, prepared as per Section 4.3.2.3 are shown in Figure 4.3-18. All three samples were found to be crystalline. Interestingly, only the 1:2 mixture of ITZ and SUC shows crystals grown into characteristic spherulitic shapes (Figure 4.3-18c).

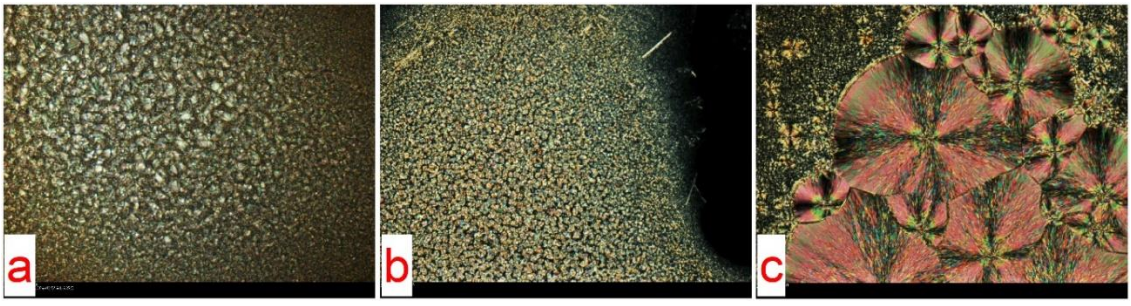

Figure 4.3-18 Microscopic images at RT, of melted and cooled to room temperature physical mixtures of ITZ and SUC, where a, b, and c correspond to 2:1, 1:1, and 1:2 molar composition of ITZ and SUC, respectively.

4.4 Conclusions

The behaviour of binary mixtures of ITZ and SUC was investigated and analysed using thermal analysis, X-ray diffraction and infrared spectroscopy. Two thermodynamic phase diagrams were constructed based on the DSC results from the first and second heating. The phase diagram constructed from the results of the first heating, suggested a new phase formation with a stoichiometry of 2:1 of ITZ and SUC (ITZ-SUC). Furthermore, three eutectic phases were identified as: a metastable (m-E, T_m= 132.8 ± 0.22 °C), a stable eutectic phase composed of ITZ-SUC and SUC (E_1, T_m= 147.9 ± 0.08 °C) and another stable eutectic phase made by ITZ-SUC and ITZ (E_2, T_m= 157.1 ± 0.28 °C). The phase diagram constructed from the results of the second heating, confirmed formation of ITZ-SUC. The composition of E_1 and E_2 phases were determined from the Tamman plot. The E_1 mixture was produced by crystallisation from acetone solution and its identity confirmed by DSC and PXRD analysis. A new crystallisation method of ITZ-SUC using acetone as a "green alternative" to the solvents used by other researchers was optimised. The formation of another polymorphic form of SUC, the α form, was observed upon flash cooling of the melted ITZ and SUC mixtures for samples with prevalent SUC content.

Chapter 5: Solid State Characterisation and Solubility Behaviour of Itraconazole–Succinic Acid and Itraconazole–Succinic Acid-Polymer Systems

5.1 Introduction

As previously discussed in Chapter 1, itraconazole (ITZ) is a BCS II compound. Its aqueous solubility is extremely low and pH-dependent. Many marketed drugs, including other antifungal azoles, are weak bases or weak acids and show pH-dependent solubility. An approach that can be utilised to improve solubility of such actives is to formulate them with acidic (for basic drugs) or basic (for acidic drugs) excipients to create a favourable pH-microenvironment and thus enhance bioavailability of drugs. A desirable release profile should be pH independent to resist the pH changes occurring in the gastrointestinal tract (GIT).[207] Thoma and Ziegler [208] reported that succinic acid (SUC) improved fenoldopam dissolution at higher pH-values. Tatavarti and Hoag[209] described that adding malic acid into the formulation resulted in creating of microenvironmental pH to and led to pH-independent release of trimethoprim.[209] Streubel et al.[210] investigated the effect of addition of organic acids such as fumaric, SUC or adipic acid into the drug-polymer system on drug release. They reported that the release of verapamil hydrochloride from tablets composed of ethylcellulose (EC) or methylcellulose acetate succinate (HPMC) and mentioned above, organic acids were found to be pH-independent.[209] The resent study published by Parikh et al.[211] involved preparation of amorphous solid dispersions (ASDs) of ITZ with weak organic acids, including glutaric, tartaric, malic and citric acid. They reported that in the presence of these acids the solubility and dissolution rate of ITZ was greatly enhanced.[211]

In addition to small organic acids, polymers can also be suited to manipulate microenvironmental pH. Tatavarti and Hoag[209] described that incorporation of the enteric polymer Eudragit L100-55 into matrix tablets, consisting of pH-dependent drug (trimethoprim) and hydroxypropyl methylcellulose (HPMC), lead to a marginal release enhancement in the simulated intestinal fluid (SIF) media. They noted that the effect of the enteric polymer on drug release was related to the pH modulation exerted by the polymer. Miller et al.[124] investigated ternary ASDs of ITZ in Eudragit L 100-55 containing either 20% or 40% Carbopol® 974P produced by hot melt extrusion. They reported that addition of 20% Carbopol 974P reduced the acid phase release at 2 h and retarded ITZ release following the acid-to-neutral pH change. The maximum ITZ release was reported to occur occurring 30 min after the pH change. However, the duration of supersaturation was substantially improved.[124]

Having investigated the miscibility of ITZ with acidic polymers in Chapter 3 and interactions of ITZ with SUC, which can also be employed as a microenvironmental pH-modifier, in Chapter 4, the work in this Chapter concentrates on investigating if a combination of changing the solid

state of ITZ (amorphisation) and pH-modification can enhance ITZ solubility. As discussed in detail in Chapter 1, amorphisation can increase the apparent solubility of drugs.

The most common techniques of preparation of amorphous solids follow the thermodynamic pathway (e.g. melt quench method) or the kinetic pathway (e.g. milling method).[51] Preparation of disordered ITZ by the melt quench method is described in Chapter 3. Preparation of disordered ITZ via kinetic pathway was also reported[51] [212] Grobelny et al.[212] studied amorphisation of ITZ by inorganic pharmaceutical excipients. The dissolution study conducted in SGF (pH 1.2) at 37 °C showed solubility improvement for both milled and melt-quenched ITZ. However, the dissolution of melt-quenched ITZ was slow with only 75% dissolved at 2 h. Based on the above, amorphisation by milling was selected as the process of choice.

In relation to SUC being able to increase solubility of ITZ, literature accounts show the values for the cocrystal form (details on the formation and physicochemical characterisation of this cocrystal can be found in Chapter 4). The solubility of the cocrystal (ITZ-SUC) conducted in 0.1M HCl solution at 25 °C was a ~4-fold higher compared to that of ITZ.[45] However, it has not been shown if the cocrystal formation with SUC can improve its solubility in neutral pH environment. Another interesting aspect of the work presented in this Chapter was to study the properties of milled ITZ-SUC to ascertain if the amorphous sample retains some characteristics of the cocrystal sample.

Summarising, the aim of this work was to investigate if the combination of the solid state and microenvironmental pH manipulation is a viable approach towards improving solubility of ITZ. A number of binary (ITZ and SUC as well as ITZ and polymer (Eudragit L100-55)) and ternary (ITZ, SUC and Eudragit L100-55) systems were prepared by milling and their solid state properties along with solubility in acidic (pH=1.2) and buffer (pH=6.5) media were studied.

5.2 Materials and Methods

5.2.1 Materials

Itraconazole (ITZ) was donated by Welding GmbH (Hamburg, Germany). Methacrylic acid - ethyl acrylate copolymer (Eudragit L100-55, EUD) was kindly donated by Evonik Industries AG (Germany). Potassium hydroxide (KOH) pellets were obtained from Riedel-de Haën, (Germany); sodium phosphate monobasic dihydrate $NaH_2PO_4 \cdot H_2O$ from Merck (Germany). Succinic acid (SUC), potassium phosphate monobasic (KH_2PO_4), 37% hydrochloric acid (HCL), sodium chloride (NaCl), and acetonitrile (HPLC grade) were purchased from Sigma-Aldrich Ireland Ltd., (Ireland).

5.2.1.1 Preparation of Media for Solubility Studies

A potassium phosphate buffer pH 6.8 was prepared by dissolving 6.8 g of KH_2PO_4 in 800 ml of purified water. The pH was adjusted to 6.8 using KOH pellets, and the solution was brought up to 1000 ml of purified water at room temperature.

A sodium phosphate buffer pH 6.5 was prepared as follows: 0.420 g of NaOH, 3.954 g of $NaH_2PO_4*H_2O$, 6.19 g of NaCl were dissolved in approximately 900 mL of purified water. The pH was adjusted to 6.5 with 37% HCl. The volume was made up to 1000 mL with purified water at room temperature.

The simulated gastric fluid (SGF) was prepared by dissolving 2 g of NaCl in approximately 900 ml of purified water. The pH was adjusted to 1.6 using 37% HCl and made up to the volume of 1000 mL with purified water.

The fasted state simulated intestinal fluid (FaSSIF) was prepared by adding 2.24 g SIF Powder Original (biorelevant.com, Surrey, UK) to 500 ml of sodium phosphate buffer pH 6.5. When the powder dissolved, the solution was made up to 1000 ml with sodium phosphate buffer pH 6.5 and was left to stand for two hours before use. The FaSSIF fluid was used within 48 hours at room temperature.

5.2.2 Synthesis of Itraconazole and Succinic Acid Cocrystal (ITZ-SUC)

ITZ-SUC was synthesised as described in Chapter 4.

5.2.3 Preparation of Milled Samples

All milled samples were prepared by ball milling at 400 rpm for 2 hours, with a planetary ball mill PM 100 (Retsch, Germany) at room temperature. The total amount of powder, 2 g, was loaded into the stainless-steel milling container with a volume of 50 ml, and three stainless steel balls (Ø = 20 mm) of the same material were used. Milled samples were sieved through 100 µm stainless still sieve Afnor NFX 11-501 (France). Collected samples were stored in a desiccator over silica gel at 5˚C until use.

The binary systems composed of ITZ and SUC in molar ratios of 2:1, 1:1, 1:2, and ternary systems composed of ITZ, SUC, and EUD were prepared by Mr David Goulding in TCD.

5.2.4 Differential Scanning Calorimetry (DSC)

DSC was performed using a Mettler Toledo DSC (Schwerzenbach, Switzerland) with an RP-100 LabPlant refrigerated cooling system (Filey, UK), which was calibrated using an indium and zinc standards. Nitrogen was used as the purge gas. Hermetically sealed 40 µl aluminium pans with three vent holes were used throughout the study, and sample weights varied between 3 and 7 mg. A heating rate of 10 °C/min was implemented in all DSC measurements. Mettler Toledo STARe software (version 6.10) was used to analyse the thermograms.

5.2.5 Powder X-ray Diffraction (PXRD)

PXRD was performed as described in Chapter2.

5.2.6 Solid-State Fourier Transform Infrared Spectroscopy (FT-IR)

FT-IR was performed as described in Chapter 3.

5.2.7 Dynamic Solubility Study

The solubility study was performed in SGF and FaSSIF media prepared as per Section 5.2.1.1. A volume of 25 ml of media was added to a 50 ml glass vial, placed in a jacketed cylinder connected to a Lauda M12 water bath (Lauda-Königshofen, Germany). The media was equilibrated to 37 °C. The amount of 100 mg of the analysed sample was added to the vial and continuously stirred at 1000 rpm. Aliquots of 1 ml were taken at 2, 5, 10, 20, 30, 60, 90 and 120 minutes for the SGF studies, and additional time points of 180 and 240 minutes were included in the FaSSIF studies. The samples taken at different time points were immediately filtered using 0.45 µm PTFE filters,

diluted with the mobile phase and analysed by HPLC (Section 5.2.7). For SGF studies, 200 µl of the filtrate was diluted to 800 µl with mobile phase and mixed in the HPLC vial. For FaSSIF studies, 500 µl of the filtered sample was added to 500 µL mobile phase and mixed in the HPLC vial. The pH of the solutions was measured at the end of the study using a Thermo Orion 420A+ pH meter (Thermo Scientific, Hampshire, UK). The solid material remained in the vials at the end of the study was filtered and analysed by PXRD.

Part of this study was performed with help of Mr David Goulding in TCD. His work involved conducting the solubility studies in SGF and FaSSIF media and preparation of samples for HPLC analysis including milled ITZ, milled systems composed of ITZ and SUC in molar ratios of 2:1, 1:1, 1:2, and milled systems composed of ITZ, SUC and EUD.

5.2.8 High-Performance Liquid Chromatography (HPLC)

The content of ITZ was measured using a Waters 2695 Separations module equipped with a temperature programmable autosampler and Waters 2996 photodiode array detector (Milford, MA, USA). The mobile phase consisted of 4 parts of potassium phosphate buffer pH 6.8 and 6 parts (by volume) of acetonitrile HPLC grade. Preparation of the potassium phosphate buffer pH 6.8 is described in Section 5.2.1.1. The mobile phase was degassed by sonication for 10 minutes. Separation was performed using a Waters Symmetry C18 (4.6 mm x 150 mm) column. Samples were analysed at a UV detection wavelength of 260 nm. An injection volume of 50 µl was used. The elution was carried out isocratically with a flow rate of 1 ml/min. The total run time was 15 minutes per sample. The temperature of the column chamber was maintained at 25 °C for the entire analytical process. The retention time of ITZ was found to be 10.3 minutes. Empower software was used for peak evaluation. Calibration curves were used to determine the ITZ concentration at the various time points. This HPLC method was previously reported by Mugheirbi et al.[213] LOD and LOQ were found to be 0.31 µg/ml and 0.94 µg/ml in SGF media and 0.32 µg/ml and 0.96 µg/ml in FaSSIF media .

5.2.9 Dynamic Vapour Sorption (DVS)

Vapour sorption experiments were performed for milled samples of ITZ-SUC and a physical mixture of ITZ and SUC 2:1 (mole:mole) using a DVS Advantage-1 automated gravimetric sorption analyser (Surface Measurement Systems, Alperton, UK). The experiments were carried out at 25.0 ± 0.1 oC in water and ethanol vapour and 40 ± 0.1 oC in water vapour. Approximately 10 mg of powder was loaded on to the sample basket. All samples were first pre-dried at 0% relative humidity (RH) until a constant mass was obtained, defined as dm/dt ≤ 0.002 mg/min.

The reference mass was recorded, and a sorption-desorption analysis was then carried out between 0 and 90% RH, in steps of 10% RH. At each stage, the sample mass was equilibrated ($dm/dt \leq 0.002$ mg/min for at least 10 min) before the RH was changed. An isotherm was calculated from the complete sorption and desorption profile. Samples at the end of the DVS study were collected and analysed by PXRD and DSC.

5.2.10 Computer Modelling

The single crystal structures of α-SUC (SUCACB07), β-SUC (SUCACB06), and ITZ-SUC (REWTUK) were obtained from the Cambridge Structural Database (CSD). The software Mercury (version 3.9) (Cambridge Crystallographic Data Centre, UK) was used to generate the theoretical powder X-ray patterns based on the single crystal structures.

5.4 Results and Discussion

5.4.1 Thermal Behaviour of Milled ITZ

Disordered ITZ was produced via melt quenching (ITZq) in the DSC or by vibrational ball milling (ITZm) (Section 5.2.3). The thermal behaviour of ITZ prepared by both methods is compared in Figure 5.4-1.

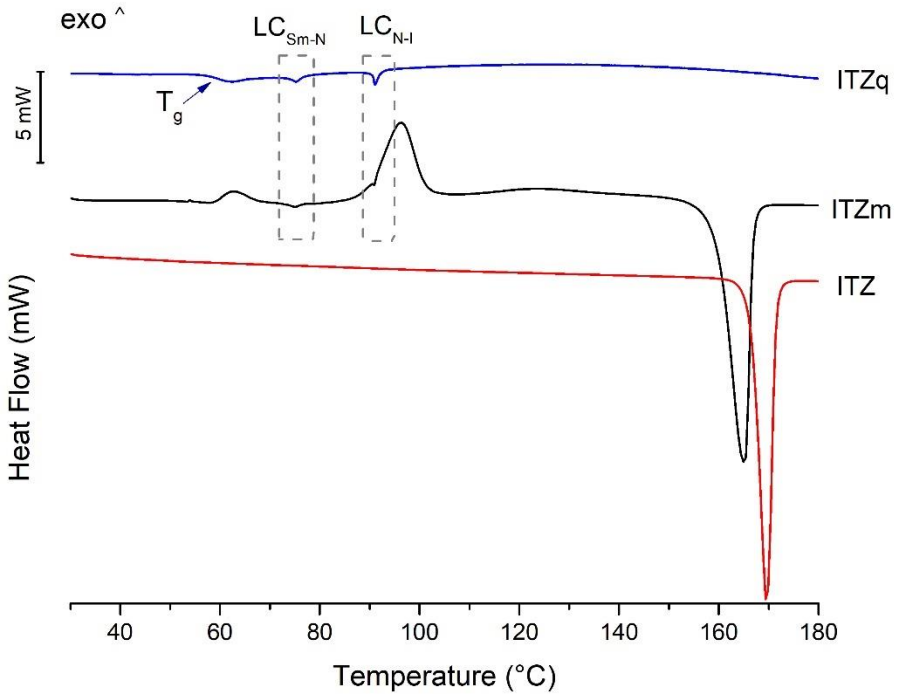

Figure 5.4-1 DSC thermograms of crystalline ITZ (ITZ) and disordered ITZ produced by melt quench (ITZq) and milling (ITZm) methods.

Preparation of ITZq was previously described in Chapter 3, Section 3.3.1. It included heating of crystalline ITZ in situ in the DSC pan at a heating rate of 10 °C/min above ITZ melting temperature (up to 180 °C) followed by fast cooling at a heating rate of 300 °C/min. ITZq showed a glass transition temperature (T_g) at 59.3 ± 0.25 °C, followed by two endothermic liquid crystalline (LC) transitions events at 73.2 ± 0.4 °C and 90.4 ± 0.35 °C, attributed to smectic (LC_{Sm-N}) and nematic (LC_{N-I}) LC transition, respectively (Figure 5.4-1). ITZm showed three exothermic events at 58.7 ± 0.37 °C, 89.9 ± 0.08 °C, and 159.4 ± 0.14 °C, as well as three endothermic events at 72.4 ± 0.04 °C, 89.4 ± 0.30 °C and 59.4 ± 0.14 °C (Figure 5.4-1).

The first major difference in the thermal behaviour of ITZq and ITZm was in the cold crystallisation behaviour, as ITZq did not crystallise on heating, while ITZm showed multiple crystallisation events. The exothermic event at 58.7 ± 0.37 °C may be related to surface

crystallisation. It has been perceived that below T_g, the molecular mobility of material is reduced, and the material is "kinetically frozen" in a thermodynamically unstable glassy state.[46] However, recent studies found that a thin layer of molecules near the surface may possess higher molecular mobility than the bulk molecules and enable crystallisation near or below the T_g. The surface crystallisation was reported to occur for amorphous indomethacin [48][214], griseofulvin[5] and nifedipine[215] Another explanation for the exothermic peak at 58.7 ± 0.37 °C recorded on ITZm thermogram is that amorphous materials prepared by ball milling may still contain a large number of nuclei. These nuclei can act as seeds and induce crystallisation.[51] For example, Trasi et al.[216][217] observed double exothermic peaks on the DSC thermogram for milled griseofulvin. They attributed the first exothermic peak to surface crystallisation, which was a result of crystallisation of particles having nuclei on their surface. The second exothermic peak was reported as bulk crystallisation and was related to crystallisation of interior (bulk) particles along with particle surfaces without nuclei. [216][217]

The endothermic events at 72.4 ± 0.04 °C and 89.4 ± 0.30 °C observed on ITZm DSC thermogram (Figure 5.4-1) correspond to smectic (LC_{Sm-N}) and nematic (LC_{N-I}) LC transition, respectively. The LC transitions of ITZ are described in Chapter 3.

The melting endotherm of ITZm observed at 159.4 ± 0.14 °C (Figure 5.4-1), showed a slight broadening and depression of onset melting temperature (Tm), in comparison to melting of crystalline ITZ (166.6 ± 0.32 °C). The heat of fusion (ΔHm) of ITZm (85.5 ± 0.61 $J \cdot g^{-1}$) was also lower than that of crystalline ITZ (75.7 ± 0.32 $J \cdot g^{-1}$). Such differences may be related to a different particle size of ITZm and crystalline ITZ and lower crystallinity of the DSC in situ crystallised ITZm, resulting in lower Tm and lower ΔHm. Sun and Simon[218] reported that as the particle size of aluminium nanoparticles was decreased, the melting temperature and the heat of fusion was also decreased. Feng et al.[219] also reported that ΔHm and Tm of cryo-milled griseofulvin were lower than those of the crystalline drug.

To provide more information about the thermal behaviour of ITZm, and to exclude the possibility that a different polymorphic form of ITZ formed upon heating a simple experiment was performed. In this experiment samples of ITZm were heated in the DSC pan, up to 65, 100, 120, and 145 °C, and analysed by PXRD (Figure 5.4-2).

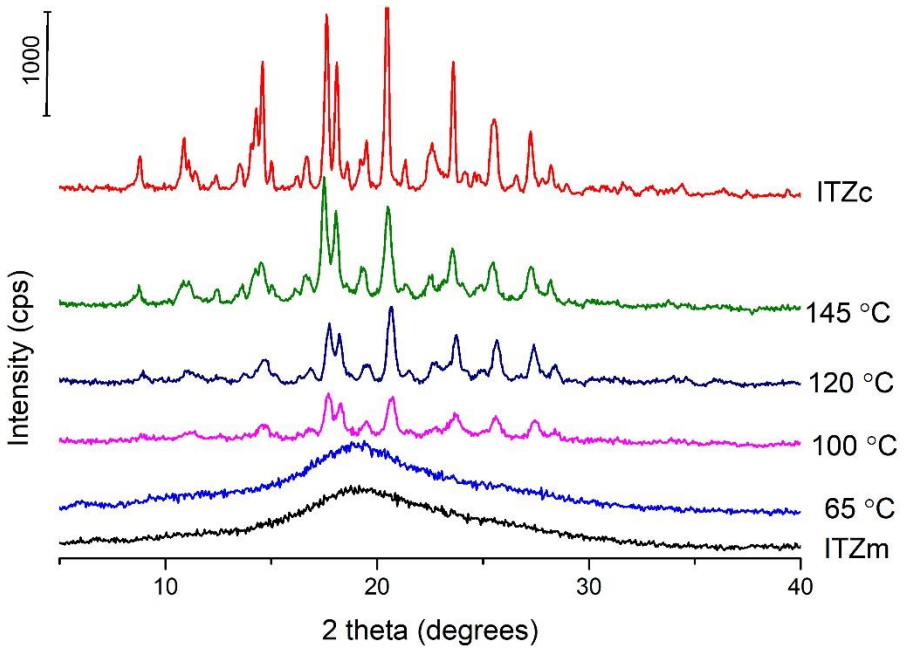

Figure 5.4-2 The XRPD pattern of crystalline ITZ (ITZ) and milled ITZ (ITZm) heated in the DSC pan up to a temperature of 65, 100, 120, and 145 °C.

As mentioned above, the exothermic event at 58.7 °C may be related to surface crystallisation. However, the PXRD patterns of ITZm heated up to 65 °C did not show any perceptible crystallinity (Figure 5.4-2). It is possible that the formed crystals were too small to be detected by PXRD. Samples heated up to 100 °C and above showed clear crystalline peaks. As the position of these peaks perfectly matched that of a commercially available stable polymorph of ITZ[152], [159], [220], a polymorphic transformation upon heating of the milled sample was excluded.

The FT-IR spectrum of ITZm were compared to those of crystalline ITZ and ITZq (Figure 5.4-3). The characteristic peaks visible in the spectrum of crystalline ITZ were previously discussed in detail in Chapter 4, Section 4.4.3. As shown in Figure 5.4-3 the spectrum of ITZ prepared by melt quench and milling method were identical, however, when compared to that of crystalline ITZ, some differences were noticed. Some peaks shown in the FT-IR spectrum of disordered ITZ (ITZm and ITZq) were broader than the corresponding peaks of the crystalline ITZ (Figure 5.4-3). The observed differences are most likely caused by changes in molecular arrangement due to an alteration in molecular packing between amorphous and crystalline forms. [221]

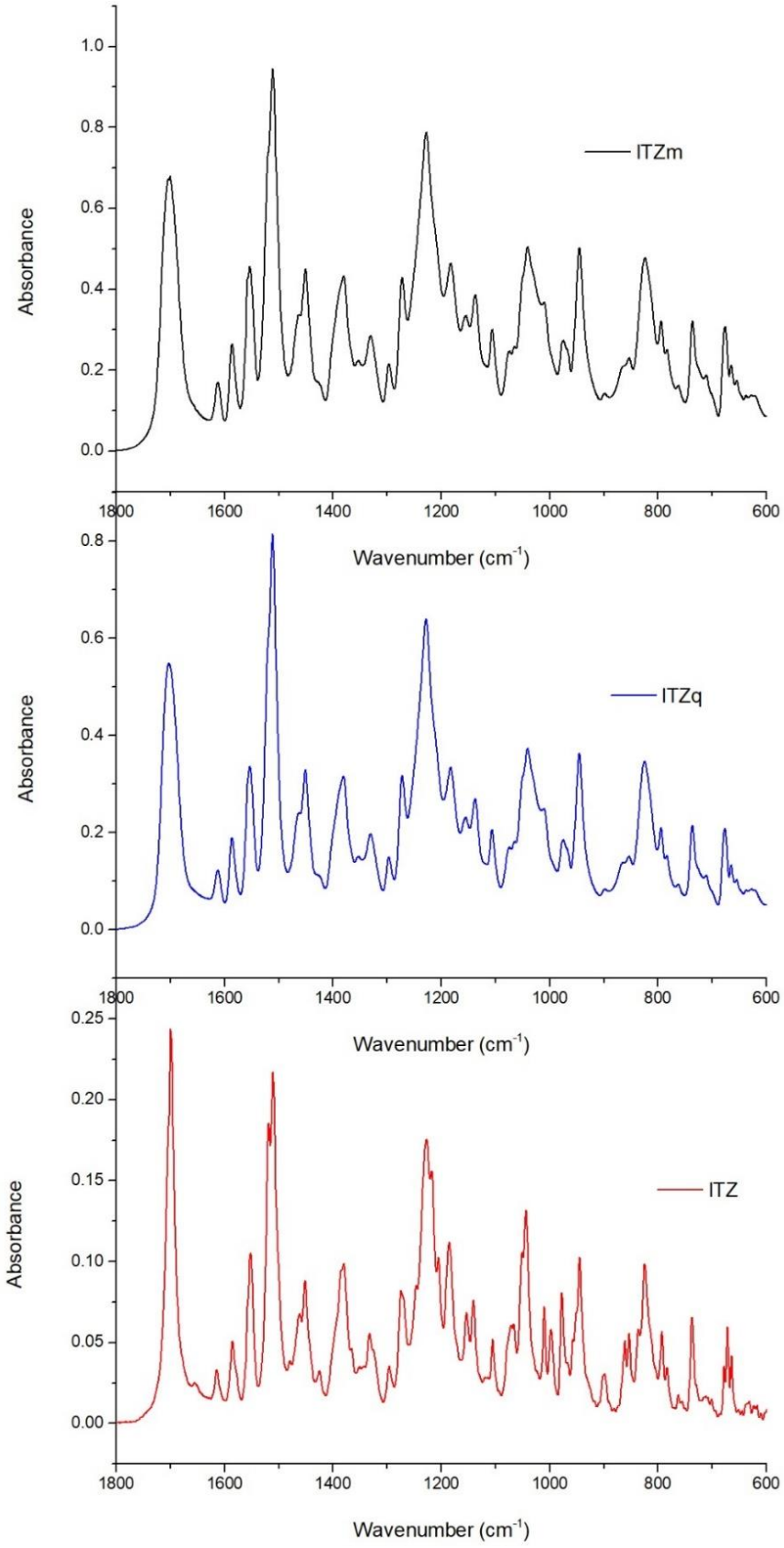

Figure 5.4-3 FT-IR fingerprint regions of crystalline ITZ (ITZ), milled ITZ (ITZm), and melt quenched ITZ (ITZq).

The results from this study suggest that the preparation technique (melt quench or ball milling) used to prepare disordered ITZ affected its physical stability. It was previously proposed that amorphous materials prepared by ball milling may still contain a large number of nuclei which can subsequently act as seeds and induce crystallisation.[25] The melt-quenched samples may have a small number of nuclei, which consequently gives them better physical stability.[51], [217], [222]

5.4.2 Comparison of Physicochemical Properties of Milled ITZ-SUC and Milled Physical Mixture of ITZ and SUC in a 2:1 Molar Ratio

The ITZ and SUC cocrystal (ITZ-SUC) was produced by the crystallisation method described in Chapter 4. To investigate the effect of milling, ITZ-SUC was milled (ITZ-SUCm) as described in Section 5.2.3, and analysed by DSC, PXRD, FT-IR, and DVS. The results were compared to those of a milled mixture of ITZ and SUC 2:1 (mole/mole) (ITZ:SUC2:1m).

The thermal behaviour of ITZ-SUCm and ITZ:SUC2:1m is shown in Figure 5.4-4. The DSC thermogram of milled ITZ-SUCm showed two exothermic events at 53.5 ± 0.01 °C and 111.3 ± 0.01 °C, followed by one endothermic peak a 158.6 °C ± 0.13 °C. Similarly, the DSC results recorded for ITZ:SUC2:1m also showed two exothermic peaks at 53.8 ± 0.08 °C and 113.4 ± 0.09 °C, followed by one endothermic peak at 158.5 °C ± 0.13 °C.

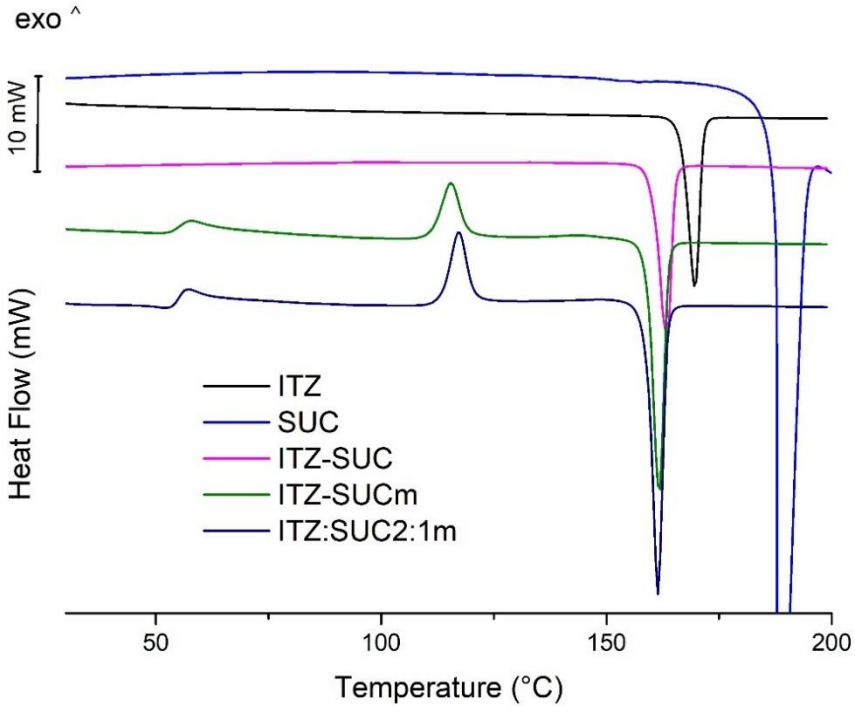

Figure 5.4-4 DSC thermograms of crystalline ITZ, SUC, ITZ-SU and milled ITZ-SUCm and ITZ:SUC2:1m.

The first exothermic event, observed at around 54 °C for both samples (ITZ-SUCm and ITZ:SUC2:1m), may be related to surface crystallisation, which was also observed for ITZm (Section 5.3.1). The melting of ITZ-SUCm and ITZ:SUC2:1m, recorded at 158.6 and 158.5 °C, respectively, matched the melting temperature of ITZ-SUC (159.8 °C ± 0.37 °C). Thus both systems, ITZ-SUCm and ITZ:SUC2:1m, crystallise to ITZ-SUC.

As seen in Figure 5.4-5a, PXRD patterns of both milled samples, ITZ-SUCm and ITZ:SUC2:1m, showed the typical halo characteristic for disordered materials. Upon heating, during the DSC run, both ITZ-SUCm and ITZ:SUC2:1m showed an event that could be ascribed to surface crystallisation, followed by another crystallisation peak. To provide more information about these exothermic events, samples of ITZ-SUCm and ITZ:SUC2:1m were heated in situ in the DSC beyond each exothermic event up to 100 and 130 °C and subsequently analysed by PXRD (Figure 5.4-5b and c). Both, ITZ-SUCm and ITZ:SUC2:1m, presented identical XRPD patterns (Figure 5.4-5b). Furthermore, when heated up to 100 °C, two characteristic peaks of ITZ-SUC at 6.08° and 9.04° 2θ were visible for both of the samples. The XRPD patterns of both materials heated up to 130 °C matched well the theoretical pattern of ITZ-SUC (Figure 5.4-5c).

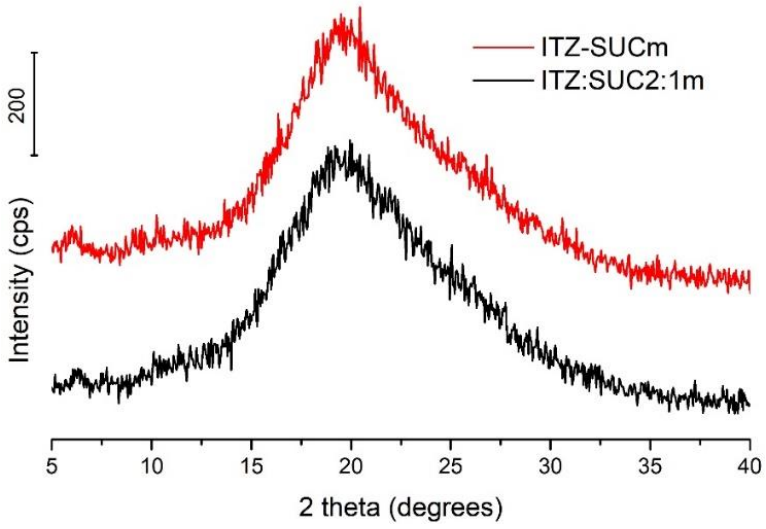

a)

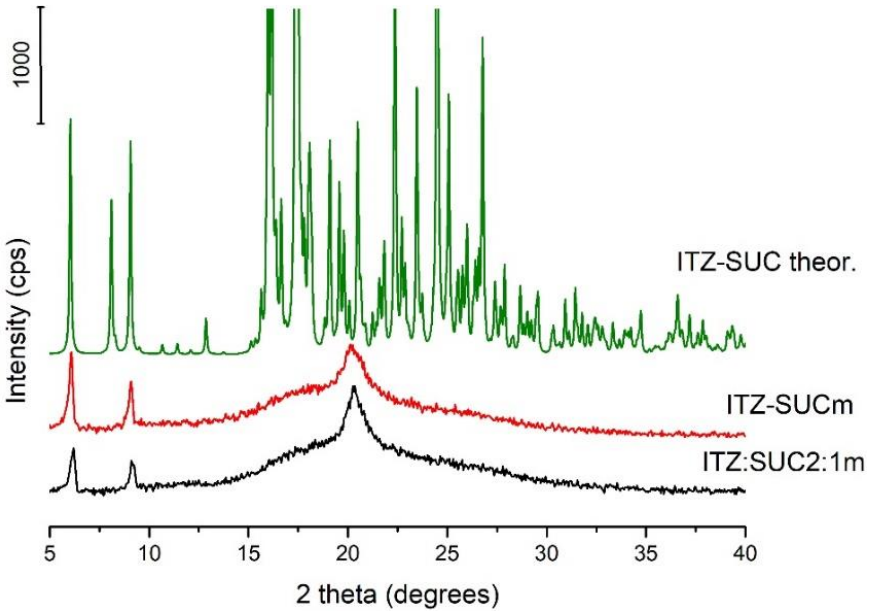

b)

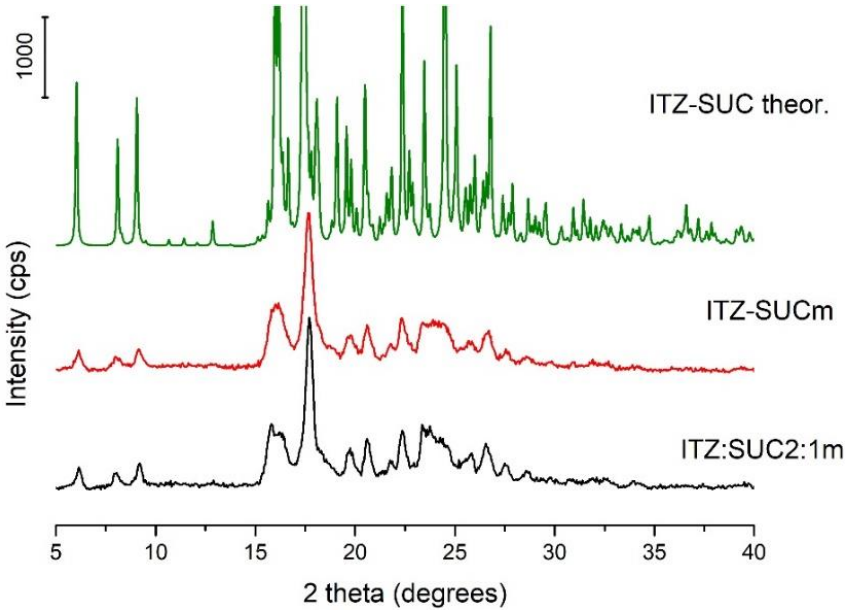

c)

Figure 5.4-5 PXRD patterns of: a) milled ITZ-SUCm and ITZ:SUC2:1m; b) milled ITZ-SUCm and ITZ:SUC2:1m after heating to 100 °C; b) milled ITZ-SUCm and ITZ:SUC2:1m after heating in to 145 °C. The theoretically calculated PXRD pattern of ITZ-SUC was generated based on the single crystal data (CSD, REWTUK).

The characteristic peaks seen in the FT-IR spectra of ITZ and SUC were analysed in Chapter 4, Section 4.4.3. The molecule of ITZ-SUC is made by two antiparallel ITZ molecules, which form a pocket filled by a SUC molecule. The SUC is connected to the 1,2,4,-triazole group of ITZ by a hydrogen bond. [45], [182], [193] When a hydrogen bond is formed with either the carbonyl oxygen (HO-C=O) or the hydroxyl hydrogen (HO-C=O), the C=O stretching frequency is downshifted.[201] As shown in Figure 5.4-6a, the peak corresponding to the C=O group in the

FT-IR spectrum of SUC at 1731 cm^{-1} was downshifted to 1711 cm^{-1} in the ITZ-SUC spectrum. The peak corresponding to the carbonyl group in the FT-IR spectrum of ITZ at 1700 cm^{-1} was also downshifted to 1692 cm^{-1} in the spectrum of ITZ-SUC, suggesting hydrogen bond formation between ITZ and SUC (Figure 5.4-6a). To analyse the effect of milling on crystalline ITZ-SUC, the FT-IR spectrum of ITZ-SUC was compared to those of ITZ-SUC, ITZ:SUC2:1m, and ITZm. The spectrum of ITZ-SUCm was identical to that of ITZ:SUC2:1m (Figure 5.4-7). Furthermore, ITZ-SUCm and ITZ:SUC2:1m matched the FT-IR spectrum of ITZm (Figure 5.4-6b, and Figure 5.4-7), suggesting that milling breaks the hydrogen bonds between ITZ and SUC and leads to the formation of a disordered mixture of ITZ and SUC. The shoulder peak present in the FT-IT spectrum of ITZ-SUCm at 1731 cm^{-1} might be related to the presence of SUC in the sample (Figure 5.4-6b). No other peaks corresponding to SUC were recorded in the FT-IR spectrum of ITZ-SUCm. However, this may be related to the low concentration of SUC in ITZ-SUCm and ITZ:SUC2:1m samples. Converting the mole (2:1) ratio to the weight ratio of ITZ to SUC in these sample, which is 14:1, and considering that SUC does not have strongly vibrating or rotating chemical groups, the SUC concentration in the system may be below the detection limit.

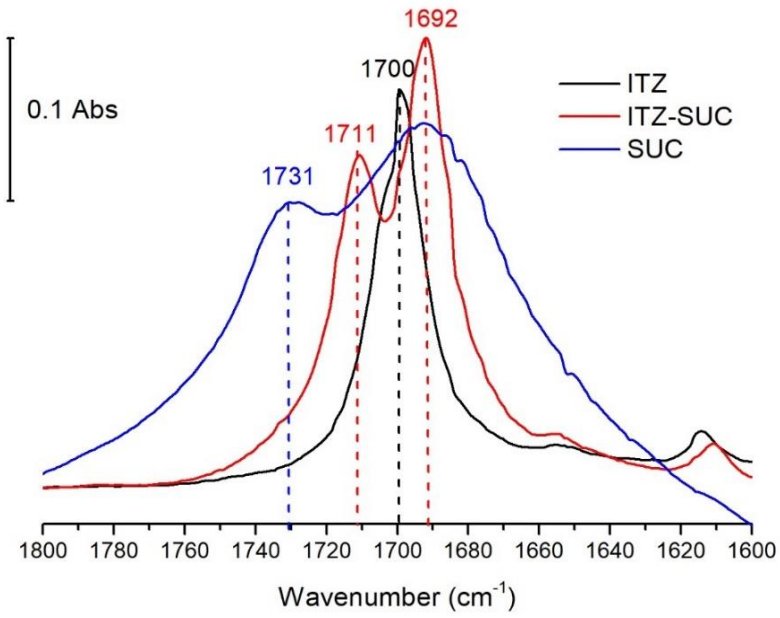

a)

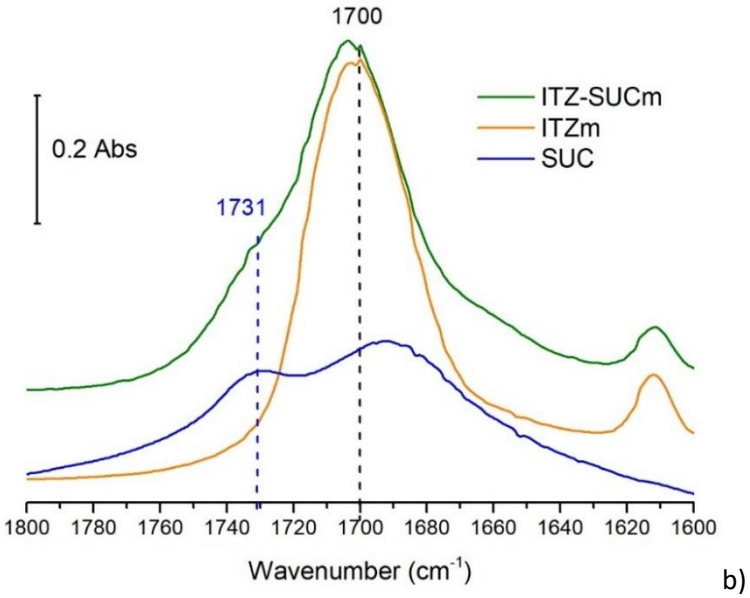

Figure 5.4-6 The carbonyl region of FT-IR spectra of a) ITZ, ITZ-SUC, SUC; b) ITZ-SUCm, ITZm, SUC.

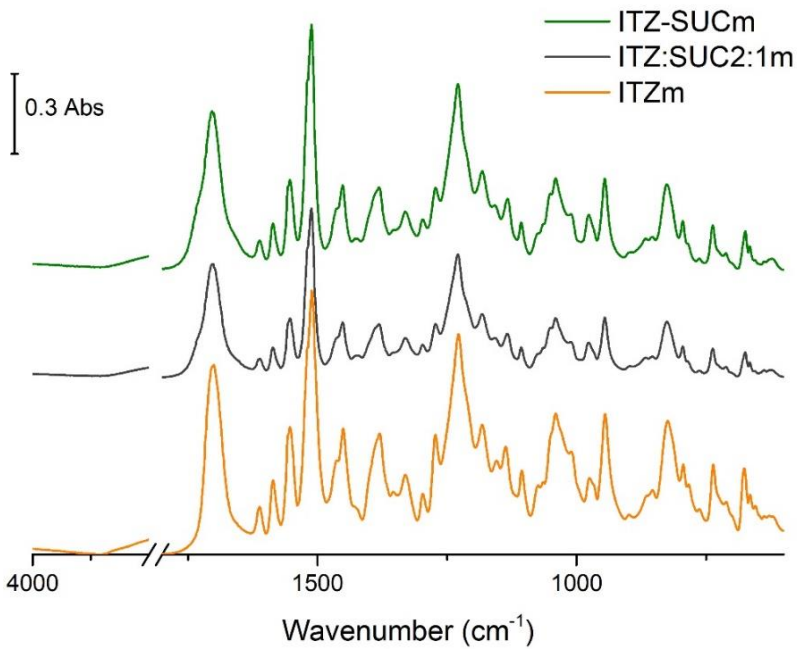

Figure 5.4-7 FT-IR fingerprint regions of ITZm, ITZ_SUCm, and ITZ:SUC2:1m.

The DVS experiments were performed to investigate the crystallisation behaviour of ITZ-SUCm and ITZ:SUC2:1m induced by solvent vapour. The initial DVS experiments were performed using water as the adsorbate. However, due to the hydrophobic nature of ITZ, samples showed negligible water uptake (data not shown). Figure 5.4-8a shows the DVS isotherms of a sorption-

desorption cycle in ethanol vapour. The maximum ethanol sorption was recorded at 70% p/p_0 and was 2.45% and 2.25% for ITZ-SUCm and ITZ:SUC2:1m, respectively. At 80% p/p_0, both samples showed a similar mass loss of 0.76% and 0.82% for ITZ-SUCm and ITZ:SUC2:1m, respectively. The mass loss is attributed to crystallisation induced by ethanol vapour.

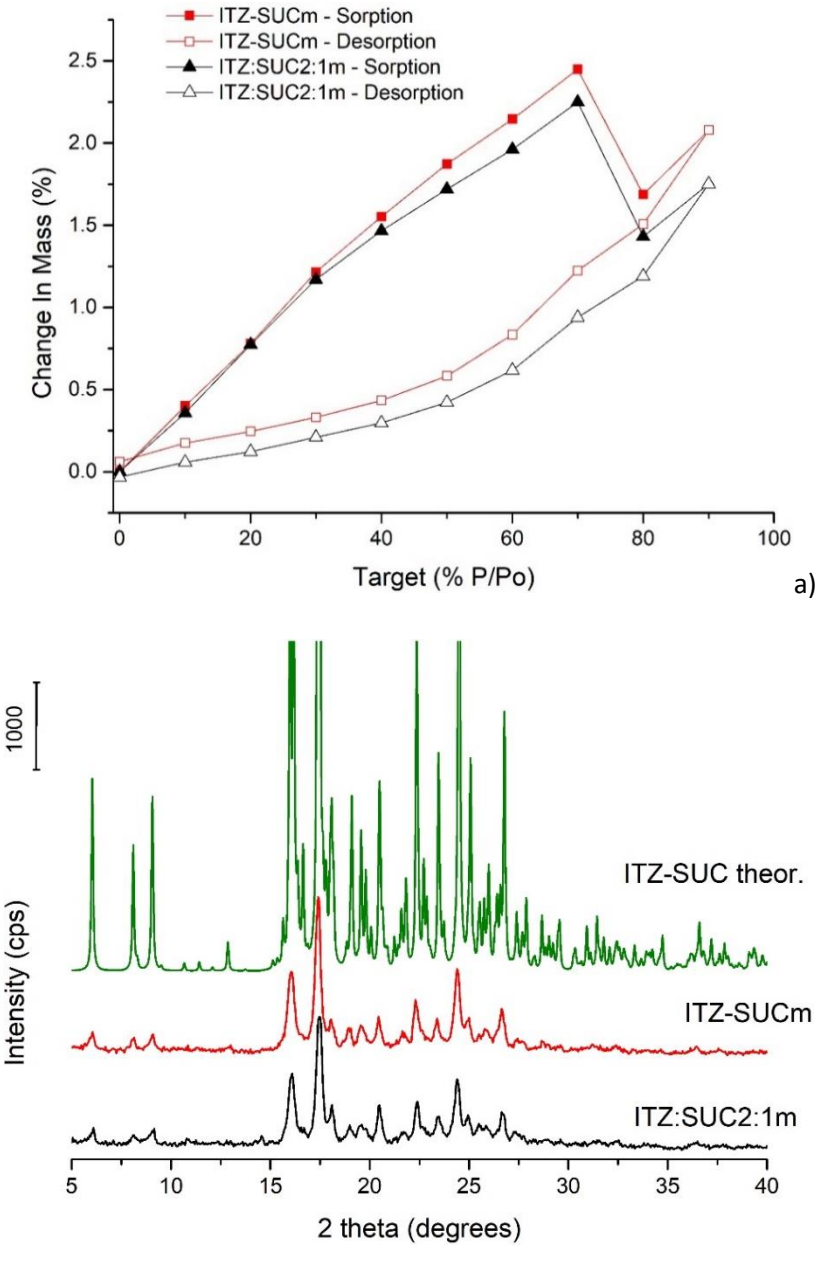

Figure 5.4-8 a) DVS sorption-desorption isotherms of ITZ-SUCm and ITZ:SUC2:1m at 25 °C in ethanol vapour. b) PXRD patterns of ITZ-SUCm and ITZ:SUC2:1m collected after the DVS analysis at 25 °C in ethanol vapour. The experimental results are compared to the theoretically calculated PXRD pattern of ITZ-SUC.

Both samples were collected at the end of the DVS experiments and analysed by PXRD, DSC and FT-IR. The PXRD results suggest that both the milled samples crystallised to ITZ-SUC (Figure 5.4-8b). The characteristic peaks, corresponding to ITZ-SUC, were observed in the PXRD diffraction pattern of ITZ-SUCm and ITZ:SUC2:1m, at 6.06°, 9.04, 16.04°, 17.45°, 20.48°, and 24.47° 2ϑ. The DSC thermograms recorded for remained powders from DVS experiment showed a single melting peak at 158.3 and 158.0 °C for ITZ-SUCm and ITZ:SUC2:1m, respectively. The FT-IR spectra of ITZ-SUCm and ITZ:SUC2:1m after crystallisation by DVS, were compared to the spectrum of ITZ-SUC and no differences were noticed (data not shown).

Overall, the results of this study indicate that milling of ITZ-SUC weakens/breaks intermolecular interactions between ITZ and SUC and leads to the disordered system. Milling of ITZ and SUC in a molar ratio equivalent to ITZ-SUC also resulted in the production of a disordered system. Both, ITZ-SUCm and ITZ:SUC2:1m were seen to crystallise to ITZ-SUC upon heating or in ethanol vapour (DVS).

5.4.3 Preparation of Solid Dispersions (SDs) of ITZ and SUC

One of the aims of this study was to investigate microenvironmental pH manipulation on solubility of ITZ. Therefore, ITZ and SUC were co-milled, as described in Section 5.2.3, in molar ratios of 2:1 (ITZ:SUC2:1m), 1:1 (ITZ:SUC1:1m), and 1:2 (ITZ:SUC1:2m) of ITZ and SUC. Considering that the ITZ-SUC cocrystal has a stoichiometry of 2:1 ITZ:SUC, and was seen on milling to form a disordered material comparable with the equivalent milled physical mixture, it was of interest to investigate other combinations of these two components: 1:1 and 1:2 mole/mole of ITZ and SUC. In addition, the choice of these molar ratios was based on the results obtained from the phase diagrams constructed for the ITZ/SUC system (Chapter 4). It was shown that the 1:2 molar composition of ITZ and SUC produced a eutectic (E_1) phase (although it should be acknowledged that E_1 is composed of ITZ-SUC and SUC). The 1:1 molar composition of ITZ and SUC was found to be an intermediate phase between the cocrystal (ITZ-SUC) and E_1.

The thermal behaviour of ITZ:SUC2:1m, ITZ:SUC1:1m and ITZ:SUC1:2m is shown in Figure 5.4-9. The temperature of the events seen in the DSC thermograms of the SDs prepared by co-milling ITZ and SUC are presented in Table 5.4-1. All binary, milled ITZ and SUC samples showed two exothermic events, ascribed to surface and main crystallisation events (Figure 5.4-9 and Table 5.4-1).

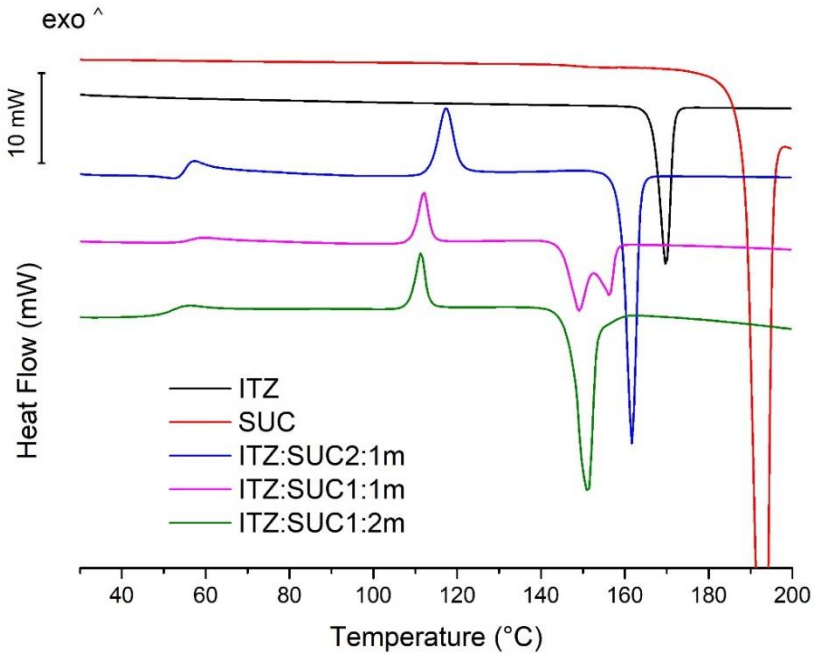

Figure 5.4-9 DSC thermograms ITZ, SUC, and binary SDs of ITZ and SUC prepared by milling.

Table 5.4-1 The temperature of the thermal events occurring on heating of SDs of ITZ and SUC with/without EUD, at a heating rate of 10 °C/min.

System	LC_{Sm-N} transition (°C)	LC_{N-I} transition (°C)	Surface crystallisation (°C)	Main crystallisation (°C)	Melting (°C)
ITZ:SUC2:1m	Not detected	Not detected	53.5 ± 0.01	113.4 ± 0.01	158.5 ± 0.13
ITZ:SUC1:1m	Not detected	Not detected	53.5 ± 0.43	109.4 ± 0.17	145.7 ± 0.28 153.9 ± 0.62
ITZ:SUC1:2m	Not detected	Not detected	52.7 ± 0.08	108.4 ± 0.03	147.2 ± 0.02
ITZ/EUD20m	70.9 ± 0.35	Not detected	51.2 ± 0.30	82.4 ± 0.15 107.01 ± 0.08	159.2 ± 0.06
ITZ:SUC2:1/EUD20m	Not detected	Not detected	54.6 ± 0.03	114.5 ± 0.14	158.0 ± 0.31
ITZ:SUC2:1/EUD40m	Not detected	Not detected	54.4 ± 0.11	115.1 ± 0.14	154.4 ± 0.03
ITZ:SUC1:1/EUD20m	Not detected	Not detected	53.0 ± 0.45	109.3 ± 0.06	144.4 ± 0.06 152.5 ± 0.67
ITZ:SUC1:2/EUD20m	Not detected	Not detected	51.8 ± 0.48	108.3 ± 0.02	146.4 ± 0.04
ITZ:SUC1:2/EUD40m	Not detected	Not detected	52.5 ± 0.43	108.5 ± 0.29	142.5 ± 0.16

Figure 5.4-10 shows PXRD patterns of milled samples composed of ITZ and SUC in the molar ratios 2:1, 1:1, and 1:2. The PXRD pattern of ITZ:SUC2:1m sample showed the typical halo characteristic of disordered materials. However, ITZ:SUC1:1m and ITZ:SUC1:2m showed small crystalline peaks, corresponding to either α-SUC or β-SUC polymorphic form.[202]–[206] Therefore, the peaks are seen in the diffractograms of ITZ:SUC1:1m and ITZ:SUC1:2m at 22.01°, 27.20°, and 32.32° 2θ correspond to the α-SUC polymorph and peaks seen at 20.17°, 31.47° and 38.40° 2θ correspond to the β-SUC polymorphic form. The peak at 26.15° 2θ may be related to either α-SUC or β-SUC. To investigate if milling could induce a polymorphic transition of β-SUC to α-SUC, a sample of β-SUC (commercially available form) was milled for 120 minutes at 400 rpm and analysed by PXRD. After milling, all crystalline peaks of β-SUC remained unchanged, therefore milling did not induce a polymorphic transition of SUC (Figure 5.4-11). However, co-milling of ITZ and SUC affected the polymorphic stability of SUC and resulted in a transition to form α.

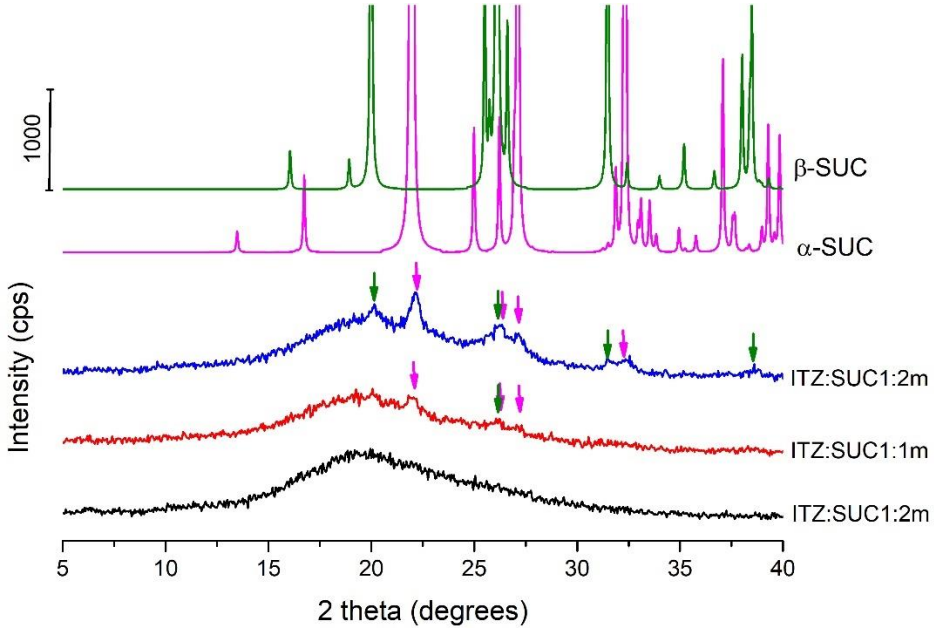

Figure 5.4-10 PXRD patterns of ITZ:SUC2:1m, ITZ:SUC1:1m, and ITZ:SUC2:1m. The experimental results are compared to the theoretically calculated PXRD patterns of α-SUC and β-SUC polymorphs. The pink and green arrows show the position of peaks corresponding to α-SUC and β-SUC form, respectively.

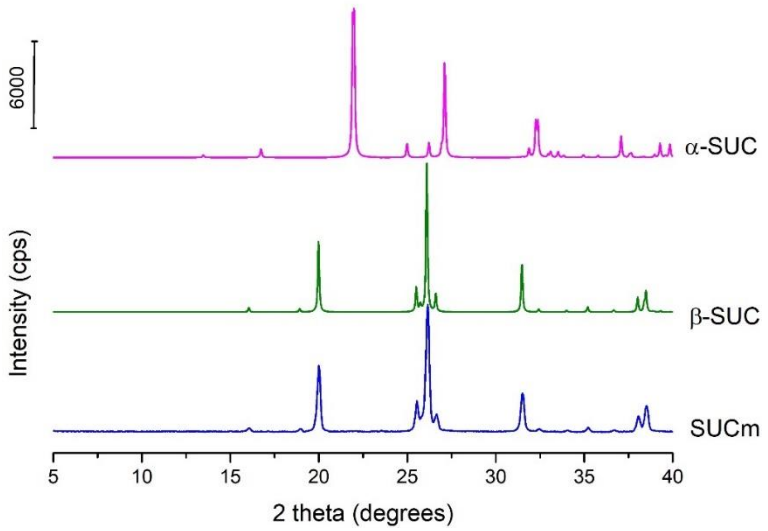

Figure 5.4-11 The PXRD pattern of a milled sample of SUC (SUCm) and the theoretically calculated PXRD patterns of α-SUC and β-SUC polymorphs.

The melting temperature of 147.2 °C recorded for ITZ:SUC1:2m was very close to that of E_1 at 147.9 °C (Chapter 4), therefore to investigate it further, a sample of ITZ:SUC1:2m was heated to 100 or 130 °C in the DSC and analysed by PXRD. As shown in Figure 5.4-12, the peaks corresponding to ITZ-SUC are dominant in the sample crystallised at 130 °C, but the crystalline peaks corresponding to α-SUC and β-SUC polymorphs are also present.

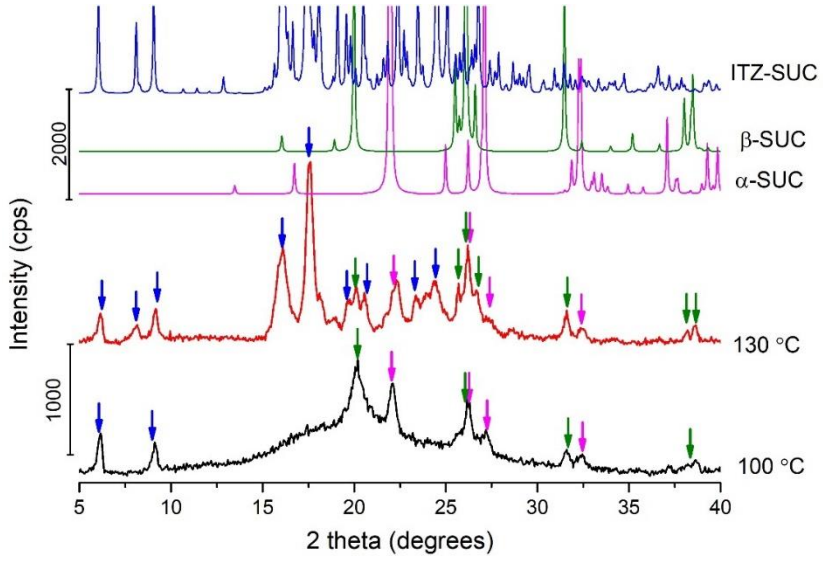

Figure 5.4-12 PXRD patterns of ITZ:SUC1:2m heated to 100 and 130 °C. The experimental results are compared to the theoretically calculated PXRD patterns of ITZ-SUC, α-SUC and β-SUC. The blue, pink and green arrows are showing the position of peaks corresponding to ITZ-SUC, α-SUC and β-SUC, respectively.

The characteristic peaks seen in the FT-IR spectra of ITZ and SUC were analysed in Chapter 4, Section 4.4.3. The FT-IR spectrum of ITZ:SUC2:1m was discussed in Section 5.3.2 of this chapter. All peaks seen in the spectrum of ITZ:SUC2:1m matched the position of peaks seen in the FT-IR spectrum of ITZm, except for a small shoulder peak at 1731 cm-1. As discussed in Section 5.3.2 this shoulder peak may be related to the presence of SUC in the sample. The FT-IR spectrum of ITZ:SUC1:2m is shown in Figure 5.4-13, and it appears as a combination of spectra of ITZm and SUC. The SUC peaks were seen at 2632, 2538, 1731, 1420, 1310, 1201, 803 and 637 cm-1 (Figure 5.4-13). For visibility reason, only FT-IR fingerprint regions are shown in Figure 5.4-13. The spectrum of ITZ:SUC1:1m matched that of ITZ:SUC1:2m. However, the absorbance of peaks corresponding to SUC and seen in the spectrum of ITZ:SUC1:1m was reduced compared to the corresponding SUC peaks seen in the spectrum of ITZ:SUC1:2m (data not shown).

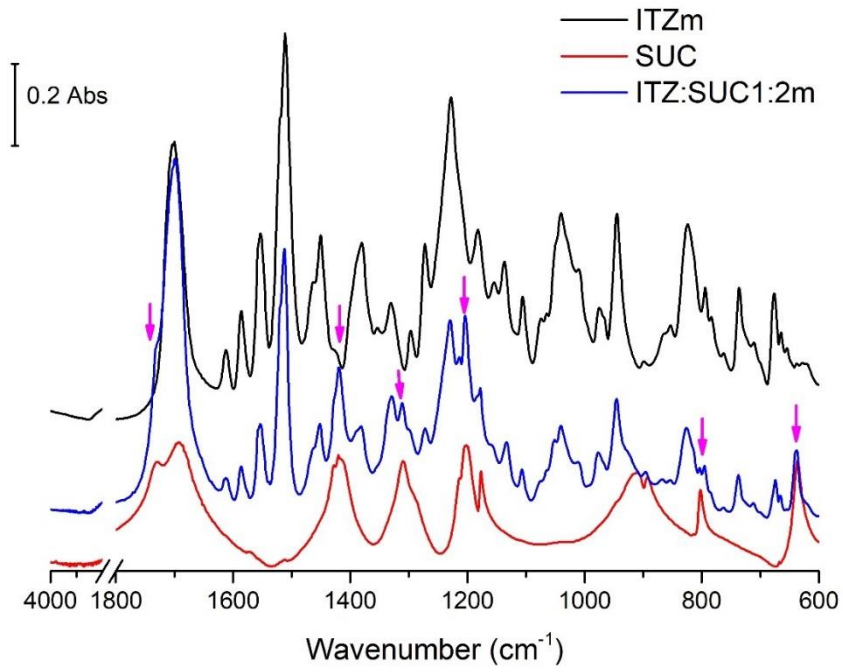

Figure 5.4-13 FT-IR spectra of ITZm, SUC, and ITZ:SUC1:2m. The pink arrows show the position of SUC peaks visible in the ITZ:SUC1:2m spectrum.

5.4.4 Preparation of Solid Dispersions of ITZ and SUC with Eudragit L100-55

Thermodynamic phase diagrams were generated for ITZ and three acidic polymers, Eudragit L100-55 (EUD), Carbopol 981, and HPMCAS-MG and are described in Chapter 3. The LC nature of ITZ was considered, and it was concluded that if ITZ was present in an SD in a liquid crystalline phase, immiscibility as a result of molecule anisotropy might be expected. Furthermore, the constructed phase diagrams suggested that, depending on the polymer, the LC phase might be

present even at a relatively large content of polymer in the binary combination, even up to 50% w/w. However, for the ITZ/EUD combination, the smectic phase (LC_{Sm-N}) was determined to be present in the system for ITZ concentration above 60% w/w, while the nematic phase (LC_{N-I}) was persistent for ITZ contents above 85% w/w. Based on these results, the EUD concentration of 20% and 40% as w/w, was chosen for the preparation of SDs of ITZ and SUC with EUD. The composition of these SDs is shown in Table 5.4-2.

Table 5.4-2 The composition of SDs of ITZ and/or SUC with EUD prepared by milling.

Sample name	The molar ratio of ITZ:SUC (mol/mol)	The content of ITZ:SUC mixture (w/w, %)	The content of Eudragit L100-55 (w/w, %)
ITZ/EUD20m	1:0	80 (pure ITZ)	20
ITZ:SUC2:1/EUD20m	2:1	80	20
ITZ:SUC1:1/EUD20m	1:1	80	20
ITZ:SUC1:2/EUD20m	1:2	80	20
ITZ:SUC2:1/EUD40m	2:1	60	40
ITZ:SUC1:2/EUD40m	1:2	60	40

The thermal behaviour of these SDs is shown in Figure 5.4-14. The temperature of the events seen in the DSC thermograms recorded for each system is gathered in Table 5.4-1.

The LC_{Sm-N} transition was recorded, at 70.9 ± 0.35 °C, only for the ITZ/EUD20m system, showing a decrease in the temperature of this event compared to the LC_{Sm-N} transition of pure ITZ (73.2 ± 0.4 °C, Chapter 3). A similar decrease in the onset value of LC_{Sm-N} transition, to 70.0 ± 0.08 °C, was seen for ITZ/EUD20 system prepared by melt quench method (Chapter 3), suggesting some miscibility of liquid crystalline phase of ITZ in EUD.

As shown in Figure 5.4-14 and Table 5.4-1, the melting temperatures recorded for ITZ:SUC2:1/EUD and ITZ:SUC1:2/EUD decreased as the concentration of EUD increased. As described in Chapter 2, the melting point depression phenomenon (chemical potential reduction) resulting from the drug-polymer interactions is related to the solubility of a drug in the polymer.[223] For instance, the hydrogen bonds between two drugs (griseofulvin and progesterone) and poly[N-(2-hydroxypropyl)methacrylate] (PHPMA) were confirmed by FT-IR.[224] It was reported that in the physical mixtures containing 90% (v/v) of PHPMA, melting of

griseofulvin (219°C) and progesterone (129°C) were depressed to 194°C and 118°C, respectively. In contrast, melting of phenindione remained unchanged, which was attributed to the absence of interactions between phenindione and PHPMA.[224]

To investigate if depression of the melting point recorded for ITZ:SUC2:1/EUD and ITZ:SUC1:2/EUD systems is related to intermolecular interactions, FT-IR analysis was performed for all SDs as described in Section 5.2.6. However, it was observed that all peaks seen in the FT-IR spectrum of ITZ/EUD20m matched the peaks seen in the FT-IR spectrum of ITZm (data not shown), suggesting that there were no strong intermolecular interactions between ITZ and EUD. No differences were found between SDs composed of ITZ, SUC and EUD, where EUD content was 20 or 40%. Furthermore, the spectra of SDs composed of ITZ, SUC and EUD, matched those without EUD (data not shown), again indicating lack of strong intermolecular interactions between components.

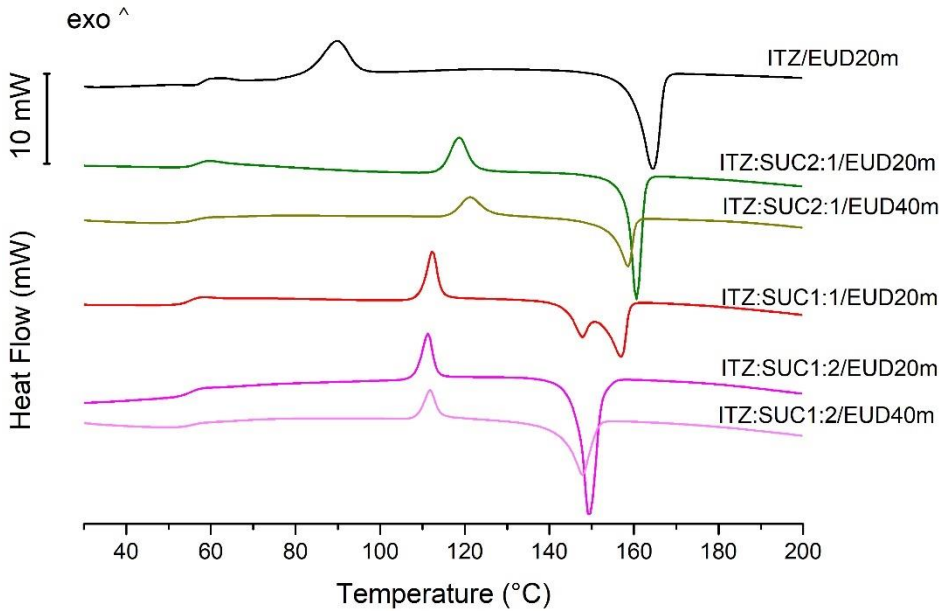

Figure 5.4-14 DSC thermograms of SDs prepared by milling of ITZ and/or SUC with EUD.

The PXRD patterns of the prepared SDs are shown in Figure 5.4-15. ITZ/EUD20m, ITZ:SUC2:1m/EUD20m and ITZ:SUC2:1m/EUD40m showed a typical halo characteristic of disordered materials. However the diffractograms recorded for ITZ:SUC1:1/EUD20m, ITZ:SUC1:2/EUD20m and ITZ:SUC1:2/EUD40m showed the presence of small crystalline peaks. The peak seen at 2θ= 22.05° corresponds to the α-SUC polymorphic form, and the peaks visible

at 20.18°, 25.52°, 27.20° and 32.32° 2θ correspond to the β-SUC polymorph. The peak seen at 2θ=26.32° may be related to either α or β form of SUC. [202]–[206]

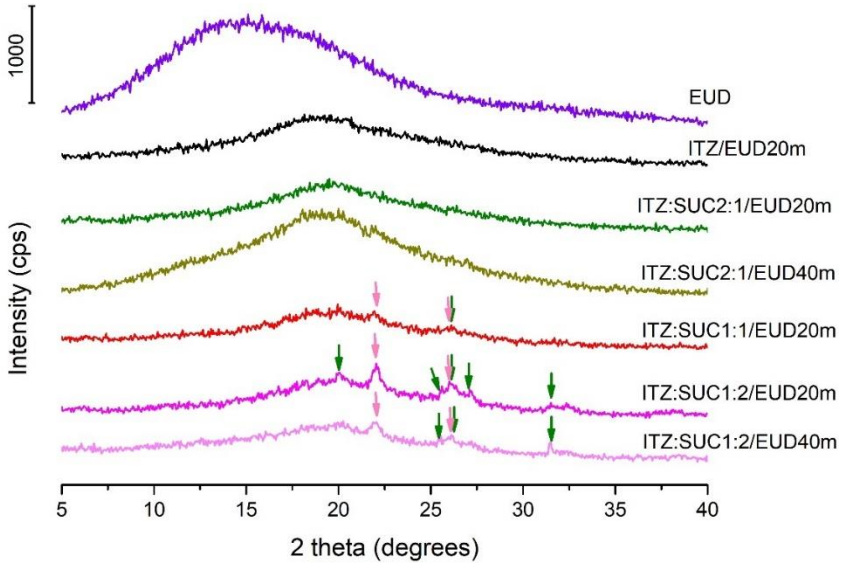

Figure 5.4-15 PXRD patterns of SDs prepared by milling of ITZ and/or SUC with EUD. The pink and green arrows show the position of peaks corresponding to α-SUC and β-SUC polymorphs, respectively.

To summarise, a depression of melting was recorded for both, ITZ:SUC2:1/EUD and ITZ:SUC1:2/EUD, compared to the corresponding systems without EUD, indicating some miscibility between ITZ and EUD. The ITZ/EUDm, ITZ:SUC2:1/EUD20m, and ITZ:SUC2:1/EUD40m systems were the only X-ray amorphous solid dispersions. The systems with a higher SUC content were partially amorphous as crystalline peaks corresponding to SUC were recorded by PXRD.

5.4.5 Dynamic Solubility Studies

The dynamic solubility studies in the simulated gastric fluid (SGF) and in the fasted state simulated intestinal fluid (FaSSIF) media were performed as described in Section 5.2.7. Based on data published by Lang et al.[225] degradation of ITZ under solubility test conditions, described in Section 5.2.7 was assumed to be negligible. Lang and co-workers investigated the chemical stability of ITZ in acidic pH media (0.1N HCl aqueous solution with 10% DMSO) at an elevated temperature of 60 °C. It was reported that ITZ underwent chemical degradation in acidic environment during storage. However, the degradation rate of ITZ was found to be slow, as

approximately 80% of the drug remained unchanged after four weeks of storage at accelerated conditions.[225]

The dynamic solubility studies were performed for ITZm, ITZ-SUC, ITZ-SUCm, ITZ:SUC2:1m, ITZ:SUC1:1m, ITZ:SUC1:2m, ITZ/EUD20m, ITZ:SUC2:1/EUD20m, ITZ:SUC1:1/EUD20m, ITZ:SUC1:2/EUD20m, ITZ:SUC2:1/EUD40m, and ITZ:SUC1:2/EUD40m. Tables 5.3-3 and 5.3-4 give the summary of the key parameters resulting from the solubility studies of the above listed systems in SGF and FaSSIF, respectively. Both tables include the maximum concentration (C_{max}), time to C_{max}, duration of supersaturation and the final ITZ concentration at the end of the solubility study. The solubility profiles of all materials tested in SGF and FaSSIF media are shown in Figure 5.4-16 and Figure 5.4-17, respectively.

The equilibrium solubility of ITZ in 0.1N HCl is reported as 4 µg/ml and 1 ng/ml in the neutral pH.[114][115] These values were used as a reference to present ITZ supersaturation levels generated during solubility study.

The solubility profiles of ITZm, ITZ-SUC, and ITZ-SUCm in the SGF media are shown in Figure 5.4-16a, while Figure 5.4-16b shows SGF solubility results for the systems prepared by milling ITZ and SUC in three different molar ratios (ITZ:SUC2:1m, ITZ:SUC1:1m, and ITZ:SUC1:2m). Figure 5.4-16c and Figure 5.4-16d show solubility profiles of SDs produced with EUD, where EUD concentration in the SDs is 20% and 40% (w/w), respectively. As shown in Figure 5.4-16, all systems, except for ITZ-SUC, gave similar results. The supersaturation was generated rapidly until C_{max} was achieved at 10 min into the solubility study, and from 10 minutes until the end of the study (120 min) a decline in the ITZ concentration was observed. Looking at these results it may be concluded that the addition of SUC had no improvement on solubility of ITZ in SGF as the solubility profiles of ITZm and milled binary ITZ/SUC systems were similar. Furthermore, the incorporation of EUD into the formulation composed of ITZ and SUC also did not show any improvement in solubility of the drug. However, it should be highlighted that these milled systems generated drug supersaturation levels of ~17.5-fold higher than that of crystalline ITZ at this pH.

Table 5.4-3 Summary of the key parameters of solubility study in SGF media, where C_{max} is the maximum concentration

System	C_{max} (mg/ml)	Time to C_{max} (min)	Duration of supersaturation (min)	Final concentration after 120 min (mg/ml)
ITZm	67.9 ± 0.4	10	120	4.6 ± 1.1
ITZ-SUC	30.9 ± 0.4	10	120	10.07 ± 1.0
ITZ-SUCm	64.1 ± 0.7	10	120	4.1 ± 1.1
ITZ:SUC2:1m	68.8 ± 4.9	10	90	1.6 ± 0.4
ITZ:SUC1:1m	69.1 ± 4.5	10	120	4.1 ± 0.2
ITZ:SUC1:2m	68.1 ± 2.5	10	120	4.3 ± 2.3
ITZ/EUD20m	64.1 ± 2.2	5	120	5.8 ± 0.8
ITZ:SUC2:1/EUD20m	66.6 ± 4.6	5	90	3.1 ± 2.2
ITZ:SUC1:1/EUD20m	66.5 ± 7.4	10	90	2.5 ± 0.2
ITZ:SUC1:2/EUD20m	68.5 ± 7.3	10	60	2.4 ± 0.4
ITZ:SUC2:1/EUD40m	65.7 ± 4.6	5	90	2.2 ± 2.2
ITZ:SUC1:2/EUD40m	68.1 ± 0.4	10	120	4.5 ± 1.7

Table 5.4-4 Summary of the key parameters of solubility study in FaSSIF media, where C_{max} is the maximum concentration.

System	C_{max} (µg/ml)	Time to C_{max} (min)	Final concentration after 240min (µg/ml)
ITZm	4.5 ± 0.1	5	1.4 ± 0.2
ITZ-SUC	3.3 ± 0.2	20	0.9 ± 0.2
ITZ-SUCm	5.7 ± 0.3	5	1.5 ± 0.4
ITZ:SUC2:1m	4.7 ± 0.3	10	1.7 ± 0.2
ITZ:SUC1:1m	6.1 ± 0.2	10	1.4 ± 0.2
ITZ:SUC1:2m	5.3 ± 0.4	10	2.8 ± 1.0
ITZ/EUD20m	4.0 ± 0.3	10	1.3 ± 0.2
ITZ:SUC2:1/EUD20m	5.2 ± 1.0	10	0.4 ± 0.1
ITZ:SUC1:1/EUD20m	4.7 ± 0.6	10	0.5 ± 0.2
ITZ:SUC1:2/EUD20m	4.5 ± 0.1	10	4.0 ± 0.1
ITZ:SUC2:1/EUD40m	4.8 ± 0.1	10	0.5 ± 0.0
ITZ:SUC1:2/EUD40m	25.4 ± 1.7	240	25.4 ± 1.7

As shown in Figure 5.4-16a, the solubility profile of ITZ-SUC (crystalline) in SGF media deviates from the others. The measured supersaturation (at its highest, C_{max}) was ~7.7-fold higher than that of ITZ, which is about half of the highest supersaturation level generated by the other investigated systems. However, the drug supersaturation at C_{max}, was extended up to ~30 minutes for ITZ-SUC. The concentration of ITZ after 60 and 120 minutes for ITZ-SUC system was measured as 22.3 and 10.7 mg/ml, which represents an ~5.6-fold and ~2.7-fold of ITZ supersaturation, respectively. This results are relatively close to those reported by Remenar and co-workers[45], who conducted solubility studies of ITZ-SUC in 0.1M HCl solution (pH=1.2) at 25 °C and reported that the ITZ concentration was ~4-fold higher to that of crystalline ITZ.[45]

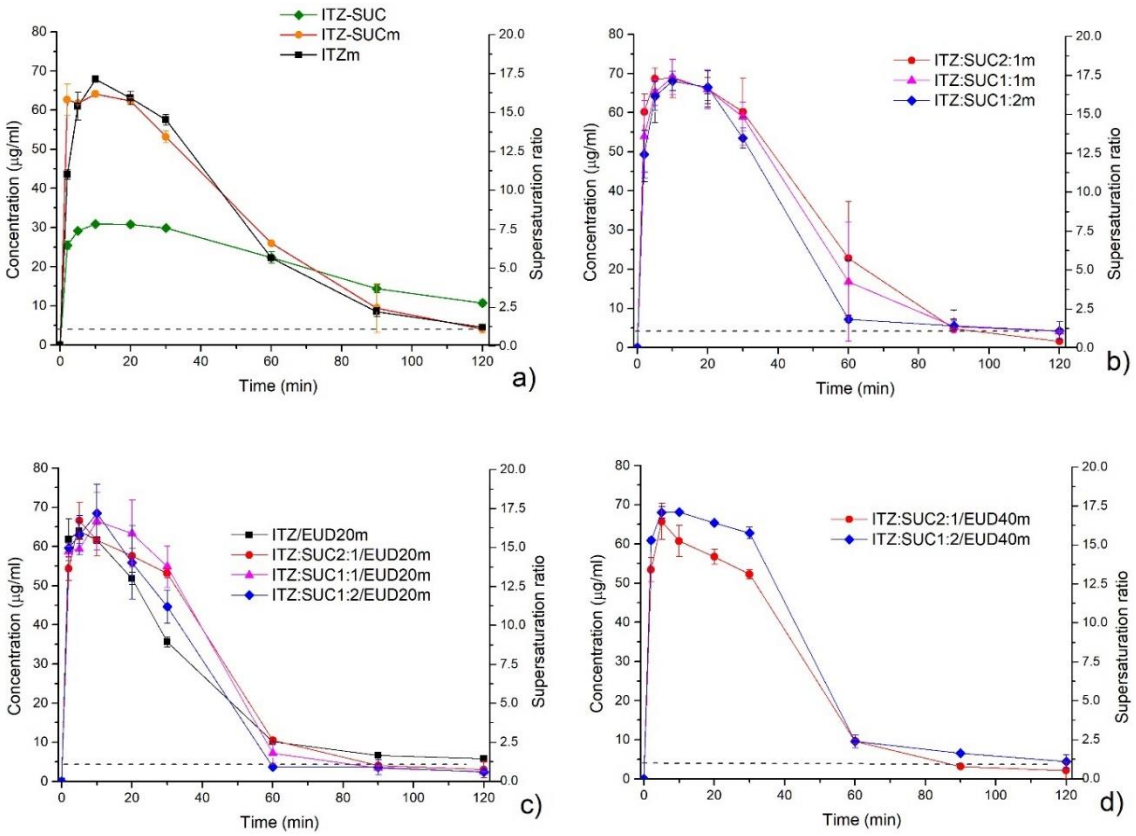

Figure 5.4-16 Dynamic solubility profiles of the various ITZ systems in SGF. The dashed lines in the graphs show the concentration of 4 µg/ml, which corresponds to the equilibrium solubility of ITZ in pH=1.2. [114][115]

The solubility study performed in the FaSSIF media are shown in Figure 5.4-17 and Table 5.4-4. Starting with profiles showed in Figure 5.4-17a and Figure 5.4-17b, one can see a similar trend for all the systems except for ITZ-SUC. For the ITZ-SUC system, the supersaturation generated was ~330-fold higher than that of the crystalline ITZ solubility and its duration was extended to 30 minutes (Figure 5.4-17a and Table 5.4-4). Afterwards the concentration of ITZ declined steadily until 180 minutes, reaching a concentration of ITZ of 1.0 µg/ml (~100-fold of crystalline ITZ solubility). From 180 minutes, until the end of the study (240 minutes), the concentration of ITZ did not change, as the final concentration (after 240 minutes) was found as 0.9 µg/ml.

Looking at Figure 5.4-17b showing solubility profiles of systems prepared by milling of ITZ and SUC in three different molar ratios (ITZ:SUC2:1m, ITZ:SUC1:1m, and ITZ:SUC1:2m), one can see that the supersaturation was generated rapidly, and C_{max} of about 5 µg/ml (~500--fold level of crystalline ITZ solubility), was achieved at 10 minutes into the solubility study (Table 5.4-4). Immediately after 10 minutes, the drug started to precipitate out of the solution. The steep decline in the ITZ concentration was recorded until 60 minutes into the solubility study. From 60

minutes, until the end of the study (240 minutes), the concentration of ITZ did not change much, and the final ITZ concentration was recorded as 1.7 and 1.4 μg/ml for ITZ:SUC2:1m and ITZ:SUC1:1m, respectively. Interestingly, the ITZ:SUC1:2m system showed a different behaviour towards the end of the study than ITZ:SUC2:1m and ITZ:SUC1:1m. As shown in Figure 5.4-17b, the concentration of ITZ recorded for this system, did not reach a plateau at 60 minutes. Instead, a slow increase in ITZ concentration, until the end of the study, was seen, reaching the final ITZ concentration of 2.8 μg/ml (~280-fold of crystalline ITZ solubility). The increase in ITZ concentration at the end of the study observed for this system appears to be related to the higher SUC content in this system. It may be possible that to create a favourable pH-microenvironment[208]–[211] that may enhance solubility of ITZ a higher ratio of SUC is required.

Figure 5.4-17c and Figure 5.4-17d show the solubility profiles of ITZ:SUC SDs with a 20 and 40% w/w of EUD. Starting with the solubility profile of ITZ:SUC2:1m/EUD40m, one can see that this system does not deviate much from the system containing 20% EUD (ITZ:SUC2:1/EUD20m) or the system without EUD (ITZ:SUC2:1m), with exception of one time point, at 240 minutes, where the ITZ:SUC2:1/EUD20m showed a rapid decrease in soluble ITZ (to 0.4 μg/ml). In contrast, at 240 minutes, ITZ:SUC1:2/EUD20m system showed increase in in soluble ITZ (to 4.0 μg/ml) in comparison to ITZ:SUC1:2m (2.8 μg/ml). The formulation with 40% of EUD in the system (ITZ:SUC1:2/EUD40m) led to an even higher increase of the final ITZ concentration, up to 25.4 μg/ml, which represent a ~2,500-fold enhancement in ITZ supersaturation (Figure 5.4-17,Table 5.4-4).

Hot melt extrusion method was applied by Sarode et al. [122] to prepare SDs of ITZ with hydrophilic polymers, including Eudragit EPO, Eudragit L-100-55, Eudragit L 100, HPMCAS-LF, HPMCAS-MF, Pharmacoat 603, and Kollidon VA-64.[122] The supersaturation levels of ITZ in non-sink conditions (dynamic solubility using conditions similar to those used in this Chapter 3) of simulated intestinal fluid (SIF) of pH=6.8, achieved with HPMCAS-LF, HPMCAS-MF, and Eudragit L 100-55 were respectively 22, 19, and 7- times higher than the equilibrium solubility of ITZ in SIF.[122] Enteric polymers, including cellulose acetate phthalate (CAP) and polyvinyl acetate phthalate (PVAP) were selected by DiNunzio et al.[123] to produce amorphous SDs by ultra-rapid freezing. ITZ-CAP formulations demonstrated a significant 2-fold improvement in the supersaturation level of ITZ in the neutral media in comparison to the currently marketed product Sporanox®.[123]

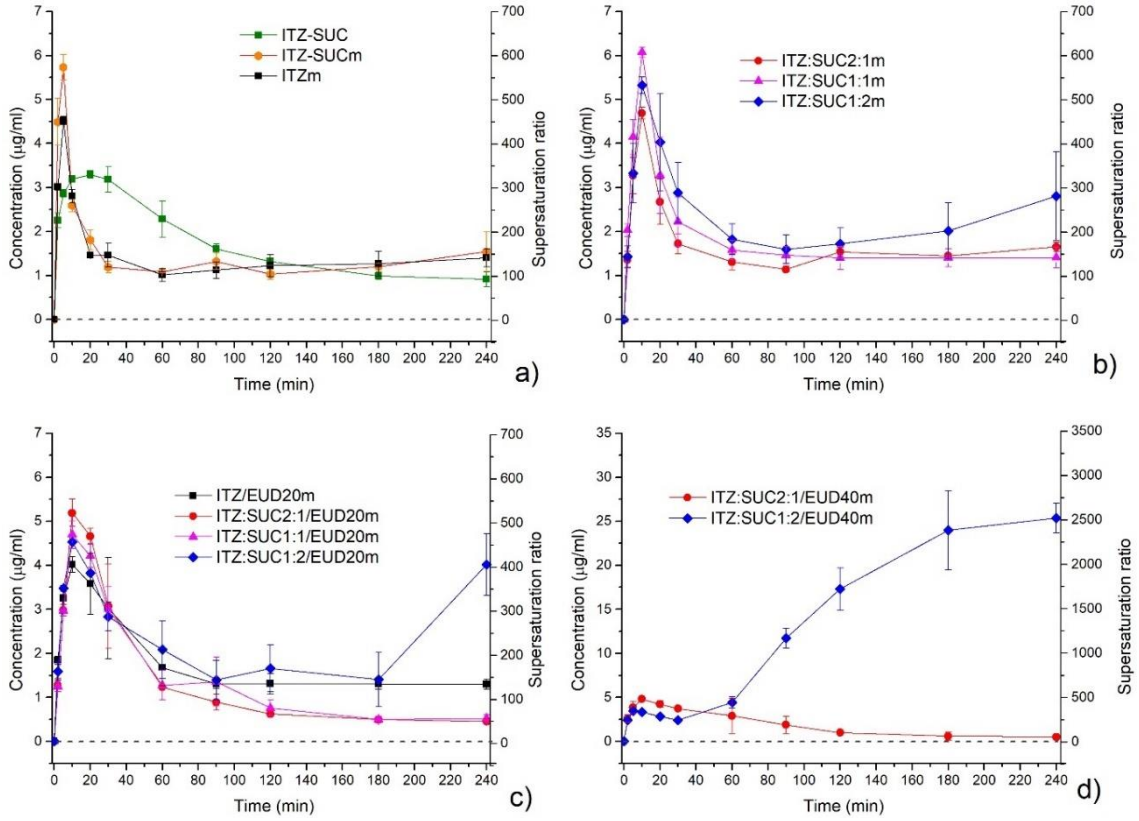

Figure 5.4-17 Dynamic solubility profiles of the various ITZ systems in FaSSIF. The dashed lines in the graphs show the concentration of 1ng/ml, which corresponds to the equilibrium solubility of ITZ in natural pH. [114][115]

Statistical analysis was not performed for the dynamic solubility studies due to the small sample size (n=2). However, looking at the solubility profiles in SGF media, it is clear, that ITZ-SUC profile significantly differs from other analysed samples. Results obtained from FaSSIF media, show that the final concentration of ITZ, measured at the end of the study (after 240 minutes) was significantly different for ITZ:SUC1:2/EUD20 and ITZ:SUC1:2/EUD40 samples. Furthermore, the profile of ITZ:SUC1:2/EUD40 recorded after 60 minutes of the study, until the end of the study significantly differs from other analysed samples.

Looking at these results it appears that the outstanding performance of ITZ:SUC1:2/EUD40m system must be related to concentration of both SUC and EUD in the formulation. Van den Mooter et al. [226] reported that polymers containing acidic functional groups may have a stabilising effect on weakly basic drugs in the supersaturated solution state and in the amorphous solid state. They attributed the improvement of solubility and amorphous state stability to the formation of a salt between basic drugs and acidic polymers.[226] Miller et al.[227] also reported that solubility improvement of ITZ in aqueous media was related to a

greater number of acidic functional groups on the polymer chain of EUD than on hypromellose phthalate (grade HP-55 and HP-55S).[227] Considering that the affinity of ITZ to acidic groups of EUD would be a reason for high solubility of ITZ generated by ITZ:SUC1:2, strong intermolecular interactions, as reported by Sarode et al.[122], would be expected to be seen in FT-IR spectra of ITZ:SUC1:2/EUD systems. However, as reported in Section 5.3.4, FT-IR analysis did not detect any intermolecular interactions for these systems. Miyazaki et al.[228] studied the influence of the drug–polymer interactions on nucleation and crystal growth of amorphous SDs composed of nitrendipine (NTR) with PVP, HPMC and HPMCP. They reported that only strong interactions, such as hydrogen bonding between NTR and PVP, which were detectable by FT-IR, resulted in a decrease in the crystal growth rate of NTR, however weak drug-polymer interactions, which were not detectable by FT-IR, may have reduced nucleation.[228]

To summarise, the addition of SUC or EUD into the formulation with ITZ had no effect on solubility of the drug in SGF as solubility profiles of these systems were comparable to that of neat ITZm. However, the incorporation of SUC and EUD into the formulation with ITZ was shown to improve solubility of ITZ in FaSSIF. The ITZ:SUC1:2/EUD40m system generated the highest ITZ supersaturation concentrations in comparison to the other investigated systems in FasSIF. The ITZ supersaturation duration from ITZ-SUC was prolonged and achieved a C_{max} at 30 minutes, in both SGF and FaSSIF.

5.5 Conclusions

The effect of milling on ITZ and ITZ-SUC was investigated and analysed by a range of methods. The results obtained for the milled cocrystal (ITZ-SUCm) were compared to those of a milled physical mixture of ITZ and SUC in the molar ratio 2:1 (ITZ:SUC2:1m). It was confirmed by FT-IR that milling breaks the hydrogen bond formed between ITZ and SUC in the cocrystal and leads to the formation of a disordered mixture of ITZ and SUC.

Solubility studies of ITZ-SUC performed in SGF and FaSSIF media showed that ITZ-SUC generated supersaturation of ~7.7-fold higher than that of crystalline ITZ, which was about half compared to supersaturation levels generated by the other investigated systems. However, the advantage of ITZ-SUC system is its supersaturation duration was prolonged and a C_{max} at 30 minutes followed by a slow and steady decrease of ITZ concentration until the end of the study (120 min for SGF studies, and 240 min for FaSSIF studies. Learning from Chapter 4, that eutectic phase E_1 is composed of ITZ-SUC and SUC and knowing that absorption of ITZ is facilitated by an acidic environment, it would be desirable to investigate the solubility behaviour of E_1 form.

Furthermore, it would be of high interest to perform a dissolution study and investigate the effect of different SUC concentrations in the formulations on the dissolution profile of ITZ. Due to the large difference between the solubility of ITZ in the neutral pH of 1ng/ml, compared to 4 µg/ml in the acidic media, it would be expected that precipitation and decrease of ITZ concentration may occur on transitioning from SGF to FaSSIF during the dissolution study. However, it would be desirable to compare different formulations, as increased SUC content may create a favourable pH-microenvironment and thus enhance solubility of ITZ.

The addition of SUC, as a pH-adjuster, was investigated in relation to the solubility of ITZ in SGF and FaSSIF media. The increasing amount of SUC in the formulation did not affect the solubility of ITZ in SGF. Also, incorporation of an enteric polymer Eudragit L100-55 (EUD) into formulations composed of ITZ and SUC, showed no effect and solubility profiles of these systems were comparable to that of ITZm. In contrast, the solubility study in FaSSIF suggested that even though the drug supersaturation levels generated at 10 minutes of the study were not affected by the SUC content in the formulation, the final ITZ concentration at the end of the study (after 240 minutes) varied. The highest ITZ concentration of 2.8 µg/ml was recorded for ITZ:SUC1:2m system. Furthermore, the incorporation of EUD into this formulation also had an impact on the final concentration of ITZ. Adding 20 and 40% of EUD into the ITZ:SUC1:2m system resulted in the final concentration of ITZ as 4.0 and 25.4 µg/ml, respectively, which represent a 400 and 2,500-fold increase in ITZ supersaturation, based on an estimated 1 ng/ml equilibrium solubility of ITZ at neutral pH.[114][115]

Chapter 6: General Discussion and Conclusions

6.1 General Discussion and Conclusions

As previously mentioned, the primary aim of this project was to produce and characterise different multicomponent systems of itraconazole ITZ and elucidate how the various forms of the drug are able to improve solubility of ITZ. Some of the more specific goals of the project were to review and characterise liquid crystalline (LC) properties of ITZ, study physical stability of polymeric SDs with ITZ by using experimental and theoretical predictions methods, produce crystalline and disordered multicomponent systems with ITZ and to establish if they can improve solubility of ITZ. From the material covered in this thesis it can be seen that all of these objectives were achieved, at least to some degree.

The development of an amorphous formulation with an optimal performance involves selecting the appropriate excipients and then an appropriate method of introducing these excipients into the formulation. The disordered materials are prone to crystallisation during storage or during dissolution.[46] Therefore, excipients (e.g. polymers) may be added to the formulation to inhibit drug crystallisation process.[126] However, it should be noted that in order to produce a physically stable formulation, drug and polymer need to be miscible/soluble in one another and form a single phase amorphous system. [92], [93] Also, the drug loading in such a stable solid dispersion must be below its saturation level to prevent phase separation or crystallisation.[129] The drug/polymer solubility may be predicted using thermal analysis methods such as including the melting point depression method, the crystallisation method and the dissolution endpoint method.[139] A comparison of these methods and solubility predictions based on the F-H theory for five model drugs at 25 °C, were conducted in Chapter 2. The results obtained for the melting point depression method and the crystallisation method were similar however it was hypothesised that they may overestimate solubility. The predictions made from the dissolution endpoint method were lower than predictions from melting point depression and crystallisation methods. However, as all three thermal analysis methods provided reproducible data, the choice of a method for the prediction of drug/polymer solubility should be based on the thermal properties of both the drug and polymer. Therefore, the melting point depression method was also used in Chapter 3 to construct phase diagrams for ITZ/polymer systems.

Chapter 3 was focused on understanding the liquid crystalline properties of ITZ on its own and in a formulation with a polymer. The reversible LC transitions observed at 73.2 ± 0.4 °C (smectic, LC_{Sm-N}) and 90.4 ± 0.35 °C (nematic, LC_{N-I}) were in agreement with the data reported by Six et al.[116] PLM experiments conducted for vitrified ITZ showed colourful focal-conic fan textures as well as four-brush Schlieren textures, thus suggested a smectic (A or C) arrangement. RT-

PXRD analysis showed two sharp peaks at 2θ=2.97° and 5.96° and a major diffuse maximum at 2θ=19°. The peaks at around 3 and 19° 2θ corresponded well to the position of the predicted maxima of nematic phase, normally located at $Q = 2\pi/l_o$ and $Q=2\pi/w_o$, where Q is the scattering wavevector and l_o and w, are the length and width of the molecule, respectively.[58] However the peak at approximately 6° 2θ suggested a smectic arrangement.[58] Therefore, VT-PXRD was used to further investigate the LC phase transitions of ITZ and the obtained results clearly indicated the long range organisation of the LC phase upon cooling from melt, and thus the smectic phase formation. Keeping in mind all information gained about the LC nature of ITZ, miscibility of ITZ with three polymers including methacrylic acid - ethyl acrylate copolymer (EUD), hypromellose acetate succinate (HAS), and polyacrylic acid (CAR), was also investigated in Chapter 3. PLM-HS was applied to visually investigate if LC transitions take place in systems composed of ITZ and the polymer. The results suggested that ITZ/EUD and ITZ/HAS may form smectic and nematic phases. However, the ITZ/CAR system is more likely to form only one LC phase, possibly a nematic, which might be related to high viscosity of CAR. PLM-HS observations were supported by the DSC study. Indeed, both both, LC_{Sm-N} and LC_{N-I}, transitions were recorded for ITZ/EUD and ITZ/HAS systems and only LC_{N-I} was observed for ITZ/CAR system. Furthermore, depending on the ITZ content either one or two T_gs were recorded for ITZ/CAR which strongly suggests a phase separation. Analysing the DSC results of different ITZ/polymer compositions, an evident decrease in the onset temperature values for the LC events in comparison to the values for pure ITZ was noticed for ITZ/EUD and ITZ/HAS systems. As shown in other studies, part of the LC phase may remain separated and some of the LC phase dissolves in the polymer matrix to form a molecular dispersion.[151], [172] Therefore, the fraction of ITZ remaining in the LC phase was quantified taking into consideration the enthalpy of a LC transition. ITZ solubility limits in the polymer determined for ITZ/EUD were calculated as 0.78 and 0.845 of ITZ weight fraction for LC_{Sm-N} and LC_{N-I}, respectively. It means a minimum of 20% w/w of EUD in formulation is required to form a homogenous, non-separated blend. For the HAS systems the LC phases of the drug were well persistent at concentrations much lower than 80% w/w ITZ and a non-linear relationship of P(x) versus x was observed. To provide full information about miscibility of the analysed ITZ/polymer systems the Flory-Huggins lattice theory (successfully applied in Chapter 2 to predict solubility of five different drugs in polymers) and the Maier-Saupe-McMillan approach to model anisotropic ordering of molecules were utilised to create phase diagrams for all ITZ/polymer mixtures. It was concluded that in a supercooled ITR/polymer mix, if ITZ is present in a liquid crystalline phase, immiscibility because of molecule anisotropy is afforded.

Chapter 4 was dedicated to crystalline compositions of ITZ and SUC. The thermodynamic phase diagrams were determined experimentally, using DSC, and theoretically, using Schroeder-Van Laar[188] and Prigogine-Defay[189] equations. Depending on the composition of ITZ and SUC mixtures, several peaks were detected in DSC thermograms, representing different points on the constructed phase diagram. For the composition range of 0.05 < *x*(ITZ) < 0.86 an endothermic peak at around 133 °C, immediately followed by an exothermic peak (peaking at around 140 °C) were recorded during the first heating cycle. The endothermic transition seen at 133 °C was associated with the formation of an metastable eutectic phase (m-E) and the exothermic peak seen immediately after m-E melting was associated with the cocrystal (ITZ-SUC) formation.[185], [186], [229] Two other eutectic phases were identified as E_1, 147.9 ± 0.08 °C (composed of ITZ-SUC and SUC), and E_2, 157.1 ± 0.28 °C (composed of ITZ-SUC and ITZ). The compositions of E_1 and E_2 were determined from the Tamman plot as *x*(ITZ)=0.31 and *x*(ITZ)=0.67, respectively. The E_1 phase was successfully produced by a fast-evaporation crystallisation method.

Chapter 5 investigated a combination of solid state and microenvironmental pH manipulation on solubility of ITZ. The binary (composed of ITZ and SUC as well as ITZ and EUD) and ternary (composed of ITZ, SUC and EUD) systems were prepared by ball milling. It was discovered that the SUC content in the formulation influenced the solid state of the formed solid dispersions (SDs). Only formulations where the molar ratio of ITZ and SUC was 2:1 were X-ray amorphous. All other formulations with higher SUC content showed the presence of crystalline peaks corresponding to SUC (α and/or β) by PXRD. The effect of milling on the stability of cocrystal of ITZ and SUC (ITZ-SUC) was also investigated as part of this study. It was discovered that during milling the hydrogen bonding between ITZ and SUC brakes/weakens, which leads to the formation of an X-ray disordered system, which crystallises to ITZ-SUC. Dynamic solubility profiles were completed for the mentioned above formulations. In the SGF medium the supersaturation generated by ITZ-SUC was ~7.7-fold higher than that of ITZ and was persistent up to 30 minutes. The concentration of ITZ from the ITZ-SUC form after 60 and 120 minutes was measured as 22.3 and 10.7 µg/ml, which represents ~5.6-fold and ~2.7-fold of ITZ supersaturation, respectively. In the FaSSIF medium supersaturation generated by ITZ-SUC was ~330-fold higher than that of ITZ, it was extended up to 30 minutes, and then it declined slowly and after 240 minutes measured as ~90-fold of ITZ supersaturation. The SUC and EUD content in the formulations with ITZ had no effect on solubility of ITZ in SGF. However, in FaSSIF, the addition of SUC and EUD was related to improvement of ITZ solubility. The ternary system composed of ITZ and SUC in the 1:2 molar ratio and 40% of EUD (ITZ:SUC1:2/EUD40m) showed

an outstanding improvement of solubility of ITZ in FaSSIF. After 240 minutes the concentration of ITZ was ~2,500-fold higher than that of ITZ thermodynamic concertation, based on an estimated 1 ng/ml equilibrium solubility of ITZ at neutral pH.[114][115]

In conclusion, the primary aim of this project was achieved and several formulations of ITZ were synthesised and analysed. Due to the lack of comprehensive studies examining liquid crystalline properties of ITZ in relation to drug-polymer stability, the work presented in Chapter 3 is substantial addition to the body of knowledge concerning disordered forms of this drug. The detailed analysis of capability of ITZ to form various crystalline solid state forms, such as cocrystal and eutectic forms, presented in Chapter 4, may be used as a model to explore the possibility of formation of new crystalline forms of ITZ with different compounds. While all the produced SDs formulations of ITZ, as shown in Chapter 5, were able to increase apparent solubility of ITZ, the ITZ-SUC and ITZ:SUC1:2/EUD40m systems are perhaps the most promising and should be the subject of further research.

6.2 Main Findings

- The comparative study of three different thermal methods for predicting drug solubility and/or miscibility in polymers may be used as general guidance for the selection of the most suitable thermal analysis method for the screening of drug/polymer solubility.
- For the first time, for a pharmaceutical drug substance, a full thermodynamic phase diagram including the presence of smectic and nematic phases of ITZ was constructed. The Flory-Huggins theory for isotropic systems and the Maier-Saupe-McMillan approach for anisotropic mixing were utilised for this purpose.
- It was shown that that binary mixtures of ITZ with polymers produced by quench cooling do not always form fully disordered systems. Depending on the itraconazole and polymer ratio, anisotropic, liquid crystalline and phase separated mixtures may form.
- A comprehensive review of the LC nature of ITZ was delivered in this study and could be used as a guide to predict the correct identity of the phases, of a key relevance to stability and formulation design.
- For the first time, a full binary phase diagram for the ITZ-SUC cocrystal was experimentally determined using thermal analysis method and three eutectic phases in the phase diagram were identified.
- E_1 phase, composed of ITZ_SUC and SUC was successfully produced by a fast-evaporation crystallisation method.

- A new method for the ITZ-SUC cocrystal crystallisation using acetone as a "green alternative" to the solvents used by other researchers was optimised.
- The formation of another polymorphic form of SUC, the α form, was observed upon flash cooling of the melted ITZ and SUC mixtures for samples with prevalent SUC content.
- It was confirmed that ball milling leads to the breakage of the hydrogen bond formed between ITZ and SUC in the cocrystal and consequently leads to the formation of a disordered mixture of ITZ and SUC.
- The ITZ-SUC cocrystal demonstrated an improved solubility in comparison to crystalline ITZ and ITZ supersaturation at C_{max} obtained by dissolving the cocrystal was extended up to 30 minutes followed by a slow and a steady decrease in ITZ concentration during the dynamic solubility studies in SGF and FaSSIF media.
- All the binary and ternary SDs obtained by ball milling physical mixtures of ITZ and SUC; ITZ and EUD as well as ITZ, SUC and EUD showed enhanced drug solubility when compared to that of crystalline ITZ.
- Addition of SUC, as a pH-adjuster, increased solubility of ITZ in FaSSIF.
- Addition of EUD into the ball milled ITZSUC1:2m system significantly enhanced solubility of ITZ in FaSSIF. The concentration of ITZ after 240 minutes of the studies was recorded to be 4.0 and 25.4 μg/ml for ITZ:SUC1:2/EUD20m and ITZ:SUC1:2/EUD40m, respectively, which represent 400- and 2,500-fold enhancement in the ITZ supersaturation.

6.3 Future Directions

- The thermodynamic phase diagram constructed in Chapter 3 addressed the liquid crystalline properties of ITZ. Therefore, this model may be applied to study miscibility of other ITZ/polymer systems.
- As the ITZ-SUC cocrystal showed an enhanced solubility performance it would be desirable to formulate it into an oral solid dosage form. However, it should be kept in mind, that the physical stress that may be created during a formulation process may result in disruption of the hydrogen bond between the components and change its physical properties. It would be of interest to study the behaviour of this cocrystal under stress created by compression.
- It was observed that incorporation EUD into the binary system composed of ITZ and SUC in a molar ratio of 1:2 (ITZ:SUC1:2) greatly improved solubility of ITZ in FaSSIF. Perhaps, an increase in the EUD content up to 50 or 60% in a solid dispersion could lead to even

higher solubility of ITZ. Also, other polymers, or combination of polymers could be tested with ITZ:SUC1:2 system.

- It was shown that in FaSSIF the system composed of ITZ and SUC in a molar ratio of 1:2 resulted in better ITZ solubilisation than the systems composed of ITZ and SUC in a molar ratio 2:1 or 1:1. Therefore it would be desirable to study solubility of formulations with a higher SUC content.
- The E1 phase produced by the fast crystallisation method required using a large excess of SUC, where the molar ratio of ITZ to SUC was 1:20. Such a high ratio of SUC to ITZ was chosen to generate the supersaturation required for cocrystal formation. However, the phase diagram test showed that E1 form is composed of ITZ-SUC and SUC, where molar content ITZ to SUC is 1:2. Therefore it would be desirable to optimise this method further by reducing content of SUC.
- The eutectic phase E_1, composed of ITZ-SUC and SUC, was observed to form during the phase diagram tests. However, due to time and equipment restrictions, solubility studies were not conducted for the E_1 phase. It was previously reported that eutectic mixtures can significantly improve solubility and dissolution rate of drugs.[66]–[68] Thus, it would be highly recommended to conduct solubility and dissolution studies of the E_1 phase.
- For the most promising ITZ systems, it would also be compelling to perform stability studies under certain temperature and humidity conditions, which may further discriminate their suitability for formulation studies.
- Following on the stability studies, small scale formulation tests on incorporating the ITZ systems into capsules or tablets, would be advantageous. Direct comparisons in relation to e.g. ITZ dissolution kinetics could be made between the selected formulation prototypes and the commercial Sporanox® capsules to discern if they offer any benefit.

References

[1] A. Siew, *Solving Poor Solubility with Amorphous Solid Dispersions*, vol. 38, no. 10. 2014.

[2] C. Lipinski, "Poor solubility - an industry wide problem in drug discovery," *Am. Pharm. Rev.*, vol. 5, no. January, pp. 82–85, 2002.

[3] W. Curatolo, "Physical chemical properties of oral drug candidates in the discovery and exploratory development settings," *Pharmaceutical Science and Technology Today*. 1998.

[4] G. L. Amidon, H. Lennernäs, V. P. Shah, and J. R. Crison, "A Theoretical Basis for a Biopharmaceutic Drug Classification: The Correlation of in Vitro Drug Product Dissolution and in Vivo Bioavailability," *Pharm. Res. An Off. J. Am. Assoc. Pharm. Sci.*, 1995.

[5] J. M. Butler and J. B. Dressman, "The Developability Classification System: Application of Biopharmaceutics Concepts to Formulation Development," *J. Pharm. Sci.*, vol. 99, no. 12, pp. 4940–4954, Dec. 2010.

[6] Fda, Cder, Purdie, and Florine P, "Waiver of In Vivo Bioavailability and Bioequivalence Studies for Immediate-Release Solid Oral Dosage Forms Based on a Biopharmaceutics Classification System Guidance for Industry," 2017.

[7] D. D. S. Particle Sciences, "Biopharmaceutical Classification System and Formulation Development," vol. 9, pp. 1–2, 2011.

[8] B. T. Smith, *Physical Pharmacy*. Pharmaceutical Press, 2016.

[9] H. R. Guzmán, M. Tawa, Z. Zhang, P. Ratanabanangkoon, P. Shaw, C. R. Gardner, H. Chen, J. P. Moreau, Ö. Almarsson, and J. F. Remenar, "Combined use of crystalline salt forms and precipitation inhibitors to improve oral absorption of celecoxib from solid oral formulations," *J. Pharm. Sci.*, vol. 96, no. 10, pp. 2686–2702, Oct. 2007.

[10] K. Sugano, A. Okazaki, S. Sugimoto, S. Tavornvipas, A. Omura, and T. Mano, "Solubility and Dissolution Profile Assessment in Drug Discovery," 2007.

[11] A. A. Noyes and W. R. Whitney, "The rate of solution of solid substances in their own solutions," *J. Am. Chem. Soc.*, vol. 19, no. 12, pp. 930–934, 1897.

[12] W. Nernst, "Zur Theorie der Reaktionsgeschwindigkeit in heterogenen Systemen," *Zeitschrift für Phys. Chemie*, vol. 47, pp. 52–55, 1904.

[13] E. Brunner, “Reaktionsgeschwindigkeit in heterogenen Systemen,” *Zeitschrift für Phys. Chemie*, vol. 43, no. 1897, pp. 56–102, 1904.

[14] D. Horter and J. B. Dressmä, “Influence of physicochemical properties on dissolution of drugs q in the gastrointestinal tract,” *Adv. Drug Deliv. Rev.*, vol. 46, pp. 75–87, 2001.

[15] M. E. Aulton and K. Taylor, *Aulton’s pharmaceutics : the design and manufacture of medicines*. Churchill Livingstone/Elsevier, 2013.

[16] H. D. Williams, N. L. Trevaskis, S. A. Charman, R. M. Shanker, W. N. Charman, C. W. Pouton, and C. J. H. Porter, “Strategies to Address Low Drug Solubility in Discovery and Development,” *Pharmacol. Rev. Pharmacol Rev*, vol. 65, pp. 315–499, 2013.

[17] J. P. Möschwitzer, “Drug nanocrystals in the commercial pharmaceutical development process,” *Int. J. Pharm.*, vol. 453, pp. 142–156, 2013.

[18] N. Rasenack, H. Hartenhauer, and B. W. Müller, “Microcrystals for dissolution rate enhancement of poorly water-soluble drugs,” *Int. J. Pharm.*, vol. 254, pp. 137–145, 2003.

[19] L. Yu, “Amorphous pharmaceutical solids: preparation, characterization and stabilization,” *Adv. Drug Deliv. Rev.*, vol. 48, pp. 27–42, 2001.

[20] C. L. Stevenson, D. B. Bennett, and D. Lechuga-Ballesteros, “MINIREVIEW Pharmaceutical Liquid Crystals: The Relevance of Partially Ordered Systems,” *J. Pharm. Sci.*, vol. 94, no. 9, pp. 1861–1880, 2005.

[21] L. R. Hilden and K. R. Morris, “Physics of amorphous solids.,” *J. Pharm. Sci.*, vol. 93, no. 1, pp. 3–12, Jan. 2004.

[22] N. Schultheiss and A. Newman, “Pharmaceutical cocrystals and their physicochemical properties,” *Crystal Growth and Design*, vol. 9, no. 6. pp. 2950–2967, 2009.

[23] J. Haleblian and W. McCrone, “Pharmaceutical applications of polymorphism,” *J. Pharm. Sci.*, vol. 58, no. 8, pp. 911–929, 1969.

[24] D. Singhal and W. Curatolo, “Drug polymorphism and dosage form design: A practical perspective,” *Advanced Drug Delivery Reviews*, vol. 56, no. 3. pp. 335–347, 2004.

[25] D. K. Bučar, R. W. Lancaster, and J. Bernstein, “Disappearing Polymorphs Revisited,” *Angew. Chemie - Int. Ed.*, vol. 54, no. 24, pp. 6972–6993, 2015.

[26] R. Liu, *Water insoluble drug formulation*. CRC Press, 2008.

[27] S. R. Byrn, G. Zografi, and X. S. Chen, *Solvates and Hydrates*. 2017.

[28] M. Pudipeddi and A. T. M. Serajuddin, "Trends in solubility of polymorphs," *J. Pharm. Sci.*, vol. 94, no. 5, pp. 929–939, 2005.

[29] S. M. Berge, L. D. Bighley, and D. C. Monkhouse, "Pharmaceutical Salts," *J. Pharm. Sci.*, vol. 66, no. 1, pp. 1–19, Jan. 1977.

[30] D. P. Elder, R. Holm, and H. Lopez De Diego, "Use of pharmaceutical salts and cocrystals to address the issue of poor solubility," *Int. J. Pharm.*, vol. 453, pp. 88–100, 2013.

[31] P. H. Stahl and C. Wermuth, *Handbook of Pharmaceutical Salts: Properties, Selection, and Use*. VHCA, 2002.

[32] S. L. Childs, G. P. Stahly, and A. Park, "The salt-cocrystal continuum: The influence of crystal structure on ionization state," *Mol. Pharm.*, vol. 4, no. 3, pp. 323–338, 2007.

[33] A. J. Cruz-Cabeza, "Acid–base crystalline complexes and the pKa rule," *CrystEngComm*, vol. 14, no. 20, pp. 6362–6365, 2012.

[34] A. O. Surov, A. P. Voronin, A. A. Simagina, A. V Churakov, and G. L. Perlovich, "Pharmaceutical salts of biologically active hydrazone compound salinazid: Crystallographic, solubility, and thermodynamic aspects," *Cryst. Growth Des.*, vol. 16, no. 5, pp. 2605–2617, 2016.

[35] M. Z. P. Vishweshwar, J. McMahon, J. Bis, "Pharmaceutical Co-Crystals," *Int. J. Drug Dev. Res.*, vol. 3, no. 2, pp. 26–33, 2011.

[36] R. Thakuria, A. Delori, W. Jones, M. P. Lipert, L. Roy, and N. Rodríguez-Hornedo, "Pharmaceutical cocrystals and poorly soluble drugs," *Int. J. Pharm.*, vol. 453, pp. 101–125, 2013.

[37] Fda and Cder, "Regulatory Classification of Pharmaceutical Co-Crystals Guidance for Industry Regulatory Classification of Pharmaceutical Co-Crystals Guidance for Industry Contains Nonbinding Recommendations." [Online]. Available: http://www.fda.gov/Drugs/GuidanceComplianceRegulatoryInformation/Guidances/default.htm. [Accessed: 18-Jun-2018].

[38] S. Kumar, A. Nanda, and a, "Pharmaceutical Cocrystals: An Overview," *Indian J. Pharm. Sci.*, vol. 79, no. 6, pp. 858–871, Jan. 2017.

[39] N. Blagden, M. de Matas, P. T. Gavan, and P. York, "Crystal engineering of active

pharmaceutical ingredients to improve solubility and dissolution rates," *Adv. Drug Deliv. Rev.*, vol. 59, no. 7, pp. 617–630, 2007.

[40] G. R. Desiraju, "Supramolecular Synthons in Crystal Engineering—A New Organic Synthesis," *Angew. Chemie Int. Ed. English*, vol. 34, no. 21, pp. 2311–2327, 1995.

[41] M. C. Etter, "Encoding and Decoding Hydrogen-Bond Patterns of Organic Compounds," *Acc. Chem. Res.*, vol. 23, no. 4, pp. 120–126, 1990.

[42] Ö. Almarsson and M. J. Zaworotko, "Crystal engineering of the composition of pharmaceutical phases. Do pharmaceutical co-crystals represent a new path to improved medicines?," *Chemical Communications*, no. 17. pp. 1889–1896, 2004.

[43] H.-G. Lee, G. G. Z. Zhang, and D. R. Flanagan, "Cocrystal Intrinsic Dissolution Behavior Using a Rotating Disk," *J. Pharm. Sci.*, vol. 100, no. 5, pp. 1736–1744, May 2011.

[44] M. L. Cheney, D. R. Weyna, N. Shan, M. Hanna, L. Wojtas, and M. J. Zaworotko, "Coformer Selection in Pharmaceutical Cocrystal Development: a Case Study of a Meloxicam Aspirin Cocrystal That Exhibits Enhanced Solubility and Pharmacokinetics," *J. Pharm. Sci.*, vol. 100, no. 6, pp. 2172–2181, Jun. 2011.

[45] J. F. Remenar, S. L. Morissette, M. L. Peterson, B. Moulton, J. M. MacPhee, H. R. Guzmán, and O. Almarsson, *Crystal engineering of novel cocrystals of a triazole drug with 1,4-dicarboxylic acids.*, vol. 125, no. 28. 2003.

[46] B. Hancock and G. Zografi, "Characteristics and significance of the amorphous state in pharmaceutical systems," *J. Pharm. Sci.*, vol. 86, no. 1, pp. 1–12, 1997.

[47] K. A. Graeser, J. E. Patterson, J. A. Zeitler, and T. Rades, "The Role of Configurational Entropy in Amorphous Systems.," *Pharmaceutics*, vol. 2, no. 2, pp. 224–244, May 2010.

[48] M. Yoshioka, B. C. Hancock, and G. Zografi, "Crystallization of Indomethacin from the Amorphous State below and above Its Glass Transition Temperature," *J. Pharm. Sci.*, vol. 83, no. 12, pp. 1700–1705, 1994.

[49] B. C. Hancock, S. L. Shamblin, and G. Zografi, "Molecular Mobility of Amorphous Pharmaceutical Solids Below Their Glass Transition Temperatures," *Pharmaceutical Research: An Official Journal of the American Association of Pharmaceutical Scientists*, vol. 12, no. 6. pp. 799–806, 1995.

[50] B. C. Hancock and S. L. Shamblin, "Molecular mobility of amorphous pharmaceuticals

determined using differential scanning calorimetry," *Thermochim. Acta*, vol. 380, no. 2, pp. 95–107, Dec. 2001.

[51] L. I. Blaabjerg, E. Lindenberg, T. Rades, H. Grohganz, and K. Löbmann, "Influence of preparation pathway on the glass forming ability," *Int. J. Pharm.*, vol. 521, no. 1–2, pp. 232–238, Apr. 2017.

[52] K. A. Graeser, C. J. Strachan, J. E. Patterson, K. C. Gordon, and T. Rades, "Physicochemical properties and stability of two differently prepared amorphous forms of simvastatin," *Cryst. Growth Des.*, vol. 8, no. 1, pp. 128–135, 2008.

[53] P. Karmwar, K. Graeser, K. C. Gordon, C. J. Strachan, and T. Rades, "Investigation of properties and recrystallisation behaviour of amorphous indomethacin samples prepared by different methods," *Int. J. Pharm.*, vol. 417, pp. 94–100, 2010.

[54] M. Otsuka, J.-I. Nishizawa, N. Fukura, and T. Sasaki, "Characterization of Poly-Amorphous Indomethacin by Terahertz Spectroscopy," *J. Infrared, Millimeter, Terahertz Waves*, vol. 33, no. 9, pp. 953–962, 2012.

[55] R. Lefort, A. De Gusseme, J.-F. Willart, F. Danède, and M. Descamps, "Solid state NMR and DSC methods for quantifying the amorphous content in solid dosage forms: an application to ball-milling of trehalose," *Int. J. Pharm.*, vol. 280, pp. 209–219, 2004.

[56] M. J. Stephen and J. P. Straley, *Physics of liquid crystals Liquid Crystals in General*, vol. 46, no. 4. 1974.

[57] S. Kumar, *Liquid Crystals: Experimental Study of Physical Properties and Phase Transitions*. Cambridge University Press, 2001.

[58] V. V. D. Demus, J. Goodby, G. W. Gray, H.-W. Spiess, *Handbook of Liquid Crystals*. Weinheim, Germany: Wiley-VCH Verlag GmbH, 1998.

[59] K. Binnemans, "Lanthanidomesogens," *Handb. Phys. Chem. Rare Earths*, vol. 43, pp. 1–158, 2013.

[60] M. Barón, "Definitions of basic terms relating to low-molar-mass and polymer liquid crystals (IUPAC Recommendations 2001)," *Pure Appl. Chem.*, vol. 73, no. 5, 2001.

[61] A. A. Collyer, Ed., *Liquid Crystal Polymers: From Structures to Applications*. Dordrecht: Springer Netherlands, 1993.

[62] P. J. Collings, "Introduction to Liquid Crystals: Chemistry and Physics," *Am. J. Phys.*, vol.

66, no. 6, p. 551, 1998.

[63] W. L. Chiou and S. Riegelman, “Pharmaceutical applications of solid dispersion systems,” *J. Pharm. Sci.*, vol. 60, no. 9, pp. 1281–1302, 1971.

[64] S. J. Dengale, H. Grohganz, T. Rades, and K. Löbmann, “Recent advances in co-amorphous drug formulations,” *Adv. Drug Deliv. Rev.*, vol. 100, pp. 116–125, May 2016.

[65] C. Leuner and J. Dressman, “Improving drug solubility for oral delivery using solid dispersions.,” *Eur. J. Pharm. Biopharm.*, vol. 50, no. 1, pp. 47–60, 2000.

[66] S. Cherukuvada and A. Nangia, “Fast dissolving eutectic compositions of two anti-tubercular drugs,” *CrystEngComm*, vol. 14, no. 7, pp. 2579–2588, 2012.

[67] D. Law, W. Wang, E. A. Schmitt, Y. Qiu, S. L. Krill, and J. J. Fort, “Properties of rapidly dissolving eutectic mixtures of poly(ethylene glycol) and fenofibrate: The eutectic microstructure,” *J. Pharm. Sci.*, vol. 92, no. 3, pp. 505–515, 2003.

[68] A. Górniak, A. Wojakowska, B. Karolewicz, and J. Pluta, “Phase diagram and dissolution studies of the fenofibrate-acetylsalicylic acid system,” *J. Therm. Anal. Calorim.*, vol. 104, no. 3, pp. 1195–1200, 2011.

[69] R. Laitinen, P. A. Priemel, S. Surwase, K. Graeser, C. J. Strachan, H. Grohganz, and T. Rades, “Theoretical Considerations in Developing Amorphous Solid Dispersions,” Springer, New York, NY, 2014, pp. 35–90.

[70] A. H. Goldberg, M. Gibaldi, and J. L. Kanig, “Increasing Dissolution Rates and Gastrointestinal Absorption of Drugs via solid Solutions and Eutectic mixtures II,” *J. Pharm. Sci.*, vol. 55, no. 5, pp. 482–487, May 1966.

[71] A. H. Goldberg, M. Gibaldi, and J. L. Kanig, “Increasing dissolution rates and gastrointestinal absorption of drugs via solid solutions and eutectic mixtures III: Experimental evaluation of griseofulvin-succinic acid solid solution,” *J. Pharm. Sci.*, vol. 55, no. 5, pp. 487–492, 1966.

[72] A. H. Goldberg, M. Gibaldi, J. L. Kanig, and M. Mayersohn, “Increasing Dissolution Rates and Gastrointestinal Absorption of Drugs Via Solid Solutions and Eutectic Mixtures IV: Chloramphenicol—Urea System,” *J. Pharm. Sci.*, vol. 55, no. 6, pp. 581–583, Jun. 1966.

[73] M. K. Mishra, U. Ramamurty, and G. R. Desiraju, “Solid solution hardening of molecular crystals: Tautomeric polymorphs of omeprazole,” *J. Am. Chem. Soc.*, vol. 137, no. 5, pp.

1794–1797, 2015.

[74] S. Baghel, H. Cathcart, and N. J. O'Reilly, "Polymeric Amorphous Solid Dispersions: A Review of Amorphization, Crystallization, Stabilization, Solid-State Characterization, and Aqueous Solubilization of Biopharmaceutical Classification System Class II Drugs," *J. Pharm. Sci.*, 2016.

[75] J. Yang, K. Grey, and J. Doney, "An improved kinetics approach to describe the physical stability of amorphous solid dispersions," *Int. J. Pharm.*, vol. 384, pp. 24–31, 2010.

[76] G. Van, S. Janssens, and G. Van Den Mooter, "Review: physical chemistry of solid dispersions," *JPP*, vol. 61, pp. 1571–1586, 2009.

[77] H. Konno and L. S. Taylor, "Influence of Different Polymers on the Crystallization Tendency of Molecularly Dispersed Amorphous Felodipine," *J. Pharm. Sci.*, vol. 95, no. 12, pp. 2692–2705, Dec. 2006.

[78] "SPORANOX® (itraconazole) Capsules." [Online]. Available: https://www.accessdata.fda.gov/drugsatfda_docs/label/2009/020083s040s041s044lbl.pdf. [Accessed: 06-Aug-2018].

[79] "CESAMET™ (nabilone) Capsules." [Online]. Available: https://www.accessdata.fda.gov/drugsatfda_docs/label/2006/018677s011lbl.pdf. [Accessed: 06-Aug-2018].

[80] "PROGRAF® tacrolimus capsules tacrolimus injection (for intravenous infusion only)." [Online]. Available: https://www.accessdata.fda.gov/drugsatfda_docs/label/2009/050708s027,050709s021lbl.pdf. [Accessed: 06-Aug-2018].

[81] C. A. McCarthy, R. J. Ahern, R. Dontireddy, K. B. Ryan, and A. M. Crean, "Mesoporous silica formulation strategies for drug dissolution enhancement: a review," *Expert Opin. Drug Deliv.*, vol. 13, no. 1, pp. 93–108, 2016.

[82] K. K. Qian and R. H. Bogner, "REVIEWS Application of Mesoporous Silicon Dioxide and Silicate in Oral Amorphous Drug Delivery Systems," *J Pharm Sci*, vol. 101, pp. 444–463, 2011.

[83] N. Chieng, J. Aaltonen, D. Saville, and T. Rades, "Physical characterization and stability of amorphous indomethacin and ranitidine hydrochloride binary systems prepared by mechanical activation," *Eur. J. Pharm. Biopharm.*, vol. 71, no. 1, pp. 47–54, 2009.

[84] A. Newman, S. M. Reutzel-Edens, and G. Zografi, “Coamorphous Active Pharmaceutical Ingredient–Small Molecule Mixtures: Considerations in the Choice of Coformers for Enhancing Dissolution and Oral Bioavailability,” *J. Pharm. Sci.*, vol. 107, no. 1, pp. 5–17, 2018.

[85] R. Laitinen, K. Löbmann, C. J. Strachan, H. Grohganz, and T. Rades, “Emerging trends in the stabilization of amorphous drugs,” *Int. J. Pharm.*, vol. 453, pp. 65–79, 2013.

[86] K. L€ Obmann, R. Laitinen, H. Grohganz, K. C. Gordon, C. Strachan, and T. Rades, “Coamorphous Drug Systems: Enhanced Physical Stability and Dissolution Rate of Indomethacin and Naproxen,” *Mol. Pharm.*, vol. 8, pp. 1919–1928, 2011.

[87] R. B. Chavan, R. Thipparaboina, D. Kumar, and N. R. Shastri, “Co amorphous systems: A product development perspective,” *Int. J. Pharm.*, vol. 515, no. 1–2, pp. 403–415, Dec. 2016.

[88] K. Löbmann, H. Grohganz, R. Laitinen, C. Strachan, and T. Rades, “Amino acids as co-amorphous stabilizers for poorly water soluble drugs--Part 1: preparation, stability and dissolution enhancement.,” *Eur. J. Pharm. Biopharm.*, vol. 85, no. 3 Pt B, pp. 873–81, Nov. 2013.

[89] K. Löbmann, R. Laitinen, C. Strachan, T. Rades, and H. Grohganz, “Amino acids as co-amorphous stabilizers for poorly water-soluble drugs--Part 2: molecular interactions.,” *Eur. J. Pharm. Biopharm.*, vol. 85, no. 3 Pt B, pp. 882–8, Nov. 2013.

[90] D. J. Van Drooge, W. L. J. Hinrichs, M. R. Visser, and H. W. Frijlink, “Characterization of the molecular distribution of drugs in glassy solid dispersions at the nano-meter scale, using differential scanning calorimetry and gravimetric water vapour sorption techniques,” *Int. J. Pharm.*, vol. 310, pp. 220–229, 2006.

[91] P. Srinarong, J. H. Faber, M. R. Visser, W. L. J. Hinrichs, and H. W. Frijlink, “Strongly enhanced dissolution rate of fenofibrate solid dispersion tablets by incorporation of superdisintegrants,” *Eur. J. Pharm. Biopharm.*, vol. 73, pp. 154–161, 2009.

[92] P. J. Marsac, S. L. Shamblin, and L. S. Taylor, “Theoretical and practical approaches for prediction of drug-polymer miscibility and solubility,” *Pharm. Res.*, vol. 23, no. 10, pp. 2417–2426, 2006.

[93] P. J. Marsac, T. Li, and L. S. Taylor, “Estimation of drug-polymer miscibility and solubility in amorphous solid dispersions using experimentally determined interaction

parameters," *Pharm. Res.*, vol. 26, no. 1, pp. 139–151, 2009.

[94] A. C. F. Rumondor, I. Ivanisevic, S. Bates, D. E. Alonzo, and L. S. Taylor, "Evaluation of drug-polymer miscibility in amorphous solid dispersion systems.," *Pharm. Res.*, vol. 26, no. 11, pp. 2523–34, Nov. 2009.

[95] F. Qian, J. Huang, and M. Hussain, "Drug–polymer solubility and miscibility: Stability consideration and practical challenges in amorphous solid dispersion development," *J. Pharm. Sci.*, vol. 99, no. 7, pp. 2941–2947, 2010.

[96] W. Brostow, R. Chiu, I. M. Kalogeras, and A. Vassilikou-Dova, "Prediction of glass transition temperatures: Binary blends and copolymers," *Mater. Lett.*, vol. 62, no. 17–18, pp. 3152–3155, Jun. 2008.

[97] M. Gordon and J. Taylor, "Ideal copolymers and the second-order transitions of synthetic rubbers. I. Non-crystalline copolymers," *J. Appl. Chem.*, vol. 2, no. 9, pp. 493–500, 1952.

[98] G. Van Den Mooter, J. Van Den Brande, P. Augustijns, and R. Kinget, "Glass forming properties of benzodiazepines and co-evaporate systems with poly (hydroxyethyl methacrylate)," *J. Therm. Anal.*, vol. 57, pp. 493–507, 1999.

[99] Charles M. Hansen, "The three dimensional solubility parameter and solvent diffusion coefficient. Their Importance In Surface Coating Formulation," Danish Technical Press, Copenhagen, 1967.

[100] C. M. Hansen, *Hansen solubility parameters : a user's handbook*. CRC Press, 2007.

[101] D. J. Greenhalgh, A. C. Williams, P. Timmins, and P. York, "Solubility parameters as predictors of miscibility in solid dispersions," *J. Pharm. Sci.*, vol. 88, no. 11, pp. 1182–1190, 1999.

[102] D. W. van Krevelen and K. te Nijenhuis, *Properties of Polymers. Their Correlation with Chemical Structure. Their Numerical Estimation and Prediction from Additive Group Contributions.*, 4th ed. Elsevier, 2009.

[103] T. Kitak, A. Dumičič, O. Planinšek, R. Šibanc, S. Srčič, T. Rades, H. Grohganz, and K. Löbmann, "Determination of solubility parameters of ibuprofen and ibuprofen lysinate," *Molecules*, vol. 20, no. 12, pp. 21549–21568, 2015.

[104] I. Teraoka, *Polymer Solutions: An Introduction to Physical Properties.*, vol. 3. John Wiley & Sons, Inc., 2002.

[105] C. Donnelly, Y. Tian, C. Potter, D. S. Jones, and G. P. Andrews, “Probing the Effects of Experimental Conditions on the Character of Drug-Polymer Phase Diagrams Constructed Using Flory-Huggins Theory.,” *Pharm. Res.*, no. 5, Jul. 2014.

[106] Y. Tian, V. Caron, D. S. Jones, A.-M. Healy, and G. P. Andrews, “Using Flory-Huggins phase diagrams as a pre-formulation tool for the production of amorphous solid dispersions: a comparison between hot-melt extrusion and spray drying.,” *J. Pharm. Pharmacol.*, vol. 66, no. 2, pp. 256–74, Feb. 2014.

[107] Y. Tian, J. Booth, E. Meehan, D. S. Jones, S. Li, and G. P. Andrews, “Construction of drug-polymer thermodynamic phase diagrams using Flory-Huggins interaction theory: identifying the relevance of temperature and drug weight fraction to phase separation within solid dispersions.,” *Mol. Pharm.*, vol. 10, no. 1, pp. 236–48, Jan. 2013.

[108] P. J. Marsac, T. Li, and L. S. Taylor, “Estimation of drug-polymer miscibility and solubility in amorphous solid dispersions using experimentally determined interaction parameters.,” *Pharm. Res.*, vol. 26, no. 1, pp. 139–51, Jan. 2009.

[109] Y. Zhao and P. Inbar, “Prediction of the thermal phase diagram of amorphous solid dispersions by Flory–Huggins theory,” *J. Pharm. Sci.*, vol. 100, no. 8, pp. 3196–3207, 2011.

[110] S. Thakral and N. Thakral, “Prediction of drug–polymer miscibility through the use of solubility parameter based flory–huggins interaction parameter and the experimental validation: PEG as,” *J. Pharm. Sci.*, vol. 102, no. 7, pp. 2254–2263, 2013.

[111] M. Yang, P. Wang, and C. Gogos, “Prediction of acetaminophen’s solubility in poly(ethylene oxide) at room temperature using the Flory-Huggins theory.,” *Drug Dev. Ind. Pharm.*, vol. 39, no. 1, pp. 102–8, Jan. 2013.

[112] C. J. Arrighi V, Cabral J, *Miscibility in: Encyclopedia of Polymer Science and Technology*, vol. 7. John Wiley & Sons, Inc., 2002.

[113] M. Rubinstein and R. H. Colby, *Polymer Physics*. Oxford University Press, 2003.

[114] J. Peeters and P. Neeskens, “Characterization of the interaction of 2-hydroxypropyl-β-cyclodextrin with itraconazole at pH 2, 4, and 7,” *J. Pharm. Sci.*, vol. 91, no. 6, pp. 1414–1422, 2002.

[115] H. S. Ghazal, A. M. Dyas, J. L. Ford, and G. A. Hutcheon, “In vitro evaluation of the dissolution behaviour of itraconazole in bio-relevant media,” *Int. J. Pharm.*, vol. 366, no. 1–2, pp. 117–123, 2009.

[116] K. Six, G. Verreck, J. Peeters, K. Binnemans, H. Berghmans, P. Augustijns, R. Kinget, and G. Van den Mooter, “Investigation of thermal properties of glassy itraconazole: Identification of a monotropic mesophase,” *Thermochim. Acta*, vol. 376, pp. 175–181, 2001.

[117] P. Gilis, V. De Conde, and R. Vandecruys, “Pellets having a core coated with an antifungal and a polymer,” 18-Mar-2005.

[118] S. Jaruratanasirikul and A. Kleepkaew, “Influence of an acidic beverage (Coca-Cola) on the absorption of itraconazole,” *Eur. J. Clin. Pharmacol.*, vol. 52, no. 3, pp. 235–237, 1997.

[119] J. A. Barone, B. L. Moskovitz, J. Guarnieri, A. E. Hassell, J. L. Colaizzi, R. H. Bierman, and L. Jessen, “Food interaction and steady-state pharmacokinetics of itraconazole oral solution in healthy volunteers.,” *Pharmacotherapy*, vol. 18, no. 2, pp. 295–301, 1998.

[120] K. De Beule and J. Van Gestel, “Pharmacology of Itraconazole,” *Drugs*, vol. 61, no. Supplement 1, pp. 27–37, 2001.

[121] J. Brouwers, S. Geboers, R. Mols, J. Tack, and P. Augustijns, “Gastrointestinal behavior of itraconazole in humans – Part 1: Supersaturation from a solid dispersion and a cyclodextrin-based solution,” *Int. J. Pharm.*, vol. 525, no. 1, pp. 211–217, 2017.

[122] A. L. Sarode, H. Sandhu, N. Shah, W. Malick, and H. Zia, “Hot melt extrusion (HME) for amorphous solid dispersions: Predictive tools for processing and impact of drug-polymer interactions on supersaturation.,” *Eur. J. Pharm. Sci.*, vol. 48, no. 3, pp. 371–384, Dec. 2012.

[123] J. C. Dinunzio, D. A. Miller, W. Yang, J. W. McGinity, and R. O. Williams, “Amorphous compositions using concentration enhancing polymers for improved bioavailability of itraconazole,” *Mol. Pharm.*, vol. 5, no. 6, pp. 968–980, 2008.

[124] D. a Miller, J. C. DiNunzio, W. Yang, J. W. McGinity, and R. O. Williams, “Targeted intestinal delivery of supersaturated itraconazole for improved oral absorption.,” *Pharm. Res.*, vol. 25, no. 6, pp. 1450–9, Jun. 2008.

[125] G. Van Den Mooter, “The use of amorphous solid dispersions: A formulation strategy to overcome poor solubility and dissolution rate,” *Drug Discov. Today Technol.*, vol. 9, no. 2, 2012.

[126] J. Maincent and R. O. 3rd Williams, “Sustained-release amorphous solid dispersions.,” *Drug Deliv. Transl. Res.*, 2018.

[127] L. Yu, “Amorphous pharmaceutical solids: Preparation, characterization and stabilization,” *Adv. Drug Deliv. Rev.*, vol. 48, no. 1, pp. 27–42, 2001.

[128] Y. E. Sun, J. Tao, G. G. Z. Zhang, and L. Yu, “Solubilities of Crystalline Drugs in Polymers : An Improved Analytical Method and Comparison of Solubilities of Indomethacin and Nifedipine in PVP , PVP / VA , and PVAc,” *J. Pharm. Sci.*, vol. 99, no. 9, pp. 4023–4031, 2010.

[129] Y. Huang and W.-G. Dai, “Fundamental aspects of solid dispersion technology for poorly soluble drugs,” *Acta Pharm. Sin. B*, vol. 4, no. 1, pp. 18–25, Feb. 2014.

[130] R. Mohan, H. Lorenz, and A. S. Myerson, “Solubility Measurement Using Differential Scanning Calorimetry,” *Ind. Eng. Chem. Res.*, vol. 41, no. 19, pp. 4854–4862, 2002.

[131] X. Xie, R. Li, S. Tjong, and C. Tang, “Flory-huggins interaction parameters of LCP/thermoplastic blends measured by DSC analysis,” *J. Therm. Anal. …*, vol. 70, pp. 541–548, 2002.

[132] P. J. Marsac, S. L. Shamblin, and L. S. Taylor, “Theoretical and practical approaches for prediction of drug-polymer miscibility and solubility.,” *Pharm. Res.*, vol. 23, no. 10, pp. 2417–26, Oct. 2006.

[133] J. Tao, Y. Sun, G. G. Z. Zhang, and L. Yu, “Solubility of small-molecule crystals in polymers: D-Mannitol in PVP, indomethacin in PVP/VA, and nifedipine in PVP/VA,” *Pharm. Res.*, vol. 26, no. 4, pp. 855–864, 2009.

[134] D. Lin and Y. Huang, “A thermal analysis method to predict the complete phase diagram of drug-polymer solid dispersions.,” *Int. J. Pharm.*, vol. 399, no. 1–2, pp. 109–15, Oct. 2010.

[135] V. Caron, L. Tajber, O. I. Corrigan, and A. M. Healy, “A comparison of spray drying and milling in the production of amorphous dispersions of sulfathiazole/polyvinylpyrrolidone and sulfadimidine/polyvinylpyrrolidone.,” *Mol. Pharm.*, vol. 8, no. 2, pp. 532–42, Apr. 2011.

[136] A. Mahieu, J.-F. F. Willart, E. Dudognon, F. Daneìde, and M. Descamps, “A new protocol to determine the solubility of drugs into polymer matrixes,” *Mol. Pharm.*, vol. 10, no. 2, pp. 560–566, 2013.

[137] M. M. Knopp, N. E. Olesen, P. Holm, P. Langguth, R. Holm, and T. Rades, “Influence of Polymer Molecular Weight on Drug-Polymer Solubility: A Comparison between

Experimentally Determined Solubility in PVP and Prediction Derived from Solubility in Monomer," *J. Pharm. Sci.*, vol. 104, no. 9, pp. 2905–2912, 2015.

[138] K. Wlodarski, W. Sawicki, A. Kozyra, and L. Tajber, "Physical stability of solid dispersions with respect to thermodynamic solubility of tadalafil in PVP-VA," *Eur. J. Pharm. Biopharm.*, vol. 96, pp. 237–246, Oct. 2015.

[139] M. M. Knopp, L. Tajber, Y. Tian, N. E. Olesen, D. S. Jones, A. Kozyra, K. Löbmann, K. Paluch, C. M. Brennan, R. Holm, A. M. Healy, G. P. Andrews, and T. Rades, "Comparative Study of Different Methods for the Prediction of Drug-Polymer Solubility," *Mol. Pharm.*, vol. 12, no. 9, pp. 3408–3419, 2015.

[140] T. Nishi and T. Wang, "Melting point depression and kinetic effects of cooling on crystallization in poly (vinylidene fluoride)-poly (methyl methacrylate) mixtures," *Macromolecules*, vol. 8, no. 6, 1975.

[141] A. C. F. Rumondor, P. J. Marsac, L. a Stanford, and L. S. Taylor, "Phase behavior of poly(vinylpyrrolidone) containing amorphous solid dispersions in the presence of moisture.," *Mol. Pharm.*, vol. 6, no. 5, pp. 1492–505, 2009.

[142] R. Pinal, "Entropy of Mixing and the Glass Transition of Amorphous Mixtures," *Entropy*, vol. 10, no. 3, pp. 207–223, Aug. 2008.

[143] A. Kini and S. B. Patel, "Pharmaceutical Development and Technology Phase behavior, intermolecular interaction, and solid state characterization of amorphous solid dispersion of Febuxostat Phase behavior, intermolecular interaction, and solid state characterization of amorphous so," *Pharm Dev Technol*, vol. 22, no. 1, pp. 45–57, 2017.

[144] A. Alzghoul, A. Alhalaweh, D. Mahlin, and C. A. S. Bergströ, "Experimental and Computational Prediction of Glass Transition Temperature of Drugs," *J. Chem. Inf. Model*, vol. 54, 2014.

[145] L. Z. Benet, "The role of BCS (biopharmaceutics classification system) and BDDCS (biopharmaceutics drug disposition classification system) in drug development.," *J. Pharm. Sci.*, vol. 102, no. 1, pp. 34–42, Jan. 2013.

[146] J. Patterson, A. Bary, and T. Rades, "Physical stability and solubility of the thermotropic mesophase of fenoprofen calcium as pure drug and in a tablet formulation," *Int. J. Pharm.*, vol. 247, no. 1–2, pp. 147–157, 2002.

[147] B. C. Hancock and M. Parks, "What is the true solubility advantage for amorphous

pharmaceuticals?," *Pharm. Res.*, vol. 17, no. 4, pp. 397–404, Apr. 2000.

[148] E. Shalaev, K. Wu, S. Shamblin, and J. F. Krzyzaniak, "Crystalline mesophases: Structure, mobility, and pharmaceutical properties," *Adv. Drug Deliv. Rev.*, vol. 100, pp. 194–211, May 2016.

[149] T. Rades, Y. Padmadisastra, and C. C. Müller-Goymann, "Thermal behaviour and solubility of fenoprofen calcium," *Pharmazie*, vol. 51, no. 11, pp. 846–851, 1996.

[150] A. Serajuddin, "Solid dispersion of poorly water soluble drugs: early promises, subsequent problems, and recent breakthroughs," *J. Pharm. Sci.*, vol. 88, no. 10, 1999.

[151] M. Mucha, "Polymer as an important component of blends and composites with liquid crystals," *Progress in Polymer Science (Oxford)*, vol. 28, no. 5. pp. 837–873, 2003.

[152] K. Six, C. Leuner, J. Dressman, G. Verreck, J. Peeters, N. Blaton, P. Augustijns, R. Kinget, and G. Van den Mooter, "Thermal properties of hot-stage extrudates of itraconazole and eudragit E100. Phase separation and polymorphism," *J. Therm. Anal. Calorim.*, vol. 68, no. 2, pp. 591–601, 2002.

[153] S. Janssens, A. De Zeure, A. Paudel, J. Van Humbeeck, P. Rombaut, and G. Van den Mooter, "Influence of Preparation Methods on Solid State Supersaturation of Amorphous Solid Dispersions: A Case Study with Itraconazole and Eudragit E100," *Pharm. Res.*, vol. 27, no. 5, pp. 775–785, 2010.

[154] M. Tarnacka, K. Adrjanowicz, E. Kaminska, K. Kaminski, K. Grzybowska, K. Kolodziejczyk, P. Wlodarczyk, L. Hawelek, G. Garbacz, A. Kocot, and M. Paluch, "Molecular dynamics of itraconazole at ambient and high pressure," *Phys. Chem. Chem. Phys.*, vol. 15, no. 47, pp. 20742–20752, 2013.

[155] E. U. Mapesa, M. Tarnacka, E. Kamińska, K. Adrjanowicz, M. Dulski, W. Kossack, M. Tress, W. K. Kipnusu, K. Kamiński, and F. Kremer, "Molecular dynamics of itraconazole confined in thin supported layers," *RSC Adv.*, vol. 4, no. 54, pp. 28432–28438, 2014.

[156] N. A. Mugheirbi, K. Fleischer, and L. Tajber, "A Rare Case of Mesomorphic Behavior–Molecular Reorientation of Itraconazole Liquid Crystal Induced by a Hygrothermal Treatment," *Cryst. Growth Des.*, vol. 16, no. 3, pp. 1329–1336, Mar. 2016.

[157] S. Janssens, H. N. de Armas, J. P. Remon, and G. Van den Mooter, "The use of a new hydrophilic polymer, Kollicoat IR®, in the formulation of solid dispersions of Itraconazole," *Eur. J. Pharm. Sci.*, vol. 30, no. 3–4, pp. 288–294, 2007.

[158] P. Pharmacy, “Miscibility of Itraconazole-Hydroxypropyl Methylcellulose Blends- Insights with High Resolution Analytical Methodologies,” 2015.

[159] S. Zhang, T. W. Y. Lee, and A. H. L. Chow, “Crystallization of Itraconazole Polymorphs from Melt,” *Cryst. Growth Des.*, p. acs.cgd.6b00342, 2016.

[160] L. M. Dwyer, V. K. Michaelis, M. O’Mahony, R. G. Griffin, and A. S. Myerson, “Confined crystallization of fenofibrate in nanoporous silica,” *CrystEngComm*, vol. 17, no. 41, pp. 7922–7929, 2015.

[161] H. Sackmann, “Thermodynamic aspects of polymorphism in liquid crystals,” *Pure Appl. Chem.*, vol. 38, no. 4, pp. 505–527, 1974.

[162] S. P. Bhardwaj, K. K. Arora, E. Kwong, A. Templeton, S. D. Clas, and R. Suryanarayanan, “Correlation between molecular mobility and physical stability of amorphous itraconazole,” *Mol. Pharm.*, vol. 10, no. 2, pp. 694–700, 2013.

[163] M. P. Fernandez-Ronco, M. Salvalaglio, J. Kluge, and M. Mazzotti, “Study of the preparation of amorphous itraconazole formulations,” *Cryst. Growth Des.*, vol. 15, no. 6, pp. 2686–2694, 2015.

[164] P. Piccinni, Y. Tian, A. McNaughton, J. Fraser, S. Brown, D. S. Jones, S. Li, and G. P. Andrews, “Solubility parameter-based screening methods for early-stage formulation development of itraconazole amorphous solid dispersions,” *J. Pharm. Pharmacol.*, p. n/a-n/a, 2016.

[165] S. Rauch, C. Selbmann, P. Bault, H. Sawade, G. Heppke, O. Morales-Saavedra, M. Y. M. Huang, and A. J??kli, “Glass forming banana-shaped compounds: Vitrified liquid crystal states,” *Phys. Rev. E - Stat. Nonlinear, Soft Matter Phys.*, vol. 69, no. 2 1, pp. 1–7, 2004.

[166] E.-J. Donth, *The Glass Transition*, vol. 48. Berlin, Heidelberg: Springer Berlin Heidelberg, 2001.

[167] J. W. P. Schmelzer, I. S. Gutzow, O. V. Mazurin, A. I. Priven, S. V. Todorova, and B. P. Petroff, *Glasses and the Glass Transition*. Weinheim, Germany: Wiley-VCH Verlag GmbH & Co. KGaA, 2011.

[168] J. Kerč and S. Srčič, “Thermal analysis of glassy pharmaceuticals,” *Thermochim. Acta*, vol. 248, no. 94, pp. 81–95, 1995.

[169] G. Rehage and J. Frenzel, “The Glass Transition and the Glassy State in Isotropic and Liquid

Crystalline Polymers," *Br. Polym. J.*, vol. 14, no. 4, pp. 173–179, 1982.

[170] J. Dong, Y. Ozaki, and K. Nakashima, "Infrared, Raman, and Near-Infrared Spectroscopic Evidence for the Coexistence of Various Hydrogen-Bond Forms in Poly(acrylic acid)," *Macromolecules*, vol. 30, no. 4, pp. 1111–1117, 1997.

[171] G. P. Crawford and S. Žumer, *Liquid crystals in complex geometries*. Taylor & Francis, 1996.

[172] E. R. Soul, N. Mohieddin Abukhdeir, and A. D. Rey, "Thermodynamics, Transition Dynamics, and Texturing in Polymer-Dispersed Liquid Crystals with Mesogens Exhibiting a Direct Isotropic/Smectic-A Transition," *Macromolecules*, vol. 42, pp. 9486–9497, 2009.

[173] L. Bedjaoui-Alachaher, F. Semdani, R. Meziane, and U. Maschke, "Thermophysical analysis of smectic a domains confined into a thermoplastic polymer matrix," *Mol. Cryst. Liq. Cryst.*, vol. 546, pp. 87–94, 2011.

[174] J. K. Srivastava, R. K. Singh, R. Dhar, and S. Singh, "Phase diagrams and morphology of polymer-dispersed liquid crystals: An analysis," *Liq. Cryst.*, vol. 39, no. 11, pp. 1402–1413, 2012.

[175] F. Benmouna, U. Maschke, X. Coqueret, and M. Benmouna, "Mixtures of Polymer Networks and Nematic Liquid Crystals," *Mol. Cryst. Liq. Cryst. Sci. Technol. Sect. A. Mol. Cryst. Liq. Cryst.*, vol. 330, no. 1, pp. 475–482, 1999.

[176] R. Benmouna and M. Benmouna, "Thermophysical and phase properties of polymer/liquid crystal systems: Theoretical aspects and experimental examples," *J. Chem. Eng. Data*, vol. 55, no. 5, pp. 1759–1767, 2010.

[177] A. Forster, J. Hempenstall, I. Tucker, and T. Rades, "Selection of excipients for melt extrusion with two poorly water-soluble drugs by solubility parameter calculation and thermal analysis," *Int. J. Pharm.*, vol. 226, pp. 147–161, 2001.

[178] B. A. Schuld, Norbert; Wolf, "Solvent quality as reflected in concentration- and temperature-dependent Flory-Huggins interaction parameters.," *J. Polym. Sci. Part B Polym. Phys.*, vol. 39, no. 6, pp. 651–662, 2001.

[179] K. Kamide, K. Sugamiya, T. Kawai, and Y. Miyazaki, "The Concentration Dependence of the Polymer–Solvent Interaction Parameter for Polystyrene–Methylcyclohexane System," *Polym. J.*, vol. 12, no. 1, pp. 67–69, Jan. 1980.

[180] M. M. Knopp, N. E. Olesen, Y. Huang, R. Holm, and T. Rades, “Statistical Analysis of a Method to Predict Drug-Polymer Miscibility,” *J. Pharm. Sci.*, vol. 105, no. 1, pp. 362–367, 2016.

[181] J. L. Calahan, S. C. Azali, E. J. Munson, and K. Nagapudi, “Investigation of Phase Mixing in Amorphous Solid Dispersions of AMG 517 in HPMC-AS Using DSC, Solid-State NMR, and Solution Calorimetry,” *Mol. Pharm.*, vol. 12, no. 11, pp. 4115–4123, 2015.

[182] A. Shevchenko, I. Miroshnyk, L. O. Pietilä, J. Haarala, J. Salmia, K. Sinervo, S. Mirza, B. Van Veen, E. Kolehmainen, Nonappa, and J. Yliruusi, “Diversity in itraconazole cocrystals with aliphatic dicarboxylic acids of varying chain length,” *Cryst. Growth Des.*, vol. 13, no. 11, pp. 4877–4884, 2013.

[183] A. Shevchenko, L. M. Bimbo, I. Miroshnyk, J. Haarala, K. Jelínková, K. Syrjänen, B. van Veen, J. Kiesvaara, H. A. Santos, and J. Yliruusi, “A new cocrystal and salts of itraconazole: comparison of solid-state properties, stability and dissolution behavior.,” *Int. J. Pharm.*, vol. 436, no. 1–2, pp. 403–9, Oct. 2012.

[184] C. A. Ober and R. B. Gupta, “Formation of itraconazole-succinic acid cocrystals by gas antisolvent cocrystallization.,” *AAPS PharmSciTech*, vol. 13, no. 4, pp. 1396–406, Dec. 2012.

[185] H. Yamashita, Y. Hirakura, M. Yuda, T. Teramura, and K. Terada, “Detection of Cocrystal Formation Based on Binary Phase Diagrams Using Thermal Analysis,” *Pharm. Res.*, vol. 30, no. 1, pp. 70–80, 2013.

[186] T. Y. K. Sekiguchi, I. Himuro, I. Horikoshi, T. Tsukada, T. Okamoto, “Thermal Analysis of Organic Medicinals. I. Detection of the Molecular Compound Formation by the Differential Thermal Analysis and by the Differential Scanning Calorimetry,” *Chem. Pharm. Bull.*, vol. 17, no. 1, pp. 191–199, 1969.

[187] H. Yamashita, Y. Hirakura, M. Yuda, and K. Terada, “Coformer screening using thermal analysis based on binary phase diagrams,” *Pharm. Res.*, vol. 31, no. 8, pp. 1946–1957, 2014.

[188] Y. Corvis, P. Négrier, M. Lazerges, S. Massip, J. M. Léger, and P. Espeau, “Lidocaine/ l - menthol binary system: Cocrystallization versus solid-state immiscibility,” *J. Phys. Chem. B*, vol. 114, no. 16, pp. 5420–5426, 2010.

[189] A. O. L. Évora, R. A. E. Castro, T. M. R. Maria, M. R. Silva, J. H. ter Horst, J. Canotilho, and

M. E. S. Eusébio, “Co-crystals of diflunisal and isomeric pyridinecarboxamides – a thermodynamics and crystal engineering contribution,” *CrystEngComm*, vol. 18, no. 25, pp. 4749–4759, 2016.

[190] S. Shah and M. A. Repka, “Melt Extrusion in Drug Delivery: Three Decades of Progress,” 2013, pp. 3–46.

[191] E. Stoler and J. C. Warner, “Non-Covalent derivatives: Cocrystals and eutectics,” *Molecules*, vol. 20, no. 8, pp. 14833–14848, 2015.

[192] D. R. Weyna, T. Shattock, P. Vishweshwar, and M. J. Zaworotko, “Synthesis and Structural Characterization of Cocrystals and Pharmaceutical Cocrystals: Mechanochemistry vs Slow Evaporation from Solution,” *Cryst. Growth Des.*, vol. 9, no. 2, pp. 1106–1123, 2009.

[193] Nonappa, M. Lahtinen, E. Kolehmainen, J. Haarala, and A. Shevchenko, “Evidence of Weak Halogen Bonding: New Insights on Itraconazole and its Succinic Acid Cocrystal,” *Cryst. Growth Des.*, vol. 13, no. 1, pp. 346–351, Jan. 2013.

[194] C. R. Hargreaves and J. B. Manley, “ACS GCI Pharmaceutical Roundtable Collaboration to Deliver a Solvent Selection Guide for the Pharmaceutical Industry,” in *Collaboration to Deliver a Solvent Selection Guide for the Pharmaceutical Industry*, 2008, pp. 1–19.

[195] Fda and Cder, “Q3C — Tables and List Guidance for Industry Q3C — Tables and List Guidance for Industry Q3C — Tables and List Guidance for Industry.” [Online]. Available: http://www.fda.gov/Drugs/GuidanceComplianceRegulatoryInformation/Guidances/default.htm. [Accessed: 04-Oct-2017].

[196] Sigma-Aldrich, “Succinic acid SigmaUltra,” 2003. [Online]. Available: https://www.sigmaaldrich.com/content/dam/sigma-aldrich/docs/Sigma-Aldrich/Product_Information_Sheet/s3674pis.pdf. [Accessed: 15-Sep-2017].

[197] N. Blagden, D. J. Berry, A. Parkin, H. Javed, A. Ibrahim, P. T. Gavan, L. L. De Matos, and C. C. Seaton, “Current directions in co-crystal growth,” *New J. Chem.*, vol. 32, no. 10, p. 1659, 2008.

[198] A. Ainouz, J.-R. Authelin, P. Billot, and H. Lieberman, “Modeling and prediction of cocrystal phase diagrams,” *Int. J. Pharm.*, vol. 374, pp. 82–89, 2009.

[199] N. Rodríguez-Hornedo, S. J. Nehm, K. F. Seefeldt, Y. Pagán-Torres, and C. J. Falkiewicz, “Reaction crystallization of pharmaceutical molecular complexes,” *Mol. Pharm.*, vol. 3, no. 3, pp. 362–367, 2006.

[200] M. Susuki and T. Shimanouchi, “Infrared and Raman Spectra of Succinic Acid Crystal,” *J. Mol. Spectrosc.*, vol. 28, no. 1968, pp. 394–410, 1968.

[201] B. Nie, J. Stutzman, and A. Xie, “A vibrational spectral maker for probing the hydrogen-bonding status of protonated Asp and Glu residues.,” *Biophys. J.*, vol. 88, no. 4, pp. 2833–47, Apr. 2005.

[202] V. Chikhalia, R. T. Forbes, R. A. Storey, and M. Ticehurst, “The effect of crystal morphology and mill type on milling induced crystal disorder,” *Eur. J. Pharm. Sci.*, vol. 27, no. 1, pp. 19–26, Jan. 2006.

[203] G. D. Rieck, “The crystal structure of α-succinic acid,” *Recl. des Trav. Chim. des Pays-Bas*, vol. 63, no. 9, pp. 170–180, 1944.

[204] Q. Yu, L. Dang, S. Black, and H. Wei, “Crystallization of the polymorphs of succinic acid via sublimation at different temperatures in the presence or absence of water and isopropanol vapor,” *J. Cryst. Growth*, vol. 340, no. 1, pp. 209–215, 2012.

[205] A. V. Trask, N. Shan, W. D. S. Motherwell, W. Jones, S. Feng, R. B. H. Tan, and K. J. Carpenter, “Selective polymorph transformation via solvent-drop grinding,” *Chem. Commun.*, vol. 0, no. 7, p. 880, Feb. 2005.

[206] K. M. Carver and R. C. Snyder, “Unexpected polymorphism and unique particle morphologies from monodisperse droplet evaporation,” *Ind. Eng. Chem. Res.*, vol. 51, no. 48, pp. 15720–15728, 2012.

[207] H. Wen and K. Park, *Oral controlled release formulation design and drug delivery : theory to practice.* Wiley, 2013.

[208] K. Thoma and I. Ziegler, “The pH-independent release of fenoldopam from pellets with insoluble film coats,” *Eur. J. Pharm. Biopharm.*, vol. 46, no. 1, pp. 105–113, 1998.

[209] A. S. Tatavarti and S. W. Hoag, “Microenvironmental pH Modulation Based Release Enhancement of a Weakly Basic Drug from Hydrophilic Matrices,” *J. Pharm. Sci.*, vol. 95, no. 7, pp. 1459–1468, Jul. 2006.

[210] * A Streubel, J. Siepmann, A. Dashevsky, and R. Bodmeier¨college, “pH-independent release of a weakly basic drug from water-insoluble and-soluble matrix tablets,” 2000.

[211] T. Parikh, H. K. Sandhu, T. T. Talele, and A. T. M. Serajuddin, “Characterization of Solid Dispersion of Itraconazole Prepared by Solubilization in Concentrated Aqueous Solutions

of Weak Organic Acids and Drying," *Pharm Res*, vol. 33, pp. 1456–1471, 2016.

[212] P. Grobelny, I. Kazakevich, D. Zhang, and R. Bogner, "Amorphization of itraconazole by inorganic pharmaceutical excipients: comparison of excipients and processing methods.," *Pharm. Dev. Technol.*, vol. 7450, pp. 1–10, Oct. 2014.

[213] N. a Mugheirbi, K. J. Paluch, and L. Tajber, "Heat induced evaporative antisolvent nanoprecipitation (HIEAN) of itraconazole.," *Int. J. Pharm.*, vol. 471, no. 1–2, pp. 400–11, Aug. 2014.

[214] T. Wu and L. Yu, "Surface Crystallization of Indomethacin Below T g," *Pharm. Res.*, vol. 23, no. 10, pp. 2350–2355, Oct. 2006.

[215] L. Zhu, L. Wong, and L. Yu, "Surface-enhanced crystallization of amorphous nifedipine," *Mol. Pharm.*, vol. 5, no. 6, pp. 921–926, 2008.

[216] N. S. Trasi, S. X. M. Boerrigter, and S. R. Byrn, "Investigation of the milling-induced thermal behavior of crystalline and amorphous griseofulvin," *Pharm. Res.*, vol. 27, no. 7, pp. 1377–1389, 2010.

[217] N. S. Trasi and S. R. Byrn, "Mechanically Induced Amorphization of Drugs: A Study of the Thermal Behavior of Cryomilled Compounds," *AAPS PharmSciTech*, vol. 13, no. 3, pp. 772–784, 2012.

[218] J. Sun and S. L. Simon, "The melting behavior of aluminum nanoparticles," *Thermochim. Acta*, vol. 463, no. 1–2, pp. 32–40, Oct. 2007.

[219] T. Feng, R. Pinal, and M. T. Carvajal, "Process Induced Disorder in Crystalline Materials:Differentiating Defective Crystals from the Amorphous Form of Griseofulvin," *J. Pharm. Sci.*, vol. 97, no. 8, pp. 3207–3221, Aug. 2008.

[220] M. Doty, J. Kipp, C. Rebbeck, J. Werling, and J. Wong, "Polymorphic form of itraconazole, US20030100568A1," vol. 1, no. 19, 2003.

[221] A. Heinz, K. C. Gordon, C. M. McGoverin, T. Rades, and C. J. Strachan, "Understanding the solid-state forms of fenofibrate – A spectroscopic and computational study," *Eur. J. Pharm. Biopharm.*, vol. 71, no. 1, pp. 100–108, Jan. 2009.

[222] J. A. Baird, B. van Eerdenbrugh, and L. S. Taylor, "A Classification System to Assess the Crystallization Tendency of Organic Molecules from Undercooled Melts," *J. Pharm. Sci.*, vol. 99, no. 9, pp. 4215–4227, 2010.

[223] P. J. Flory, *Principles of polymer chemistry*. Cornell University Press, 1953.

[224] H. Al-Obaidi, P. Ke, S. Brocchini, and G. Buckton, “Characterization and stability of ternary solid dispersions with PVP and PHPMA.,” *Int. J. Pharm.*, vol. 419, no. 1–2, pp. 20–7, Oct. 2011.

[225] B. Lang, S. Liu, J. W. McGinity, and R. O. Williams, “Effect of hydrophilic additives on the dissolution and pharmacokinetic properties of itraconazole-enteric polymer hot-melt extruded amorphous solid dispersions,” *Drug Dev. Ind. Pharm.*, vol. 42, no. 3, pp. 429–445, 2016.

[226] D. K. G. van den Mooter, G. Verreck, M. Brewster, J. Peeters, I. Weuts, A. DeCorte, K. Heymans, “Solid Dispersions of a Basic Drug Compound and a Polymer Containing Acidic Groups,” WO2005117834, 2005.

[227] D. a Miller, J. C. DiNunzio, W. Yang, J. W. McGinity, and R. O. Williams, “Enhanced in vivo absorption of itraconazole via stabilization of supersaturation following acidic-to-neutral pH transition.,” *Drug Dev. Ind. Pharm.*, vol. 34, no. 8, pp. 890–902, 2008.

[228] T. Miyazaki, Y. Aso, S. Yoshioka, and T. Kawanishi, “Differences in crystallization rate of nitrendipine enantiomers in amorphous solid dispersions with HPMC and HPMCP,” *Int. J. Pharm.*, vol. 407, no. 1–2, pp. 111–118, 2011.

[229] H. Yamashita, Y. Hirakura, M. Yuda, T. Teramura, and K. Terada, “Detection of cocrystal formation based on binary phase diagrams using thermal analysis.,” *Pharm. Res.*, vol. 30, no. 1, pp. 70–80, 2013.